UCSF RADIOLOGICAL INFORMATICS RESEARCH

A Progress Report

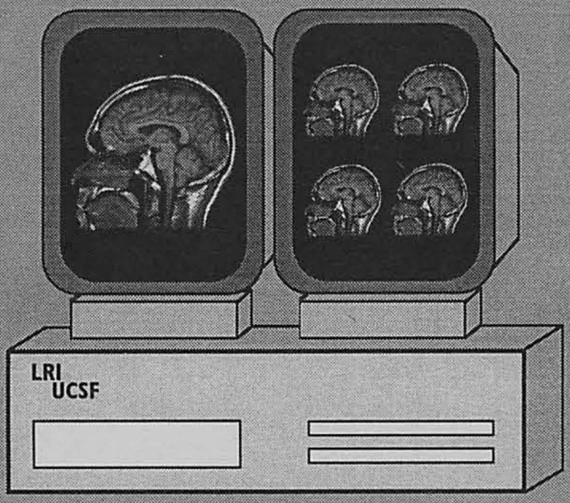

February 1997

Laboratory for Radiological Informatics
Department of Radiology
University of California, San Francisco
530 Parnassus Avenue, Rm CL-158
San Francisco, CA 94143-0628

Tel (415) 476-5941
Fax (415) 502-3217

SUMMARY

During the past year, several major events happened. First, after one year of clinical operation, our hospital-integrated PACS was ready to be transferred to the department for its continuing operation and upgrade. On April 1996, a clinical PACS team was formed to oversee the daily operation. This team is composed of some original members of the laboratory and some new recruits. Most of the laboratory staff members continue their research on future PACS development and other related topics. Second, in September 1996 we received two major contracts from the US. Army Medical Research and Development Command and the HPCC Program, National Library of Medicine (NLM). The Army contract entitled "Full-Field Direct Digital Telemammography" allows us to research one of the unsolved problems in PACS, namely, how to include breast imaging in PACS. The NLM contract on "Medical Image Infrastructure for Collaborative Health Care" provides us with the opportunity to investigate the utilization of the large amount of data in the existing PACS database. Both research topics are derived from our past experience in PACS research and implementation which will hopefully set the trend for our future research direction.

This report summarizes the current status of PACS and image informatics research in our laboratory including image processing, PACS, workstation design, integration of database, data and knowledge extraction, and image compression. It contains preprints of papers which will appear in the Proceedings of *International Society for Optical Engineering, SPIE Medical Imaging* 1997: volumes 3031, 3035, Newport Beach, California, February 22-28, 1997. This report also contains selected reprints published during the last year; abstracts and presentations from the 82nd RSNA, November - December, 1996 and the Preface and Table of Contents of the new book: PACS in Biomedical Imaging, 1996 by Bernie Huang.

This work is currently supported by:

- NLM contract N01-LM-4-3508
- NLM contract N01-LM-6-3547
- NCHS BPA 50257C-95, National Center for Health Statistics
- US Army Medical R&D DAMD 17-94-J-4338
- US Army Medical R&D DAMD 17-96-C-6111
- Lumisys (equipment)
- Fuji Medical Systems USA, Inc. (equipment)
- Abe Sekkei, Japan (equipment)
- Philips Medical Systems DPA 109
- California Breast Research Program 1RB-0148

TABLE OF CONTENTS

PREPRINTS FROM SPIE

SELECTED REPRINTS

UCSF Radiological Informatics Research
- A Progress Report -

Laboratory for Radiological Informatics -- LRI

__Faculty__

Ronald Arenson, M.D.
Professor and Chairman
Department of Radiology

H.K. Huang, D.Sc.
Professor and Vice Chairman, Dir LRI
Department of Radiology

David Avrin, M.D., Ph.D.
Clinical Associate Professor

Katherine Andriole, Ph.D.
Assistant Professor

Robert Gould, Ph.D.
Professor

Shyh-Liang (Andrew) Lou, Ph.D.
Assistant Professor

Stephen Wong, Ph.D.
Assistant Professor

__Postdoctoral Fellows__

Fei Cao, Ph.D.
Postdoctoral Fellow

Mohammed Jahangiri, M.D, MPH
Postdoctoral Fellow

__Graduate Students__

Kent Soo Hoo
Ph.D. Candidate

__Staff__

Todd Bazzill, B.S.E.E.
PACS Engineer

David Hoogstrate, B.A.
Programmer/Analyst

Christopher Jovais
RIS Manager

Michael Linnolt, B.S.
Programmer/Analyst

Laura Snarr, B.S.
Administrative Assistant

Albert Wong, B.S.
Software System Manager

Lloyd Yin, B.S.
Programmer/Analyst

__Visiting Faculty and Fellows__

Ewa Pietka, Ph.D..
Visiting Assistant Professor (Poland)

Jianguo Zhang, Ph.D.
Fellow (Assoc. Prof. Chang Chun Inst., Chinese Acad. Sci)

Guang Pu Lei
Fellow (Prof. Shanghai Med U,China)

Koun Sik Song, M.D.
Visitng Scholar (AMC, S. Korea)

Stephan Erberich
Visiting Scholar (Germany)

Hong Zhang
Visiting Scholar (China)

__Collaborators__

Robert Knowlton, M.D.
Neurology, UCSF

James Sayre, Ph.D.
Statistician, UCLA

Edward Sickles, M.D.
Professor and Chief, Breast Imaging

William Dillon, M.D.
Professor and Chief, Neuroradiology

Department of Radiology, UCSF Network Architecture

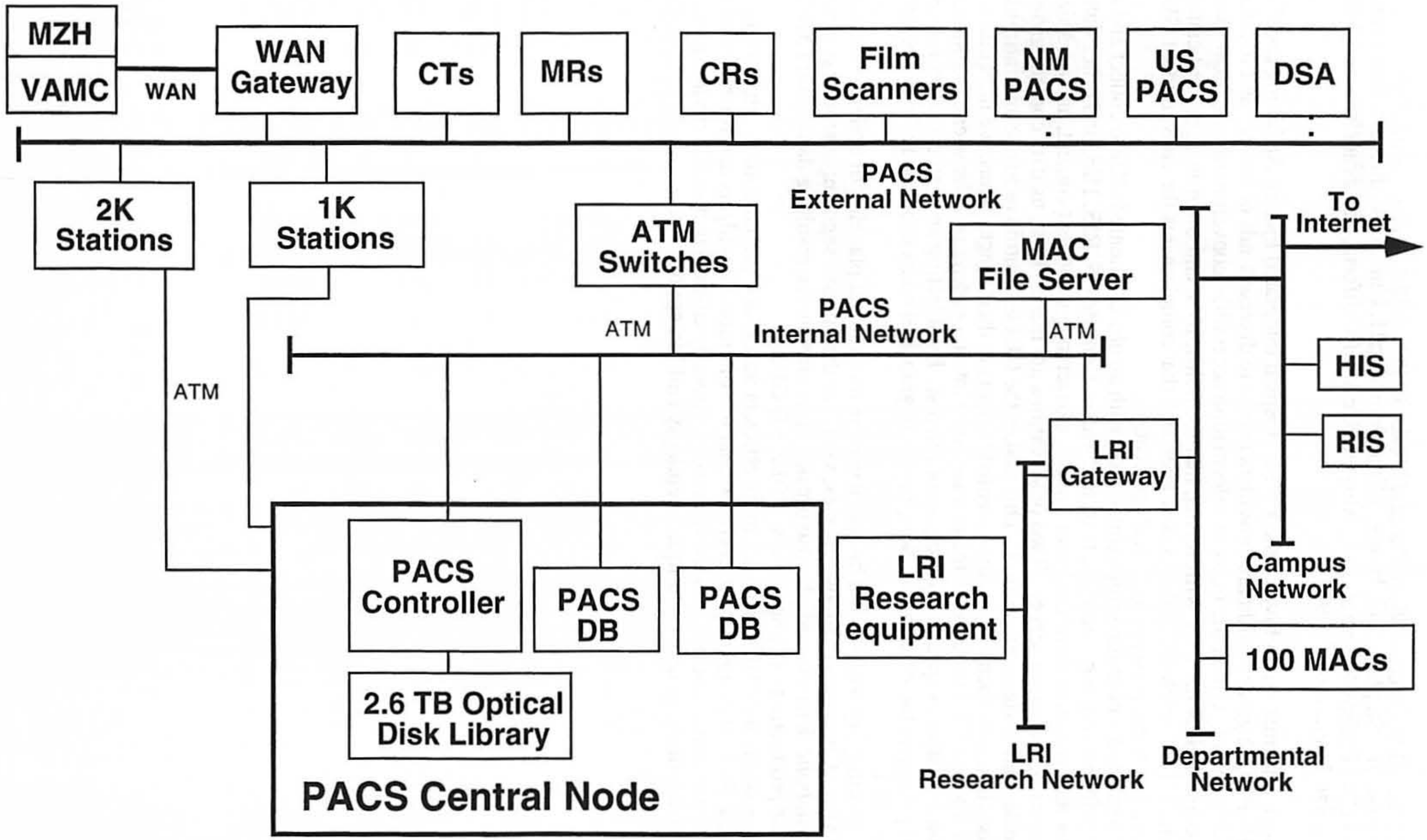

Medical workstation design: Enhancing graphical interface with 3-D anatomical atlas.

Kent Soo Hoo, Jr., Stephen T.C. Wong, Ellen Grant (KSH, Univ. of California, San Francisco/Berkeley, CA 94143) (STCW, Philips Research Palo Alto and Univ. of Califoria, San Francisco, CA 94143) (EG, Univ. of California, San Francisco, CA 94143)

The huge information archive of the UCSF Hospital Integrated Picture Archiving and Communication System (HI-PACS) gives healthcare providers access to diverse kinds of images and text for diagnosis and patient management. Given the mass of information accessible, conventional graphical user interface (GUI) approach overwhelms the user with forms, menus, fields, lists, and other widgets and causes "information overloading." This article describes a new approach that complements the conventional GUI with 3-D anatomical atlases and presents a clinical application.

We constructed a neuroimaging workstation with an object-oriented GUI to collect and display a wide variety of information, e.g., images, text, and video, from PACS, RIS, HIS, and other data sources. The user can register and visualize different brain images, extract image and text content, and organize the processed data into databases of a content server. Two observations are made. First, as data content grows, more icons, menus, fields, and widgets are added. This makes the GUI less intuitive to use and intimidates the users. Second, the clinicians focus on image-oriented widgets in their usage. Thus, we integrate a 3-D anatomical brain atlas into the GUI to serve as the primary user interface element. The user can rotate, segment, and walk through the 3-D atlas to specify any region of interest. By selecting an anatomical region of the brain, the user dynamically triggers the creation of the appropriate graphical widgets on the fly to query and display multimedia data.

The neuroimaging workstation has been used in the surgical planning of epilepsy and diagnosis of multiple sclerosis (MS). Clinicians compose queries, visualize the images, segment anatomical structures, quantitate volume, metabolic activity, and glucose uptake, and correlate the resulting data among MRI, MEG, PET, and MRS. Their productivity is improved with the 3-D GUI.

3-D atlas augmented GUI provides more efficient access and presentation of multimedia medical data than conventional GUI. It combines the conventional use of graphical widgets and forms-based user interface with 3-D anatomical atlases and enables the user to dynamically customize his GUI environment. This research successfully applied this new technique to epilepsy and MS applications.

Mammography display station and its application in a digital teaching file

Fei Cao, H.K. Huang, Edward A. Sickles

Department of Radiology, The University of California, San Francisco, CA 94143-0628

ABSTRACT

We implemented a high resolution display system for viewing digitized mammograms at real-time speeds. This display system has been utilized at the UCSF to develop a digital breast imaging teaching file.

The mammography display station is built on a Sun workstation and Pixar processing hardware. It is capable of real-time 2K image display and manipulation, and serves as a basic platform for our digital mammographic teaching file. The teaching file is designed on a sophisticated computer-aided instruction (CAI) model, which simulates the work-up sequences used in imaging interpretation. Our CAI model not only provides answers to questions, but also allows user's detection of imaging abnormalities by pointing at the image. We also developed a software tool with an easy-to-use user interface to manage patient images and related information, and manipulate the large quantity of digital mammograms.

The display station is found to be adequate for fast display of high resolution digital mammograms. Our sophisticated CAI model integrates the vast image and textual data with visualization software into an interactive mammographic teaching file. This teaching file can be used as a real teaching tool for training radiology residents in mammography.

Keywords: digital imaging, mammogram, display station, interactive teaching file, computer-aided instruction

1. INTRODUCTION

Routine screening with physical examination and periodic mammography has been proved to be effective for early detection of breast cancer and in lowering its death rate among women in the United States.[1-2] Because of the manpower shortage in interpreting breast imaging due to insufficient training resources and facilities, there is a need to develop an alternate method to supplement or replace the current film-based method of training. A digital breast imaging teaching file can alleviate this shortage since a digital teaching file can be duplicated easily and disseminated widely for continuing medical education. This will help to improve the quality of breast imaging interpretation and thereby facilitate mass screening with mammography and problem-solving imaging evaluation of screening-detected abnormalities.

There is still no digital mammographic teaching file currently adequate for clinical use. That is due in part to the lower resolution of currently affordable display monitors and the slower speed in manipulating large digital mammograms (10MByte each). The basic requirement for general use of mammography display station is the ability to show an entire breast with such fine detail that tiny structures are readily visible. Furthermore, since routing mammographic interpretation involves four images of a current examination compared with four images from a prior examination, digital display workstations must be able to utilize monitors so that two or more whole-breast mammograms are displayed per monitor and can be manipu-

Further author information

F.C.(correspondence): Email: fcao@lri.ucsf.edu; WWW: http://www.lri.ucsf.edu; Tel: 415-502-4288; Fax: 415-502-3217

H.K.H.: Email: bernie_huang@radmac1.ucsf.edu; WWW: http://www.lri.ucsf.edu; Tel: 415-476-6044; Fax: 415-502-3217

E.A.S.: Email:edwards@email.his.ucsf.edu; Tel: 415-885-7417; Fax: 415-885-7829

lated at nearly real-time speeds. Computer-aided instruction for mammogram teaching file has been applied to radiology also with limited success because of the difficulties in handing the required images and in simulating an interactive teaching session.

We use a high resolution (50μm spot size) laser film digitizer for mammogram digitization and a high resolution 2,000 by 2,500 line multi-monitor display workstation for viewing digital mammograms. The quality of the digital images produced and subsequently read meets the standards laid out by the American College of Radiology (ACR)[3] and is found to be adequate for clinic applications[4-5]. We also developed a sophisticated CAI model to simulate a real teaching session. With carefully structured questions, each user can be prompted to respond by making his/her own observations, assessments, and work-up decisions just as if the patient were being examined at that time. This effectively replaces a "show-and tell" teaching experience with the interactive, response-driven type of instruction that currently must be taught in person.

In this paper, we describe our high-resolution mammographic display station for viewing mammograms and the interactive mammographic teaching file implemented on this display station.

2. MAMMOGRAPHY DISPLAY STATION

Our 2K mammography display station is sketched in Figure 1. The 2K station is based on a Sun Sparc 470 workstation, two 21" diagonal 2K MegaScan monitors, Pixar image processing hardware and a 7 GByte fast storage disk.

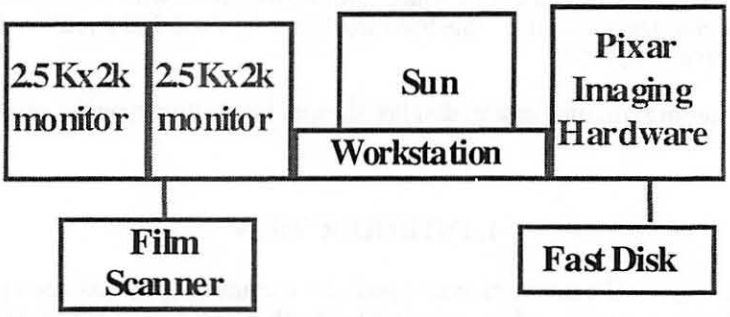

Figure 1. Configuration of mammography display station.

The Sun 470 workstation (64MB system memory) serves as a platform for the display station. Each of two gray scale monitors is able to display 2048 pixels by 2560 scan lines with 10 bit resolution. The Pixar image processing system can directly access the digital image stored in the Fast-disk. A 10MB digital mammogram takes less than 2 seconds to retrieve from the Fast-disk and display on the 2K monitors. The Pixar hardware also comes with two 32MB frame buffers and the optimized image processing routines. That makes it possible for four mammograms (<10MB each), in a typical display mode, to be easily manipulated on screen in a nearly real time. The 7 GB Fast-disk is capable of storing 1,000 digital mammograms for fast retrieving by the Pixar system.

The laser film digitizer is provided by Abe Sekkei, Inc. in Japan.[6] It is a high-resolution scanner specially designed and developed for mammograms, with a 50μm spot size, a 50μm sampling distance and 12Bits resolution. This scanner also has the capability of minimizing scanning artifacts due to grid lines. An 8" x 10" mammogram will yield 2000 x 2500 x 2byte = 10MB image with 100μm sampling distance or 4000 x 5000 x 2 byte =40MB image with 50μm sampling distance. In our teaching file, the mammograms, depending on their original film size, were digitized in either 50μm or 100μm resolution to fit the 2K display monitors.

Routing mammographic interpretation requires displaying four or eight images. A special display mode is therefore developed for the digital teaching file. The display mode takes advantage of the fact that most breast images can be fitted into a narrow rectangle. Thus, we can split the 2K x 2K monitor into two 2K x 1K display areas. A standard setting is shown in Figure 2, where the left monitor is for LCC and RCC (Cranio Caudal view of Left and Right breast) and the right monitor for LMLO and RMLO (MLO: Mediolateral Oblique view of Left or Right breast).

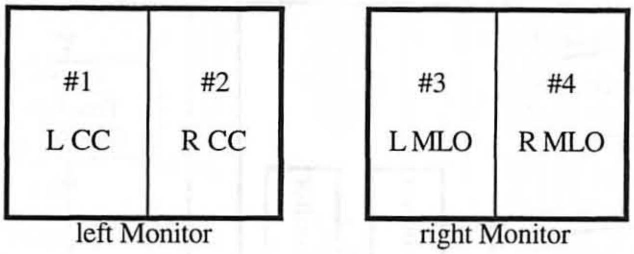

Figure 2 Display mode for four mammograms on the two 2K monitors. Each screen is split into two 2K x 1K regions to accommodate two mammograms.

A toggle button is used for alternative display of current or past four mammograms. Total of eight mammograms can then be shown and examined.

3. TEACH FILE DATA COLLECTION

The UCSF film-based breast imaging teaching file has been in constant use since 1976 by radiology residents and fellows. The teaching file consists of over 1,000 pathologically proved cases, each of which begins with a screen-film mammography examination no more than 7 years old. The case material demonstrate the various problem-solving imaging approaches available in reaching accurate imaging diagnoses. 1,000 cases from this teaching file have been selected and will be converted to a digital imaging file.

Figure 3 summarizes the processes for image digitization and teaching file data collection. Mammograms, as well as breast ultrasonographs, CT and MRI (if they are included in the case) are digitized with the high-resolution film scanner connected with Sun Workstation #1. Related medical information and image description textual data are inserted into the header record of the image files. The digitized images are then send via network to our mammography display station #2 where they are decoded, processed and then stored in the fast-disk ready for retrieving. Meanwhile, the image information are extracted from the raw image header file and well indexed for later uses in image retrieving and in the digital teaching file. The digitized images are currently formatted to an ACR/NEMA 2 standard and backed up in 14GB Extrabyte tape drive. They can be reformatted to DICOM 3 standard later and sent to our PAC system for permanent archiving.

It is a tedious task to input 60,000 questions and answers, 10,000 digitized images (2K x 2K) and regions of interest (ROI) for a large teaching file of 1,000 cases. The interactive, response-driven type of CAI for imaging work-up of all cases also has to be specified. In order to input this voluminous data, it is necessary to develop a simple teaching file script (TFS) integrating this data with the CAI.

The TFS is similar to but much simpler than the Hypertext Markup language used in the Web Home page. It is simply an ordinary text file together with tags that tell the computer how to identify each of elements in the teaching file, how to query and display images, and how to response to user's actions. A navigation browser is developed and then used by the users on the mammography display system to read and navigate through the TFS file, simulating an interactive and response-driven type of teaching session.

Radiologists indicate that the TFS is simple enough for them to learn quickly and create their own teaching sessions. The TFS is a plain text file, easy to update and to port to the other systems. All tags used in the TFS are listed in Appendix A, while the GUI of the teaching file navigation browser is shown and explained in Section 5.

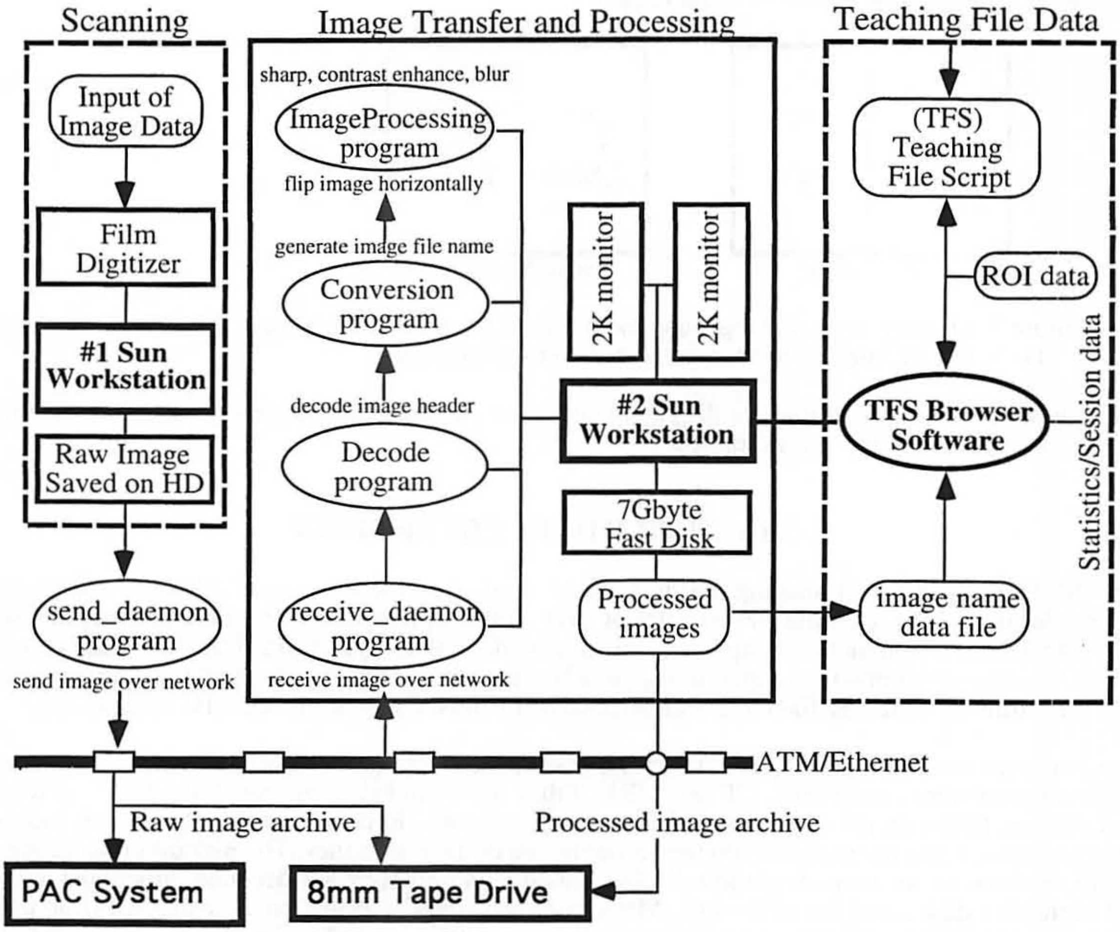

Figure 3. Sketch for digitization process and teaching file database establishment

4. COMPUTER-AIDED INSTRUCTION MODEL

Our CAI model specifies the sequence of questions, image display, instructions, and explanations of cases dynamically based on the user response during the interactive teaching session. It not only provides answers to questions and image visualization, but also provides follow-up questions and allows user's detection of imaging abnormalities by pointing.

Figure 4 shows the general control flow of this model and imaging work-up sequences. At the start of each case, the system presents to the user a set of initial screening mammograms. After examination of those images, the user will be asked to use mouse pointer identifying on the 2K monitors the mammographic abnormalities. The user's selection is compared with the pre-recorded ROI data. If the user succeeds in identifying the ROI, he/she will proceed to a multiple choice or true/false type of question that is relevant to his/her findings, or the user has to try again. If the user still can not mark the abnormality after three tries, the system will display the ROI on the 2K monitor with an explanation and then proceed to the question item. Based on the user response to the question item, the computer system will call up different work-up sequences, defined in the CAI model as illustrated in Figure 4. The system will provide the instruction and answers, guiding the user towards the next question. Whenever necessary, addition images will also be shown.

Often, there is more than one suitable approach to working up a specific breast imaging problem. The questions and instruction sequences built into the digital teaching file system support this by accepting more than one correct choice and allowing different follow-up questions, as illustrated in Figure 5.

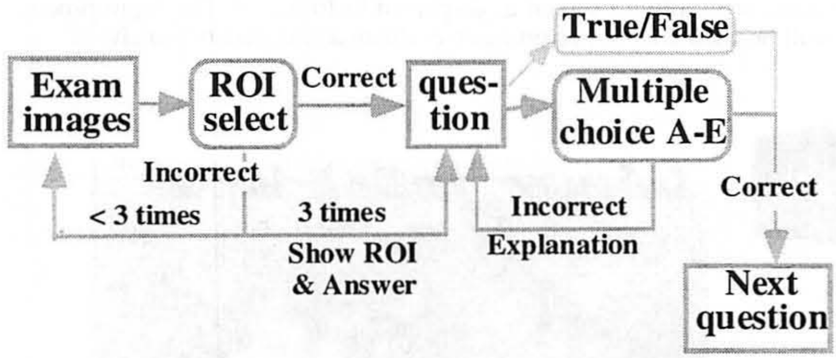

Figure 4 A general algorithm for the CAI model and the basic work-up sequences

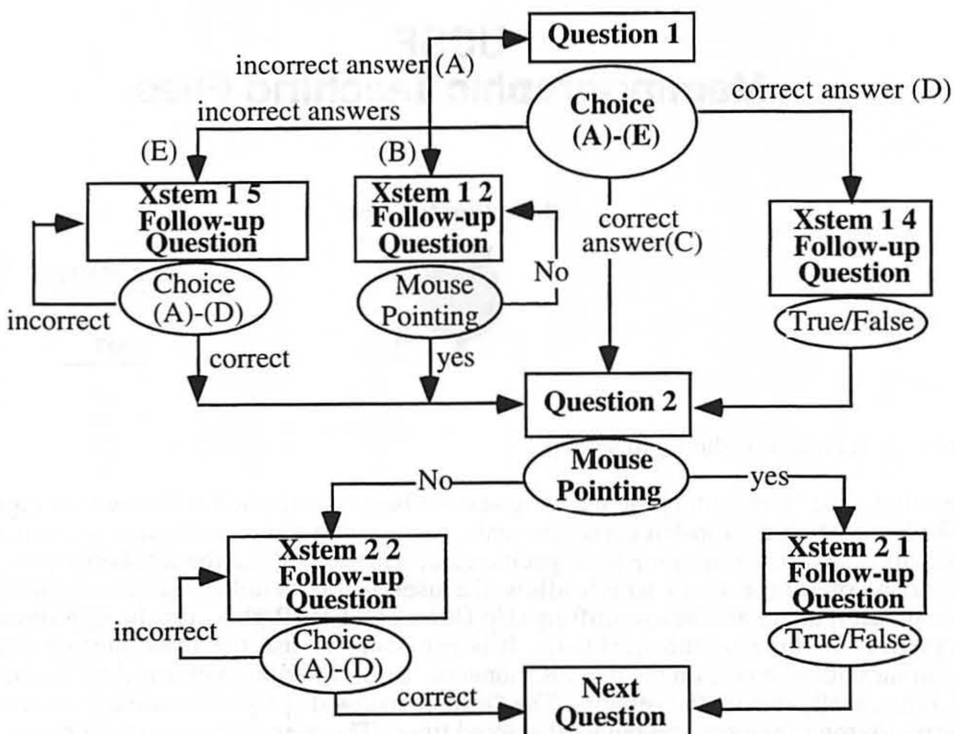

Figure 5. An example of nested building blocks and different work-up sequences for the same question.

Marking the abnormality, multiple choice and true/false questions are three basic building blocks of our interactive teaching file. They can be nested together to create an effective teaching session as what radiologists want.

5. GRAPHICAL USER INTERFACE (GUI)

An easy-to-use graphical user interface is well designed for our interactive teaching file. It responses dynamically to every user's action with detailed instruction. Combined with an on-line help, the GUI makes the user easy to manipulate the digital mammograms and navigate through the teaching session.

The teaching file starts with a login screen as displayed in Figure 6. The login process will capture the user's profile that will be used later in performance evaluation and statistics analysis.

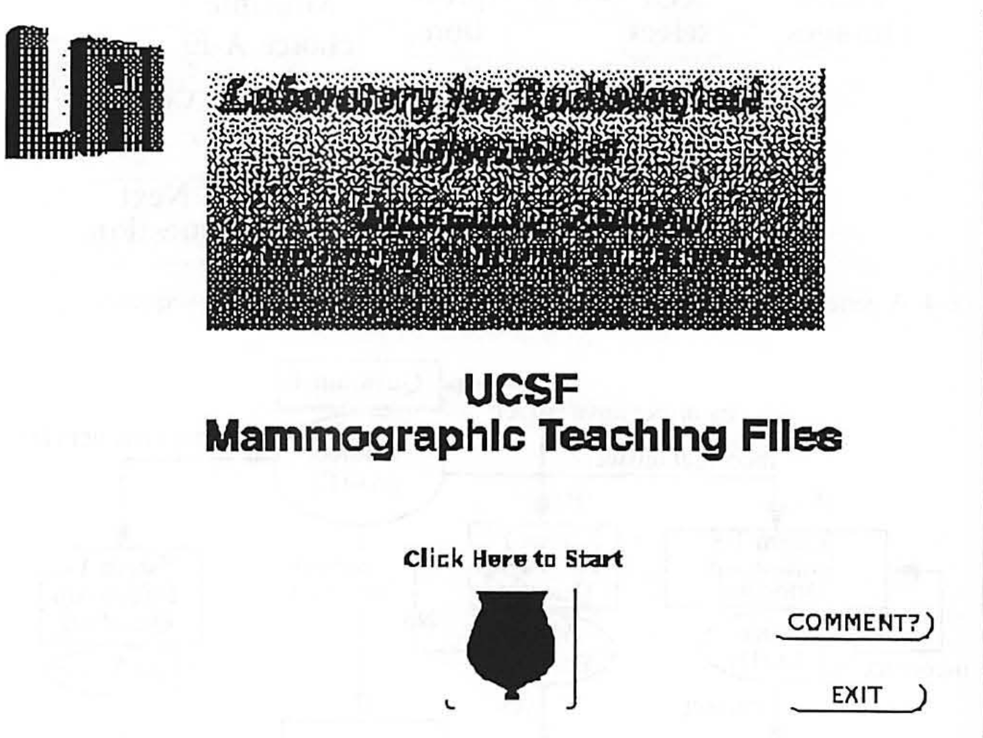

Figure 6. Screenshot of the login screen.

After the user clicks the start button, the teaching session begins with the GUI shown in Figure 7. The "START HERE" button on the top-left corner presents the user with a choice of starting a new session, resuming the previous session or jumping to a specific case. On the left and the left-bottom of the screen, there are an array of image tools which allow the user to do Window-Level adjustment, image magnification, measurement, and image shifting (Up/Down and Left/Right). On the right-bottom corner, there is a depiction of three-button trackball. It is necessary to use the three buttons especially in manipulating an individual image on the two 2K monitors. Brief description of trackball button usage will be displayed dynamically during the session. The "Info" window displays the case/question number, the number of correct/wrong answers and the total elapsed time. The user navigation buttons are located on the middle of the control screen. The user will be asked to click these buttons making choices, answering questions, initiating the pointer for marking abnormalities on the 2K monitors. In the "text window", the questions/answers and the system instructions are shown dynamically according to user's actions.

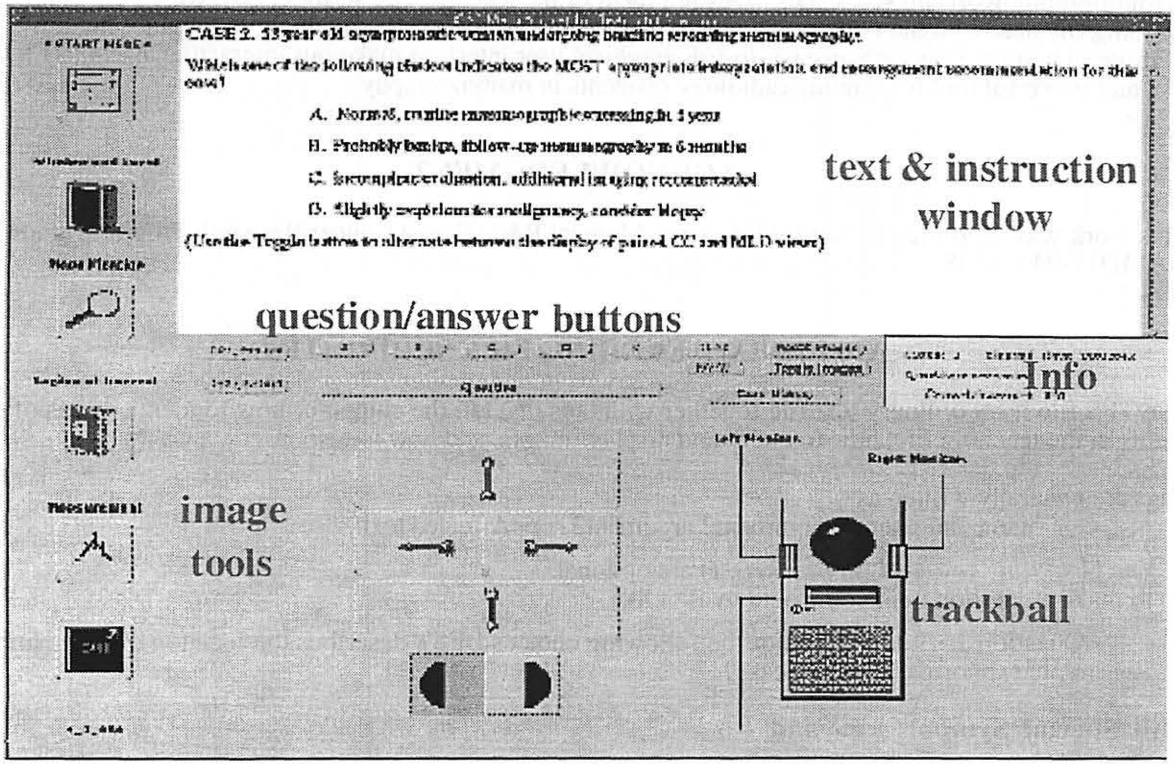

Figure 7. Screen shot of the main control screen of the interactive teaching file.

6. SUMMARY

We implemented a high resolution display system for viewing digitized mammograms at real-time speeds. This display system, combined with a sophisticated computer-aided instruction (CAI) model, has been utilized to create an interactive teaching file as a real teaching tool for training radiology residents in mammography.

A mammography display has to be able to portray the entire breast with such fine detail that tiny structures are readily visible and in a near real-time speed. The quality of digital mammograms is dictated by the film digitizer and display system while the speed of image display and on-screen manipulation is determined by the system hardware architecture and the imaging processing software. In this paper, we described our 2K display station and high resolution film digitizer. The image quality of the digitized and displayed mammograms is found to be adequate and acceptable to clinic applications. The Pixar image hardware with two large frame buffers and the optimized processing software, combined with the fast retrieving of images from the fast-disk, makes nearly real time mammogram reading and on-screen manipulating possible. We also developed a special display mode to directly show on the two 2K monitors a set of four mammograms or eight if toggled with. Such display mode is necessary and needed in a mammography interpretation.

Using the high resolution display station, we create a large interactive mammographic teaching file. The teaching file is designed on a sophisticated computer-aided instruction (CAI) model to simulate the real mammography work-up sequences. Development of the teaching file script (TFS), which integrates vast teaching file data with the CAI, makes it easy for breast imaging experts to create a digital teaching file. All of those in conjunction with an easy-to-use graphical user interface make our interactive teaching file as a real and powerful tool for training radiology residents in mammography.

ACKNOWLEDGMENT

This work was supported in part by US Army Medical R&D Breast Cancer Research Program, grant No: DAMD17-94-J-4338.

APPENDIX: TEACHING FILE SCRIPT (TFS)

The TFS file is an ordinary text file together with tags that tell the computer how to identify each of elements in the teaching file, how to query and display images, and how to response to a user's action.

Tags are generally written as

<tag_name augment1 (argument2 argument3 ...)> Affected text .

Note: *any keywords in brackets* () are optional.

So to make a question item you would mark it like

<Question 2> Which ONE of the following choices BEST describes the location of the mammographic abnormality in this case?

Two Special Symbols < > and { }

< > Angle brackets are a special default to identify the tags or keywords.

{ } Braces: are used to contain a block of physicians/programmers' comments. The computer will skip any text enclosed in { }.

Tags and Keywords

<Section number> text:

---identify the beginning of the 'number'th case, followed by the 'text' description of the case history if any. e.g. <Section 89> for 89th case.

Note: this tag must be the first one for each case.

<Patient>text

---optional tag: identify a patient's name and ID. 'text' contains any useful information about the patient. A suggested format:

<Patient> lastName, First 8-digit-ID-number others

Note: this tag is purely for physicians/programmers' purpose. The patient ID and names will not be shown to a user.

<Question number> text:

---identity the 'text' as the 'number'th question. e.g. <Question 3>

<Image number1 (number2) (yes)> (pointers to images):

---display images.

'number1' (maximum of 4) is the number of images to be shown.

'number2' (maximum of 4) is the number of images to be toggled with if any.
'yes' : if this keyword is specified, the images will not be shown until a correct answer is given.

pointers to images: image file names will be read in automatically from an image data file. Normally, you don't have to specify the image names. However, if one wants to show the images in a previous question or case, one has to specify the pointers to the images, which can be one of the following two formats

#l-num1 q-num2 l-num3
#l-num1 filename

where 'l-num1' is the 'number'th of current images to be loaded in, 'q-num2' and 'l-num3' are the previous question number and the 'number'th image which 'l-num1' points to, 'filename' is any image file name. e.g.

<Image 2 2 yes>
#2 2 1
#3 credo/case2/CC_30:09:94_02:12:02(R)#100#.spl.fd
Show four images (<Image 2 2>) after a correct answer ('yes'). The first (#1) and forth (#4) images are read in automatically from the image data file. The second image (#2) is the same as the first image in Question 2 (#2 2 1). The third image points to the image file---credo/case2/CC....

<A (yes) (x)> text:
<B (yes) (x)> text:
<C (yes) (x)> text:
<D (yes) (x)> text:
<E (yes) (x)> text:
---Answers to the multiple choices (A)-(E).
---The keyword 'yes' is used to identify the correct answer. e.g. <B> is for wrong choice while <B yes> is used for the correct answer.
---The keyword 'x' indicates an existence of a follow-up question specified by the tag <Xstem>.
Note: maximum choices of 5 from (A)-(E).

<T (yes) (x)> text:
<F (yes) (x)> text:
---Answers to the TRUE/FALSE questions. The keyword 'yes' is used to identify the correct choice. e.g. <T> for an incorrect answer and <F yes> for a correct answer.
---The keyword 'x' indicates an existence of a follow-up question specified by the tag <Xstem>.

<Mouse (no) (x)> text1:
<Mouse yes (x)> text2:
---Answer to the question, which requires a user to identify the predetermined region on an image. The answer 'text2'will be shown if the user selects the right region on the display, or 'text1' will be shown. e.g. <Mouse> or <Mouse no> for an incorrect answer and <Mouse yes> for a correct answer.
---The keyword 'x' indicates an existence of a follow-up question specified by the tag <Xstem>.

<Xstem number1 number2>
---follow-up question, which stems out of Question 'number1' and Answer 'number2'.
'number2' = 1,2,3,4,5 for multiple choices A, B, C,D,E respectively; or
'number2' = 1, 2 for TRUE/FALSE choices T and F; or
'number2' = 1, 2 for <Mouse yes> and <Mouse no>.
See an example and its control flow chart for <Xstem> in Figure 5.

REFERENCES

1. Sickles E.A., Ominsky SH, Solitto RA, et al., Medical audit of a rapid-throughput mammography screening practice: Methodology and results of 27,114 examinations, *Radiology*, 1990; 175:323-327.

2. Feig SA, Decreased breast cancer mortality through mammographic screening: results of clinical trials, *Radiology*, 1988, 167:194-225.

3 ACR, ACR standards for the performance of screening mammography, ACR Publications

4. Lou SL, Sickles E., Wang J. Huang HK. A high resolution display system for mammograms. *Radiology* 193(P), 474, 1994.

5. Moskowitz M., Wang J, Huang HK, Sickles E, Allen J, Giles A. High Resolution Display System for Mammograms. *Proc. SPIE Medical Imaging* 2431-44, 1995.

6. Andriole K, Wang J, Gould RG, Huang HK. Digital image quality comparison between a 50μm laser digitizer and a high-resolution CR imaging plate. *Radiology*. 193(P), 250, 1994.

PACS Pitfalls and Bottlenecks

H.K. Huang, S.L. Lou, and W.K. Wong

Laboratory for Radiological Informatics
Department of Radiology, University of California San Francisco
530 Parnassus Avenue, Rm. CL-158, San Francisco, CA 94143-0628

Abstract

PACS pitfalls are mostly created from human error, whereas bottlenecks are due to imperfect design in either the PACS or image acquisition devices. These drawbacks can only be realized through accumulated clinical experience.

Pitfalls due to human error are often initiated at imaging acquisition devices and at workstations. Three major errors at the acquisition devices are entering wrong input parameters, stopping an image transmission process improperly, and incorrect patient positioning. The error occurring most often at the workstation happens when the user enters too many key strokes or clicks the mouse too often before the workstation can respond. Other pitfalls at the workstation unrelated to human error are missing location markers in a CT or MR scout view, images displayed with unsuitable look-up-tables, and white boarders in CR images due to x-ray collimation. Pitfalls created due to human intervention can be minimized by a better quality assurance program and periodic in-service training, and by interfacing image acquisition devices to the HIS/RIS.

Bottlenecks affecting the PACS operation include network contention; CR, CT, and MR images stacked up at acquisition devices; slow response from workstations; and long delays for image retrieval from the long term archive. Bottlenecks can be alleviated by improving the system architecture, re-configuring the networks, and streamlining operational procedures through a gradual understanding of the clinical environment.

We have identified most of the pitfalls and bottlenecks discussed above in our hospital-integrated PACS based on the past two years of clinical experience. This paper categorizes some of these problems, illustrates their effect on PACS operations, and suggests methods for circumventing them.

Keywords: PACS operation, image acquisition, workstations, human errors, pitfalls and bottlenecks

1. INTRODUCTION

PACS pitfalls are mostly caused by human error and operator intervention with imaging acquisition devices and various PACS components. Bottlenecks are due to design imperfections in either the PACS or image acquisition devices. These problems can only be realized through clinical experience [1-4]. This paper categorizes some of these problems, illustrates their effect on PACS operations, and suggests methods of circumvention [5].

2. PITFALLS

Pitfalls due to human error are often initiated at imaging acquisition devices and at workstations. Three major errors at the acquisition devices are entering wrong input parameters, stopping an image transmission process improperly, and incorrect patient positioning.

Human Errors at Imaging Acquisition Devices

Two most commonly occurring errors at the computed radiography (CR) acquisition are using the wrong imaging plate ID card at the reader and entering the wrong patient's ID, name, accession no., or birthday, and invalid characters at the scanner's operator console. These errors can result in a loss of images, images assigned to a wrong patient, the patient image folder containing other patient's images, orphaned images, and acquisition computer crashing due to illegal characters. Routine quality assurance (QA) procedures checking the CR operator log book or the radiology information system (RIS) log file against the PACS patient folder normally can discover these errors. If discrepancy detected early enough before images are sent to the workstation (WS), the PACS manager can perform the damage control by manually editing the PACS database to 1. correct for patient's name, ID, etc., and other typographical errors; 2. delete images not belonging to the patient and 3. append orphaned images to the proper patient image folder. Lost images in a patient's folder can usually be found in the orphaned image directory. If images have already been sent to the WS before the PACS manager has a chance to do the damage control described earlier, the PACS coordinator should alert the users immediately.

Procedure errors at Imaging Acquisition Devices

Procedure errors can be categorized in CT/MR and in the CR during image acquisition. In CT/MR, there are three most common errors: 1. terminating a scan while the last images are being transmitted, 2. the operator manually interrupting an image transmission process, and 3. the technician realigning the patient during scanning. These errors can result in CT/MR image file missing images, images out of order in the sequence, and crashing the scanner due to the interruption of the image transmission. In CR, the most common error occurs when the technologist places the imaging plate under the patient in the wrong direction during a portable examination. The result is a wrong image orientation during the display.

Another pitfall during CT acquisition which is not due to human error is in the coronal head scan protocol. In this protocol, the image appearing on the CT display monitor will have the left and right direction reversed. If film output is used, the technologist manually inputs the orientation as annotation on the screen which is then printed on the film with the image. In the PACS such an interactive step is not possible because graphics on the CT display console are not included in the DICOM image header. A method to circumvent this shortcoming is to detect the scanning protocol from the DICOM image header and automatically annotate the orientation on the image during its display on the PACS workstation.

Errors due to manually interrupting the transmission procedure can be alleviated by using the DICOM communication protocol for automatic image verification and recovery during the transmission. Images archived out of order in the sequence can be manually edited during the QA procedure. Wrong CR orientation during display can be detected by an algorithm with automatic rotation [6], or manually rotating during the QA procedure.

Pitfalls created due to human error can been minimized by scheduling regular in-service training and continued education for technologists. However, the most effective method is to use a direct HIS/RIS interface between the image acquisition device and the PACS components which in essence eliminates the human interaction for inputting patient related data. Currently, there is a CR interface to the RIS available for direct patient data input [7]. However, direct interface from RIS to CT/MR is still not available.

Errors at the Workstation(WS)

Human Error

Two human errors occur often at the WS. First, the user enters too many key strokes or clicks the mouse too often before the WS can respond to the last request. As a result from this error, the WS does not respond properly or it crashes. When the WS response is slow, the impatient user enters the next few commands while the WS is still executing the last request, it can either crash unexpectedly or hang. Another possible result is that the WS continues executing the next few commands by the user after the current one is completed. Since the user may have forgotten what commands he/she had entered, an unexpected display may appear on the screen which will cause confusion. Second, the user forgets to close the window of a previous operation. In this case, the WS may not response to the next command. If the user gets panic and enters other commands, similar errors described in the first case may occur.

Two remedies can be used. The WS can provide a big visible timer on the screen for the user to know that the last process is still in operation. This process will minimize the impatient user's error. A better solution is to have an improved WS design to tolerate this type of human error.

System Deficiency

Four system deficiencies at the WS are no localization markers on a CT/MR scout view, incorrect look up table for CT/MR display, orientation of the CT head image in the coronal scan protocol discussed earlier, and white boarders in CR due to X-ray collimation. No localization markers on a CT/MR scout view can be remedied by creating the localization lines using the information from the DICOM image header. The use of an incorrect look up table for a CT/MR display is case dependent. Correct look up tables for CT can be generated by using the histogram technique. There are still some difficulties in obtaining a uniform correct look up table for all images in a head MR sequence. Sometimes it is necessary to investigate every image individually by using the histogram method. Correction for CT head coronal scan has been discussed previously. White boarders in CR due to X-ray collimation can be corrected using an automatic background removal technique [8].

2. Bottlenecks

There are three major bottlenecks in the PACS: network contention, slow response at the WS, and slow response from the long term archive. This section summarizes what causes these bottlenecks and methods of remedy.

Network Contention

Network contention will cause many bottlenecks. First, CR/CT/MR images could stack up at the image acquisition computers. The result would cause the computer disks to overflow and eventually lose some images. Another effect is that it will take the image file a long time to collect all images at the PACS controller which can delay the transmission of the file to the WS for review. Network contention can also cause a long delay for image retrieval from the long term archive, especially when the retrieved image file is large.

Methods of correction can be divided into general and specific. In the general category, it includes redesigning the network architecture, using a faster network, and modifying the communication protocols.

An example of redesigning the network architecture is to separate the network into segments and subnets and redistribute the heavy traffic routes to different subnets. For example, CT/MR acquisition and CR acquisition can be divided into two subnets. Assign priorities to different subnets based on the use and time of day is one way to address the user's immediately need.

Using a faster network can speed up the image transfer rate. If the current network is conventional Ethernet, consider changing it to Ethernet Hub or fast Ethernet. If optical fibers are available, consider upgrading the network to asynchronous transfer mode (ATM) technology [9]. Conventional network protocols were designed for small file transfer. Changing some parameters in the protocol may speed up the transfer rate, for example, enlarging the image buffer size.

In the specific category, it depends on the operational environment. Methods of correction may involve changing the operational procedure in the radiology department. Consider two examples: CR images stacked-up at the CR reader, and CT/MR images stacked up at the scanner. Most CR applications are for portable examinations and are mostly performed in the early morning. A most obvious method of correction is to rearrange portable examination schedule at the wards. CT/MR images stacked-up at the scanner may be due to a design fault in the communication protocol at the scanner. There are two methods of correction. First, use DICOM auto-transfer mode to "push" images out from the scanner to the PACS controller or the WS. At the PACS controller or the WS, design the database to update the image file as each image arrives from the scanner. Second, from the PACS controller or the WS, use DICOM to "pull" images from the scanner.

Slow Response at the WS

A slow response at the WS is mostly due to bad WS local database design, and not sufficient image memory. An example of bad WS database design is when the database allocates a large image file in the local disk for image storage. During the initial configuration, this storage space is contiguous. As the WS starts to accumulate and delete images while it is being used, this space becomes fragmented. Fragmented space causes an inefficient I/O transfer rate rendering a slow response bringing images from the disk to the display. Insufficient image memory in the WS requires continuous disk-memory swap slowing down the image display speed. This is especially problematic when the image file is large.

Several methods for correcting a slow response at the WS are possible. First, is to increase the memory size so that the memory can accommodate a complete image file which will minimize the requirement for memory-disk swap. The use of redundant array of inexpensive disks (RAID) technology is one way to speed up the disk I/O for fast image display. A better local database design at the WS is necessary to speed up the image seeking and transfer time.

Slow Response from the Long-term Archive

A slow response from the long-term archive can be caused by slow optical disk search and read/write procedures, patient images scattering in different optical disk platters, and many simultaneous requests. Optical disk read/write normally is about 400-500 Kbytes/sec. When many large image files are requested which scatter in many platters, the seeking time and disk I/O will be slow. This will cause a slow response from the long term archive.

There are two possible methods of correction. First, an image platter manger software can be used to re-write scattered images to contiguous optical disk platters. This mechanism will minimize the seeking time for platters. Another method is to use the image prefetch mechanism which anticipates what images will be needed by the clinician for a particular patient. A combination of both mechanisms will speed up the response from the long-term archive.

SUMMARY

Pitfalls and bottlenecks are two major obstacles hindering a smooth PACS operation after its installation. We have identified most of these problems based on our clinical experience with the hospital-integrated PACS during the past two years and clinical experience from other centers. We have also suggested methods to circumvent these pitfalls and minimize the occurrence of bottlenecks.

REFERENCES

1. D.V. Smith, S. Smith, G.N. Bender, et al. 1995. Evaluation of the Medical Diagnostic Imaging Support System based on 2 Years of Clinical Experience. *J Digital Imag.* Vol. 8, No. 2, 75-87.

2. N.H. Strickland. 1996. Hammersmith PACS: Some Lessons learned in Implementing a Filmless Hospital. *Proceedings 14th Intern. EuroPACS Meeting* , October 3-5, Crete, Hellas, 12-17.

3. Z. Protopapas, E.L. Siegel, B.I. Reiner, et al. PACS Training for Physicians: Lessons Learned at the Baltimore VA Medical Center. *J Digital Imag.* Vol. 9, No. 3, 131-136.

4. H.K. Huang. 1996. Picture Archiving and Communication Systems in Biomedical Imaging. *VCH(John Wiley & Sons) Publishers,* NY, p.489.

5. H.K. Huang, A.W.K. Wong, S.L. Lou, et al. 1996. Clinical Experience with a Second Generation PACS. *J Digital Imag.* Vol. 9, No. 4, 1-16.

6. E. Pietka, H.K. Huang. 1992. Orientation Correction for Chest Images. *J. Digital Imag.* Vol. 5, No. 3, 185-189.

7. R. Tecotsky. 1996. FCR ID Gateway: Theory of operation. Private Communication.

8. J Zhang, H.K. Huang. 1996. Background Recognition and Removal of Computed Radiography images. *Radiology.* 201(P), 220.

ACKNOWLEDGMENT

We would like to thank our colleagues at UCSF for contributing their input to identify some of these pitfalls and bottlenecks and suggesting methods of remedy. Raymond Tecotsky developed the CR direct interface to the HIS/RIS shown in Figure 3. Part of this work is supported by NLM Contract N01-LM-4-3508 and CalREN grant ATMN-007, Pacific Bell.

PACS Meets Digital Library - Issues and Applications

[1,2]Stephen TC Wong, [2,3]Kent Soo Hoo, Jr, [3]Pablo Whaley, [4]Olivia Velez, [5]Camper D English, and [2]HK Huang

[1]Philips Research Laboratory, Palo Alto, CA 94304
[2]University of Califoria, San Francisco, CA 94143
[3]University of California, Berkeley, CA 94530
[4]Mount Holyoke College, MA 01075
[5]San Francisco State University, CA 94114

ABSTRACT

The purpose of this presentation is to point out the issues of incorporating digital libraries (DL) technologies into picture archiving and communication systems (PACS). The DL technologies can be used to increase the knowledge content and utilities of PACS and associated medical information systems in providing a broader range of medical services. We further illustrate certain potential application areas with examples from a research prototype developed on top of the hospital-integrated PACS of UCSF.

1. INTRODUCTION

Health care delivery systems are progressively transforming into digital media for better and more cost-effective communications. The trend is accelerated by the current environment of managed care and wide spread availability of digital imaging modalities. Digital communication and management in radiology is particularly challenging owing to large image size and high quality requirement. Over the past decade, PACS has evolved to be the predominant means for acquisition, storage, and communication of digital medical images for softcopy review. The technology of PACS is still maturing rapidly, but the fundamental knowledge of PACS is reasonably well defined. Medical imaging vendors are now offering turnkey or customized PACS solutions to achieve filmless radiology.

A digital library, on the other hand, is viewed as an electronic version of a paper-based public library, with the major differences in storage in digital form, direct communication to obtain material, and copying from a master version [1]. The objective of a digital library is to provide a single port of entry to the online documents of distributed library sites over the Internet. These documents are inherently multimedia, consisting of text, images, video, and audio. Coordinated national effort in DL research has recently been initiated with joint funding by NSF, APRA, and NASA, and new conferences and journals dedicated to the DL activities are also organized (see Web sites of these agencies and digital library project homepage at http://www.dlib.org).

Although addressing different applications, the observation is that the emerging digital library (DL) technologies can be deployed to enrich the knowledge content and utilities of current PAC systems in providing a broader range of medical services than softcopy review. This article describes potential applications and technical issues of the interplay bewteen DL and PACS and proposes areas of research to address these issues. When appropriate, we provide illustrative examples taken from our research prototypes.

The rest of the paper is organized in the following manner. Section 2 lists certain potential extensions to PACS, which will enlarge the functional scope of PACS for radiology and other medical specialties. The section also raises several unresolved research questions to these extensions. Section 3 discusses the system architecture of

PACS DL while Section 4 provides some examples of utilization. Section 5 concludes this presentation.

2. DL ISSUES OF PACS

A number of issues arise in the contexts of developing, maintaining and using PACS and its associated databases as a digital clinical library to support on line search and decision aids. Some are technical in nature, others are managerial. Many of the issues present rich opportunities for research.

Issue 1: Two-Tier Versus Three-Tier Architecture?

The major factors that impact this issue include the size of the medical databases, the number of actual and prospective users, and the types of services that are performed.

Traditional PACS is based on the two-tier client-server architecture. Even the recent development of PACS, so-called second generation PACS, still consolidates related textual information from Radiology Information System (RIS) and Hospital Information System (HIS) into one centralized archive [2]. The main advantages of the two-tier architecture are its simplicity and lower costs of development.

The two-tiered approach, however, may not always be scalable for systems distributed in different departments or hospitals, owing to the complexity in data acquisition and data modeling, the escalating storage cost, and the potential of forming a bottleneck in light of large numbers of query transactions. Moreover, data in such data warehouse cannot be independently updated by users, but rather is refreshed on a periodic basis by data extracted from various established data sources. This incurs a penalty for real-time applications.

The concept of three-tiered architecture has long been introduced in digital library systems to manage information in their heterogeneous and distributed computing environment. Major middleware standards include the Common Object Request Broker Architecture (CORBA) from Object Management Group (OMG) and Microsoft's Distributed Component Object Model (DCOM) [3]. Effort in adapting CORBA for medical community, i.e., CORBA-MED, is also underway. The main advantages of the three-tiered architecture are faster response times, better data consistency, and the ability to custom design data for each type of user community. The question is whether the advantages of a three-tiered architecture justify the additional cost and complexity in software development and maintenance.

Issue 2: Retrieval by Artificial keys or by Image Content?

The original intent of PACS is to support softcopy review, and thus images are retrieved based on artificial key, such as patient name or hospital identifier. The image document management is based on flat files. The advantage is simple design of data modeling. This approach, however, lacks the capability to search and index the large PACS data repository by content, i.e., image features or relevant keywords. It greatly hinders the usefulness of PACS for other clinical operations, such as online references and outcome studies.

Content based image retrieval (CBIR) has been a key activity in digital library research. Certain techniques developed in DL community may be adaptable for PACS [4]. Most of the existing techniques, however, deal with two-dimensional (2D) images and are concerned with searching through generic image features such as color, shape, texture, or a combination of these. For the medical imaging domain, more application-specific algorithms for feature extraction and more expressive data models for multimedia medical data must be developed to take advantage of the rich information content of PACS DL. Further, it appears that the practical approach is to supplement the CBIR with textual keywords which can be entered by manual annotation or extracted from textual reports and image file headers.

Issue 3: Fat PACS Stations versus Thin DL Clients?

Current PACS stations are based on high-end client workstations with multiple high resolution monitors. They are used to retrieve image data directly from the PACS server and are customized to provide quality image viewing and consultation. The application programs of these workstations are rather complex and large in size. Subsequently, the price of a PACS station is high, at the range of $20K and up. The question is whether to redesign these rather expensive stations in order to support new DL utilities for image browsing and decision supports.

In contrast, rather than using dedicated workstations, DL systems of other non-medical imaging domains use the World Wide Web (WWW) as the primary means to disseminate information over the Internet. The Web browsers are originally designed for the client computers to navigate and display hypermedia documents and image bitmaps stored at the server machines on the Internet. Many Web based health systems have been developed based on the WWW paradigm. Recent introduction of Web programming languages, in particular, Java, further increases the computing power and platform independency of Web based systems. Whether the Web based PACS stations can match the functions of high resolution image display stations has yet to be seen. Their advantages are ubiquitous means for image browsing and retrieval, low costs, and simple maintenance.

Issue 4: 2D Display versus Volume Visualization?

The design of PACS is to support various modes of 2D image display that can simulate the conventional review of films using the alternators. The added features of digital image display include the support of cine loop, zoom and pan, and window and leveling.

Meanwhile, there is a trend of 3D visualization of medical images due to recent advances made in 3D graphics hardware and languages. Visualization techniques currently being applied for the analysis of biomedical data include: surface rendered anatomical displays with rotation and shading, volume rendered cut-outs with enhanced emphasis of particular objects, transparent surfaces within surfaces with color shading and rotation, superimposition of multiple image datasets about the same organ, and reprojection techniques using various weightings of pixels of interest, such as maximum-intensity projection (MIP) and weighted-integrated projection [5]. Most of these functions, however, are performed off-line on powerful graphics stations.

The question is whether there is a need to provide on-line volume visualization in PACS. One argument is that the radiologists are trained with the ability to reconstruct the image volume in 3D space mentally from 2D image slices. The complex and time consuming process of volume visualization does not add any new values and may even lower their reading efficiency. Another school of thought is that the need for on-line visualization is critical for the combined interpretation or correlation of 3D anatomic and physiologic or metabolic data and for real time operations of image-guided therapy and surgery procedures. The challenge is due not only to the large size of medical images but also to the complexities of the relationships among the different data.

The implementation of visualization capabilities in PACS would likely be a strategic decision of whether one should expand the services of the system to other disciplines. One operational model is to add a high power visualization server in the middleware of the three-tiered architecture and transmit the visualization results to the client stations via high speed networks. The advantage of this configuration is to reduce the computational burden of client stations.

Issue 5: How Should the Security of Digital Images be Ensured?

Making medical information available to legitimate external parties in a timely fashion while protecting the privacy of patient data is likely to become an important issue in the coming of digital hospitals. The current practice of data security is rather simplistic, mostly involving the user authentication using passwords. With the PACS DL, medical images and associated patient data will become widely used in diagnosis, consultation, and research. Thus, there is a need to make them available outside the medical department or institution where they were initially generated and processed.

Security measures go beyond point-to-point image transmission, i.e., in PACS and teleradiology, these can be achieved through the use of encryption [6]. The past three decades of civilian research have generated many robust encryption algorithms that are freely available in the public domain and are strong enough to warrant government concerns [7]. The question is how to integrate these encryption algorithms properly into the networked medical environment with minimum overhead and intervention to existing operations.

Query screening or filtering is often implemented in digital library systems to limit the types of query allowable for the particular user group. This approach can certainly be extended to PACS DL applications. However, because queries are an inclusive, not exclusive selector of information content, the more difficult issue is how to screen the results of queries. For example, how to ensure that users do not retrieve unexpected or unauthorized patient information through a sequence of carefully designed but related queries to PACS DL. This still is an open area for research. Further, closely related to the issue of query screening is how to protect from people redistributing or reusing image data without permission.

Issue 6: What is the Best Economic Model?

How can content and value-added providers of PACS be assured that they have a reasonable chance to recover their investment if they distribute their information asset over the hospital network or the Web? This is especially important in this climate of managed care and shrinking resources. Should the development and maintenance costs be paid by hospital information departments or shared by participating departments and organizations? Or, should the users be charged by monthly subscription, by session, or by document? To sustain electronic distribution of medical images and records, the system must accommodate a workable economic model and to understand the requirements of digital image distribution.

3. SYSTEM ARCHITECTURE

The UCSF HI-PACS, as with many existing PACSs, is originally designed to serve softcopy readings of radiologists only. With the technologies for storing and sending a large amount of image data readily available, we investigate the adaptation of digital library (DL) methodologies for creating and managing content of PACS multimedia data and disseminating such contents to serve a broad range of clinicians and radiologists.

Figure 1 illustrates the three-tier architecture of PACS DL. The function of each layer is briefly discussed as follows [8]:

Layer 1: Data Sources

They include databases of PACS, associated medical information systems such as RIS and HIS, other legacy clinical systems, and external files from outside hospitals. The types of information include images as well as patient demographics, medical history, still and moving images, diagnostic reports, voice dictation, and other clinical data. Most of these data are archived as flat files, such as PACS images, or in non-relational textual databases, such as hierarchical data model used in most hospital information systems (HIS). These data can be archived and shared using recognized data exchange standards and protocols, such as DICOM (Digital Imaging and Communication in Medicine) for medical images and HL7 (Health Level 7) for clinical text. The availability of raw images and other medical information in digital media permits the post-processing, creation, and presentation of image contents to serve new classes of multimedia applications in medical imaging.

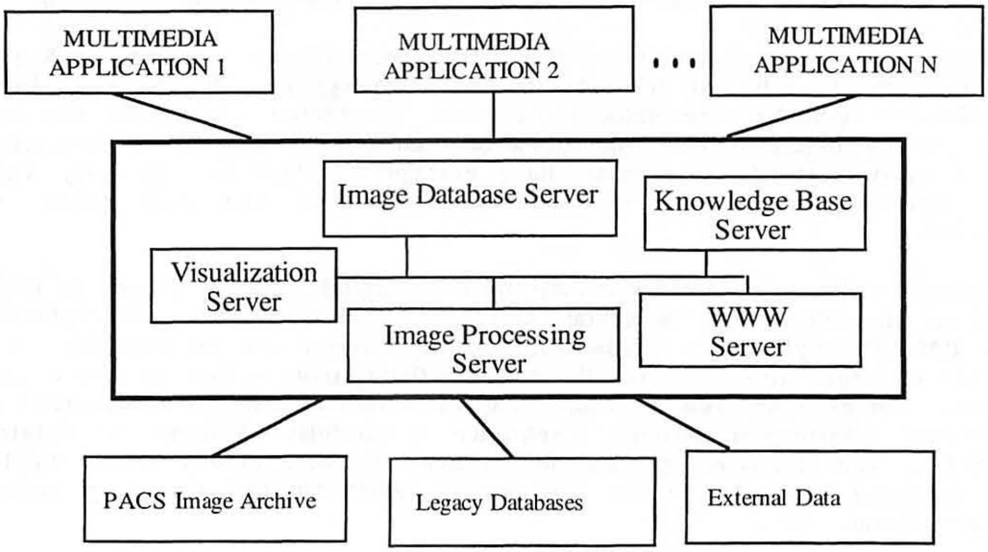

Figure 1. PACS Digital Library Architecture (three-tier).

Layer 2: Middleware Servers

A collection of servers that enable image database management, data visualization, image processing, World Wide Web access, and decision supports. These servers may not necessarily reside in the same physical machine. In our implementation, they are distributed over computers interconnected with 155 Mbps ATM and 10 BaseT networks of UCSF HI-PACS.

The image database server manages a metadata repository of underlying PACS and patient data. It merges the quantitative image features extracted from the image processing server with textual patient data into an anatomical based data model to support content based indexing. The content of a medical image includes three levels of abstraction: (i) features or attributes, such as the texture pattern of an organ, the shape of a breast tumor, and the signal strength of brain metabolites; (ii) structural objects, such as image segments corresponding to anatomical regions; and (iii) semantic information, such as the types of relationships between two objects.

In Figure 2, we illustrate the operational steps that the PACS DL takes to extract image and textual features from the underlying patient data. The feature extraction is based on the *a priori* approach, rather than the dynamic and automatic feature extraction during user query.

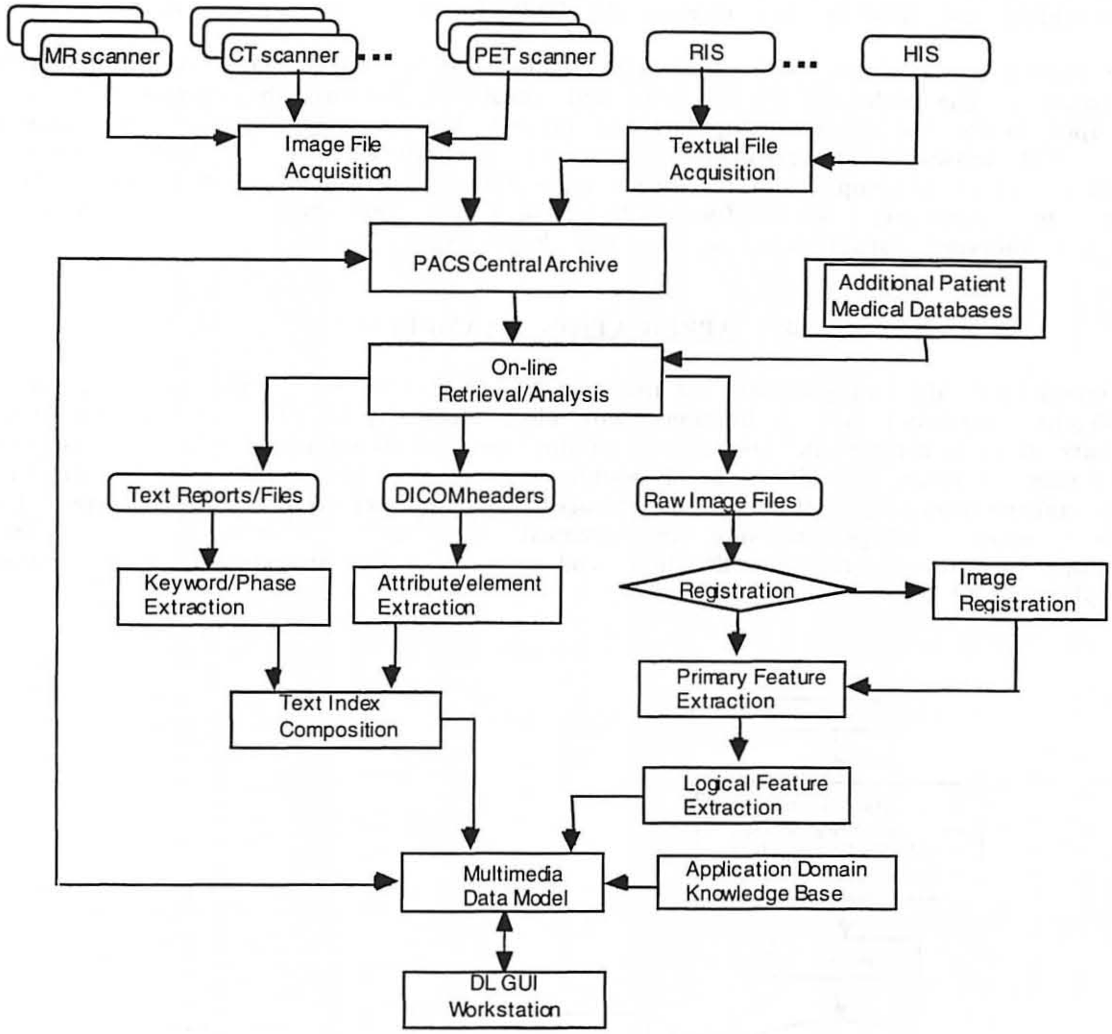

Figure 2. The workflow of extracting image and text features into a data model for subsequent content-based indexing in PACS DL. Rules are used to aid the query and navigation.

The extraction and composition of textual data from the diagnostic reports and the DICOM (Digital Imaging and Communications in Medicine) header fields can be automatic, whereas the segmentation and extraction of medical images often are done interactively. The image features are further divided into primitive and logical. Primitive features are directly obtained from the medical images, such as volume, shape, and texture of certain organs in CT images or metabolic activities of brain tissue in PET scans. Logical features are abstract representations of images at various levels of detail and deeper domain semantics. For example, whether the volume of an anatomic structure is normal or whether certain brain tissue is hypometabolic in reference to an established data. These logical features are synthesized from primitive ones and additional domain knowledge. All extracted features and keywords are entered into object attributes defined in a metadata model to facilitate subsequent information query by content. Note that the original image data are still stored in PACS.

Layer 3: Client Workstations

Each client workstation provides a graphical user interface (GUI) for the local user to request applications of the PACS DL to perform information retrieval, manipulation, analysis, and update. A client workstation may also contain simple image processing capabilities, such as thresholding and filtering, but accesses the IDBS for more sophisticated database services.

Our current client front-end workstations include Motif, Tcl/Tk, Java, Gain Momentum and Web browsers. The underlying object-oriented database contains the objects that allow the client applications to access, manipulate, or present the underlying multimedia data in the server. Web browsers are efficient hypermedia navigation tools for "public domain" file documents. To allow complex, hierarchical representation of database information, however, we have to incorporate new software tools, such as JDBC and CGI-Perl, with extensive multimedia querying capabilities into the web browsers.

4. APPLICATION EXAMPLES

To understand the requirements of incorporating DL capabilities into PACS, we have been steadily implementing applications with clear clinically-driven goals for the past four years to demonstrate the usefulness of this new development of PACS. The multi-tiered system architecture allows rapid prototyping of new applications by leveraging existing information infrastructure of storage and communication infrastructure. In addition to general image browsing and retrieval, we briefly illustrate representative applications in clinical practice, education, and research being investigated at UCSF. For details please refer to [9].

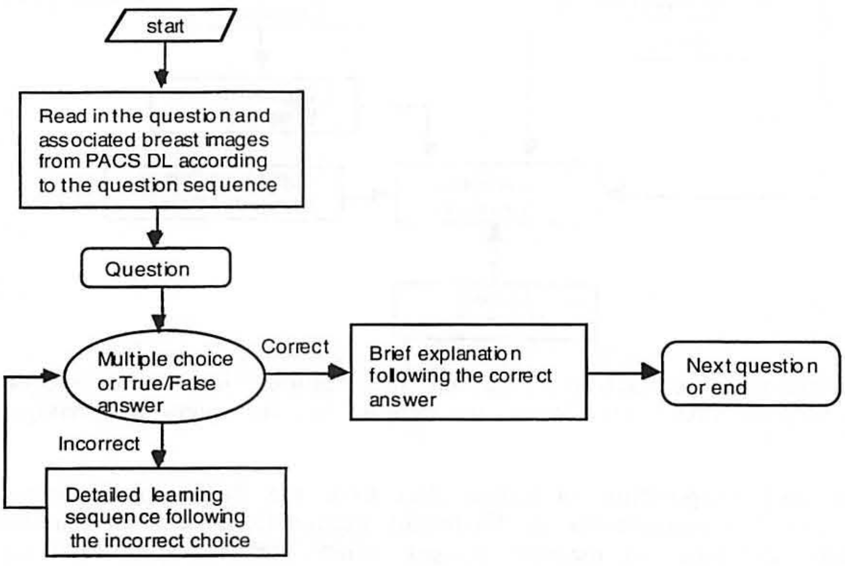

Figure 3. Using PACS DL for Breast Imaging Education.

4.1 Education (Breast Imaging Teaching File)

The objective of this application program is to provide an interactive learning environment for breast imaging teaching file on the World Wide Web [10]. Figure 3 shows the generic algorithm used in the PACS DL to support the digital breast imaging teaching file. The implementation of this algorithm separates program control from medical data.

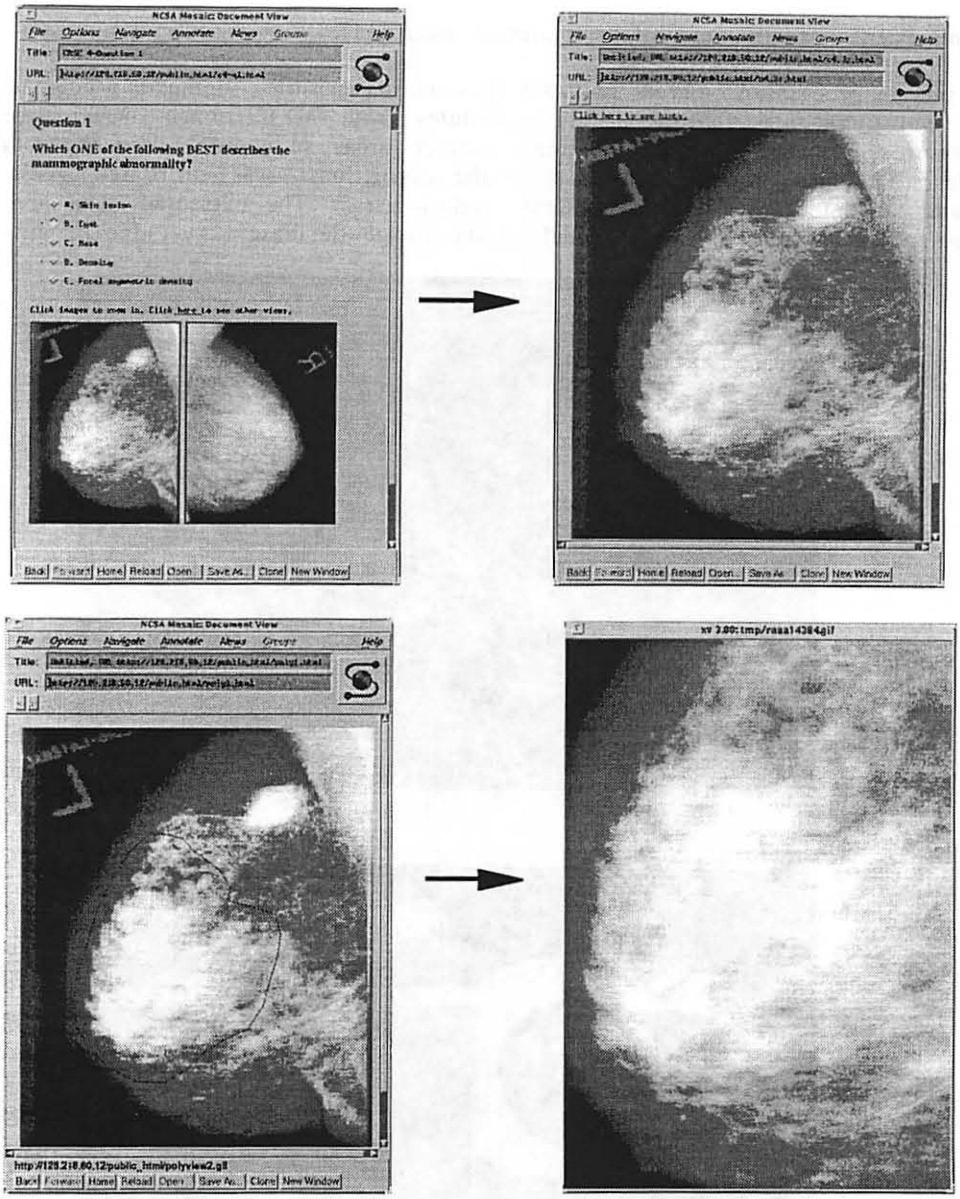

Figure 4. Snapshots of Web-Based Breast Imaging Teaching File.

The computer-aided algorithm is implemented as an application-specific module in the knowledge base server. The visualization server allows the manipulation and visualization of digitized breast images. It has the PolyMap routines that enhance the users ability to "interact" with the software by making predefined regions of interest on the image "clickable." For example, a region of an image that is predefined using the Polymap will become outlined in blue when the user passes over it with the mouse. This region can be linked to a “close-up” image, providing the user with a enhanced view of that specified region. Figure 4 shows certain snapshots of the imaging teaching file.

4.2 Clinical Research (Temporal Lung Nodule Analysis)

The objective of this application is to track and analyze progression of lung nodules over time using spiral CT (Computed Tomography) scans such that the results can be used to determine the effectiveness of a treatment plan [11].

The image processing server of PACS DL contains a suite of image processing tools to segment and quantitate features of lung nodules from 3D CT images semi-automatically. These features include volumes, locations, surface areas of nodules, and the total number of nodules. The quantitation accuracy of the algorithms was calibrated with phantom studies and validated by two independent radiologists. The extracted data are classified and organized in a temporal data model of the image database server for on line analysis.

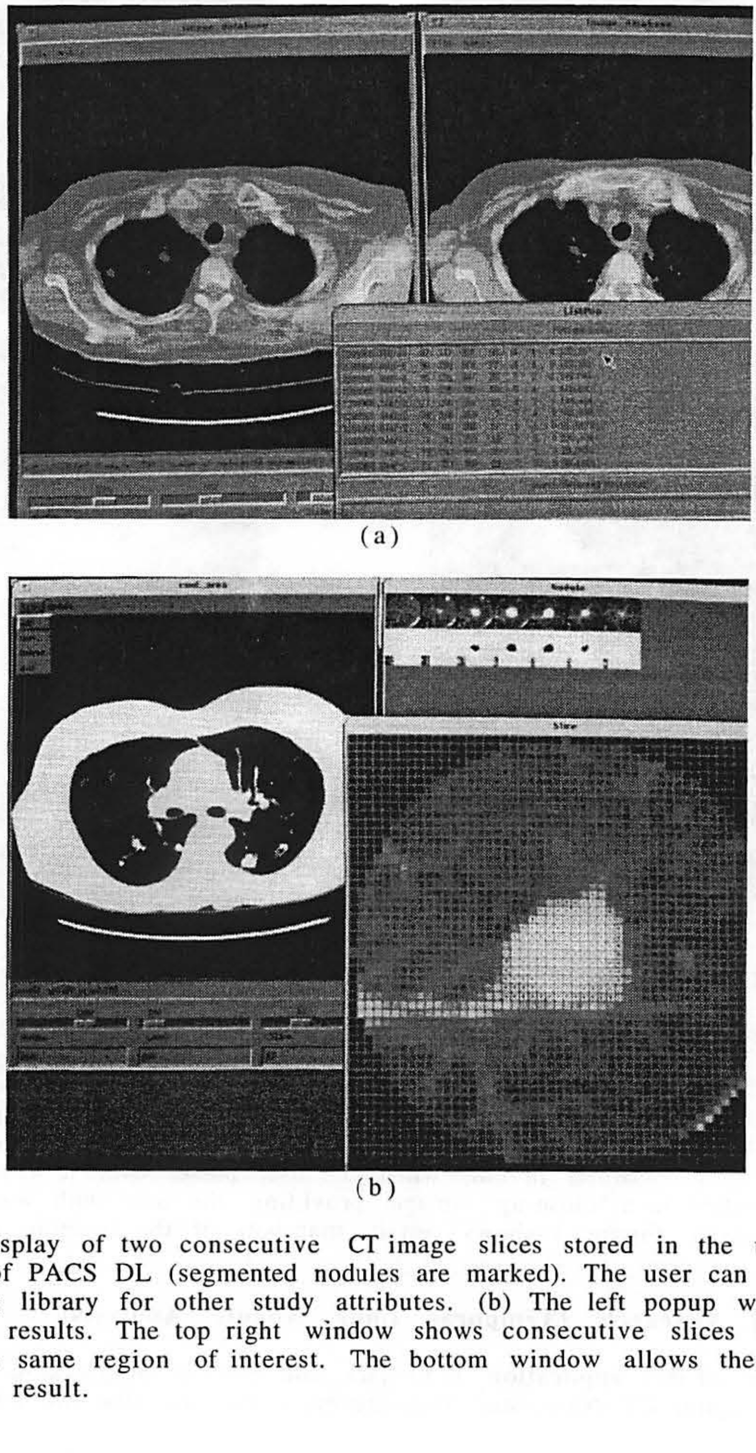

Figure 5. (a) Display of two consecutive CT image slices stored in the temporal chest imaging database of PACS DL (segmented nodules are marked). The user can use the GUI to query the imaging library for other study attributes. (b) The left popup window displays the segmentation results. The top right window shows consecutive slices of the selected nodule within the same region of interest. The bottom window allows the correction of the segmentation result.

In Figure 5, we show certain GUI displays. Figure 5.a illustrates two consecutive CT image slices retrieved (lesions are marked). The lower right window shows the list of nodule parameters extracted from this CT image dataset, e.g., patient ID, study number, nodule coordinates, volume, surface area, and nodule that it associates with in the previous study and following-up study. Figure 5.b shows the GUI developed to allow the user to correct the segmentation result on pixel-by-pixel bases; a pixel can be included or excluded simply by a mouse click.

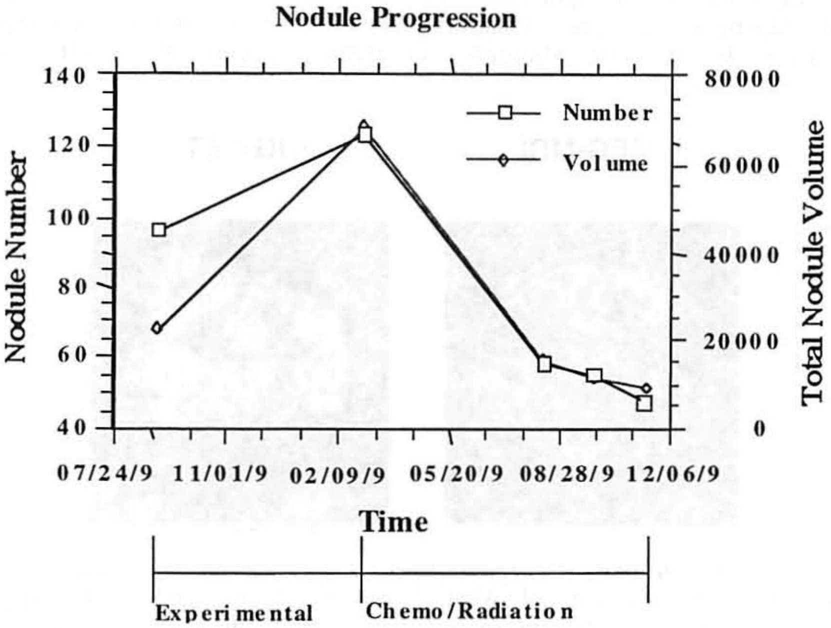

Figure 6. History of the patient nodule number and the total nodule volume. The volume is measured in mm^3 (from [11]).

Figure 6 illustrates a patient case of lung metastases to demonstrate the usefulness of the PACS DL for temporal image data analysis. This female patient is diagnosed with breast cancer that has subsequently spread out to her chest. The horizontal axis marked the periods of the five spiral CT scans she took. Below the horizontal axis, we draw two lines to denote the intervals during which the patient is under different treatment plans. One can see that total nodule number is tripled during the early drug treatment procedures. This triggered a change of treatment protocol to a combination of radiation therapy and chemotherapy, that was proved to be effective. The total volume of the cancer reduced by a factor of 5 from its peak value near March 1995. The system also provides the capability to track the progression of individual nodules over time.

4.3 Clinical Practice (Non-invasive Epilepsy Surgical Planning)

The current gold standard for evaluating surgical candidates of medically refractory epilepsy is intracranial electroencephalography (EEG) recording. An intracranial EEG study requires invasive surgery to place electrodes for recording brain electrical activity during spontaneous seizures. The purpose of this DL application is to provide accurate, noninvasive localization of epileptogenic tissue for surgical resection using multimodal imaging techniques and to resolve discordant or inconclusive imaging evaluations [12].

The image processing server contains a suite of image processing tools for 3D co-registration, image segmentation, and extraction of functional and structural information of brain regions of interest. These features include volumes, glucose uptakes, neurochemical spectra, and dipole locations. Segmentation of fine anatomical structures such as hippocampus, is done interactively. The image database server organizes PACS image indices, annotated pictures, extracted features, clinical text, and outcome data into a metadata model for epilepsy diagnosis. The visualization server provides 3D construction of medical images for better understanding of neuroanatomy and neurophysiologic pathway.

Figure 7 illustrates the registration of MSI (Magnetic Source Imaging), PET (Positron Emission Tomography), and EEG for on line planning an epilepsy case. Figure 8 shows a 3D view of combined MRI (Magnetic Resonance Imaging) and PET for a temporal epilepsy case. Such 3D views are useful for the non-radiologists to appreciate clinical significance of registration findings.

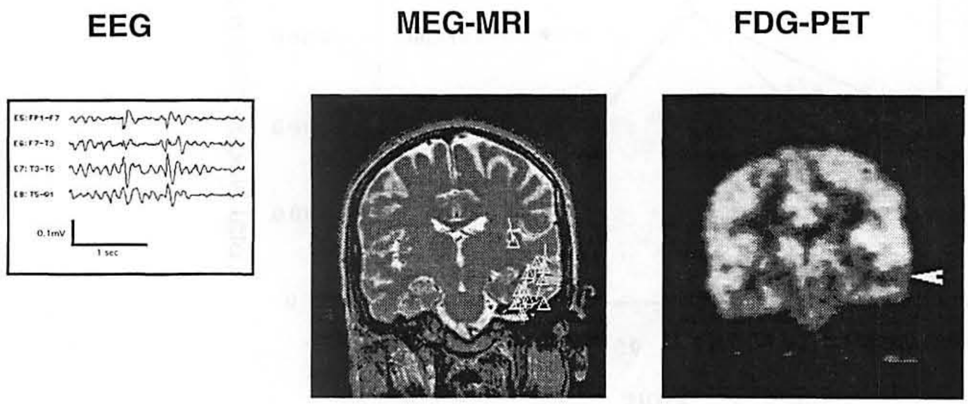

Figure 7. Left: scalp EEG recording of patient's epileptiform spike activity recorded over the left temporal region; middle: T2 weighted coronal MRI slice with dipole sources (triangles), which correspond to EEG spikes, localized adjacent to a focal area of increased T2 in the left middle temporal gyrus; right: coregistered FDG-PET slice reveals focal relative hypometabolism (white arrow) in the same region of the left middle temporal gyrus (Data courtesy, Departments of Radiology and Neurology, UCSF).

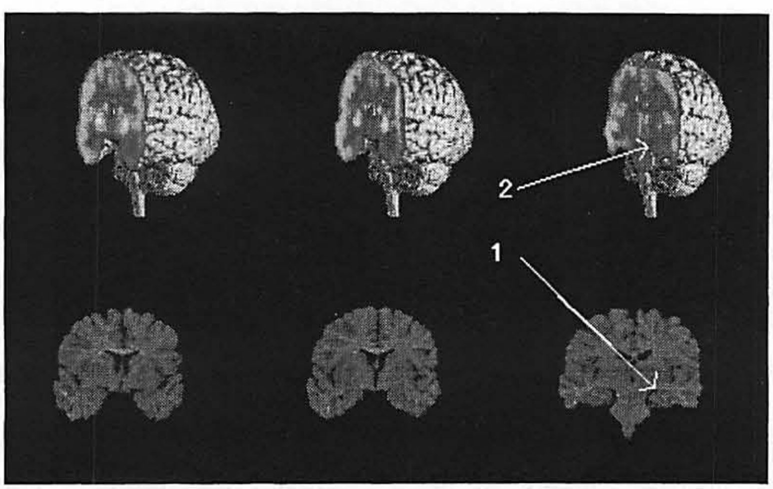

Figure 8. Visualization of a mesial temporal epilepsy case. Top: PET viewed on the cut surface of registered 3D MRI volume. Arrow 2 indicates hypometabolism in the left temporal lobe region. Bottom: The corresponding MRI coronal slice shows subtle structural atrophy of hippocampus within the left mesial temporal lobe (arrow 1).

5. CONCLUSIONS

This article points out a new direction of PACS development. It describes how the DL technologies can be adapted and integrated into PACS to increase the usefulness of the image management system in medicine. In specific, we present the multi-tiered DL-PACS architecture, discuss certain operational models, and describe new capabilities of such systems. Incorporating the emerging DL technologies into PACS will have the potential to lead to new services and markets of PACS. In this presentation, we identified some of the requirements for such systems and provided solutions to these requirements based on our prototyping experience on the UCSF HI-PACS.

REFERENCES

[1] G Wiederhold. Digital libraries, value, and productivity. *Communication of ACM*, 38(4), 1995, pp. 85-96.

[2] M Osteaux (ed.) *A second generation PACS concept*. Berlin: Springer-Verlag, 1992.

[3] R Otte, P Patrick, and M Roy. *Understanding CORBA*, Prentice Hall, 1996.

[4] STC Wong, Kent Soo Hoo, and HK Huang. Empower PACS with content-based queries and 3D image visualization. Proc. SPIE, vol. 2711, 1996, pp. 569-579.

[5] JK Udupa and GT Herman. *3D imaging in medicine*. CRC Press, 1991.

[6] STC Wong. A cryptologic based trust center for medical images. *J. AMIA*, vol. 3, no. 6, 1996, pp. 410-421.

[7] B Schneier. *Applied cryptography: Protocols, algorithms, and source code in C*. New York: John Wiley & Sons, 1993.

[8] STC Wong and HK Huang. Design methods and architectural issues of integrated medical image database systems. *Comp. Med. Imaging & Graphics*, vol. 20, no. 4, 1996, pp. 285-299.

[9] STC Wong and HK Huang. Networked multimedia in medical imaging, *IEEE Multimedia* 1997 Special Issue on Multimedia in Medicine, to appear.

[10] STC Wong, PS Whaley, A Cheong, K Soo Hoo, J Wang, and HK Huang. Interactive query and visualization of medical image data on the World Wide Web. *SPIE* vol. 2707, 1996, pp. 390-401.

[11] X Zhu, KN Lee, DL Levin, STC Wong, HK Huang, K Soo Hoo, G Gamsu, and WR Webb. Temporal image database design for outcome analysis of lung nodules. *Comp. Med. Imaging & Graphics*, vol. 20, no. 4, pp. 347-356, 1996.

[12] STC Wong, RC Knowlton, RA Hawkins, and KD Laxer. Multimodal image fusion for noninvasive epilepsy surgery planning. *IEEE Comp. Graphics & Appl.* vol 16, no. 1, 1996, pp. 30-38.

Adaptation of DICOM to an operational PACS

Albert W.K. Wong, H.K. Huang, Ronald L. Arenson

albert_wong@radmac1.ucsf.edu
Laboratory for Radiological Informatics
Department of Radiology
University of California, San Francisco (UCSF)
San Francisco, CA 94143-0628

ABSTRACT

Image communication between PACS applications and radiologic imaging equipment has always been difficult due to the proprietary communication protocols and data formats used by the individual manufacturers. With the introduction of DICOM, image communication among PACS components and radiologic imaging devices becomes feasible. We have integrated our PACS into a DICOM-compliant system that facilitates the communication of radiologic images between individual PACS components and radiologic imaging equipment.

The image communication software implemented in our PACS was based on the Mallinckrodt's central test node (CTN) software with several enhanced features. These features included dual network interface support, adjustable TCP buffer size, prioritizing job control, and computer host verification. The enhanced DICOM-based communication software has demonstrated a reliable yet efficient transfer for images in a PACS environment. This paper describes our implementation strategy of adapting DICOM to the UCSF PACS and the utilization of DICOM in the PACS operation.

KEY WORDS: Digital imaging and communications in medicine (DICOM), data encoding, transmission control protocol/Internet protocol (TCP/IP), PACS infrastructure, asynchronous transfer mode (ATM), DICOM Query/Retrieve Service Class.

1. INTRODUCTION

One major effort in the early development of the UCSF PACS[1] in 1993 was to interface the existing radiologic imaging equipment to acquire radiologic images into the PACS. These imaging equipment, which generated images that did not comply to DICOM[2] or ACR/NEMA[3] standard, required the development of sophisticated image acquisition software based on the proprietary communication protocols and data structures that were used by the individual manufacturers. Our goals in integrating these imaging equipment into the PACS included: (1) providing reliable communication for images between the imaging equipment and the PACS components such as the acquisition computers, the archive server, and the display stations; (2) archiving the multi-vendor, multi-modal radiologic images to long-term storage devices in a unified data format that would comply to DICOM standard once DICOM becomes available.

In February 1994, we successfully connected four magnetic resonance (MR) imagers, three computed tomographic (CT) scanners, two computed radiography (CR) systems, and one laser film digitizer to our PACS. Images acquired from these radiologic imaging equipment were archived to an optical disk library for future retrieval and routed to the designated display stations for clinical review.

2. METHOD

2.1 Implementation Strategy

We applied a three-phase implementation strategy in adapting DICOM to the UCSF PACS. These three phases of implementation, which ensured a smooth transition of integrating the PACS into a future DICOM-compliant system, were as follow:

Phase One: Adapt the ACR/NEMA standard[4]

Phase Two: Migrate from ACR/NEMA to DICOM

Phase Three: Integrate DICOM into PACS

2.2 Three Phases of Implementation

Phase One: Adaptation of ACR/NEMA Standard (1993 - 1994)

The major effort in Phase One was to develop interface software to acquire digital images from a wide variety of existing radiologic imaging equipment in the radiology department. These images, after acquired, were converted to ACR/NEMA 2.0 format for archiving and distribution. The following paragraphs provide the details of the implementation.

Image Acquisition and Data Encoding: An image acquisition process running on a PACS computer communicated with the radiologic imaging device using the manufacturer's proprietary communication protocol. Pixel data and relevant information were then extracted from the acquired images and converted to ACR/NEMA format via a reformatting process. This process performed the following tasks:

- Extracting header information and pixel data from an acquired image based on the manufacturer's proprietary image file structure
- Converting extracted header and pixel data to ACR/NEMA format
- Preserving manufacturer's raw header in the ACR/NEMA header as a shadow group
- Packaging slice images from one CT or MRI scan into a single file for archiving

Image Storage: All images were archived to the optical disk library in ACR/NEMA format on a per-scan-per-file (CT and MR images) or per-exposure-per-file (CR and Digitized images) basis[5].

Image Communication: Tansmission of images between individual PACS components such as the acquisition computers, the archive server, and the display stations were handled by UCSF's proprietary TCP/IP-based client/server communication software[6, 7].

Phase Two: Migration from ACR/NEMA to DICOM (1995 - 1996)

In Phase Two, we developed a DICOM converter to translate ACR/NEMA images to the DICOM 3.0 format. In addition, the Mallinckrodt CTN software was modified and used for transfer of DICOM images to any DICOM-compliant systems. The following describes the Phase Two implementation.

Image Acquisition and Data Encoding: All images acquired from the radiologic imaging equipment were converted to ACR/NEMA file format (No change from Phase One).

Image Storage: All images were archived in ACR/NEMA file format (No change from Phase One).

Image Communication: Transfer of images between individual PACS components in Phase Two was handled by two types of client/server communication software, the UCSF proprietary communication software and the Mallinckrodt CTN-based communication software.

The UCSF proprietary communication software was used for the transfer of packaged ACR/NEMA images between individual PACS computers (no change from Phase One). On the other hand, the DICOM converter, capable of translating ACR/NEMA images to DICOM format, incorporated the Mallinckrodt CTN-based communication software to distribute the packaged ACR/NEMA images as individual DICOM images to the DICOM-compliant systems.

Phase Three: Integration of DICOM (Current Implementation)

In Phase Three, we are focusing on a full integration of DICOM into our operational PACS. Our basic goals include:

- Acceptance of both DICOM and non-DICOM images from the radiologic imaging equipment
- Archiving images in DICOM file format
- Supporting DICOM standard Query/Retrieve services such as C-FIND, C-MOVE, and C-GET in the retrieval of images

We have modified Mallinckrodt's CTN software by adding several enhanced features to facilitate the communication of radiologic images between individual PACS components and radiologic imaging equipment (see Section 2.3). Currently, we are implementing DICOM's Query/Retrieve Service Class in the archive system to support online retrieval of images system-wide. The data encoding software for both DICOM and non-DICOM images have been developed and are illustrated in Figure 1 and Figure 2, respectively.

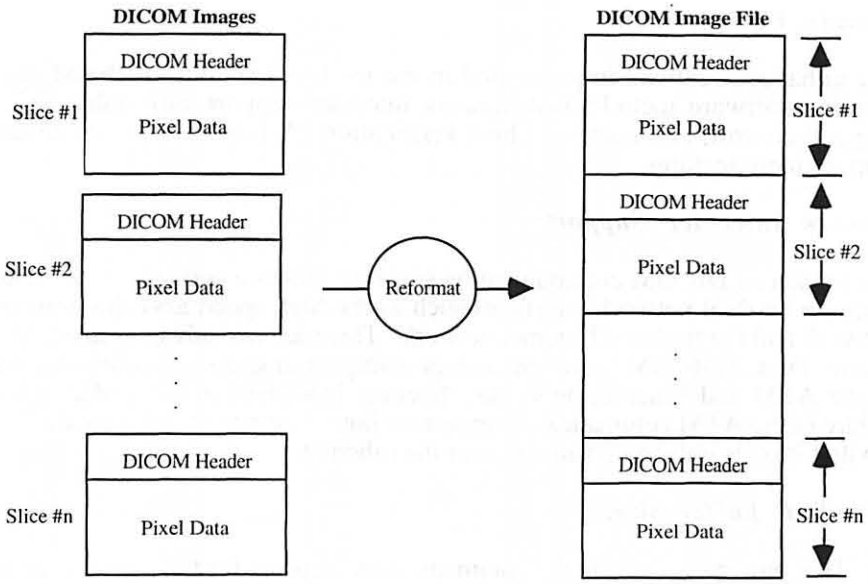

Figure 1. Data encoding of DICOM images. A PACS acquisition computer communicates with the DICOM-compliant imaging device and acquires the digital images using standard DICOM communication protocol. The acquired slice images from one CT or MRI scan are packaged into a single file for archiving. After archiving, these slice images, when retrieved, are unpacked from the multi-slice image file and transmitted individually to the requesting station.

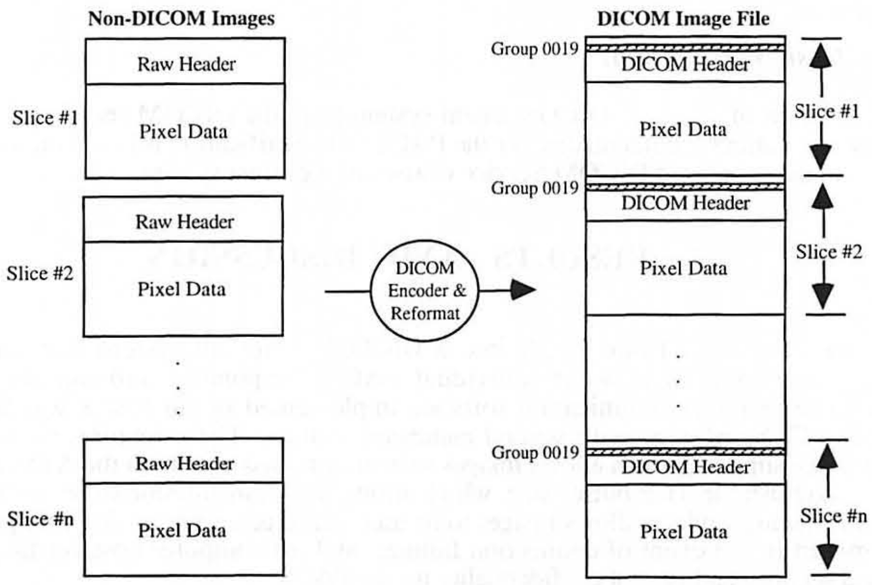

Figure 2. Data encoding of Non-DICOM images. A PACS acquisition computer communicates with the imaging device and acquires the digital images using the manufacturer's proprietary communication protocol. The acquired images are converted to DICOM via the DICOM encoder. The manufacturer's raw headers are preserved in the corresponding DICOM headers as shadow group 0019. Slice images from one CT or MRI scan are packaged into a single file for archiving.

2.3 Software Enhancement

The enhanced features implemented in the modified version of the Mallinckrodt CTN communication software include dual network interface support, adjustable TCP buffer size, prioritizing job control, and computer host verification. What follows is a description of the functionality of these features.

Dual Network Interface Support:

The enhanced DICOM communication software allows a server or a client host system to be configured with dual network interfaces such as the high-speed asynchronous transfer mode (ATM) network and the tradition Ethernet network. There are two advantages of the dual network configuration. First, a DICOM server can accept multiple transmissions of images simultaneously over both the ATM and Ethernet networks. Second, Ethernet can be used as a backup for the ATM. Failure of the ATM automatically triggers the host system to reconfigure the communication network so that images will be transmitted over the Ethernet.

Adjustable TCP buffer size:

The TCP buffer size used in the communication software for transmission of images can be adjusted to achieve better network throughputs. This is important because the optimal buffer sizes for ATM and Ethernet are different.

Prioritizing Job Control:

The job control mechanism implemented in the communication software allows images to be transmitted according to different priority levels or re-transmitted in the event of connection failure.

Computer Host Verification:

Verification of a remote DICOM client system from the DICOM server system provides data security and patient confidentiality for the PACS. The verification is based on the IP address, host name, and the supported DICOM Service Classes of the client system.

3. RESULTS AND DISCUSSION

We have integrated our PACS into a DICOM-compliant system that facilitates the communication of images between individual PACS components and radiologic imaging equipment. The image communication software implemented in our PACS was based on the Mallinckrodt's CTN software with several enhanced features. These features include: (a) dual network interface support, which allows images to be transmitted over both the ATM and Ethernet networks; (b) adjustable TCP buffer size, which allows data transmission to be optimized; (c) a job control mechanism, which allows images to be transmitted according to different priority levels or re-transmitted in the event of connection failure; and (d) computer host verification, which provides data security and patient confidentiality for the PACS.

The enhanced DICOM-based communication software has demonstrated a reliable yet efficient transfer for images in a PACS environment. Our PACS infrastructure currently provides DICOM connectivity for multi-vendor equipment. The system accepts both DICOM and Non-

DICOM images from the radiologic imaging equipment, and distributes images in either ACR/NEMA or DICOM format.

Utilization of DICOM communication protocol and data format in PACS requires overhead which tends to slow down the processing and transmission of the radiologic images. On the other hand, DICOM provides interoperability between individual PACS components and radiologic imaging equipment, but does not guarantee reliable transmission of images on the network. Therefore, much effort in software integration is necessary in order to increases operation efficiency and data integrity of a PACS that will comply to DICOM standard.

4. REFERENCES

1. H.K. Huang, R.L. Arenson, S.L. Lou, A.W.K. Wong, K.P. Andriole, et al, "Second generation picture archiving and communication systems", SPIE Med. Imaging Proceedings, Vol 2165:527-535, 1994.

2. NEMA Standards Publication PS3.3, "Digital imaging and communications in medicine (DICOM)", National Electrical Manufacturers Association, 1993.

3. ACR/NEMA Standards Publication No. 300, "Digital imaging and communications", National Electrical Manufacturers Association, 1989.

4. J.K. Lee, L. Yin, H.K. Huang, A.W.K. Wong, "Adaptation of industry standards to PACS", SPIE Med. Imaging Proceedings, Vol 2165:397-402, 1994.

5. A.W.K. Wong, H.K. Huang, R.L. Arenson, J.K. Lee, "Digital archive system for radiologic images", RadioGraphics, Vol 14:1119-1126, 1994.

6. H.K. Huang, R.L. Arenson, W.P. Dillon, S.L. Lou, T. Bazzill, A.W.K. Wong, "Asynchronous transfer mode technology for radiologic image communication", Am. J. Roentgenology, Vol 164:1533-1536, 1995.

7. A.W.K. Wong, H.K. Huang, T.M. Bazzill, J.K. Lee, I. Bobkov, M.J. Moskowitz, "Performance characteristics of a digital imaging network with asynchronous transfer mode technology", Radiology, Vol 197(P):259, 1995.

The Utilization of a Multimedia PACS Workstation for Surgical Planning of Epilepsy

Kent Soo Hoo, Jr.[a], Stephen T.C. Wong[b,a,c,d], Randall A. Hawkins[c,a], Robert Knowlton[e], Kenneth D. Laxer[d], Howard Rowley[c]

[a] Joint Program in Bioengineering, UCSF/UCB, CA 94143
[b] Philips Research Palo Alto, CA 94304
[c] Department of Radiology, UCSF
[d] Department of Neurology, UCSF
[e] Swedish Medical Center, Seattle, WA 98114

ABSTRACT

Surgical treatment of temporal lobe epilepsy (TLE) requires the localization of the epileptogenic zone for surgical resection. Currently, clinicians utilize electroencephalography (EEG), various neuroimaging modalities, and psychological tests together to determine the location of this zone. We investigate how a multimedia neuroimaging workstation built on top of the UCSF Picture Archiving and Communication System (PACS) can be used to aid surgical planning of epilepsy and related brain diseases. This usage demonstrates the ability of the workstation to retrieve image and textual data from PACS and other image sources, register multimodality images, visualize and render 3D data sets, analyze images, generate new image and text data from the analysis, and organize all data in a relational database management system.

Keywords: PACS, workstation, multimedia, epilepsy, surgical planning

1. INTRODUCTION

Epilepsy is a condition characterized by recurrent seizures. Approximately 0.5 - 1% of the United States population suffers from epilepsy, and 20% of these people do not have their seizures controlled by anti-epileptic drugs. Of this 20%, one-half are candidates for surgical treatment because the candidates must have partial (focal) seizures. In surgical treatment the epileptogenic zone (focus) is localized and resected. Invasive intracranial interictal and ictal video EEG monitoring is considered the gold standard for localizing the epileptogenic zone and involves the implantation of depth electrodes and/or placement of subdural grids to monitor the brain for epileptiform activity. This procedure is both costly in terms of money ($30,000 - $50,000/exam) and patient morbidity, so noninvasive methods of localization are being pursued in hopes of expediting the surgical treatment of larger populations of epilepsy patients [Laxer 93].

Two thirds of all surgeries undertaken for intractable seizures are temporal lobectomies [Engel 87]. In fact, the structures of the mesial temporal lobe of the brain are of particular interest because depth electrode recordings from patients with intractable temporal lobe epilepsy have revealed that seizure onset is usually in the mesial temporal lobe [Wieser 91]. Mesial temporal sclerosis (hippocampal sclerosis) is the most common underlying pathology in temporal lobe epilepsy and primarily involves the amygdala and hippocampus. This pathology exhibits certain anatomic and pathophysiologic traits which are detectable by various noninvasive neuroimaging modalities.

At the UCSF Northern California Comprehensive Epilepsy Center, the anatomy and pathophysiology of the amygdala and hippocampus is assessed in TLE patients using the following neuroimaging modalities: magnetic resonance imaging (MRI), ^{18}fluorodeoxyglucose positron emission tomography (FDG-PET), magnetoencephalography (MEG), and magnetic resonance spectroscopic imaging (MRSI). MRI provides unsurpassed anatomic detail of brain structure and is the principal imaging technique for evaluating patients with partial epilepsy. MRI reveals gross structural abnormalities such as hippocampal atrophy in patients with partial seizure disorders. However, a substantial fraction of TLE patients have non-concordant MRIs with less optimum surgical outcome. Also, some patients suffering from partial seizures sometimes exhibit normal anatomical images.

Further author information -
K.S.H. (correspondence): Email: hoo@lri.ucsf.edu; WWW: http://lri.ucsf.edu/~hoo; Telephone: 415-502-4288; Fax: 415-502-3217
S.T.C.W.: Email: swong@lri.ucsf.edu; WWW: http://lri.ucsf.edu/~swong

FDG-PET scanning is employed to measure the localized cerebral glucose metabolism in the temporal lobe. The incidence of temporal lobe hypometabolism (focal reduced glucose uptake) varies from 60% to 90% of TLE patients [Laxer 93]. MRSI exploits the principal that every chemically distinct nucleus in a compound resonates at a slightly different frequency. MRSI measures the concentration of metabolites in brain tissue, and the epileptogenic zone has decreased levels of N-acetyl-aspartate (NAA), phosphocreatine, and adenosine triphosphate and increased levels of inorganic phosphate, lactate, and hydrogen. MEG uses three-dimensional dipole localization methods to analyze weak magentic signals generated by neuronal electrical activity. MEG can noninvasively pinpoint the source and time sequence of electrical activities in the brain.

Currently, the fusion of all the above image information to localize the epileptic focus is placed squarely on the shoulders of the clinicians. Each imaging study must be reconstructed mentally by the clinician to correlate the pathologic findings of each respective image set. This task is complicated by the fact that the output of each imaging modality differs with respect to resolution, acquisition plane, and parameter measured. The purpose of this paper is to demonstrate the utilization of a multimedia PACS workstation that provides enhanced software utilities to enable the combination and correlation of this diverse information offered in the four neuroimaging modalities in the surgical planning of TLE patients.

The organization of this paper is as follows. Section 2 briefly describes the epilepsy surgical planning procedures followed at the UCSF Northern California Epilepsy Center. Section 3 presents the workstation system architecture, and section 4 describes a typical workup scenario of evaluating the neuroimages with the workstation. Lastly, sections 5 and 6 present our preliminary results and conclusions.

2. EPILEPSY SURGICAL PLANNING

In the past three years, we have been designing and developing a multimedia client workstation on top of UCSF PACS for neurosurgical planning [Wong 95]. This work reports the utilization results of the multimedia PACS workstation in supporting the analysis of neuroimages as part of the general surgical planning in epilepsy at UCSF. The patients involved in this study come from the population of epilepsy patients followed at the Northern California Comprehensive Epilepsy Center. The image and text data of 40 patients have been analyzed by neurologists, nuclear medicine clinicians, and neuroradiologists using the multimedia workstation.

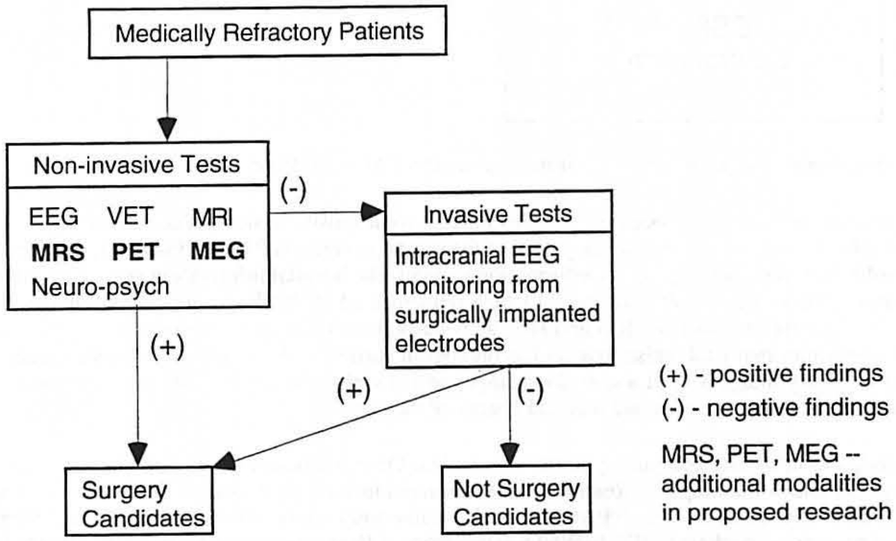

Figure 1 outlines the general diagnostic workup for presurgical epilepsy diagnosis. Patients entering this protocol are medically refractory; their seizures are not controlled by anti-epileptic drugs, or the side-effects from such drugs are intolerable. The successful finding of concordance among the non-invasive imaging modalities precludes the necessity to perform invasive intracranial EEG monitoring from surgically implanted electrodes. The tools provided by the multimedia workstation increase the likelihood of obtaining positive findings from the non-invasive tests.

3. WORKSTATION ARCHITECTURE

Our strategy of multimedia workstation development is to use, modify, and integrate off-the-shelf computing hardware and software to enable rapid prototyping and to better focus on user interface design. The capabilities of this workstation include on-line access to the image and textual data from PACS and other image sources by patient name or hospital identification (ID), automatic image registration, 2D and 3D visualization, image processing, and persistent storage of extracted data. The workstation must be easy to use because this design feature ultimately determines its usefulness and acceptance to the clinicians and therefore its ability to aid in supporting the localization of the epileptogenic zone.

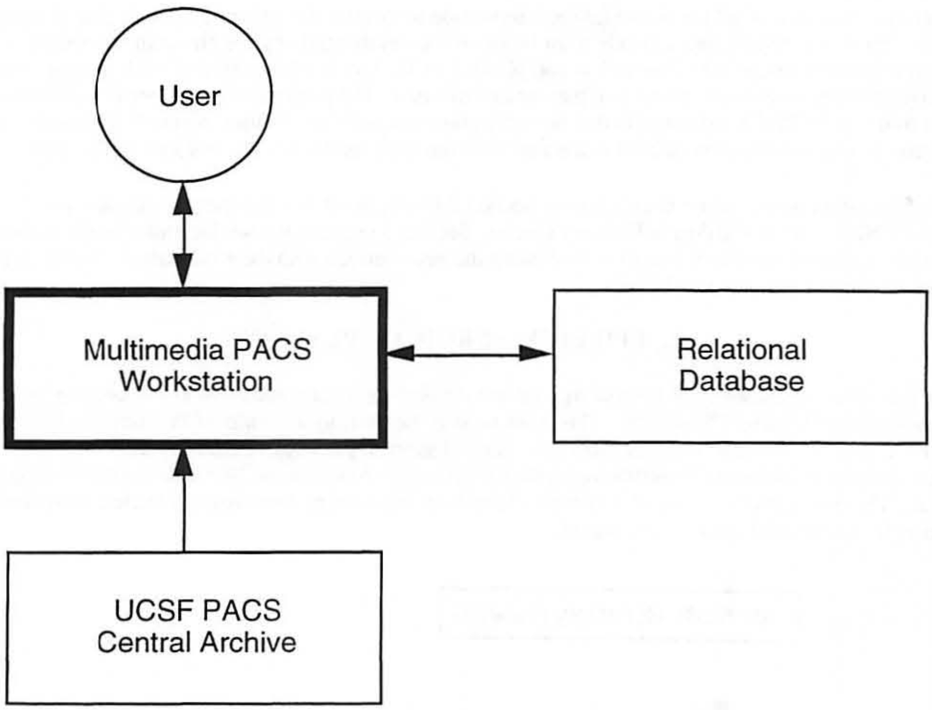

Figure 2. The distributed system architecture of the multimedia PACS workstation.

First generation PACS have been the prevalent means for acquisition, storage, communication, and display of digital medical images [Huang 96]. The recent development of the second generation PACS [Huang 93, Osteaux 92] has included the integration of PACS with heterogeneous information systems like hospital information system (HIS) and radiological information system (RIS). The hospital-integrated PACS implemented at UCSF acquires digital images from various remote scanners, as well as patient records from RIS and HIS, and consolidates them into a central data store. Accessing this large data repository overcomes many administrative and technological barriers in collecting the necessary multimodal patient data files for this work. Every image dataset acquired is complemented with the textual reports that describe the qualitative diagnostic findings about the image set and medical history of the patient.

The workstation's basic computing platform is an SGI Onyx Workstation (Silicon Graphics, Inc., Mountain View, CA) running Irix 5.3 and containing two Reality Engines for rapid image visualization. The workstation's software routines access the centralized archive of the UCSF PACS by patient name and hospital ID and contain three dimensional (3D) image visualization and processing packages: 3DVIEWNIX (University of Pennsylvania) and Volumetric Image Display and Analysis (University of Iowa), a set of automated image registration (AIR) programs based on Wood's algorithms [Woods 93], and region of interest (ROI) analysis tools from Lawrence Berkeley National Laboratory. All of the above disparate software components are integrated into an easy-to-use multimedia workstation user interface based on the object-oriented Gain Momentum Multimedia User Interface (Sybase, Inc., Emeryville, CA). This graphical user interface (GUI) utilizes graphical widgets to present information, launch 3DVIEWINIX and VIDA, make calls to registration algorithms, and manage data contained in the relational database managed by a SQL server (Sybase, Inc.) on a 4-processor SUN SPARC 690MP running Solaris Operating System.

4. WORKUP SCENARIO

When a clinician sits down at the workstation to initiate an analysis session, the first step is to retrieve image and textual data from PACS and other data sources. Figure 3 shows a screenshot taken during the retrieval of image and textual information from the PACS to the workstation. In the upper left, the patient name is entered and sent to the PACS (the patient name has been changed to maintain privacy). The PACS returns descriptions of the imaging studies corresponding to the specified patient name, and these items are displayed as rows in the upper scroll widget. Clicking on a row triggers the retrieval of the diagnostic report from the PACS, and clicking on the "Retrieve Image" button triggers the retrieval of the selected image dataset and storage on the local workstation hard drive in a user-specified UNIX file. The PET, MEG, and MRS image datasets are retrieved via file transfer protocol from the respective scanners. After retrieval the images can be visualized by launching either 3DVIEWNIX or VIDA from the GUI.

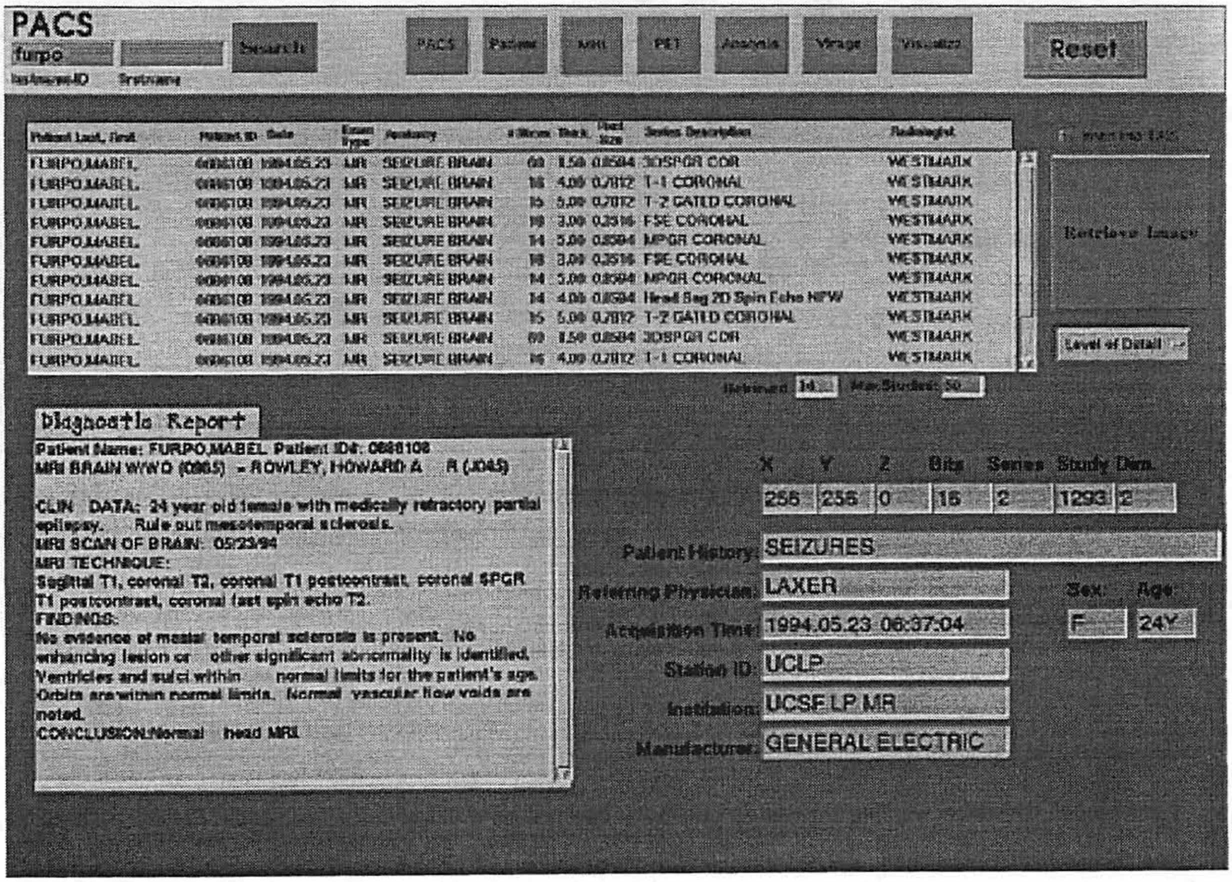

Figure 3. A screenshot taken from the multimedia PACS workstation showing the textual information retrieval from the PACS central node.

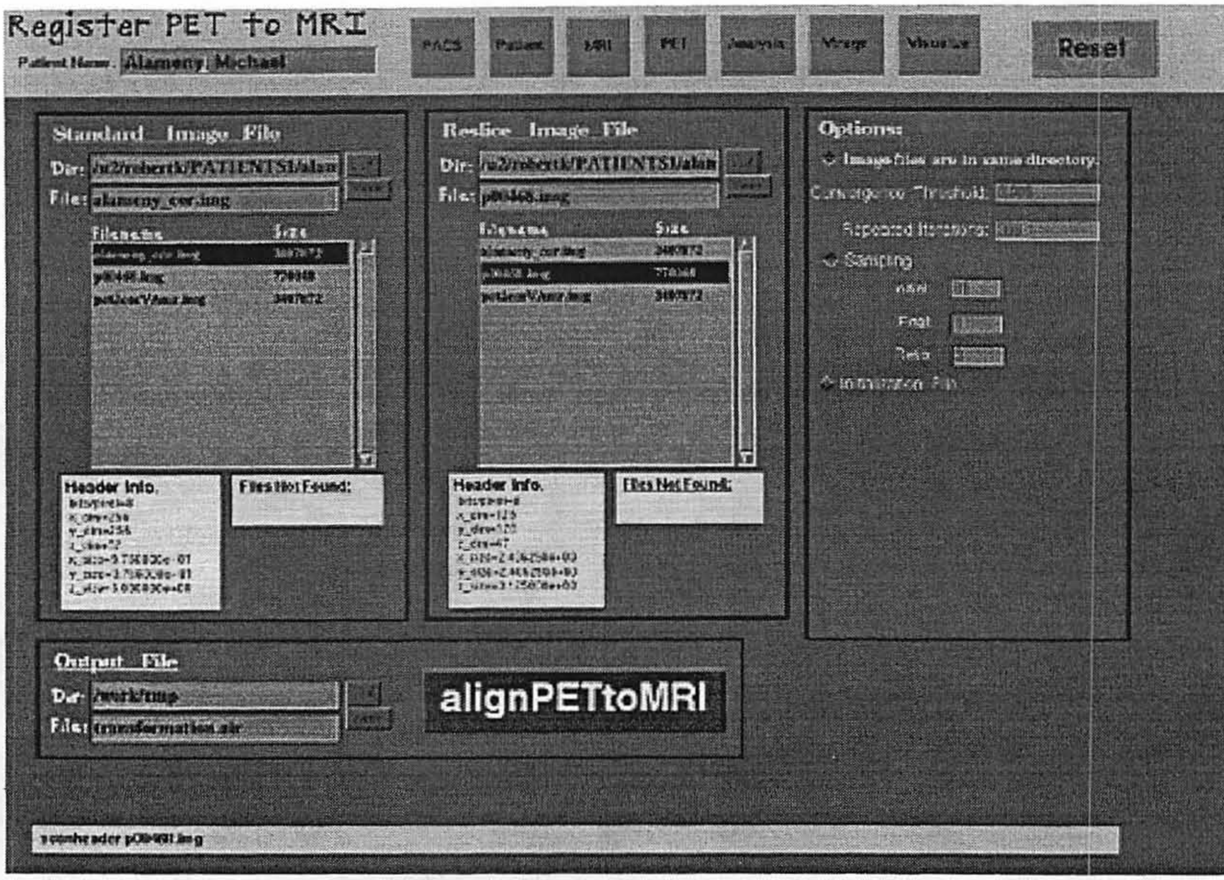

Figure 4. A screenshot taken from the multimedia PACS workstation showing the registration of PET to MRI.

With the imaging studies now reside on the workstation, biomedical information is quantitated, extracted, and combined in various ways to aid in the localization process. First, the nonbrain structures, e.g. scalp and skull, are interactively segmented from the MRI dataset, and then, a transformation matrix is generated using the AIR package to co-register the PET with the newly processed MRI dataset. Several registration parameters such as sampling, iterations, thresholds, and initialization files can all be set via the GUI.

Exploiting MRI's excellent anatomic detail, the hippocampus and amygdala are interactively segmented using the ROI utilities of VIDA (see Figure 5). The resulting segmentation parameters are combined with the transformation matrix and PET sinogram files to yield glucose counts for these mesial temporal structures. Such quantitative data, volumes and glucose counts, cannot be obtained by conventional workups and are important in determining the suitability of patients for surgical treatment. MRSI registration is done prospectively before each data acquisition. A coordinate transformation from the MEG space to the MRI space allows the projection of all or parts of the reconstructed dipole pathway into a multislice or three dimensional MR image of the patient. With the temporal lobe structures of the amygdala and hippocampus now segmented and analyzed for volume, metabolic rate, electrical activity, and metabolite concentration, the epileptogenic zone can be lateralized and localized if there is sufficient concordance of pathological findings.

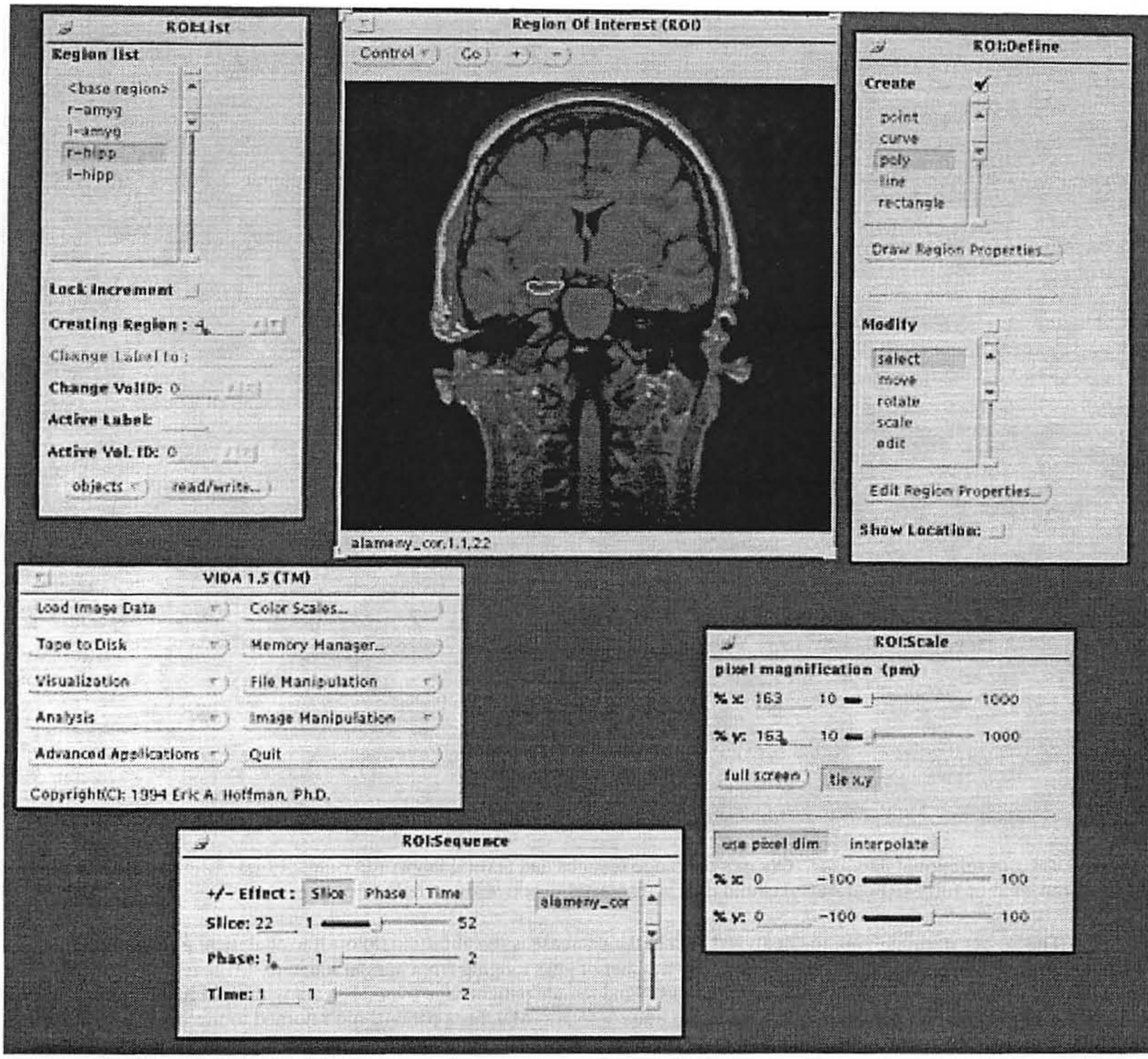

Figure 5. A screenshot taken from the multimedia PACS workstation showing the interactive segmentation of temporal lobe structures from MR images.

After the workup, the clinician saves all the analyzed results into the relational database for future reference. This includes not only the final numerical values of volume, glucose counts, electrical spike magnitude and location, and metabolite concentration, but also the scalp-less MRI, segmentation parameters, and transformation matrix that were generated at the workstation. This data can then be accessed again at a future date for reference purposes, allowing the assessment of the accuracy of segmentation and findings and comparison to new cases. The database can manage and store the analysis work of multiple clinicians on multiple patients. Figure 6 shows a GUI to the relational database.

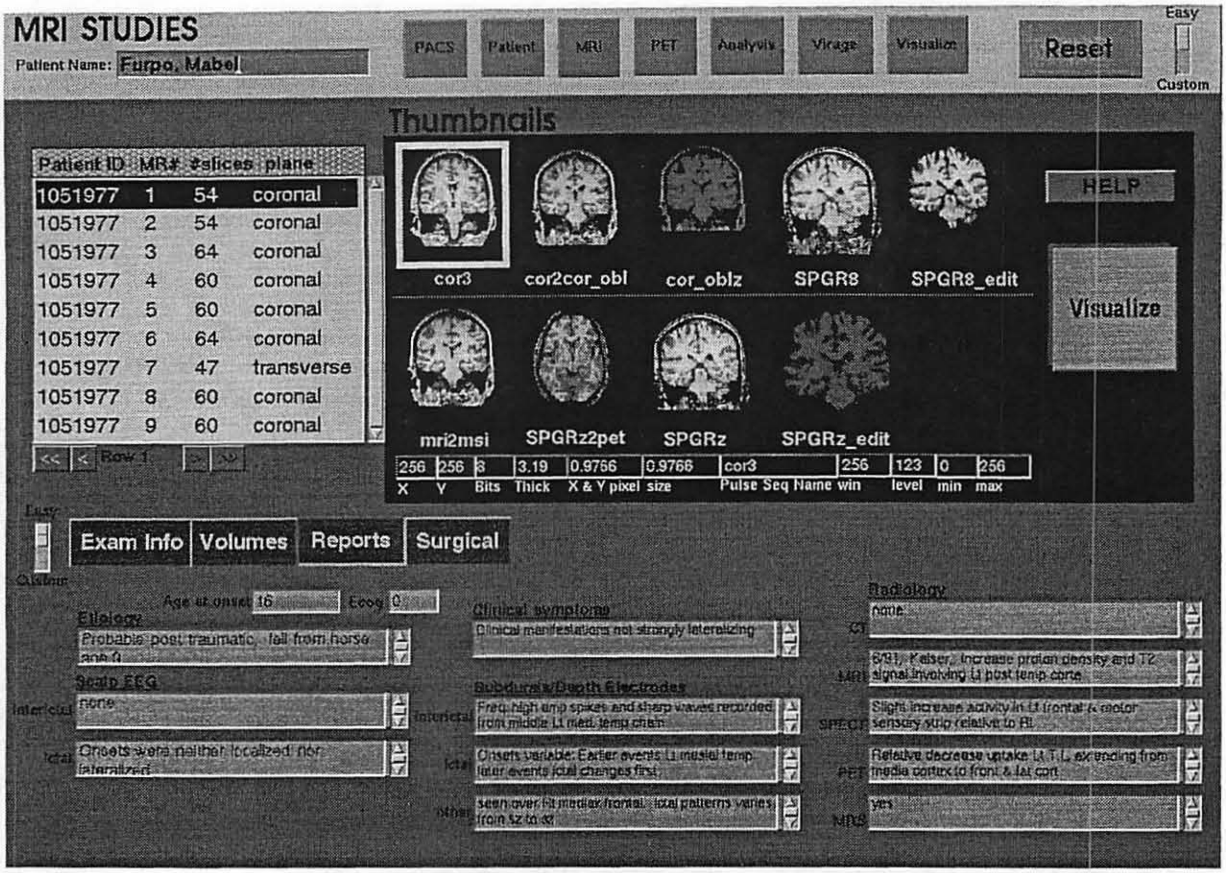

Figure 6. GUI to relational database. Queries on image features and textual keywords is supported. Clicking on thumbnails triggers retrieval of full MRI dataset. Textual data is displayed in text widgets below.

The power of organizing the analyzed data in the database is the ability to do on-line analytical processing of the collected data. The database can be queried on any number of keys ranging from patient name to image features to report keywords. Complex queries can be executed such as "Find female patients age over 21 years with right hippocampal atrophy > 10% and corresponding depletion of N-acetyl-aspartate > 15%." Matching patients are returned to the workstation, and full image datasets can be retrieved by clicking on the thumbnail images. The textual information is displayed in a variety of lists, entry fields, and textboxes. Thus, not only is it possible to index into the textual data, but also into the images themselves and the quantitative data they contain. The workstation expands the utilization of PACS data beyond radiologic soft-copy display and also augments the knowledge base of PACS by storing the results of analysis, segmentation of image features, quantitated image features, registration parameters, and textual reports.

5. RESULTS

The workstation has been utilized to analyze brain images of 40 patient cases. In cases where there were no hippocampal abnormalities on MRI, the co-registered MRI was used to increase the ability to interpret subtle lateralized abnormalities on PET. In all of 7 cases lateralized relative hypometabolism was identified concordant with ictal EEG findings. In preliminary results, missed abnormalities and false interpretations of independently interpreted high resolution FDG-PET were correctly identified with co-registration to MRI, allowing both an increase in sensitivity and specificity in the detection of hypometabolism in patients with partial epilepsy of mesial and neocortical temporal origin.

The following example demonstrates the identification and correct interpretation of focal hypometabolism only after co-registration on the workstation. Figure 7 shows an FDG-PET scan from a patient with right neocortical temporal lobe epilepsy. The scan was originally interpreted as "probably normal". Although intracranial ictal EEG recordings were non-localizing, interictal data from MEG spike source localization an intracranial EEG suggested that the epileptogenic zone was located in the right lateral temporal region. MRI in this region as well as mesial temporal structures was normal. After co-registration of MRI, interpretation of focal hypometabolism on PET in the posterior superior lateral temporal region became unequivocal. Confidence from co-localization of the local PET abnormality and focal neurophysiologic disturbance directed surgery leading to a seizure free outcome for the patient.

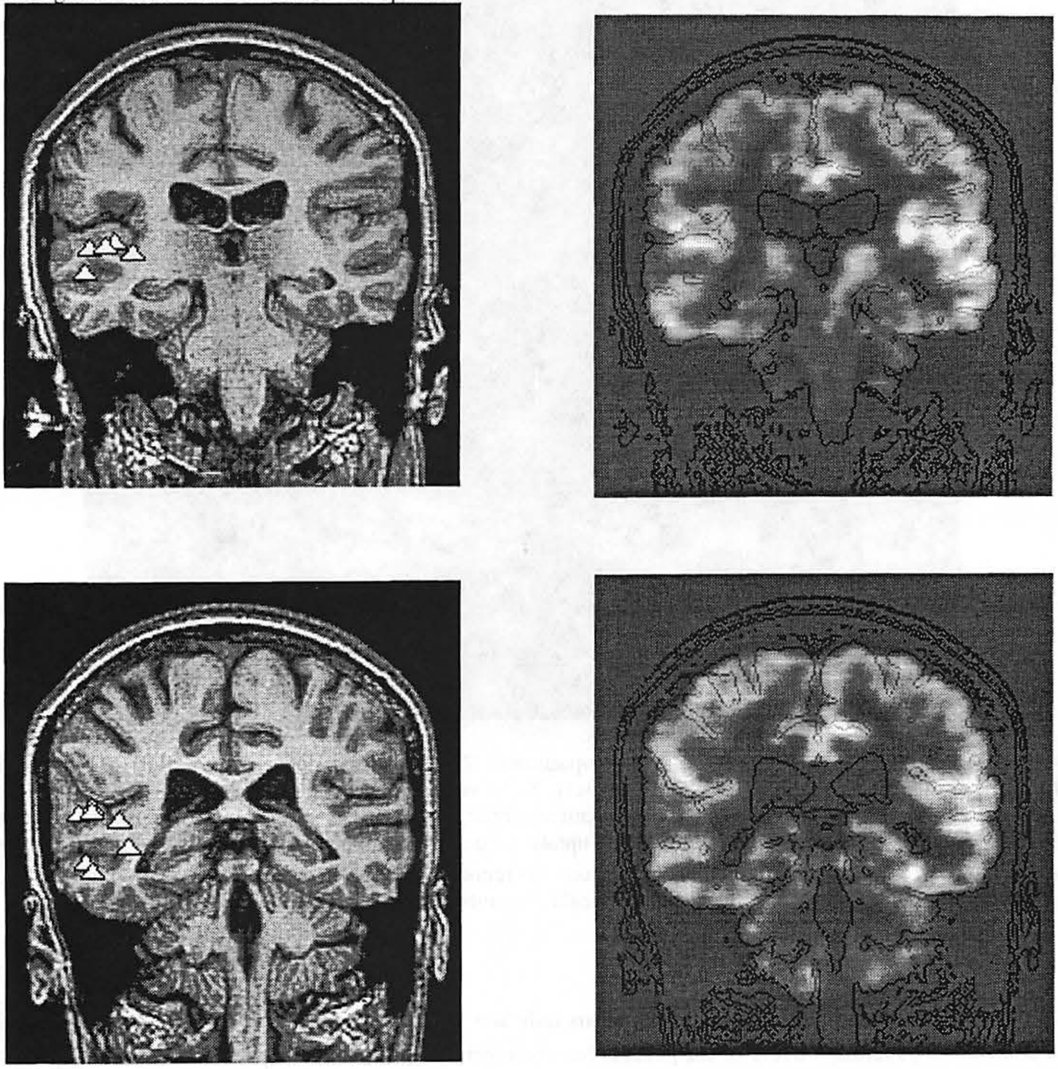

Figure 7. MRI-PET-MEG co-registration to detect a focal electrophysiologic and metabolic interictal disturbance. Left--MEG spike dipole source localization (white triangles) overlaid on selected co-registered coronal MRI slices from the temporal lobes--dipole sources correspond to an active disturbance of epileptiform activity recorded bipolarly over the right temporal lobe with scalp-sphenoidal EEG (sharp waves maximum at T4); the MRI is normal. Right--corresponding FDG-PET slices with overlayed contours from MRI anatomy--focal hypometabolism is present in the right superior temporal gyrus, remarkably colocalized with MEG spike sources. Pathologic examination cortical resection confined to the superior temporal gyrus and superior bank of the posterior middle temporal gyrus revealed hamartomatous dysplasia. Co-registration was performed with AIR©.

Direct comparison of quantitative data between different metabolic imaging volumes of interests can be done on the workstation. In figure 8 two types of metabolic data--the concentration of NAA (a marker for neuronal cell density) and glucose uptake (a measure of synaptic activity)--are calculated for the same volume, in this case a single voxel within the hippocampus. Further application afforded by co-registered MRI anatomy is the ability segment the MRSI voxel such that only the contribution from hippocampal or parahippocampal grey matter is sampled in the metabolite signal analysis.

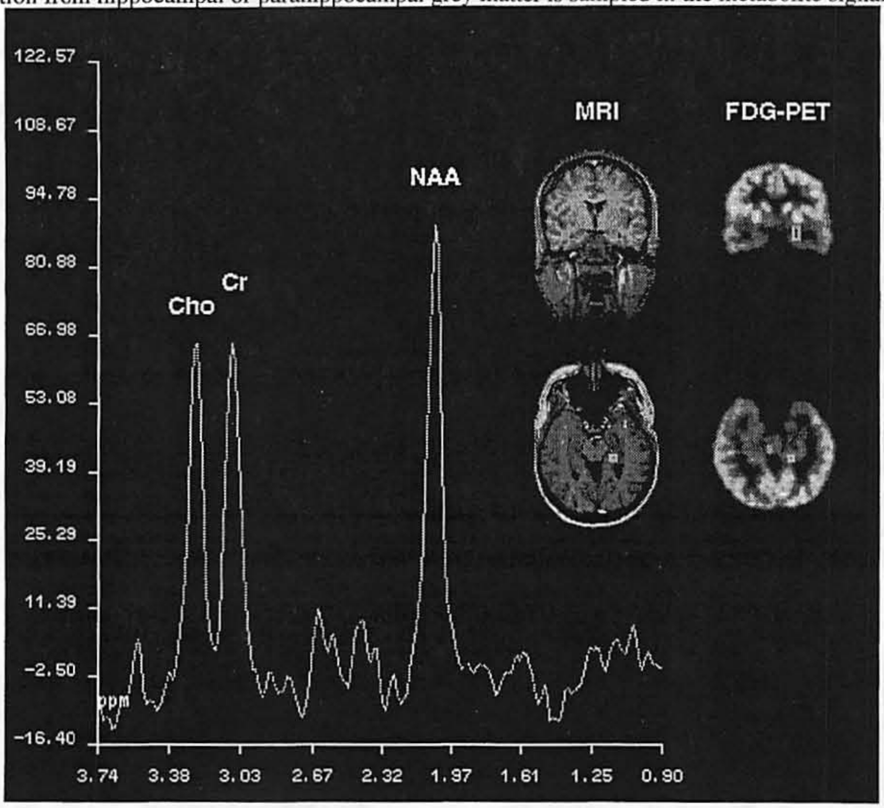

Figure 8. MRI/MRSI-PET co-registration for direct comparison of [NAA] and specific activity of glucose uptake. 1H-MRS spectra from voxel in left hippocampus on MRI (left inset). Same voxel is placed on coregistered FDG-PET (right inset). The normalized [NAA] (using water as an internal standard reference) for this region of the hippocampus can be directly compared to the normalized specific activity of glucose uptake (or actual metabolic rate of glucose metabolism if arterial blood flow curve of FDG is available) of this same region. Co-registration was performed with AIR©. Spectroscopy courtesy of Gabriele Ende (Central Institut of Mental Health, Mannheim, Germany, 1995).

Results of our preliminary image data analysis indicates that dipole sources of interictal spikes were able to be estimated in 19 of 40 patients. Twelve of the patients have had their outcomes assessed while the remaining patients will be reported in the future. All twelve patients had a MEG study, and eleven had a PET study. The imaging results and outcomes of the these twelve epilepsy patients are given in Table 2. Seven of the twelve patients had localizing MEG studies, and 6 of eleven patients displayed hypometabolic activity lateralized to a specific lobar region. The six patients who had both localizing MSI and PET all localized to the same lobar region; four were in the medial temporal lobe and 2 in the lateral temporal lobe. Five of the six patients had sublobar region of seizure onset agreement. Case C0028 is exceptional because both ictal EEG and MRI provided no localization information. The PET scan was originally interpreted as normal by blinded nuclear medicine specialists. Only with co-registration to the MEG spike sources were clear focal hypometabolism in the corresponding region revealed. In the group as a whole correlation of MSI with final localization of the epileptogenic zone was higher than either video EEG, MRI, or high resolution PET. MSI and PET provided the highest correlation of any combination of non-invasive modalities.

Case no.	Ictal EEG	MRI	PET	EEG/MEG	Surgery	Outcome (months)
C0003	LT	L hipp atrophy	NL	not done/neg.	LTL	Sz. free (5)
C0015	LT	L hipp atrophy & focal increase T2	-	FP1,F7,F3,SP1/LMT	LTL	Engel II (15)
C0026	LT	Normal	LMT	F7,T3/LMT	LTL	Engel II (15)
C0029	LT	L hipp atrophy	LT	neg/neg	LTL	Sz free (15)
C0039	LT	Normal	LMT	SP1/LMT	LTL	Sz free (5)
C0075	RT	Normal	NL	neg/neg	RTL	Sz free (8)
C0081	RT	R hipp atrophy & increased T2	RMT	neg/neg	RTL	Sz free (8)
C0088	RT	R hipp atrophy & focal increase T2	RT	F8,T4/RLT	RTL	Sz free (9)
C0091	RT	Rt. hipp atrophy	RT	neg/neg	RTL	Sz free (7)
C0096	LT	L hipp atrophy & focal increase T2	LMT	SP1/LMT	LTL	Sz free (5)
C0028	NL (SDE)	Normal	RLT (focal)	T4/RLT	RSTG/MTG topectomy	Sz free except some SPS (10)
C0055	NL (SDE)	L lateral temporal focal increase T2	LLT (focal)	T3/LLT	LLT lesionectomy and additional AILT resection	Sz free (4)

Table 2. Patient Clinical Features and Epilepsy Evaluation. These patients have either Mesial Temporal Lobe Epilepsy (MTLE) or Neocortical Epilepsy

Table legends:

Ictal EEG
LT = Left Temporal
RT = Right Temporal
NL = Non-Localizing
SDE = Subdural Electrodes

PET
LMT = Left Medial Temporal
NL = Non-Lateralized
RLT = Right Lateral Temporal
- = study not done

EEG/MEG
LLT = Left Lateral Temporal
LMT = Left Medial Temporal
RLT = Right Lateral Temporal

Surgery
AILT = Anterior Inferior Lateral Temporal

LLT = Left Lateral Temporal
LTL = Left Anterior Temporal Lobectomy
MTG = Medial Temporal Gyrus
RSTG = Right Superior Temporal Gyrus
RTL = Right Anterior Temporal Lobectomy

6. CONCLUSION

The multimedia PACS workstation enables clinicians to more effectively evaluate epilepsy patient data from PACS through the use of registration, 3-D rendering and visualization, ROI analysis, and database management. It also enables better understanding of the epileptogenic process itself and promises to facilitate multimodality investigation of brain functions and anatomy in other brain diseases such as multiple sclerosis. The intuitive GUI frees the clinician to concentrate on the clinical aspects of the case, and its integrated software utilities expand the utilization of PACS to clinicians outside the radiology department. By storing the extracted image and text data in the relational data model, the workstation increases the knowledge base of PACS. This knowledge augmentation increases the power of PACS for clinical applications.

ACKNOWLEDGEMENTS

This work was supported by the U.S. Public Health Service under Project 1 F37 LM00044-01 and a Whitaker Foundation Biomedical Engineering Research Grant.

REFERENCES

K.D. Laxer, P.A. Garcia, "Imaging Criteria to Identify the Epileptic Focus", *Neurosurgery Clinics of North America* **4**, No. 2 pp. 199-209. April 1993.

J. Engel, "Outcome with respect to epileptic seizures", *In* J. Engel (ed): *Surgical Treatment of the Epilepsies,*. pp. 553-571, Raven Press, New York, 1987.

R.P. Wood, J.C. Mazziotta, and S.R. Cherry, "MRI-PET registration with automated algorithm", *J Computer Assisted Tomography,* 17(4): 536-546, 1993.

H.G. Wieser, "Ictal manifestations of temporal lobe seizures", *In* D. Smith, D. Treiman, M. Trimble (eds), *Advances in Neurology*, vol 55, pp. 301 Raven Press, New York, 1991.

S.T.C. Wong, R.C. Knowlton, K. Soo Hoo, H.K. Huang, "Use of multidimensional, multimodal imaging and PACS to support neurological diagnosis", *SPIE vol. 2433,* pp. 236-247, 1995.

H.K. Huang, *PACS for biomedical imaging.* VCH, New York, 1996.

H.K. Huang, R.L. Arenson, et al., "Second generation PACS at UCSF", *Radiology*, Vol. 189(p), p. 290, Nov., 1993.

M. Osteaux. *A second generation PACS concept* (Ed.). Springer-Verlag, 1992.

R.P. Woods, J.C. Mazziotta, S.R. Cherry, "MRI-PET registration with automated algorithm", *Journal of Computer Assisted Tomography* , 17(4), pp. 536-546, 1993.

Computed Radiographic(CR) Image Post-processing in Picture Archiving and Communication Systems(PACS)

Jianguo Zhang, Katherine P. Andriole and H. K. Huang
Laboratory for Radiological Informatics, Department of Radiology,
University of California, San Francisco, CA94143-0628

Abstract

This paper present the key post-processing algorithms of CR images used in our second generation PACS and its software implementation based on the algorithm features, fault tolerance and multilevel adaptive control in order to achieve the benefits of image processing, get good performance and results on post-processing speed and reliability.

Key words: Computed radiography, PACS, post-processing algorithms, and adaptive process control.

1. Introduction

As digital imaging becomes more important in daily radiology practice, the need of converting images from projection radiography to digital format becomes apparent. CR system is one of digital methods which aim to replace the present screen/film system of analog X-ray[1]. It uses portable imaging plate(IP) as X-ray sensor which stores X-ray energy in latent image form. After laser scanning the IP, the optical image generated from the latent image is converted to a digital format.

Digital-based picture archiving and communication systems have gradually replace conventional film-based operations in radiology departments. The CR imaging subsystem in PACS can be considered to involve three modules, image acquisition, image archiving, and image display. Raw images generated by CR systems must be post-processed in many complex computational steps before archiving into PACS or transmitting to remote display workstations. This kind processing involves a sequential operations of intertwined computational procedures, including image reformatting, automatic background recognition and removal (ABRR)[2], orientation correction(OC)[3], automatic lookup table adjustment(ALUTA), and image encoding. Some processes (e. g., ABRR) are irreversible, and some are hardware related or input parameters dependent (e. g., ALUTA, OC). The quality of processed images, the performance and results of these processes, and speed and reliability of image delivered are relied on the algorithm features, the strategy of their software implementation in PACS environment. In this paper, we present the key post-processing algorithms of CR images used in our PACS and its software implementation based on the algorithm features, fault tolerance and multilevel adaptive control in order to achieve the benefits of image processing, get good performance and results on post-processing speed and reliability.

2. Data flow of CR images in PACS

The department of radiology at UCSF operates two CR systems(Fuji 9000 and Fuji AC-2) generating about 1.2 gigabits of image data daily. Figure 1. shows a diagram of data flow of CR images in PACS. The patient information coming from RIS/HIS is used for identifying specific study and encoding image format to DICOM.

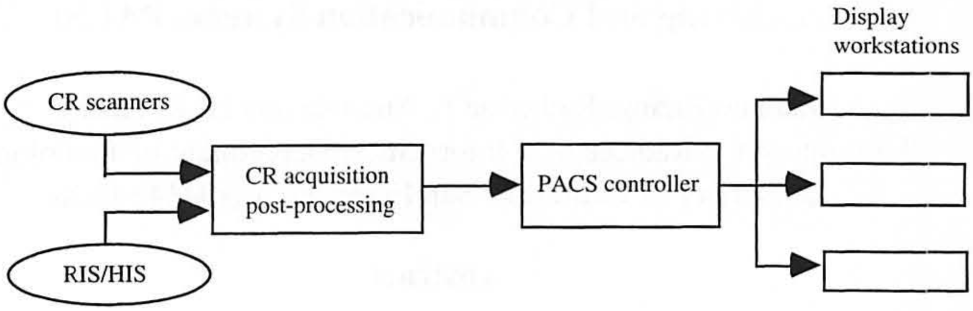

Figure 1. A diagram of CR data flow in PACS

There are seven processes involved in the CR acquisition and post-processing. The functions of these routines are as follow: (1) **DASM_server** process acquires images from a Fuji system; (2) **communication** process transfers data between acquisition and post-processing workstations; (3) **reformatting** process converts and formats the acquired image data from different sizes to an uniform 2K x 2K dimension for next step processing; (4) **automatic background recognition and removal** process eliminates redundant background signals in the acquired CR images caused by X-ray collimation; (5) **orientation correction** process aligns and rotates the CR image to a position suitable for viewing in display stations; (6) **automatic lookup table adjustment** process modifies the default lookup table to enhance the visual quality of aligned images; and (7) **header encoding** process converts the image from Fuji proprietary format to the standardized DICOM 3.0 .

These seven processes are independent daemons running in the background of the two SUN SPARC workstations. Processing of CR images is sequential through these steps and follows the FIFO model(first in first out). The conventional processing model of this stream line daemon procedure is illustrated in Figure 2.

Figure 2. A diagram of the stream line procedure of CR post-processing

3. CR key post-processing algorithms in PACS

3.1 Reformatting

Previous purpose of reformatting the image of various sizes to a standard size is for displaying because our old display system only can display image in fixed size(2K x 2K). Currently, most commercial display workstations can deal with different sizes of images with DICOM standard format. The reasons we still do reformatting on CR images are: (1) old display systems still keep running in clinics; (2) the algorithms of next processing steps need fixed image format.

In reformatting process, images from different IP sizes(8" x 10", 10" x 12", 14" x 14", 18" x 24", and 24" x 30") are reformatting to a standard size (2K x 2K pixels). If the size of an incoming image is larger than 2K x 2K, the reformatting takes two steps: first a 2D bilinear interpolation is performed to shrink the image in both directions; second a suitable number of blank lines is added to extend the size to 2K x 2K. For plates that produce pixel matrix sizes smaller than 2k x 2K, the image is extended to 2K x 2K by adding blank lines.

3.2 Automatic background recognition and removal

Under normal operation conditions, CR images contain unexposed areas due to X-ray collimation. In CR images, unexposed areas appeared as white in a display monitor is called background as marked by arrows in Figure 3. The purpose of background recognition and removal is to convert the background pixels from white to black.

There are four steps to remove CR background[2]. In first step, a statistical approach of CR background description is applied to CR images to calculate a specific parameter(called background score in this context) for a pixel and find the relation of this parameter with the background probability of pixel. Figure 4 shows the relation curve between the background score and its background probability of a pixel.

In second step, the signal processing methods, e. g., sampling, filtering, and angle-resolved recognition, are used to recognize those pixels which may be at the background edges of a CR image. Figure 5 gives the background edge recognition results for the CR image as shown in Figure 3. There are four peak signals in Figure 5 corresponding to four edges of the CR image.

In third, in order to achieve high successful ratio of full background removal meanwhile make this removal much more reliability, a peak threshold adaptively controlled by the total score of one side as shown by the curve in Figure 6 determines whether to fit lines which are coincided with background edges.

Finally, three consistently reliable estimation rules are applied to the background removal operation to make sure no valid information being removed. Figure 7 is the background removed image of Figure 3.

3.3 Automatic orientation correction

Since CR cassette can be placed at various orientations to accommodate the examination condition in clinics, orientation of CR images displayed in PACS display workstations becomes one of the quality assurance problems that has to be addressed before a workstation can successfully run in clinics. Therefore, it is necessary to implement a computerized algorithm to orient CR images to a proper direction in CR post-processing procedure.

The orientation correction method used in the CR post-processing is based on recognizing anatomical features of different types of images[3]. First, the anatomical information of an image is taken from the image header, then the analysis on the image is performed in three steps(using chest as example): (1) the orientation of the spine within the image is determined; (2) a function searches for upper extremities and sub diaphragm; and (3) the lungs are extracted and their areas are compared to indicate whether the image needs to be y-axis flipped. These three steps set the value of three parameters on the basis of which the final rotation angle is determined.

In order to get high successful ratio of correct orientation, the orientation recognition algorithm should be assigned to the image only rather than to the image and its background combined. So, the result of ABRR on original CR images determines the performance of the automatic orientation correction in our post-processing procedure.

3.4 Automatic lookup table adjustment

CR image readers(IRD) usually have built-in sensitivity/image range automatic setting mechanism to control the imaging characteristics so as to realize image density stability, i. e., modifying the image density instability due to over- or under- exposure during X-ray imaging. For most clinical CR images, there are other factors affecting the image visual quality on PACS display workstations: (1) most CR images have background due to X-ray collimation and automatic setting mechanism in IRD only adjusts image density for whole image, not specifically for anatomical areas; (2) some CR images need gradation processing to enhance specific anatomical features; and (3) CRT-based monitors usually do not produce a linear response across the full range of pixel values, and this kind nonlinear response is quite different between monitors.

For providing visual quality of CR soft copy competitive with hard copy and getting consistent output among display monitors, we apply lookup table correction operation on both CR raw image data and monitors.

In software processing, automatic lookup table adjustment process recalculates the histogram of anatomical parts of CR images by using the results of ABRR and gets correct display parameters (e. g., window/level), then extracts anatomical information from the image header and adjusts pixel values to do gradation processing according to related gradation processing curves[4] as shown in Figure 8. This processing significantly improves the image visual quality.

In hardware, we choose Dome display boards with 10 bits Digital/Analog conversion (Md2/PCI for 1K x 1K NT-based display workstation, Md5/Sbus for 2K x 2K UNIX-based high-resolution workstation) to support display monitors. Use a calibrator to do Gamma correction by adjusting DAC lookup table and get the linear relation between digital pixel value input and luminance output. Figure 9 shows the relation curves between the luminance output and pixel value input in a 1280 x 1600 portrait monitor before and after gamma correction. This hardware correction guarantees that finally image processing results mentioned above can be properly presented on screens.

4. Adaptive process control for CR post-processing

In CR post-processing, some processes run slower than others, causing computational bottleneck. Subsequently, this delays the transmission of images from the CR system to display stations, like in the ICU for which the quick response to user query is critical. Furthermore, some of these processes manipulate images based on the header information entered by the operators. However, illegal parameters, software bugs, or system errors often crash the processes. We develop a control theory and a fault tolerance algorithm to circumvent such problems.

4.1 Control theory

The idea of the control theory is based on the fact that all the CR processes have equal priority in accessing the CPU of a multitasking operating system(as UNIX, or NT). Suppose that there are m processes running in a multitasking computer and f_0 is the clock speed, or processing frequency of this computer. Let us further denote that the processing frequency of the ith CR daemon process is f_i and the number of computer cycles required by this process in finishing one job is S_i. Every process's frequency is assigned by the CPU and the sum of all process's frequencies is roughly equal to the CPU frequency or clock speed, so we have the equation described by the following:

$$f_0 \approx f_1 + f_2 + ... + f_m \quad (1)$$

The processing time required by the ith process is S_i / f_i. Assuming the CR processes occupy most of the CPU time, the total processing time to process one image by m daemon processes, T, can be approximated as follows:

$$T \approx S_1/f_1 + S_1/f_1 + ... + S_1/f_1 \quad (2)$$

Our purpose is to attain the minimum T by adjusting f_i, for i = 1, 2, ..., m. Since f_0 is a constant, Equations (1) - (2) now become an extreme value problem under certain conditions. With the solution of extreme value under conditions developed in mathematics, we find the frequency of ith process assigned by CPU should be given by the following formula:

$$f_i = \sqrt{S_i} \cdot f_0 \left(\sum_{j=1}^{m} \sqrt{S_j} \right) \quad (3)$$

In time period ΔT, assuming that the number of jobs done by the ith process is n_i, the unit time spent for one job by the this process then is $\Delta T / n_i$. This should be approximately equal to S_i / f_i. That is:

$$\Delta T / n_i = S_i / f_i \quad (4)$$

Substituting Equation (3) into Equation (4), we have:

$$n_i = \Delta T \cdot f_0 \Big/ \left[\sqrt{S_i} \cdot \left(\sum_{j=1}^{m} \sqrt{S_j} \right) \right] \quad (5)$$

Since S_i can be pre-determined, f_0 is a constant and ΔT is same for all processes, we can attain the statistical minimum of the total processing time required by all processes to handle a CR image by controlling the number of jobs done in every process specified by Equation (5).

4.2 Fault tolerance algorithm

Some illegal parameters in the image header can be predicted while some cannot. To recognize the latter errors, an algorithm is developed to guarantee that an image that causes a process crash will not be processed again. Every medical image has its own identification information, such as the serial number and the scanning time. We use these parameters to recognize those images which cause processes to crash. Suppose D_i {d_{1i}, d_{2i}, ..., d_{li}} is a vector representing the identification of the ith medical image and d_{ji} is its jth branch vector. We define that d_{ji} does not correlate with d_{jk} if $< d_{ji}, d_{jk} >= 0$, i.e., $d_{ji} \neq d_{jk}$. Thus, if image i does not correlate with image k, then their identification

$$\langle D_i, D_k \rangle = 0 \quad (6)$$

Otherwise, we say that image i correlates with image k.

Now, we apply the correlative recognition algorithm developed above to all the processes in order to identify the images which cause process crashing. After getting a job from a queue_in, a process must compare the image identification parameters with the previous image according to Equation (6). If these two images correlate with each other, it means that this job has been processed more than one time but was not completed. Then, the process removes this job from its queue_in and gets the next job in the queue. Implementing this algorithm in the multilevel processing structure which we will describe, will guarantee that all jobs are processed no more than one time in every process.

4.3 Implementation of control theory and fault tolerance

To make the job control mechanism and the fault tolerance algorithm work together, an event-driven, multilevel processing structure is developed as shown in Figure 7.1. There are three process levels: monitor_server, parent, and child. The major tasks and functions of these three levels have been described following.

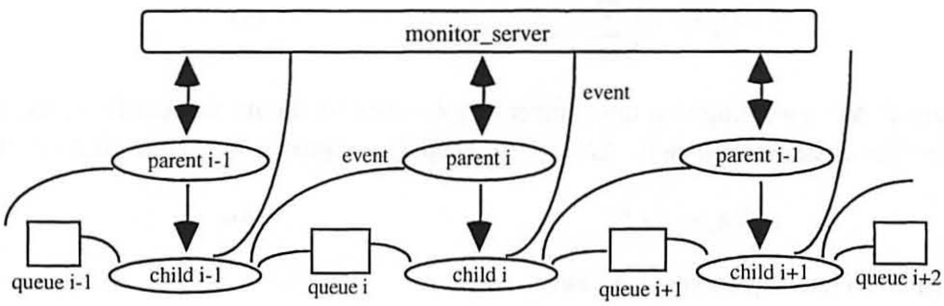

Figure 10. The diagram of multilevel adaptive process control structure

For the monitor server, apart from controlling the number of jobs of each process, it also monitors parent processes and the system environment. For example, it makes sure whether all parents are alive and whether there is enough memory space for parents to generate children. It receives events from child processes and transfers error messages to the central monitor in order to notify the system administrator.

The major functions for parent processes are: (1) check their queue_ins to detect if there is a job available; (2) generate a child process to perform desired functions; (3) monitor the processing time of the child process generated. If the child takes too long time to process a job, the parent will kill the child process. Because all these functions have nothing to do with the image data, the parent processes would not be effected by any illegal parameters or software bugs.

Every child process is composed of two parts. The first is the fault tolerance algorithm developed in Section 4.2, and the second is its image processing functions. The functions for a child are as follows: first, after being generated by its parent, it gets a job from its queue_in and applies the fault tolerance algorithm to this image. If it fails the fault tolerance criterion, i.e., the image has been processed before but not completed, the child process removes this job from its queue_in with an error message and then exits. Second, the child process reserves the image identification vector parameters in a special file in order to correlate with the next job. Third, it performs its assigned image processing function. Fourth, after completed the processing, the child moves the job into its queue_out. Finally, it deletes the job from its queue_in with the success message and then exits.

5. Results

We have implemented the CR image processing and fault tolerance algorithms with event-driven multilevel process control structure in the post-processing procedure of hospital integrated PACS at UCSF[5]. Since our CR processing algorithms are much more efficient and their software implementation is delicate, the performance and results of this processing is very acceptable in the PACS. Following, we gave some results about these algorithms implemented with adaptive process control structure in a PACS.

For ABRR, we sampled 330 consecutive CR images over a period of 5 days, of which 246 have background and 84 do not. Table 1 shows the result after applying ABRR to these images.

Table 1. Measure of success of the automatic background recognition and removal algorithm

(Total images = 330, With BKGD = 246, No BKGD = 84)

Recognition of BKGD	243(BKGD)	87(no BKGD)	99.0%
Full Removal	223		91.0%
Partial Removal	21		8.8%
No Removal	2		0.2%
Removal of valid inform	0		0.0%

For orientation correction, we acquired 268 CR images over a period of 3 days, 179 of which have incorrect orientation, and 89 have correct orientation. We measured the performance of orientation correction before and after applying ABRR to these images respectively. Table 2 lists the result of this measurement.

Table 2. Measure of success of the orientation correction algorithm

(Total images = 268, with correct orient. = 89, with incorrect orient. = 179)

	Before ABRR	After ABRR
Rotated correctly	102 (38%)	228 (85%)
Rotated incorrectly	156 (62%)	40 (15%)

For multilevel adaptive process control and fault tolerance algorithm, the measurement of their performance is given by Table 3.

Table 3. Measure of the multilevel adaptive process control and fault tolerance

	single level without controlling	multilevel with controlling
Total processing time for one image (testing 20 CR images)	4 min. 2 sec.	2 min. 56 sec.
standard deviation	1 min. 37 sec.	34 sec.
crash (monitoring six months)	once/week	None (acquired 12561 images, 272 errors, no crash, no image lost)

Figure 11 shows post-processed pediatric CR images displaying on a pediatric Intensive Care Unit display workstation.

6. Conclusions

The image processing algorithms are very useful in improving CR image visual quality and can enhance the performance of PACS in clinical environment. With the implementation of the event-driven, multilevel adaptive process control structure in CR acquisition and post-processing, the processing speed is increased and downtime is reduced while the quality assurance time and user intervention are decreased. The CR post-processing is an important step contributing to the implementation of automatic soft copy display in PACS and teleradiology.

7. References

[1]. T. T. Takano eds, *Computed Radiography,* Springer-Verlag, 1987, pp1-8
[2]. J. Zhang, et al., "Background recognition and removal of Computed Radiographic images", *Radiology* , Vol. 201(P), 1996, pp220.
[3]. E. Pieka, et al., "Orientation correction for chest images", *J. Digital Imaging,* Vol. 3, 1992, pp185.
[4]. "Digital image processing", *Fuji Computed Radiography Technical Review,* No. 1, 1993, pp8.
[5] H. H. Huang, et al., "Clinical experience with second-generation hospital-integrated picture archiving and communication system", *J. Digital Imaging,* Vol. 9, 1996, pp151.

Figure 3. An original CR image with background.

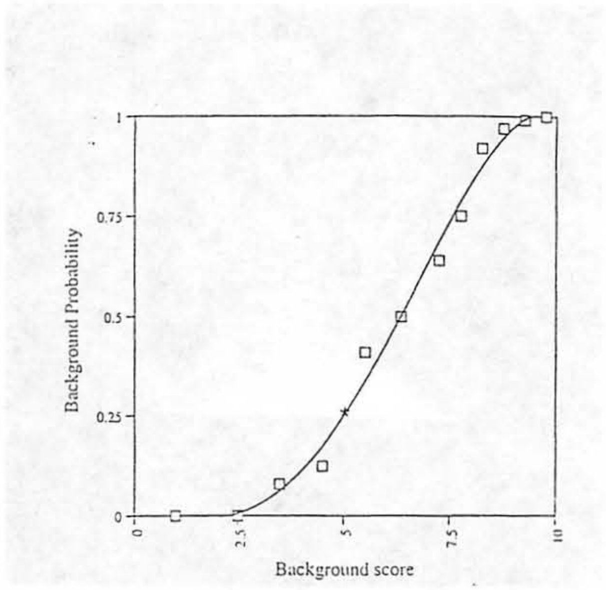

Figure 4. A relation curve between background score ant its background probability of a pixel.

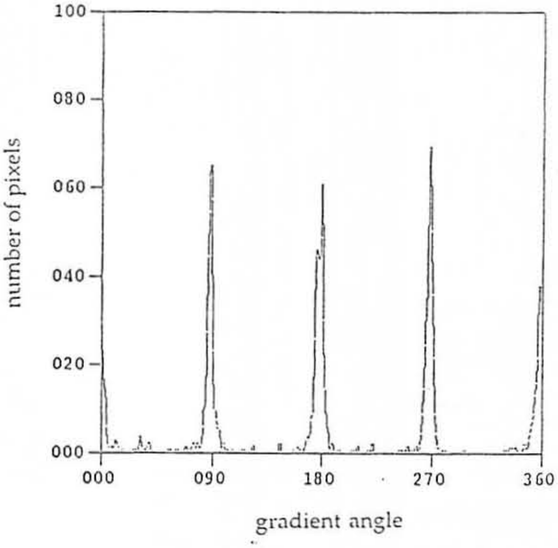

Figure 5. Angle-resolved recognition results for the CR image in Fig. 3.

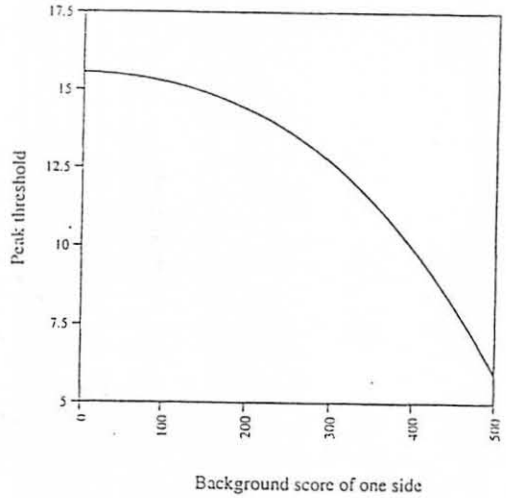

Figure 6. The threshold curve determining line fitting vs total score of one side in a CR image.

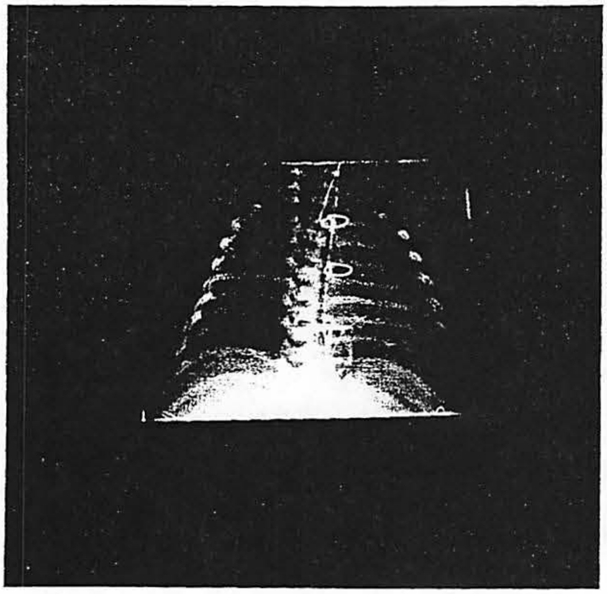

Figure 7. The background removed CR image as shown in Fig. 3.

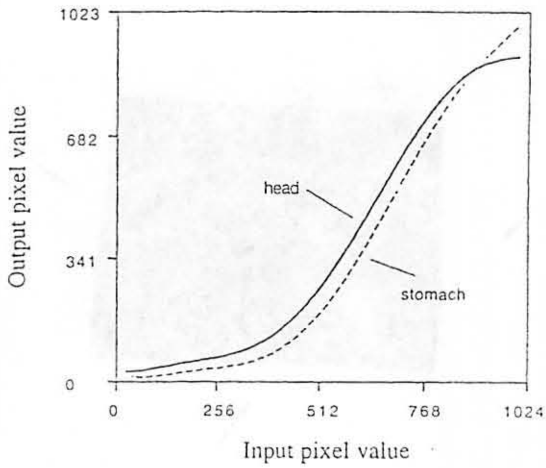

Figure 8. The gradation processing curves used in automatic lookup table adjustment.

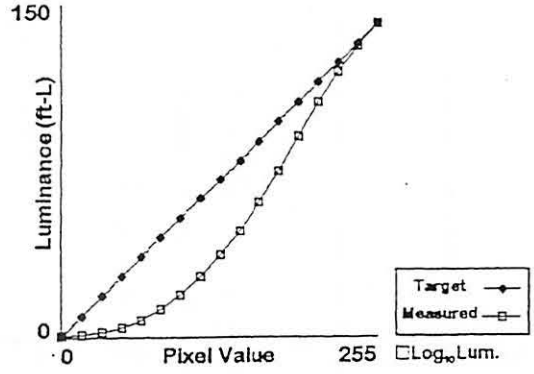

Figure 9. The measured relation curves of luminance output with pixel value input in a 1280 x 1600 portrait monitor before and after gamma correction.

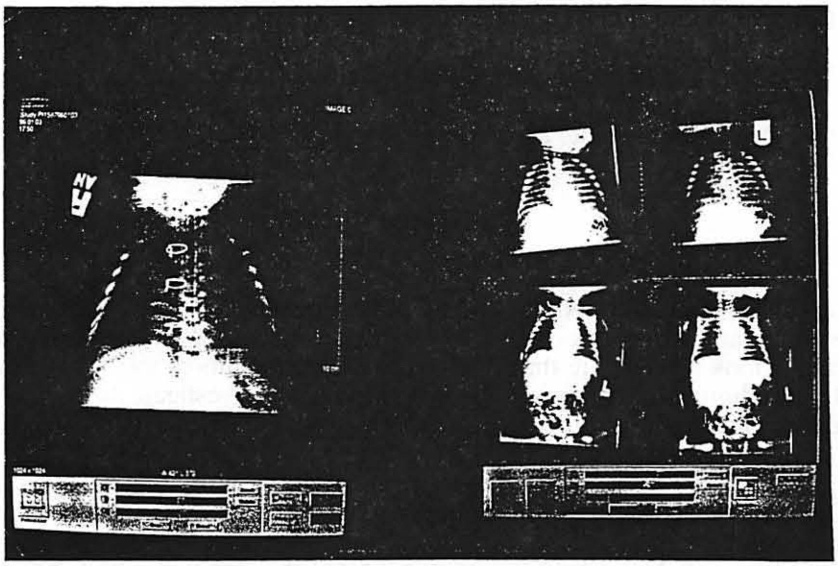

Figure 11. After passing through post-processing procedure, the CR images displayed in a pediatric ICU workstation.

Full-Field Direct Digital Telemammography -- Preliminary

S.L. Lou, Edward Sickles, H.K. Huang, Fei Cao, David Hoogstrate, Mohammad Jahangiri

Laboratory for Radiological Informatics
Department of Radiology, University of California San Francisco,
530 Parnassus Avenue, Rm. CL-158, San Francisco, CA 94143-0628

ABSTRACT

Full-field direct digital mammography has many advantages over the conventional film/screen imaging detector. Among these are larger dynamic range, lower scattering noise, and the possibility of using it for telemammography applications to alleviate the shortage of expert mammographers. We are in the process of developing a full-field direct digital telemammography imaging chain to investigate its usefulness for telediagnosis, teleconsultation, and telemanagement.

This paper describes the first phase of a three-year research program to set up a full-field direct digital mammography (FFDDM) imaging chain at the Breast Imaging Section connecting the University of California, San Francisco Medical Center and the Mt. Zion Hospital in the San Francisco Bay area. The chain consists of two FFDDM system (Fischer Imaging, Denver, CO), and two 2,500 (2K) line two-monitor workstations (VICOM, Fremont, CA). An OC-3 155 Mbits/sec asynchronous transfer mode (ATM) communication network (Pacific Bell, San Francisco, and FORE, Warrendale, PA) is used to connect the FFDDM and the two workstations. The FFDDM is based on a slot scan CCD detector which can image a full breast with 3,100 x 3,870 pixels (12 bits), and produce a direct digital image with 50 micron pixel size.

Preliminary results of the FFDDM demonstrate that it has a greater dynamic range and lower detector noise than that of a film-screen detector, and that the scattered radiation is reduced without using a grid. However, the spatial resolution is less than that of the conventional screen/film system. The 2K workstation can display simultaneously any two or four full-view mammographic images by either scrolling or subsampling on the two monitors. Display of an image takes about 1.5 seconds from the RAID disks. The ATM can transmit a 32 Mbyte digital mammogram from the FFDDM to the workstation in 3-4 seconds.

This paper also describes the three research protocols in telediagnosis, teleconsultation, and telemanagement.

Key Words: Digital mammography, teleradiology, high resolution display, asynchronous transfer mode, breast imaging

1. BACKGROUND

Breast cancer is the fourth most common cause of death among women in the United States [1]. There is no known means of preventing the disease, and available therapy has been unsuccessful in reducing the national mortality rate over the past 60 years. Current attempts at controlling breast cancer concentrate on early detection by means of mass screening, using periodic mammography and physical examination, because ample evidence is now available to indicate that such screening indeed can be effective in lowering the death rate.

Film-screen mammography has certain technical limitations which reduce its effectiveness: the film gradient must be balanced against the need for wide latitude and detection of microcalcifications. In addition, portrayal of the clarity of the margins of breast masses are reduced due to the presence of film noise in the displayed image, film processing artifacts can degrade the mammographic image, and the day-to-day variability inherent in automated film processors can produce suboptimal image quality.

Early digital mammography applications acquired data by digitizing conventional mammography films. This approach severely limits the potential of digital mammography since the resultant images can contain no more radiographic information than do the standard films from which they are produced. Indeed, most current digital images are slightly inferior in quality to their corresponding parent films, accounting in no small part for the general lack of clinical acceptance of digital mammography applications.

Direct digital mammography can overcome most of these problems, at the same time providing additional features not available with standard mammographic imaging [2]. During the past several years, due to the concentrated efforts from the National Cancer Institute and the United States Army Medical Research and Development Command, some prototype direct digital mammography systems are being developed by the jointed effort between academic institutions and the private industry. Some of these systems are ready for clinical evaluation [3]. Our full-field direct digital telemammography research program utilizes one of these prototype systems [4].

A major component in a digital mammography system is the image display. The basic requirement for general use is the ability to portray the entire breast with such fine detail that tiny structures, such as malignant microcalcifications, are readily visible. Furthermore, since routine mammographic interpretation involves four images of a current examination compared with four images from a prior examination, digital workstations either must include at least eight monitors or utilize monitors providing sufficiently fine detail that two or more whole-breast mammograms are displayed per monitor [5]. The principal theoretical advantage of direct digital mammography comes from decoupling image display from the image receptor. This permits the digital image to be captured electronically, stored digitally, and then manipulated, analyzed, and displayed however, whenever, and wherever it is needed.

Our research aims to explore teleradiology mammography, or telemammography applications. Electronic transfer of digital images to remote viewing sites can be accomplished almost as rapidly as between the standard display workstation and computer storage [6]. Numerous activities utilizing teleradiology have been devised, many of which are clearly applicable to mammography practice [7]. Radiologists who work in several different offices or hospitals will be able to monitor and interpret examinations that are carried out in a nearby or even at distant location or locations. This will permit those radiologists with the greatest interpretive expertise to manage and read in real time **all** mammography examinations, an operational procedure far superior to the alternative of choosing between deferred interpretation by expert readers or real-time interpretation by general radiologists [8,9]. Real time is defined in this context as a very rapid turnaround time between examination and interpretation. In addition, mammography screening in mobile units will be made more efficient, not only by overcoming the need to transport films from the site of examination to the site of interpretation, but also by permitting image interpretation while patients are still available for repeat or additional exposures. Furthermore, telemammography can be used to facilitate second-opinion interpretation, in effect making world-class mammography expertise immediately accessible to community-practice radiologists.

This paper describes the first phase of a three-year research program to set up a full-field direct digital telemammography chain (FFDDM).

2. THE TELEMAMMOGRAPHY CHAIN

The first phase goal is to set up a telemammography chain at the University of California, San Francisco (UCSF) Medical Center, between the comprehensive breast imaging service at UCSF-Mt Zion Hospital (MZH) and the outpatient mammography service at the UCSF-Ambulatory Care Center (ACC), with the former as the diagnostic center and the latter as the satellite site. Figure 1 shows the FFDDM telemammography. The instrumentation of setting up a real-time telemammography chain are in two stages: stage 1 is to set up a real-time local area network (LAN) with asynchronous transfer mode (ATM) technology within MZH [10], using the first full-field direct digital mammography (FFDDM) unit; stage 2 is to set up a real-time wide area network (WAN) ATM between MZH and ACC with a second FFDDM unit via the existing picture archive and communication system (PACS) infrastructure [10]. The distance between these two sites is approximately two miles.

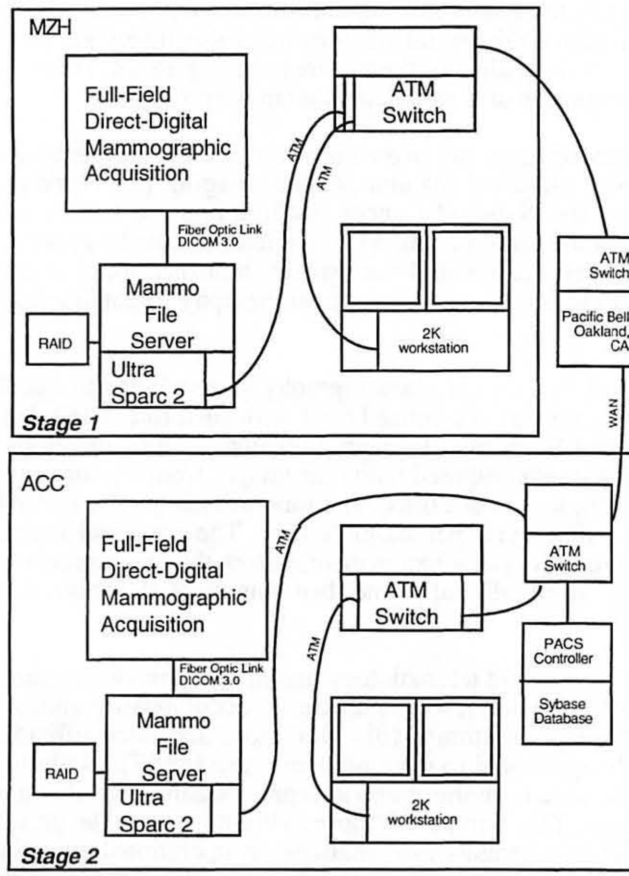

Figure 1 Systematic diagram of the real-time FFDDM telemammography chain

Full-Field Direct Digital Mammography (FFDDM)

We formed a collaborative research partnership with Fischer Imaging Corporation (Denver, CO). Fischer provides the FFDDM units and engineering support and we concentrate our effort in the telemammography chain including the system software, softcopy display, and patient research protocols. Table 1 shows the current specifications of the FFDDM.

Image Data Base

FFDDM images in DICOM 3.0 format is managed by the mammography file server (MFS). The two MF servers are in turn connected to an existing PACS centralized data base management system consisting of [10]:

1) An image archive system composed of an archive server (SUN SPARCserver 690MP, SUN Microsystems, Mountain View, CA), with a 2.6 terabyte optical library (Cranel, Ohio).

2) A mirrored relational data base server Sybase (Emeryville, CA), with a structured query language (SQL) running on two SUN SPARCserver 10.

All FFDDM images acquired is managed by this centralized data base. Figure 2 shows the connection of the two MF servers and the centralized data base.

Table 1 Specification of the Fischer FFDDM System

Image Area	193 x 240 mm
Detector	Charge-coupled devices (CCD)
Image Scan Time	slot scan, 4.5 secs (nominal)
kV Range	25-50 kVP
Tube Current	200 mA at 45 kVP
Focal Spot Size	0.30 mm (nominal)
Pixel Size	Nominal Mode: 62 x 62 microns (High res.): 31 x 31 microns
Image Matrix	3,100 x 3,870 pixels (nominal), 12 bits/pixel
Image Size	24 Mbytes
Spatial Resolution	8 lp/mm (nominal), 16 lp/mm (High Res.)
Detective Quantum Eff.	less than or equal to 50% at f(0)
Scatter-to-Primary	less than or equal to 0.15

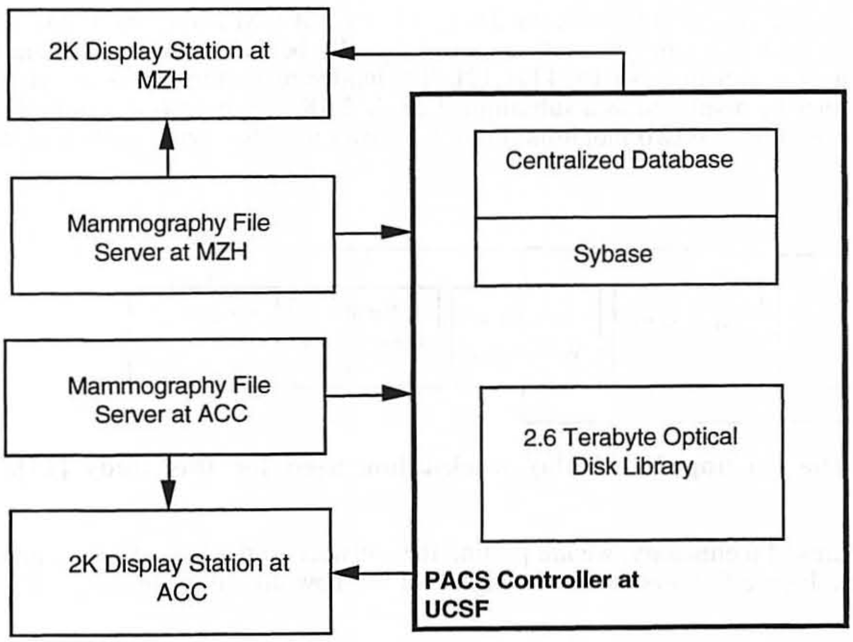

Figure 2 Dataflow between the two mammography file servers and the centralized database.

Image Communication between MZH and ACC

We use the asynchronous transfer mode (ATM) OC-3 for both WAN and LAN with the T-1 and Ethernet as the back-up networks. Table 2 shows the time required to send a 10MB (2K X 2.5K X 2 bytes) and 40MB (4K X 5K X 2 bytes) FFDDM image from MZH to ACC using T1 and ATM. With this ATM communication speed, the utility of real-time telemammography can be realized.

Table 2 Time Required to send an 10 MB, 40 MB FFDDM Image from MZH to ACC using T1 and ATM (OC3) (No Compression)

	2K x 2.5K x 2 bytes (10 MB)		4K x 5K x 2 bytes (40 MB)	
	One image	One exam 4 images	One image	One exam 4 images
T1 (1.5 mbits/s) realization 100 KB/s	100 sec (1.6 min)	400 sec (6.7 min.)	400 sec (6.7 min.)	1,600 sec (26.7 min.)
ATM (155 mbits/s) realization 60-70 mbits/s (7.5 MB/s)	1.3 sec	5.3 sec	5.3 sec	21.3 sec

Image Display

The soft copy display is based on a two monitor 2K station by VICOM (Fremont, CA). This display station was specially designed for mammographic soft copy display. We began to use this system for digital mammography teaching file display in September 1994 [11,12]. The hardware architecture is shown in Figure 3. A digital mammogram can either be displayed as a subsampled 2K X 2.5K image or as a quadrant of the full-resolution 4K X 5K image on each of the two monitors. Figure 4 shows the 2K system with four subsampled images.

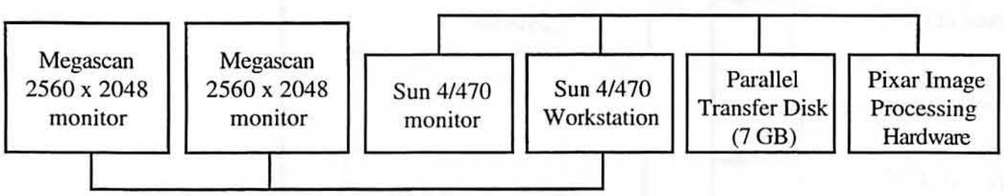

Figure 3 Architecture of the existing 2K display workstation used for this study [11].

Since this system uses five-year old technology, we are porting the software to the Ultra Sparc 2 platform with two DOME MD5/SBX boards. Figure 5 shows the block diagram of this new display system.

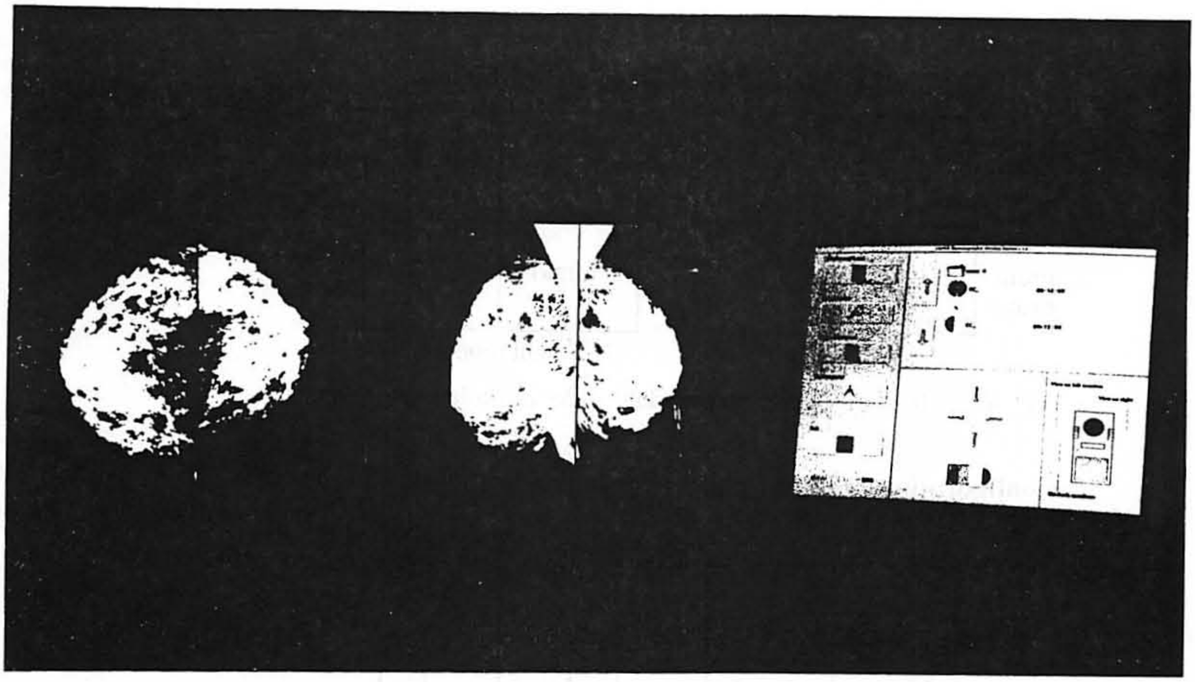

Figure 4 The 2K Station Showing four Subsampled Mammograms

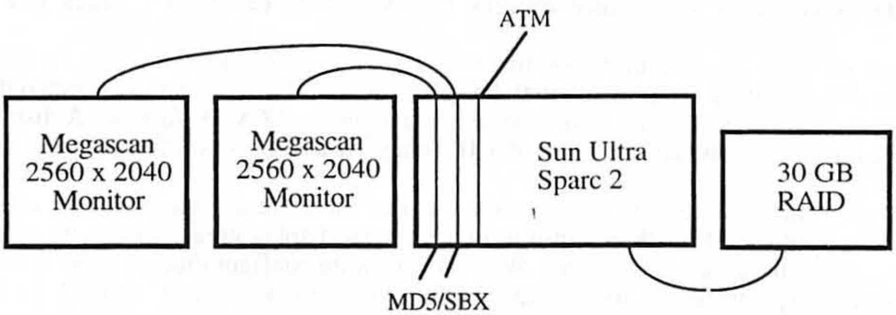

Figure 5 Schematic of the new 2K mammography display workstation

Display Modes

A standard mammographic examination consists of a craniocaudal and mediolateral oblique view of each breast, a total of four images per examination. For comparison purposes, four images from a prior examination of similar views are also used. Therefore, an optimal display mode shows eight images in proper orientation with one key stroke. Since two 2K image monitors is used for this study, we are developing display software to partition the two monitors into the following two configurations shown in Figure 6.

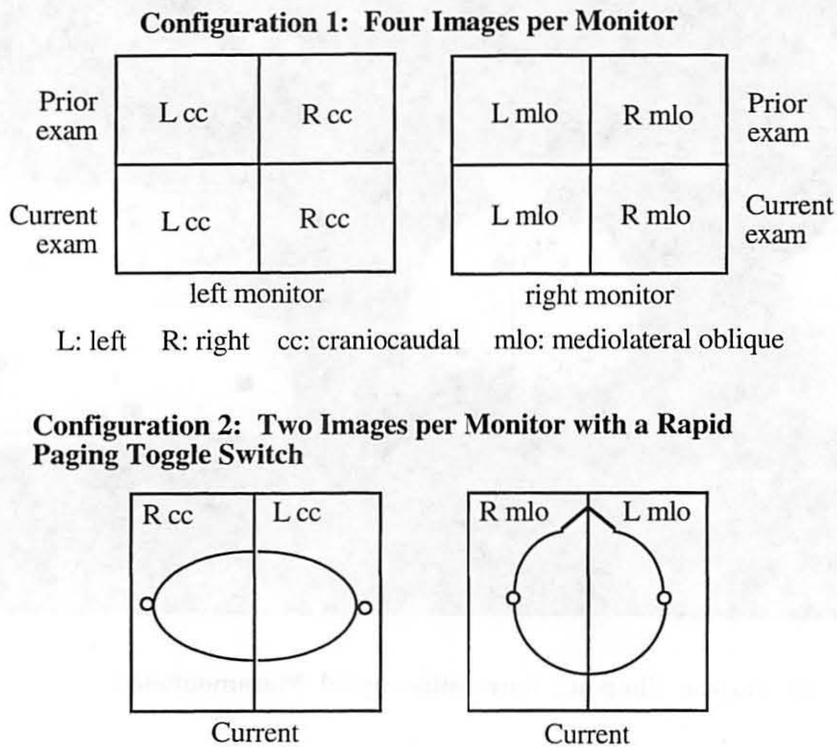

Figure 6 Display Mode (1) Four Images Per Monitor; (2) Two Images Per Monitor

A disadvantage of the first configuration is that each image will be limited to 1K x 1K pixels. To remedy this drawback we also developed a toggle switch in the display station allows the cursor-selected display of a 2K x 2K image on the other monitor that does not show the selected image in 1K x 1K format. A display program also allows the use of a 2K monitor to display a portion of a 4K image by using a scroll function.

The second configuration takes advantage of the fact that most breast images can be fitted into a narrow rectangle. Thus, we can split the 2K x 2K monitor in two 2K x 1K display areas. Four subsampled size images with proper cropping can be displayed at one time. With the hardware configuration, we can develop rapid paging software to switch current to prior examination images of the right or the left breast within 1.5 second. Again, an option can also be used to scroll a 4K image.

Optimization of Visual Image Quality

Image pre-processing is necessary to optimize the presentation of both the spatial and gray level data display on the display station. We developed three functions for special display of digital mammograms. The first algorithm optimizes the default brightness and contrast of FFDDM images presented on the display station. A preprocessing algorithm determines the histogram of each image. The 5% and 95% cumulative histogram values is used to generate the initial mean and window for the display of these images.

The second algorithm blackens all pixels beyond the x-ray collimators and outside the boundaries of the radiation field. An edge detection algorithm automatically delineates the boundaries of the radiation field. These boundaries are tested to determine if any portion of the radiation field has been excluded based on gray value deviation -- background is characterized by low deviations and the radiation field is characterized by higher deviations. The third algorithm automatically corrects the orientation of the mammogram based on left versus right side as well as specific mammographic projection.

3. RESEARCH PROTOCOLS

Our research in telemammography investigates three protocols in telediagnosis, teleconsultation and telemanagement. To complete these protocols will take three years. In this section, we summarize these protocols with emphasis in case selection and the "truth" determination.

Telediagnosis

This protocol tests the clinical effectiveness of telemammography from image transmission of full-field direct digital mammograms versus on-site interpretation of conventional film-screen mammograms.

Normal and abnormal cases are acquired from mammographic examinations done at MZH involving both film-screen and full-field direct digital images. For abnormal cases, a study is considered to be the craniocaudal and mediolateral oblique views of the abnormal breast (both the film-screen and full-field direct digital mammograms) taken in a single procedure. For normal cases, a study is considered to be the craniocaudal and mediolateral oblique views of one of the normal breasts (both the film-screen and full-field direct digital mammograms) taken in a single procedure. Case selection is made by a highly skilled mammographer based on the interpretation of bilateral film-screen mammograms by that mammographer. Putatively normal cases is selected from a pool of current bilateral film-screen mammography examinations for which we also have normal mammograms in our files from at least 2 years previously. An effort is made to select abnormal cases which in the opinion of the mammographer are considered subtle. The "truth" of the abnormal and normal cases is determined by subsequent pathologic diagnosis if biopsy is performed, or (for normal cases) by subsequent demonstration of mammographic stability over the next 2 years.

A total of four hundred (400) cases will be collected, so that a range of 40% - 60% of normal-versus-abnormal cases are included in the study. Comparison is made between interpretation of film-screen images and interpretation of transmitted FFDDM images using either the monitor display or 4K x 5K laser-printed hard copy. The procedure is as follows:

1. Film-screen mammograms is interpreted by general diagnostic radiologists at ACC.

2. At the diagnostic center (MZH), radiologists with expertise in mammography makes diagnoses of transmitted full-field direct digital images using soft copy display and laser-printed hard copy. Neither group of radiologist-interpreters has access to knowledge of the proportion of normal to abnormal cases in the test set.

3. Diagnostic results from both MZH and ACC is tabulated with respect to the known abnormal and normal cases shown in Table 3.

Table 3 Comparison Between MZH Radiologists and ACC Mammographers' Performance

ACC	MZH	TRUTH			
(1)	(2)	Abnormal		Normal	
		Frequency	Probability	Frequency	Probability
Abnormal	Abnormal	N_{11}	P_{11}	N_{01}	P_{01}
Abnormal	Normal	N_{12}	P_{12}	N_{02}	P_{02}
Normal	Abnormal	N_{13}	P_{13}	N_{03}	P_{03}
Normal	Normal	N_{14}	P_{14}	N_{04}	P_{04}
Total			π		**$1-\pi$**

Where P_{11} is the probability of both ACC radiologists and MZH mammographers diagnosed the "true abnormal" cases as abnormal; P_{12} is the probability of the ACC radiologists diagnosed the "true abnormal" cases as abnormal, whereas the MZH mammographers diagnosed them as normals; etc.;

P_{04} is the probability of both ACC radiologists and MZH mammographers diagnosed the "true normal" cases as normal; etc.

Once this table is set up, the sensitivity and specificity at ACC and MZH can be defined as

Sensitivity (ACC) = $(P_{11} + P_{12}) / \pi$
Specificity (ACC) = $(P_{03} + P_{04}) / (1-\pi)$, and
Sensitivity (MZH) = $(P_{11} + P_{13}) / \pi$
Specificity (MZH) = $(P_{02} + P_{04}) / (1-\pi)$

The null hypotheses to be tested are:

H_0: Sensitivity (ACC) = sensitivity (MZH) is equivalent to
H_0: $P_{12} = P_{13}$, and
H_0: Specificity (ACC) = specificity (MZH) is equivalent to
H_0: $P_{03} = P_{02}$

The chi-square test with 1 degree of freedom (d.f.) as described by Bennett [13]: $\chi^2 = (N_{12}-N_{13})^2 / (N_{12}+N_{13})$ with 1 d.f. is to be used to test the null hypothesis that the two sensitivities are equal versus the alternative that they differ. Estimates of sensitivity can then be calculated for MZH and ACC. Similarly, the null hypothesis that the two specificities are equal can be tested with a chi-square test: $\chi 2 = (N_{02}-N_{03})^2 / (N_{02}+N_{03})$ with 1 d.f.

This protocol tests the hypothesis that image interpretation by expert mammographers using telemammography procedure is as effective, if not better, than conventional film-screen interpretation by general diagnostic radiologists.

Teleconsultation

This protocol tests the efficacy of the previously validated image transmission and display procedure discussed in telediagnosis, used for remote consultation on **problem cases**. The aim here is to evaluate the ability of telemammography to facilitate real-time consultation between on-site general diagnostic radiologists and remotely-located expert mammographers. Currently, such consultations are tedious, time-consuming, and logistically complex, to the point where they usually are reserved for only the most confusing cases. If successful, teleconsultation should enhance the consultative process such that it becomes much more widely utilized, thereby bringing mammographic interpretive expertise to bear at the community practice level. Selected mammography examinations from ACC are chosen by the general radiologist doing mammography interpretations there, for second opinion by mammography specialists at MZH. The criterion for case selection is unresolved problem(s) in interpretation or management that require additional consultation. Past experience at MZH with non-teleradiology consultations from general radiologists at both ACC and community-practice settings, indicates that at least 20% of cases are interpreted as normal or benign after MZH consultation. Review at MZH involves transmitted full-field direct digital images from the affected breast, employing both monitor display and hard copy display.

We assume that an expert mammographer will always be in attendance at the diagnostic center (MZH), but that only general radiologists will be at the satellite station. Figure 6 shows the teleconsultation chain, which is also used for telemanagement. The steps are as follows:

1. Mammography cases for teleconsultation is selected by radiologists at ACC, once initial film-screen image interpretation has been recorded. After completion of the film-screen mammography, informed consent will be obtained from patients for two additional real-time full-field direct digital mammograms of the affected breast (in the same craniocaudal and mediolateral oblique projections just used for film-screen mammography). These images will be archived in the overall mammography data base. The data base is transparent to users in the sense that it will provide the necessary images upon request regardless of the requested site.

2. An expert mammographer at MZH diagnoses the study, and results is to be appended automatically to the film-screen study in the data base.

3. When a teleconsultation is requested, both sites will call up the same set of digital images simultaneously and discuss the case using soft-copy display. During the consultation, both parties can move a two-way cursor independently to highlight any suspicious sites. If necessary, a digital hard copy can be printed to further aid the consultation at MZH.

4. Updated diagnoses will be appended in the data base and old diagnoses will be revised. A tag will be added to the revised diagnosis for future reference.

5. The "truth" determination for cases selected for the teleconsultation study is in two stages for the abnormal and normal. Radiologic-pathologic correlation will be done for all cases for which tissue diagnosis is obtained. The "truth" for this set is therefore determined. The remaining cases, all interpreted as benign or probably benign after teleconsultation, will be confirmed in two ways. First, all cases will undergo periodic mammographic surveillance for 2 years, after which time mammographic stability will establish benignity or interval change will have prompted tissue diagnosis, and therefore pathologic proof. Second, we will track these cases retrospectively to determine if they are follow-up studies from existing over-2-year-ago examinations which had been interpreted as benign. Thus, the "truth" of benignity of a case will be determined based on either historical comparison or waiting for a period of 2 years starting from the date of examination.

Similar evaluation methodology described in Telediagnosis with the comparison between ACC radiologists and MZH mammographers (Table 3) will be used.

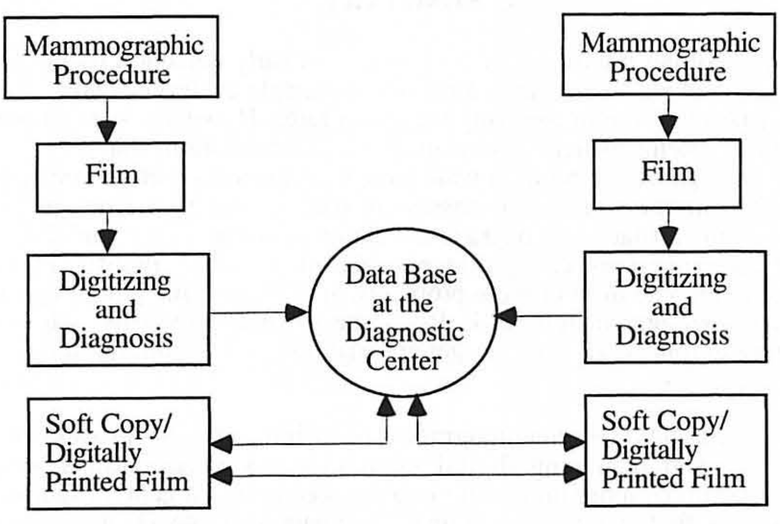

Figure 6 Teleconsultation Procedure

Telemanagement

This protocol tests the efficacy of the previously validated image transmission and display procedure discussed in Telediagnosis, but now used for **remote real-time management and interpretation** of mammography examinations. The goal of telemanagement is even more ambitious than that of teleconsultation, to completely replace the on-site general radiologist with remotely-located expert mammographers. To evaluate the ability of telemammography to permit remotely guided interpretation and work-up, the accuracy of mammographic interpretations made on site at ACC by general radiologists is compared with those made remotely but interactively in real-time by expert mammographers at MZH. Unselected ACC mammography examinations (both screening and problem-solving cases), acquired using conventional screen-film techniques, are read by the general radiologist doing mammography interpretations there, according to normal operating procedure, including the taking of any additional images that are thought to be necessary. Interpretations will be completed prior to telemanagement. Informed consent then is obtained from patients for two additional real-time full-field direct digital mammograms of one breast (in the same craniocaudal and mediolateral oblique projections just used for film-screen mammography). The affected breast is studied if the film-screen interpretation was abnormal, one breast is selected randomly if the film-screen interpretation was normal. Before each patient is sent home, the digital images are transmitted to a mammography specialist at MZH, who decides either to interpret the examination as submitted, or to request additional views to complete the mammographic work-up and then interpret the examination. The MZH-based mammographer is blind as to the interpretation rendered by the ACC radiologist and as to whether any additional images were requested by the ACC radiologist. The general radiologist's on-site interpretation of film-screen images are compared with the mammography specialist's interpretation of digitized transmitted, "tele-managed" images.

"Truth" determination for the cases for the telemanagement protocol is similar to that in teleconsultation. Malignancy will be determined by radiologic-pathologic correlation after tissue diagnosis. Benignity is determined either by radiologic-pathologic correlation after tissue diagnosis (if available) or by 2-year-old historical comparisons and by subsequent periodic mammographic surveillance for 2 years. In both latter situations, mammographic stability is used to establish the benignity of a lesion.

With the "truth" determined, similar evaluation methodology to that described in Telemammography will be used, involving sensitivity and specificity tables comparing the performance of ACC radiologists and MZH mammographers (Table 3).

4. SUMMARY

Current attempts at controlling breast cancer concentrate on early detection by means of mass screening, using periodic mammography and physical examination, because ample evidence is now available to indicate that such screening indeed can be effective in lowering the death rate. However, state-of-the-art mammography utilizes film-screen recording systems, which have several technical limitations that reduce its effectiveness: the film gradient must be balanced against the need for wide latitude and detection of microcalcifications. In addition, portrayal of the clarity of the margins of breast masses are reduced due to the presence of film noise in the displayed image, film processing artifacts can degrade the mammographic image, and the day-to-day variability inherent in automated film processors can produce suboptimal image quality. Full-field direct digital mammography promises to overcome most of these problems, at the same time providing additional features not available with standard mammographic imaging [14]. Real-time Telemammography adds to these advantages the utilization of expert mammographers (rather than general radiologists) as interpreters of the mammography examinations.

The specific aim of FFDDM telemammography is to integrate the process of acquiring, storing, communicating, visualizing, and managing digital mammography examinations within the operational environment of an expert-mammographer diagnostic imaging center and a general-radiologist mammography practice. We have described the first phase in setting up the telemammography chain as well as the three research protocols in telediagnosis, teleconsultation, and telemanagement.

ACKNOWLEDGMENTS

This research is partially supported by the California Breast Cancer Research Program: "Real-Time Telemammography" IRB-0148), the US Army Medical Research Material Command: "Full-field Direct Digital Telemammography (DAMD-96-C-6111) and "A Digital Breast Imaging Teaching File (USAMRMC DAMD17-94-J-4196), and the National HPCC Program, National Library of Medicine: A High-Performance Testbed Network for Collaborative Health Care (N01-LM-4-3508). The authors would like to thank M. Tesic and M. Piccaro of Fischer Imaging Corporation for their contributions, and James Sayre of UCLA for the experimental design.

REFERENCES

[1] Boring CC, Squires TS, Tong T. 1992. *Cancer Statistics.* CA; 42:19-38.

[2] Sickles EA. 1993. Current Status of Digital Mammography. *In* Proceedings of the 7th International Congress on Senology (Excerpta Medica International Congress Series). Amsterdam, Elsevier.

[3] Nelson MT. 1995. A Clinician's View of Digital Mammography. Proc. 4th Intern. Conf. Imag. Management and Comm. (IMAC 95).

[4] Toker E. and M. Piccaro. 1993. Design and Development of a Fiber Optic TDI CCD-Based Slot-Scan Digital Mammography System. *SPIE Proceedings*, Medical Imaging, 2009.

[5] Lou SL, Huang HK, Breant CM. 1992. A 2K Radiological Image Display Station. *Radiology* 185(P), 146.

[6] Huang H.K. 1996. Teleradiology Technologies and Some Service Models. *Comp. Med. Imaging & Graphics* 20:59-68.

[7] Fajardo LL, Yoshino MT, Seeley GW, et al. 1990. Detection of Breast Abnormalities on Teleradiology Transmitted Mammograms. *Invest Radiol.* 25: 1111-1115.

[8] Sickles EA, Ominsky SH, Sollitto RA, Galvin HB, Monticciolo DL. 1990. Medical Audit of a Rapid-throughput Mammography Screening Practice: Methodology and Results of 27,114 Examinations. *Radiology.* 175-323-327.

[9] Sickles EA. 1992. Quality Assurance: How to Audit your Own Mammography Practice. *Radiol Clin North Am.* 30:265-275.

[10] Huang HK. 1996. Clinical Experience with a Second-Generation Hospital-Integrated Picture Archiving and Communication system. *Journal of Digital Imaging* 9:151-166.

[11] M Moskowitz, J Wang, HK Huang, E Sickles, J Allen, A Giles. 1995. High Resolution Display System for Mammograms. *Proc. SPIE Medical Imaging* 2431-44.

[12] SL Lou, E Sickles, J Wang, HK Huang. 1994. A High Resolution Display System for Mammograms. *Radiology,* 193(P), 474.

[13] Bennett BM. 1985. On Tests for Equality of Predictive Values for t Diagnostic Procedures. *Stats. in Med.* 4:535-539.

[14] Tesic M. and Piccaro M.F. 1996. Digital Mammography Scanner: Performance Characteristics and Preliminary Clinical Results. The Institute of Electrical Engineers, *IEEE*, Savoy Place, London WC2R OBL, UK, pp. 3/1-3/7.

EUROPEAN JOURNAL OF
RADIOLOGY

ELSEVIER

European Journal of Radiology 22 (1996) 165

Editorial

Towards the digital radiology department

H.K. Huang[1]

Laboratory for Radiological Informatics, Department of Radiology, University of California, San Francisco, 530 Parnassus Avenue, San Francisco, CA 94143-0628, USA

To operate a digital radiology department requires a hospital-integrated picture archiving and communication system (HI-PACS) and teleradiology. PACS is a concept perceived in the early 1980s by the radiology community as a future method of practicing radiology. PACS and teleradiology consist of image acquisition devices, storage archiving units, display workstations, computer processors and database management systems. These components are integrated by a communication network system. During the past 10 years, technologies related to these components became mature and their applications have gone beyond radiology to the entire health care delivery system. As a result, PACS and teleradiology for special clinical applications as well as large scale hospital-wide PACS are being installed throughout the United States, European countries, and the world.

During the past 12 years, we have witnessed some major contributions in advancing the PACS development. Technically, the first laser film digitizers developed for clinical use by Konica and Lumisys, the development of computed radiography (CR) by Fuji and its introduction from Japan to the United States and Europe by Dr William Angus of Philips Medical Systems, and the large capacity optical disk storage by Kodak and others, all are critical. Others include the parallel transfer disk technology, 2000-line and 72-Hz display monitors, system integration methods developed by Siemens Gammasonics and Loral for large scale PACS, the DICOM Committee's effort in standardization, and the asynchronous transfer mode (ATM) technology for merging local area network and wide area network communications.

In terms of events, the annual SPIE PACS and Medical Imaging meeting in the USA, and the EuroPACS are the continuous driving force for PACS. In addition, the Computer Assisted Radiology (CAR) meeting every 2 years organized by Professor Heinz Lemke, and the Image Management and Communication (IMAC) Conference organized by Dr Seong K. Mun, provide the forum for international PACS discussion. The InfoRAD Section at the RSNA since 1993 organized by Dr Laurens V. Ackerman with the live demonstration of DICOM interface sets the tone for industrial PACS open architecture. The annual refresher course in PACS during RSNA organized first by Dr C. Douglas Maynard and then Dr Edward V. Staab provide continuing education in PACS and teleradiology to the radiology community.

Professor Michel Osteaux's 1992 edited book *Second Generation PACS* provided a vision that PACS is moving towards a hospital integrated approach. Dr Roger A. Bauman's assuming the Editor-in-Chief position of the then new journal, *Digital Imaging*, allows the consolidation of PACS and teleradiology research and development publications. U.S. Colonel Fred Goeringer instrumented the Army MDIS project resulting in several large scale PACS installations which provide a major stimulus and funding for the PACS industry.

This special edition of *European Journal of Radiology* devoted to *Towards the digital radiology department* is timely in reinforcing the importance of hospital integrated PACS and teleradiology in the practice of radiology in Europe.

[1] Fax: +1 415 5023217.

0720-048X/96/$15.00
PII: S0720-048X(96)00775-9

Pergamon

Computerized Medical Imaging and Graphics, Vol. 20, No. 4, pp. 187–188, 1996

0895-6111/96 $15.00 + .00

PII: S0895-6111(96)00011-0

EDITORIAL

Stephen T. C. Wong and H. K. Huang
Laboratory for Radiological Informatics, University of California San Francisco, CA 94143-0628, USA

During an editorial advisory board meeting held in Chicago RSNA (Radiological Society of North America) in 1994, several members felt strongly that informatics has become an emerging field of importance in medical imaging and suggested that several issues on various informatics topics should be developed. Among the topics is medical image databases. Professor Robert S. Ledley, the Editor-in-Chief, asked if we would be interested in serving as the guest editors since we are active in this area of research. We were delighted to accept his offer and would like to thank him for providing such an opportunity.

This special issue on medical image databases witnesses a new, evolving development of biomedical imaging. Medical image databases are inherently multidisciplinary. As Shiffman and Shortliffe have stated in their foreword of this special issue, the convergence of technologies of image management and textual data management is leading to the development of a new set of relationships between the biomedical imaging and informatics communities. Shiffman and Shortliffe described the importance of image information management for efficient delivery of health care and the necessity and opportunities in sharing data and applications between imaging and clinical information systems. Before all these, however, they pointed out that efforts are required to stimulate collaborations, joint training, and cross publications between medical imaging and medical informatics communities. This special issue vividly substantiates their observations. The invited articles represent a synergy among leading workers of the biomedical imaging, computer science, and clinical communities in developing this new kind of information system.

Medical image database are comprised of several major components: system architecture, image and data acquisition, feature extraction, data modeling, content-based retrieval, query languages, and workstation user interface. Among these components, content-based image retrieval attracts attention from every area of applications involving images. Content-based image retrieval requires sophisticated image processing. We witness that those works developed by many researchers since the early 1970s now bear fruit for image database research. The IEEE Computer Society Journal devoted a special issue to this topic in September 1995. However, none of the articles in that issue addressed requirements and applications in biomedical imaging. This timely issue provides a comprehensive view of current research activities of image databases in medical imaging.

The work reported in this special issue can be broadly categorized into four areas: content-based indexing; system design and architecture; data modeling; and temporal image databases. Content-based indexing constitutes one of the most important challenges of medical image databases. Several research groups are addressing this topic under a variety of approaches. Orphanoudakis, Chronaki and Vamvaka from Greece discussed a network of servers that can provide content-based query services through a World Wide Web server. They proposed description types for the representation of image content and presented performance results of a description type implemented in their network. Robinson, Tagare, Duncan and Jaffe of Yale proposed a similarity measure and an indexing mechanism for non-rigid comparison of image shape using KD-Tree algorithms. They tested their shaped-based retrieval techniques on a database containing 85 cardiac MR images. S.K. Chang introduced the new concept of active index for content-based retrieval of medical images. The applications of the active index included image prefetching and similarity matching. Bucci and colleagues proposed a content-based search engine for tomographic image databases based on the Kahrunen–Loève transform. They aimed to integrate the search engine into a radiologic image databases developed in the earlier European Union's Telemed effort for references and education purposes. Khan and Yun from Hawaii presented a drastically different mechanism. Rather than relying on symbolic representation of image content to mediate the search, they incorporated the concept of holographic associative memory into computation form to facilitate image retrieval by content.

At the systems level, Thoma, Long and Berman described a client/server system prototype developed at the National Library of Medicine for accessing multimedia biomedical databanks through the ubiquitous Internet. The challenge is to provide access to both the images, i.e. X-rays, CT and MR, and associated data by a global community for broad range of biomedical applications and research. Arya, Cody, Faloutsos, Richardson and Toga described a prototype database system developed at IBM to query and visualize 3D spatial data, focusing on the mapping of structural and functional relationships of the brain. They listed the requirement of the application, discussed the database design issues, and presented timing results of their experiments. Wong and Huang described their effort in designing and implementing vertically integrated medical image database systems. The approach they used is to integrate content-based indexing and knowledge-based techniques within the picture archiving and communication systems to make the whole image data useful in medicine. They discussed research issues and provided examples from applications implemented in the hospital integrated PACS environment at the University of California, San Francisco.

For modeling of medical image data, Adam, Holowczak and Li advocated the object-oriented approach and proposed the notion of object manifestations of medical image objects in a heterogeneous client computing environments. They provided examples of how to apply constraints and rules to represent data within objects and to cater for variations in computer platforms, networks, and user preferences. Aubry, Chameroy and Di Paola of INSERM, France, presented a more formal specification for the logical design of medical image databases, drawing on their experience in the European MIMOSA project. They tested their data model in two projects on medical image communication and image processing monitoring.

The ability to define and track temporal relation in images and related data is becoming an essential component of medical image databases. Cardenas and his UCLA colleagues in the departments of radiology and computer science presented a multimedia medical database model to support timeline-based presentation of information. A proof-of-concept prototype was developed for thoracic oncology and thermal tumor ablation therapy of the brain. Zhu, Kim, Wong, Soo Hoo and Huang, on the other hand, described a different model of temporal image database system with the ability to quantitate and monitor the progress of lung cancer of a patient under therapy treatment. Even for similar medical problems, it is interesting to observe that the former project took the perspective of database management while the latter emphasized the role of medical image processing.

Medical image databases is a rapidly growing field that has the potential to change the practice and research of biomedical imaging and to improve the efficiency of health care delivery in the coming decades. This special issue serves as an initial effort to bridge the gap between the biomedical imaging and informatics communities in addressing this new development. Finally, we would like to thank Mrs Blaire V. Mossman, Managing Editor, for guiding us through the process of getting this issue in order.

Pergamon

Computerized Medical Imaging and Graphics, Vol. 19, No. 3, pp. 251–259, 1995

0895-6111/95 $9.50 + .00

0895-6111(95)00005-4

COMPUTER-ASSISTED BONE AGE ASSESSMENT BASED ON FEATURES AUTOMATICALLY EXTRACTED FROM A HAND RADIOGRAPH

Ewa Pietka

University Hospital of Geneva, Medical Imaging Unit, 24, Rue Micheli-du-Crest, CH-1211 Geneva, Switzerland

(Received 26 May 1994; revised 14 September 1994)

Abstract—This paper presents a computer-aided classification algorithm to assist the radiologist in the bone age assessment of pediatric patients. The classification is based on features automatically extracted from two regions of Computed Radiography (CR) left hand wrist images: phalangeal region of interest (PROI) and carpal bone region of interest (CROI). Due to imprecise nature of the bone age assessment problem, a fuzzy classifier for both regions has been developed. After defining a membership function for each region, features are processed yielding a matrix which maps the set of features to a year of age within the predefined range. The grades of membership are described as membership function values in the interval [0, 1]. A classification rule based on a max-sum operator, processes the matrix assessing the bone age. Since both regions are analyzed independently, two bone age assessments are obtained. They reflect the phalangeal and carpal bones maturity individually. In pathological cases the discrepancy between both assessments may reach as much as 2 yr.

Key Words: Pediatric radiology, Skeletal age assessment, Feature selection, Fuzzy classifier

1. INTRODUCTION

Bone age assessment is a procedure frequently performed in pediatric radiology. Based on a radiological examination of skeletal development of a left hand wrist, the bone age is assessed and then compared with the chronological age. A discrepancy between these two values indicates abnormalities in skeletal development. However, there is no method accepted by radiologists as a standard. The most commonly used method (76%) (1) is the atlas matching method by Greulich and Pyle (2). Based on this method, a left hand wrist radiograph is compared with atlas patterns. The pattern which superficially appears to resemble the clinical image is selected. Since each pattern is assigned to a certain year of age, the selection assesses the bone age. However, there is still concern about the deviation in estimating the age. The disadvantage of this method is a subjective nature of the analysis performed by various observers with different levels of training. Another technique relies on a trained observer applying the Tanner and Whitehouse (TW2) method (3). This method uses a detailed analysis of each individual bone which leads to its description in terms of scores. Unfortunately, the complexity of this method prevents the rate of its application from exceeding 20%. The above presented remarks show that it is worthwhile to develop a computerized system to assist the radiologists in performing a more objective and accurate analysis.

No attempt has been made so far to computerize the bone age assessment. However, some efforts have been made in the measurement field. Michael and Nelson (4) have described a model-based computer vision system in which they have segmented-out specific phalanges and measured four parameters: perimeter, area, length of the major and minor axis. Levitt and Hedgcock (5) have applied the Bayesian inference technique to extract edges, regions, vertices, and relevant image features.

This paper presents part of a computer-aided bone age assessment study. The analysis is performed on a Computed Radiography (CR) hand wrist image. In this study three steps can be distinguished: preprocessing, feature extraction, and classification. *Preprocessing* (6) standardizes the image in terms of its background and orientation. The background standardization (7) removes parts of the image caused by blocking of the collimator during the exposure. The orientation procedure (6) rotates the image to a standard position viewed by radiologists. Due to examination conditions and the clinical environment, the standardization becomes a major problem. The CR cassette can be placed at various orientations to accommodate the examination condition. A survey in the pediatric radiology (6) shows that about 70% of images need the background to be removed and between 35–40% of procedures are not performed with a conventional image orientation.

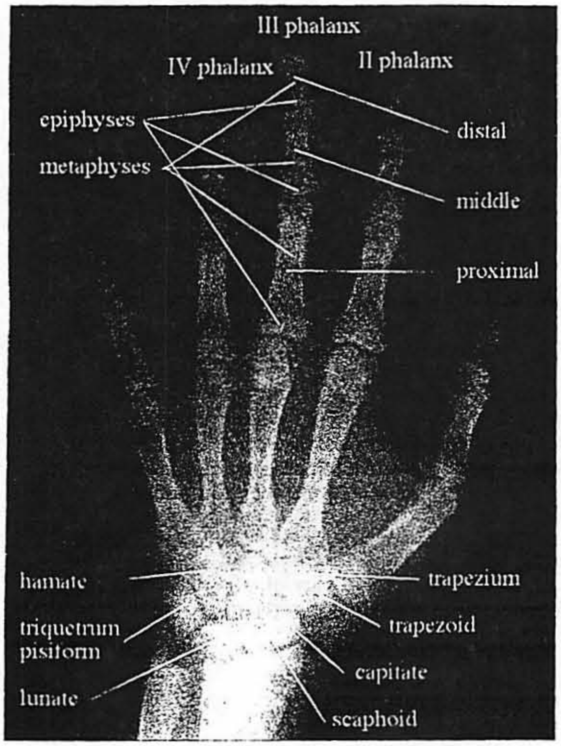

Fig. 1. Hand radiograph with anatomical structures of phalanges.

This shows the importance of this step before any computerized image analysis can be performed. This standardized image is subjected to *feature extraction* procedures performed on two regions individually. The phalangeal region of interest (PROI) containing epiphyses and metaphyses (Fig. 1) delivers epiphyseal and metaphyseal measures (8–10). The carpal bones region of interest (CROI) includes carpal bones (capitate, hamate, triquetrum, lunate, scaphoid, trapezoid, and trapezium in Fig. 1) which are separated and described in terms of features (11, 12). All features, automatically extracted, are subjected to a *classifier* (discussed in the paper) which assesses the bone age. Due to the imprecise nature of the bone age assessment problem and a possible mis-extraction of features, a fuzzy classifier has been developed.

The fuzzy theory has already been applied in different pattern recognition studies. Cluster analysis, based on partitioning a collection of data points into a certain number of groups is one of the fields frequently employing a fuzzy approach (13, 14). Since precisely defined boundaries between clusters often do not reflect real data, a fuzzy environment yields to its better description. A fuzzy approach has also been investigated as a tool for the classification of systems described by means of a decision tree (15, 16). Certain pattern classes of a hierarchical structure can be described by a formal grammar. Using fuzzy syntactic pattern recognition, handwritten capitals have been analyzed (17). Fuzzy algorithms have also been applied in the voice recognition field (18).

This paper presents a classification method which assesses the bone age based on features automatically extracted from a hand radiograph. First, features themselves are briefly summarized. For details on their extraction, the readers are referred to (8, 10, 11). Then, an approach using fuzzy theory is described. Fuzzy membership functions are defined for PROI and CROI individually. This leads to obtaining two bone age assessments: the phalangeal bone age (PBA) reflects the maturity of epiphyses and metaphyses, whereas the carpal bone age (CBA) reflects the carpal bones development. In pathological cases the discrepancy between both assessments may reach as much as 2 yr. The goals of this paper are: (i) to present a classification method able to process features, automatically extracted from a hand radiograph; (ii) to compare the bone age assessed computationally with a radiological estimation; and (iii) to compare the bone age assessed on the basis of two different hand wrist regions.

2. FEATURE SELECTION

There is no general approach to the problem of feature selection. Features should provide an adequate description of the pattern and be sensitive to the structural changes on the basis of which an image is classified. Thus, features applied to assess the bone age should reflect the morphological changes which are able to distinguish one developmental stage from the other, for example, the increase in size of epiphyses, tubular bones, or carpal bones. They may also point out an object or a change of an object which appears at a certain stage of development. The more accurate a feature is able to describe the changes between certain stages, the more reliable a classification result can be obtained. If features do not reflect the structural changes, no classifier of whatever sophistication can yield a reasonable result.

On the other hand, the features have to be extracted reliably (i.e., with a high rate of correct extraction) and cannot require too sophisticated and time consuming algorithms. It happens often that some features of a high discriminant power do not meet the above condition and cannot be extracted automatically. A recognition of a developmental stage (distinguished in the TW2 method (3)) in which the epiphysis caps the metaphysis can serve as an example. The feature

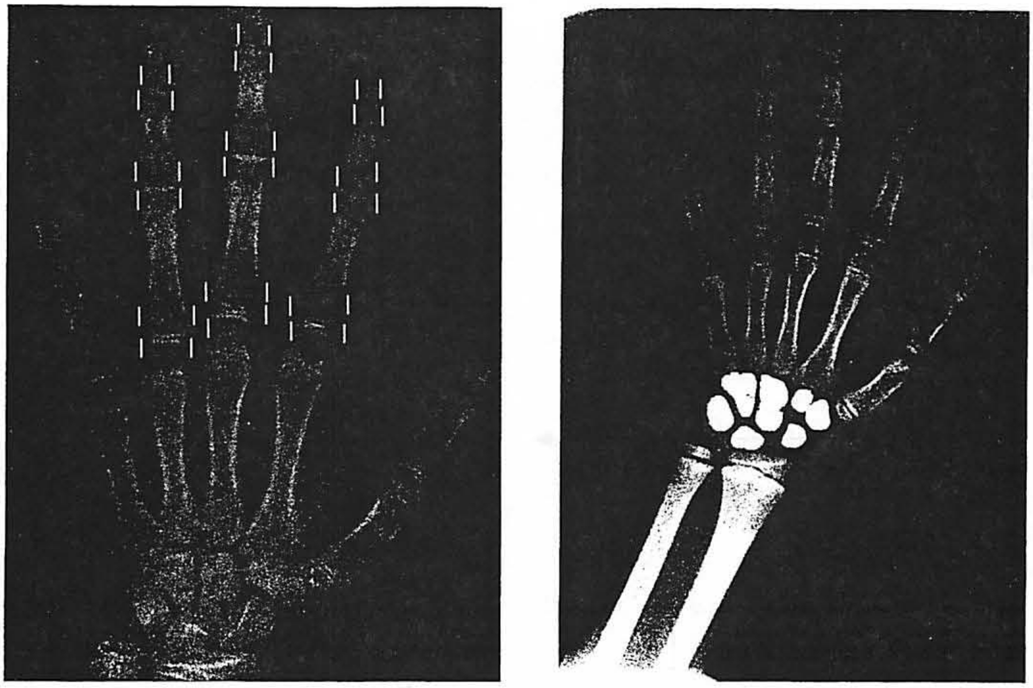

(a) (b)

Fig. 2. CR hand wrist image with (a) automatically extracted diameters, marked on the II, III, and IV phalanx; and (b) automatically extracted carpal bones superimposed on a hand radiograph.

selection step is then a compromise between the features discriminant power and the ability and reliability of their extraction. Therefore, the computerized approach often uses features which reflect the changes, yet, which have not been implemented in the clinical diagnosis.

In the phalangeal analysis three types of features have been extracted. The first type includes the length of distals, middles, and proximals. While applying the standard phalangeal length table (19) each measure can be assigned to a year of age. However, these measures do not appear to be reliable bone age indicators and are only used for a rough maturity assessment (8). The second type of features measures the diameters of epiphyses and metaphyses (distances between vertical lines in Fig. 2a). Since diameters themselves are sensitive to the size of the hand and its rotation during the examination procedure, their ratios have been calculated. This reflects to certain extent the classification done by Tanner and Whitehouse (3) who compare the epiphyseal size with the metaphyseal size. This is also a finding compared by some radiologists while applying the Greulich and Pyle method (2). In the clinical approach it is not a quantitative finding, yet, it is considered during the visual comparison of the radiographs with the atlas patterns. Plots of features clustered for each year of bone age (Fig. 3) show their different sensitivity to the hand development. The ratios of distal phalanges (Fig. 3a) are more sensitive to the growth of the hand in an early stage (up to 11 yr of age). Later the sensitivity decreases. Whereas, ratios of middle (Fig. 3b) and proximal (Fig. 3c) phalanges appear to have a reasonable sensitivity up to 13 yr of age. At the age of about 14 or 15 the fusion of epiphyses starts and the ratios do not change sufficiently enough to classify successfully the hand image and assess the bone age. The third type of the phalangeal features, again used only visually in the diagnostic procedure, describes the stage of epiphyseal fusion. In our study (20), this feature is quantified and assigned to one of four classes (no fusion, early fusion, advanced fusion, fusion completed).

Carpal bones (capitate, hamate, triquetrum, lunate, scaphoid, trapezoid, and trapezium) are another source of information in different methods of bone age assessment (21). Their development differs from the long tubular bones. In the early stage they appear as a dense pin point on a radiograph. While developing, they increase in size until finally they reach their optimal size and characteristic shape. In the developmental

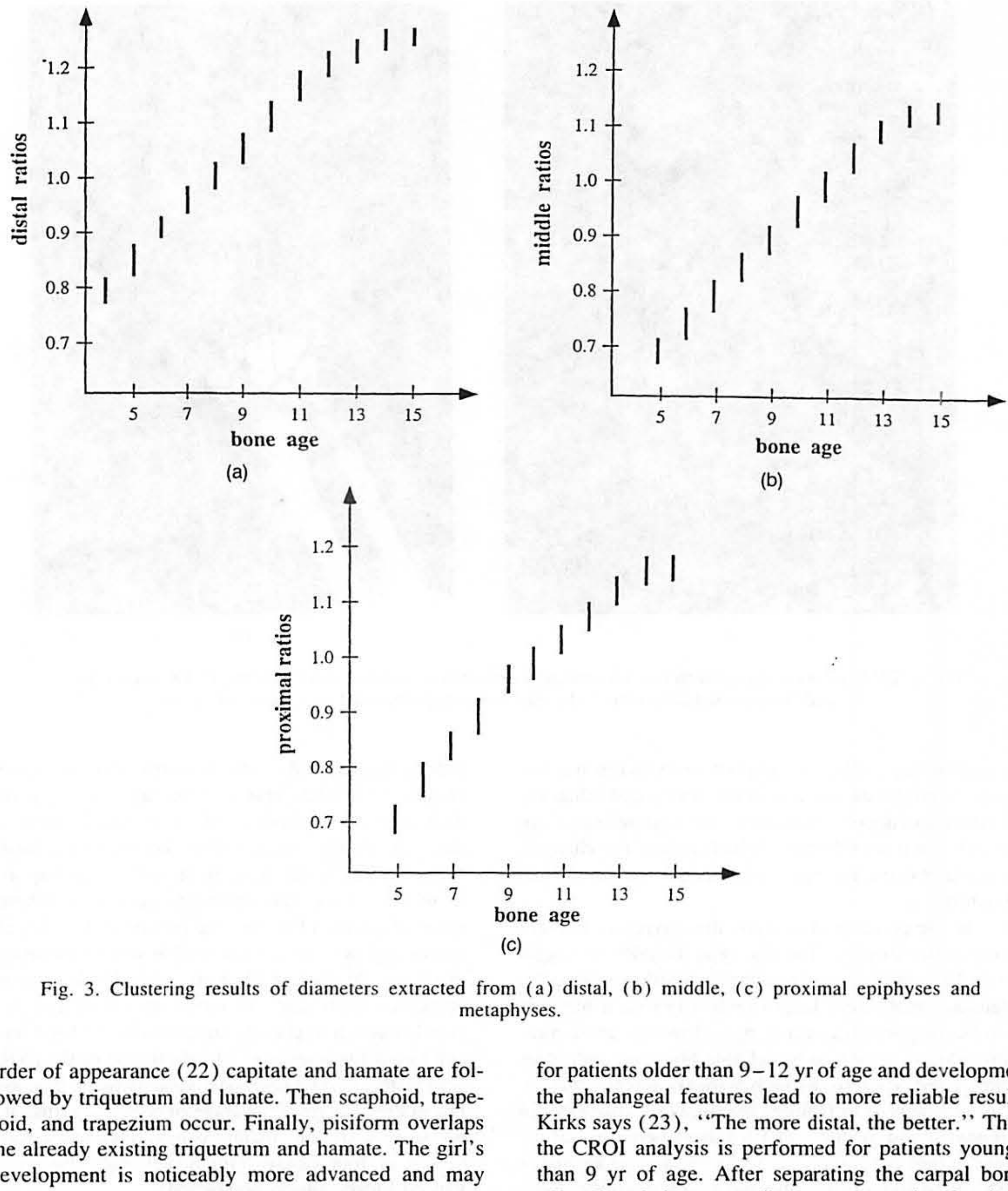

Fig. 3. Clustering results of diameters extracted from (a) distal, (b) middle, (c) proximal epiphyses and metaphyses.

order of appearance (22) capitate and hamate are followed by triquetrum and lunate. Then scaphoid, trapezoid, and trapezium occur. Finally, pisiform overlaps the already existing triquetrum and hamate. The girl's development is noticeably more advanced and may differ from boy's development as much as 3 yr.

In the early stage of development, the carpal bones appear on the radiograph individually. Their separation and description in terms of features is relatively simple. However, at the age of 9–10 they start overlapping. At this point, their separation becomes very difficult. Moreover, medical studies (21) have shown, that, due to the nature of carpal bone maturity, their analysis does not provide accurate and pertinent information for patients older than 9–12 yr of age and development the phalangeal features lead to more reliable results. Kirks says (23), "The more distal, the better." Thus, the CROI analysis is performed for patients younger than 9 yr of age. After separating the carpal bones (Fig. 2b), their area, perimeter, and a ratio of a single carpal bone area divided by the global area of all carpal bones are found (11).

In the classification phase, both regions (PROI and CROI) are considered individually. The PROI delivers nine features, namely, ratios of epiphyseal diameter divided by metaphyseal diameter for distals, middles, and proximals of the II, III, and IV phalanx. The number of features remains unchangeable for each radiograph. The CROI analysis yields three features for each carpal bone. Since the number of carpal bones increases during the developmental process, the overall number of features changes.

3. BONE AGE ASSESSMENT

In the final stage of the analysis a classifier has been developed to assess the bone age on the basis of extracted features. The classifier has to meet two conditions. Due to pathological changes, the features may exceed the limits defined for each year of age. Besides, all features have been extracted automatically with an accuracy of about 90%. This means, that on an average one feature extraction per image fails. This implies the first condition. The classifier can not be sensitive to an abnormal or mis-extracted feature.

The second condition to be met is imposed by the imprecise nature of the bone age assessment problem and, as a result, the imprecise definition of classes. The lack of a medically approved standard and a high objectivity of the clinical diagnosis performed by radiologists cause inter- and intra-observer variations ranging on an average from 0.37 to 0.6 yr (24). Different methods applied by radiologists lead also to different results.

These conditions are included in three types of inexactness (25). *Generality* features a concept applied to a variety of situation. This reflects the first condition. *Ambiguity* describes more than one distinguishable subconcept. This means, that there is more than one maximum of the membership function (membership functions are shown in the next section). *Vagueness* occurs when precise boundaries cannot be defined and functions take values other than just 0 and 1.

Since the described above recognition problem does not lend itself to a precise formulation, it requires imprecise techniques able to handle its inexactness. This justifies the selection of a fuzzy classifier which has been developed by defining membership functions and a classification rule.

3.1. *Membership function*

Let $X = \{x\}$ denotes a space of objects (or features). Then, a fuzzy set A in X is a set of ordered pairs $X = \{(x, \mu_A(x))\}$, $x \in X$, where $\mu_A(x)$ is a membership function. Intuitively, it defines the grade of membership of x in A. More precisely, it means that a membership function is a mapping from the set of features to a value from a predefined interval. We assume, that $\mu_A(x)$ is a number in the interval $[0, 1]$. The grade 1 denotes a fully membership, whereas, 0 refers to a nonmembership. The mathematical foundations of the fuzzy set theory are described in (25, 26).

The set of features, already defined in section 2, includes features extracted from two regions of interest, the PROI and the CROI. Since both can be analyzed independently leading to two bone age assessments, their classification is also performed individually. Thus, for both ROIs membership functions have been developed independently.

Definition of membership functions is based on an operator

$$\chi(a, b, x) = 1/(1 + a^*(x - b)^2). \quad (1)$$

which can be considered as a membership function component for a single year of age (a and b are parameters), a single feature (x is a variable), a single object (bone). While applying the operator to calculate the phalangeal membership function for a certain range of the year of age $(1, \ldots, n)$, it results in a vector

$$\boldsymbol{\alpha}(\mathbf{a}, \mathbf{b}, x) = \begin{bmatrix} \chi(a_1, b_1, x) \\ \vdots \\ \chi(a_n, b_n, x) \end{bmatrix}. \quad (2)$$

The extension to a multiple feature environment gives a matrix

$$\boldsymbol{\beta}(\mathbf{a}, \mathbf{b}, \mathbf{x}) = [\boldsymbol{\alpha}(\mathbf{a}, \mathbf{b}, x_1) \cdots \boldsymbol{\alpha}(\mathbf{a}, \mathbf{b}, x_m)]. \quad (3)$$

where m is the number of features.

While multiple objects (bone) occur, the matrix in eqn. 3 is extended to

$$\boldsymbol{\mu}(\mathbf{a}, \mathbf{b}, \mathbf{y}) = [\boldsymbol{\beta}(\mathbf{a}, \mathbf{b}, \mathbf{x}_1) \cdots \boldsymbol{\beta}(\mathbf{a}, \mathbf{b}, \mathbf{x}_k)]$$

where k is the number of objects $\mathbf{y} = [\mathbf{x}_1 \cdots \mathbf{x}_k]$. (4)

Parameters a and b are found on the basis of a training set. After being analyzed by a radiologist, images are grouped on the basis of patients bone age. This permits the extracted features to be clustered. Due to imprecise nature of this problem the neighbor clusters overlap. In order to define the boundaries (of fuzzy nature) between each cluster, distances between features and the center of the cluster are calculated and 10% of the features located close to borders of the cluster are excluded. This operation reduces the overlapped area, yet, in most cases does not eliminate it (Fig. 3). If it remains, the center of the common cluster between age j and age $j - 1$ is found. If two neighbor clusters are separated, then a point equally distant from the central points of both clusters is found. For each cluster two such points are located (one on each side). They serve as crossover points d_j and d_{j-1} (membership function value is equal to 0.5). These yields to a set of equations

$$\chi(a, b, d_j) = 0.5$$
$$\chi(a, b, d_{j-1}) = 0.5 \quad (5)$$

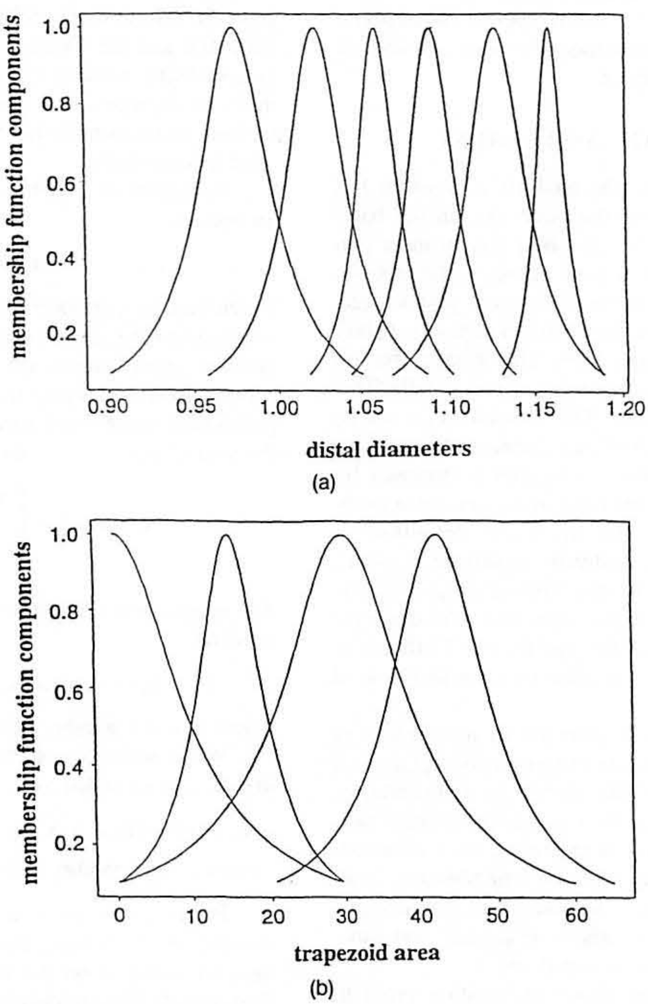

Fig. 4. Membership function components defined on the basis of (a) distal diameters for 8--13-yr-old patients and (b) area of trapezoid for 4–9-yr-old patients.

whose solution fixes the values of parameters a and b for each membership function component. As an example, membership function components defined on the basis of distal diameters of patients between 8 and 13 yr of age are shown in Fig. 4a.

Although the carpal bone membership function is also based on the operator defined in eqn. 1, the format of α differs. This is caused by the developmental order of appearance of carpal bones. Their development differs from the development of long tubular bones. In the early stage they appear as a dense pin point on a radiograph. While developing, they increase in size until finally they reach their optimal size and characteristic shape. In the developmental order of appearance (Fig. 1) capitate and hamate is followed by triquetrum and lunate (at the age of 3 or 4). Then, scaphoid, trapezoid, and trapezium occur (at the age of 5 or 6). Thus, in the CROI analysis not all carpal bones exist in the early stage. As a result, not all features have to be present at each year of age. This means, that the number of membership function components in eqn. 2 differs. Thus, α is defined as

$$\alpha(a, b, x) = \begin{bmatrix} 0 \\ \vdots \\ \chi_c(a_{j-1}, x) \\ \chi(a_j, b_j, x) \\ \vdots \\ \chi(a_n, b_n, x) \end{bmatrix}. \qquad (6)$$

The dependency of j from the object is related to the developmental order of appearance of carpal bones. Thus, for capitate and hamate j is equal to 1 and 2, respectively, for triquetrum and lunate j is, correspondingly, 3 and 4, and for scaphoid, trapezoid, and trapezium-5, 6, and 7, respectively. The membership function component related to the year of the carpal bone appearance is defined as

$$\chi_c(a_j, x) = 1/(1 + a_j x^2). \tag{7}$$

and is included in eqn. 6.

In order to determine b_j, the clustering analysis is performed (as described above) to find the d_j center and solve the equation

$$\chi_c(a_j, d_j) = 0.5. \tag{8}$$

Then, vector eqn. 6 is substituted in eqns. 3 and 4. As an example, the membership function components defined for trapezoid are shown in Fig. 4b. Since the trapezoid appears at the age of 6, four components are defined. Three of them are assigned to the age of 7–9, respectively, whereas the additional component is assigned to the age of 6. Due to a large overlap between clusters in the group age 8 and 9, the last membership function component has been shifted (Fig. 4b).

3.2. Classification rule

In the classification phase, the input vector including features of all extracted objects is processed as defined in eqn. 4. This results in a matrix which assigns each feature to a year of age from the range under consideration. The assignment is described as a grade of membership and is a number in the interval [0, 1]. The next element in the fuzzy classifiers to be defined is a classification rule which finally assesses the bone age by processing the given matrix. In this study two classification rules have been tested. The first one, called later a max-min rule is defined as

$$\max_j [\min_i \mu(x_{ij})]$$

$$\text{where } i = 1 \cdots n \text{ and } n \text{ is the number of features describing all objects} \tag{9}$$

$$j = 1 \cdots m \text{ is a year of age.}$$

It means, that for each class (year of age) a minimum membership function value is found. This gives one value for each class. Then, the maximum membership function value is found over all classes yielding the desired bone age assessment.

The second rule, called later a max–sum rule is defined as

$$\max_j \left[\sum_i \mu(x_{ij}) \right] \tag{10}$$

which means, that the minimum operator of the max–min rule is replaced by the summation over all membership function values belonging to one class. The maximum value calculated over all classes yields the bone age assessment.

As an example, a matrix of membership function values for all features extracted from the PROI is shown in Table 1 [columns marked as d1 through p3 stand for distal ratios (d), middle ratios (m), proximal ratios (p)]. These columns are followed by the result of the sum and min operator. The "age" column shows the year of age assigned to the membership function value of each feature. Comparing the results of both classification rules, one can easily notice the sensitivity of the max–min rule to features which are mis-extracted or are out of a predefined range caused by pathological conditions. Due to the shape of membership function components, their values are always close to 0. While replacing the minimum with a summation, the sensitivity is reduced. Although in the presence of the out-of-range features the overall value is reduced, it is still significantly higher than the neighbor values. Thus, in the final classification, the max-sum rule is applied.

3.3. Bone age assessment–classification phase

In the bone age assessment procedure both (PROI and CROI) regions are analyzed individually. Thus, two matrices are obtained. The max–sum classification rule is applied individually leading to two bone age assessments: the phalangeal bone age (PBA) assessment reflects the phalangeal development the carpal bone age (CBA) assessment reflects the carpal bones development. Besides, an additional condition has been imposed. If two neighbor sums differ less than 8% (refers to one month on the age axis) this value is ignored. Otherwise, an interpolation (with the accuracy of one month) yields the bone age. These two results (PBA and CBA) are compared by a radiologist who assesses the final bone age.

4. RESULTS AND DISCUSSION

This paper summarizes the feature selection phase and describes the classification step of the computerized bone age assessment study. The analysis of two regions of interest (PROI and CROI) is performed independently and leads to two bone age assessments. The features extraction techniques are based on algorithms discussed in (8, 10, 11). They have been tested on 120 pediatric CR hand images. A correct extraction of epiphyseal diameter/metaphyseal diameter ratios has been obtained in 973 out of 1080 cases (120 hand images × 9 ratios/hand image). This gives an accuracy of 90%. The mis-extractions have been noticed mostly while analyzing overexposed radiographs. For

Table 1. Membership function values calculated for a hand image

d1	d2	d3	m1	m2	m3	p1	p2	p3	sum	min	age
0.08	0.01	0.02	0.00	0.04	0.06	0.03	0.07	0.22	0.54	0.00	7
0.23	0.02	0.03	0.01	0.15	0.30	0.09	0.35	0.94	2.11	0.01	8
0.94	0.01	0.02	0.03	1.00	0.73	0.61	0.67	0.20	4.21	0.01	9
0.26	0.03	0.06	0.03	0.15	0.09	0.41	0.12	0.06	1.21	0.03	10
0.09	0.11	0.34	0.27	0.11	0.08	0.12	0.06	0.04	1.23	0.04	11
0.01	0.11	0.96	0.88	0.04	0.03	0.02	0.01	0.01	2.07	0.01	12
0.05	0.88	0.34	0.05	0.00	0.00	0.01	0.01	0.01	1.35	0.00	13

Columns marked as d1 through p3 stand, correspondingly, for features extracted from distals (d), middles (m), and proximals (p). The third and second last columns show the results of $\min_i \mu(x_{ij})$ and $\sum_i \mu(x_{ij})$ operators, respectively. The last column marks the bone age assigned to each membership function. The patients chronological age is 10 yr, the radiologically assessed bone age is 8 yr and 5 mo, whereas the phalangeal analysis results in 9 yr (max – sum result 4.21).

the CROI, a correct detection of 689 carpal bones has been obtained, giving the rate of 94%. The size of the missing carpal bones has not exceeded 3 mm in diameter. The overall comparison of the accuracy of measures has been based on a visual comparison of the detected carpal bones overlapped with the original image. A significant enlargement of the carpal bone area being caused by the soft tissue noisy objects attached to the bones has been observed in 45 (6%) cases. A mis-extraction of the area influences also the perimeter of the corresponding carpal bone. Unfortunately, causing an increase of the total carpal bone area, all ratios are influenced. Due to technical difficulties in drawing manually an exact contour of the carpal bones, leading to significant discrepancies between two corresponding values, the statistical analysis of measures does not yield reliable results.

Two tests have been made to evaluate the computerized bone age assessment. First, phalangeal bone age (PBA) and carpal bone age (CBA) have been compared with a radiological assessment (RBA) individually (Table 2). Due to the inter-observer difference of the Greulich and Pyle method applied by radiologists, the computerized bone age assessment may be accepted as being correct if it does not differ from the RBA more than 6 mo. Table 3 shows that the phalangeal parameters seem to be more reliable than the carpal bone features. Thus, phalanges appear to be more sensitive to the developmental changes than carpal bones, particularly in pathological cases. The second test (Table 3) has compared the difference between PBA and CBA and, then, referred it to the clinical results. A radiograph is assumed to be classified correctly, if the RBA falls between PBA and CBA or differs less than 6 mo. A discrepancy of more than 6 mo between PBA and CBA has been noticed mostly in pathological cases. It may reflect a difference in the development between phalanges (particular distals and middles) and carpal bones. The more distal the more the region is influenced by developmental abnormalities making the changes more noticeable.

Before a clinical evaluation of the entire algorithm, a medically approved set of digital hand images has to be collected. Both medical methods (Greulich and Pyle, and TW2) are based on data accumulated in the 1950s from highly selected patient population and does not reflect the changes which occurred in society (e.g., improved nutrition). The data base should contain images of normally developed hand wrist with the bone age assessed by 2–3 independent radiologist.

The computerized analysis still remains a computer-assisted or computer-aided diagnosis. Due to the variety of human nature none of the computer system designers are able to foresee all possible cases and, thus, none of the computerized systems are able to provide a 100% classification rate. This is true not only for the computerized systems. Additional medical consultation is often required when an unusual case is diagnosed. Therefore, each automatically performed

Table 2. Accuracy of computerized bone age assessment based on individual comparison of CBA and PBA with RBA

PBA-CBA	Differs from RBA less than 6 mo	Differs from RBA more than 6 mo
0–6 mo	54%	14%
6 mo–1 yr	20%	6%
1 yr–2 yr	3%	3%

Table 3. Accuracy of computerized bone age assessment based on discrepency between CBA and PBA with respect to RBA

	Differs from RBA less than 6 mo	Differs from RBA less than 1 yr	Differs from RBA more than 1 yr
PBA	75%	19%	6%
CBA	63%	20%	17%

analysis can serve as an assistance in order to improve the examination it terms discussed above. Yet, the clinician is still responsible for each final diagnosis.

SUMMARY

This paper presents part of an entire study leading to an estimation of skeletal maturity, called bone age assessment. In the described phase, a classifier has been developed. Due to imprecise nature of the bone age assessment problem, as well as possible misextractions, a fuzzy classifier has been defined. Based on features, automatically extracted from two regions of a CR hand wrist radiograph, the classifier delivers two values. One reflects the phalangeal stage, the other one the carpal bones developmental stage. Both values are obtained independently. The results show an agreement of 75% for the phalangeal region and 63% for the carpal bones region indicating that a more distal analysis yields better results. The discrepancy between these two estimators may suggest a difference in development of both regions, usually occurring in pathological conditions.

Acknowledgment—This work was supported by US Public Health Service grants R01 CA 39063 and P01 CA 51198, awarded by the Department of Health and Human Services.

REFERENCES

1. Miller, G.R.; Levick, R.K.; Kay, R. Assessment of bone age: A comparison of the Greulich and Pyle and the Tanner and Whitehouse methods. Clin. Radiol. 37:119–121; 1986.
2. Greulich, W.W.; Pyle, S.I., Radiographic atlas of skeletal development of hand wrist. Stanford CA: Stanford University Press; 2nd Ed.; 1971.
3. Tanner, J.M.; Whitehouse, R.H. Assessment of skeletal maturity and prediction of adult height (TW2 method) London: Academic Press; 1975.
4. Michael, D.J.; Nelson, A.C. HANDX: A model-based system for automatic segmentation of bones from digital radiographs. IEEE Trans. Med. Imaging 8:64–69; 1989.
5. Levitt, T.S.; Hedgcock, M.W. Model-based analysis of hand radiographs. Proc. SPIE 1093:563–570; 1989.
6. McNitt-Gray, M.; Pietka, E.; Huang, H.K. Image preprocessing for a Picture Archiving and Communication System. Invest. Radiol. 27:529–535; 1992.
7. McNitt-Gray, M.; Eldredge, S.; Tagawa, J. Automatic removal of unexposed background in digital radiographs. Proc. SPIE 1653:94–102; 1992.
8. Pietka, E.; McNitt-Gray, M.; Kuo, M.K.; Huang, H.K. Computer-assisted phalangeal analysis in skeletal age assessment. IEEE Trans. Med. Imaging 10:616–629; 1991.
9. Pietka, E.; Hall, T.; Huang, H.K. Bone age assessment based on the analysis of epiphyses and metaphyses. Radiology 153 (P); 1991.
10. Pietka, E.; McNitt-Gray, M.; Hall, T.; Huang, H.K., Computerized bone analysis of hand radiographs. Proc. SPIE 1652:522–528; 1992.
11. Pietka, E.; Kaabi, L.; Kuo, M.L.; Huang, H.K. Feature extraction in carpal bone analysis. IEEE Trans. Med. Imaging 12:44–49; 1993.
12. Pietka, E.; Kaabi, L.; Huang, H.K.; Kuo, M.L. Feature extraction for bone age determination. Radiology 317 (P); 1990.
13. Xie, X.L.; Beni, G. A validity measure for fuzzy clustering. IEEE Trans. Pattern Anal. Mach. Intell. 13:841–847; 1991.
14. Gath, I.; Geva, A.B. Unsupervised optimal fuzzy clustering. IEEE Trans. Pattern Anal. Mach. Intell. 11:773–781; 1989.
15. Chang, R.L.P.; Pavlidis, T. Fuzzy decision tree algorithms. IEEE Trans. Syst. Man. Cybern. SMC 7:28–34; 1977.
16. Gmytrasiewicz, P.; Hassberger, J.A.; Lee, J.C., Fault tree based diagnostics using fuzzy logic. IEEE Trans. Pattern Anal. Mach. Intell. 12:1115–1119; 1990.
17. Kickert, W.J.M.; Koppelaar, H. Application of fuzzy set theory to syntactic pattern recognition of handwritten capitals. IEEE Trans. Syst., Man, Cybern. SMC 7:148–151; 1976.
18. De Mori, R.; Laface, P. Use of fuzzy algorithms for phonetic and phonemic labeling of continuous speech. IEEE Trans. Pattern Anal. Mach. Intell. 2:136–148; 1980.
19. Garn, S.M.; Hertzog, K.P.; Poznanski, A.K.; Nagy, J.M. Metacarpophalangeal length in the evaluation of skeletal malformation. Radiology 105:375–381; 1972.
20. Pietka, E.; Huang, H.K. Epiphyseal fusion assessment based on wavelets decomposition analysis. Comp. Med. Imaging Graph. (submitted).
21. Johnston, F.E.; Jahina, S.B. The contribution of the carpal bones to the assessment of skeletal age. Am. J. Phys. Anthrop. 23:349–354; 1965.
22. Pryor, J.W. Time of ossification of the bones of the hand of the male and female and union of epiphyses with the diaphyses. Am. J. Phys. Anthrop. 401–410; 1975.
23. Kirks, D.R. Practical pediatric imaging, diagnostic radiology of infants and children Boston/Toronto: Little, Brown & Company; 1-st ed. Chap. 6; 1984: 198–201.
24. Roch, A.F.; Rohmann, C.G.; Davila, G.H. Effect of training on replicability of assessment of skeletal maturity (Greulich–Pyle), Am. J. Roentgenol. 108:511–515; 1970.
25. Kandel, A. Fuzzy techniques in pattern recognition. A Wiley-Interscience Publication, John Wiley & Sons; 1982.
26. Zadeh, L.A. Fuzzy sets. Inf. Control 8:338–353; 1965.

About the Author—EWA PIETKA, Ph.D., received her doctoral degree in Electronics from the Technical University of Silesia, Gliwice, Poland, and was an Assistant Professor in the Department of Electronics, Technical University of Silesia, Gliwice, Poland. She joined the Medical Imaging Division, Department of Radiological Sciences, ULCA, as a Postdoctoral Fellow in 1989 and became a Visiting Assistant Professor in 1991. Since 1992 Dr. Pietka has been with University Hospital of Geneva, Switzerland. Her research interests involve pattern recognition, image processing, and PACS.

Pergamon

Computerized Medical Imaging and Graphics, Vol. 19, No. 6, pp. 465–472, 1995

Printed in the USA
0895–6111/95 $9.50 + .00

0895–6111(95)00026–7

EPIPHYSEAL FUSION ASSESSMENT BASED ON WAVELETS DECOMPOSITION ANALYSIS

Ewa Pietka and H. K. Huang
UCSF Medical School, Department of Radiology, 530 Parnassus Ave, San Francisco, CA 94143-0628, USA

(*Received* 12 *April* 1994; *revised* 5 *September* 1995)

Abstract—Epiphyseal fusion is a finding frequently analysed in hand wrist radiographs. It is tested in the bone age assessment, the gonadal dysgenesis, etc. The computerized fusion analysis is performed on an automatically selected region of interest containing the lower edge of epiphysis and the upper edge of metaphysis. In the analysis a wavelets decomposition approach is employed. The wavelets decomposition components are first subjected to a preliminary test which rejects the overexposed images whose analysis would not give reasonable results. This increases the accuracy of the algorithm and a chance for an unsupervised application. Then, a quantitative measure is found. Its value decreases while the epiphyseal fusion proceeds. The analysis yields an assignment of fusion to one of four stages: no fusion, early stage of fusion, advanced stage of fusion, and fusion completed. The results show that wavelets decomposition components may efficiently be applied to a texture analysis. Copyright © 1996 Elsevier Science Ltd.

Key Words: Wavelets decomposition, Texture analysis, Epiphyseal fusion, Radius

1. INTRODUCTION

Epiphyseal fusion is a finding frequently analysed in the hand wrist radiographs. Bone age assessment is one of the medical procedures in which it is a basic feature in the later stage of skeletal development. Changes in appearance and size of ossification centers of the hand, and epiphyseal fusion are recognized as a measure of skeletal maturity. Currently, there are two basic methods: Tanner and Whitehouse (TW2) method (1), and Greulich and Pyle (G&P) method (2). The TW2 method uses a detailed analysis of each individual bone which leads to its description in terms of scores. This method is acknowledged as more objective than the G&P method, however, more time consuming and thus the rate of its application does not exceed 20%. The G&P method compares the left hand wrist radiograph with the atlas patterns. The pattern which superficially appears to resemble the clinical image is selected. Since each pattern is assigned to a certain year of age, the selection assesses the skeletal age. This method is more subjective and gives more random variation, yet, due to its simplicity (in comparison with TW2) is used more frequently (76%).

In both methods epiphyseal fusion is analysed in the later stage of skeletal development. In the G&P method, for patients older than 13 years the visual interpolation has to include the fusion analysis. Since the method is based on a subjective comparison of two images, no quantitative description can be applied. Whereas, the TW2 method offers a more objective classification of wrist bones to one of eight classes. The third last stage of development (stage G) is defined as "epiphysis caps the metaphysis" (1). In the classifier, described in this paper, this is referred to as the early stage of fusion. In stage H of the TW2 method, the separation line is partly visible and partly dense (area where fusion is proceeding). This is referred to as the advanced stage of fusion. In the final stage (I) the fusion is completed. Earlier stages (B through F) are referred to as non-fused epiphyses.

Fusion is also one of findings to be searched for in hand radiographs of patients with gonadal dysgenesis (Turner's syndrome). It has been noticed (3) that ossification centers appear normally up to the age of 13, yet afterward, a significant delay of fusion (up to 6, exceptionally to 10 years) occurs.

In this study, an attempt has been made to apply the wavelets decomposition algorithm to quantify the analysis of epiphyseal fusion. Wavelets decomposition algorithms have been tested in various signal and image processing applications. They have led to new results in the sound analysis (4) and seem to be of great promise for compact coding (5), and texture analysis (6). The idea of a multiresolution image analysis is a hierarchical interpretation of an image at lower and lower resolution. At different resolutions and in different wavelets representation components the details of an image reflect different physical structure of the object. In general applications, at a resolution step equal to two, an image (or region of an image) is convolved with a filter. In each iteration, a texture measure is found and compared with the corresponding values of other images. In the fusion assessment a different approach has been presented. After the first iteration, the wavelets representation components are tested separately. Each of them delivers a different type of information. First, over-exposed images are rejected. Their analysis would not yield reasonable results. Then, due to the sensitivity of the vertical high frequency component (VHFC) to the proceeding of fusion, it is subjected to further analysis to calculate a measure which assesses the fusion stage.

In the following section, the wavelets decomposition algorithm is described (Section 2). Then, based on previous studies (7, 8), an automatic extraction of the region of interest is shown (Section 3.1). Next, the VHFC analysis and a preliminary test of image quality are presented (Section 3.2). Finally, we discuss the sensitivity of wavelets decomposition algorithm and its applicability to the analysis of fusion (Section 4).

2. WAVELETS TRANSFORMATION OF IMAGES

2.1. *Wavelets decomposition*

In this section, we introduce a two-dimensional notation of the orthogonal wavelets representation. No proofs will be given. For more details we refer to (6, 9, 10).

A multiresolution approximation is a sequence of subspaces $\mathbf{V}_m$ of $\mathbf{L}^2(\mathbf{R}^2)$

$$\mathbf{V}_m \subset \mathbf{V}_{m+1} \qquad \text{for } m \in \mathbf{Z}$$

$$\bigcap_{m \in \mathbf{Z}} \mathbf{V}_m = \{0\}$$

and

$$\bigcup_{m \in \mathbf{Z}} \mathbf{V}_m \qquad \text{is dense in } \mathbf{L}^2(\mathbf{R}^2)$$

The $\mathbf{V}_{m+1}$ subspace is derived from $\mathbf{V}_m$ by scaling the approximated image (region or function) $f(x, y)$ by the ratio of its resolution value

$$f(x, y) \in \mathbf{V}_m \Rightarrow f(2x, 2y) \in \mathbf{V}_{m+1} \qquad \text{for } m \in \mathbf{Z}$$

In this application we approximate an image at a 2^j resolution ($j \in \mathbf{Z}$). The approximation of an image $f(x, y)$ at a resolution 2^j is equal to its orthogonal projection on the vector space $\mathbf{V}_{2^j}$. Let $\phi(x, y) \in \mathbf{L}^2(\mathbf{R}^2)$ be a scaling function such that if $\phi_{2^j}(x, y) = 2^{2j}\phi(2^j x, 2^j y)$, then for $m, n \in \mathbf{Z}^2$, $2^{-j}\phi_{2^j}(x - 2^{-j}n, y - 2^{-j}m)$ forms an orthonormal basis of $\mathbf{V}_{2^j}$. A proof for a one-dimensional case can be found in (10). For a particular case of separable multiresolution approximation, the scaling function $\phi(x, y)$ can be written as $\phi(x, y) = \phi(x)\phi(y)$ where $\phi(x)$ and $\phi(y)$ are one-dimensional scaling functions of the decomposed subspace.

Let $\psi(x)$ be the one-dimensional wavelets associated with the scaling function $\phi(x)$. Then, we can build an orthogonal basis by scaling and translating three wavelets functions

$$\Psi^1(x, y) = \phi(x)\psi(y)$$
$$\Psi^2(x, y) = \psi(x)\phi(y)$$
$$\Psi^3(x, y) = \psi(x)\psi(y)$$

The family of functions

$$m, n \in \mathbf{Z}^2 (2^{-j}\phi_{2^j}(x - 2^{-j}n)\psi_{2^j}(y - 2^{-j}m)$$
$$\psi_{2^j}(x - 2^{-j}n)\phi_{2^j}(y - 2^{-j}m)$$
$$\psi_{2^j}(x - 2^{-j}n)\psi_{2^j}(y - 2^{-j}m))$$

is an orthonormal basis of complement of $\mathbf{V}_{2^j}$ in $\mathbf{V}_{2^{j+1}}$. The proof can be found in (6). The difference of information between the projection of $f(x, y)$ at 2^{j+1} and 2^j resolution is equal to the orthonormal projection of $f(x, y)$ on this complement. Therefore, an image at a 2^{j+1} resolution can be replaced by four images at a 2^j resolution. They are described in terms of a set of inner products which are equal to two-dimensional convolution products evaluated at $2^{-j}n$

$$\begin{aligned} R^0_{2^j} &= \langle f(x, y), \Psi^0(x, y) \rangle \\ &= \langle f(x, y), \Psi^0_{2^j}(x - 2^{-j}n, y - 2^{-j}m) \rangle \\ &= (f(x, y) * \phi_{2^j}(-x)\phi_{2^j}(-y))(2^{-j}n, 2^{-j}m) \end{aligned}$$

$$\begin{aligned} R^1_{2^j} &= \langle f(x, y), \Psi^1(x, y) \rangle \\ &= \langle f(x, y), \Psi^1_{2^j}(x - 2^{-j}n, y - 2^{-j}m) \rangle \\ &= (f(x, y) * \phi_{2^j}(-x)\psi_{2^j}(-y))(2^{-j}n, 2^{-j}m) \end{aligned}$$

$$\begin{aligned} R^2_{2^j} &= \langle f(x, y), \Psi^2(x, y) \rangle \\ &= \langle f(x, y), \Psi^2_{2^j}(x - 2^{-j}n, y - 2^{-j}m) \rangle \\ &= (f(x, y) * \psi_{2^j}(-x)\phi_{2^j}(-y))(2^{-j}n, 2^{-j}m) \end{aligned}$$

$$\begin{aligned} R^3_{2^j} &= \langle f(x, y), \Psi^3(x, y) \rangle \\ &= \langle f(x, y), \Psi^3_{2^j}(x - 2^{-j}n, y - 2^{-j}m) \rangle \\ &= (f(x, y) * \psi_{2^j}(-x)\psi_{2^j}(-y))(2^{-j}n, 2^{-j}m) \end{aligned}$$

There are different approaches to the scaling function ϕ and construction function ψ. One, used by Lemarie (11) starts from a multiresolution analysis framework. Two other approaches (6, 9) start from a sequence $h(n)$. The summary of both approaches can be found in the Appendix. In this application the family of wavelets with compact support (derived in the Appendix) has been tested for $N = 11$, 13 and 15.

2.1. *Two-dimensional decomposition algorithm*

The two-dimensional wavelets decomposition algorithm, performed on a $2^j \times 2^j$ resolution region results in obtaining four images each at a $2^{j-1} \times 2^{j-1}$ resolution. The R^0_{j-1} is the low frequency in both direction component, R^1_{j-1} is the vertical high frequency component (horizontal edges), R^2_{j-1} is the horizontal high frequency component (vertical edges), and R^3_{j-1} is the high frequency in both direction component. Each of these components is obtained by two one-dimensional convolutions of rows and columns separately with ϕ and ψ filters described in the Appendix. After the convolution only every other row and column is retained. This reduces the resolution from 2^j to 2^{j-1}.

In a standard application of a wavelets decomposition algorithm, this process is repeated a predefined number of iterations. In following iterations only R^0_{j-1} components are convolved. However, in this study only the R^1_{j-1} and R^3_{j-1} components are analysed. The R^3_{j-1} component is tested in the preliminary step, whereas, the R^1_{j-1} is a basis for the fusion assessment. It preserves the horizontal edges of epiphyses and metaphyses and, therefore, reflects the stage of fusion.

3. FUSION ASSESSMENT

3.1. *Extraction of the radius region of interest*

Radius region of interest (RROI) is a subregion of a carpal bone region of interest (CROI). The CROI includes the carpal bones, parts of metacarpals, and upper parts of radius and ulna. This part of radius is subjected to the wavelets decomposition algorithm. The CROI extraction and analysis has been described in (7). In one phase of this analysis, by using a dilation/intersection reconstruction method (12), the radius is extracted. Then, the bone contour is searched for diameters of the metaphysis and epiphysis. A procedure, described in (8) is used. Next, a region including the radius is rotated to align the radius diameter with the horizontal direction. Finally, the RROI defined by both diameters (metaphyseal and epiphyseal) is extracted (Fig. 1). It is subjected to the wavelets decomposition algorithm described in Section 2.

3.2. *Assessment of epiphyseal fusion*

Subjecting the image region (Fig. 2a) to the wavelets decomposition procedure, four components are received. They correspond to the combination of low and high pass filter applied to the original image interchangeably in the horizontal and vertical direction. The top left component is a result of the low

Fig. 1. Hand image with an extracted radius region of interest (RROI).

pass filter convolved in both directions. The top right component shows the results of the vertical high frequency and horizontal low frequency analysis. It enhances mostly the horizontal lines. The bottom left component is the horizontal high frequency and vertical low frequency component in which the vertical lines are enhanced. Finally, in the bottom right component the high pass filter has been applied in both directions. It shows high gradient in both directions points.

While comparing the wavelets decomposition components of the RROI for patients at different developmental stages (Fig. 2), one can notice that their density decreases while the epiphyseal fusion proceeds. Epiphyses a–c in Fig. 2 are not fused. Fusion starts in d and e, proceeds in f–h, and is completed in i and j. The stage of fusion is described by the percentage of energy of the component calculated versus the energy of the original region and divided by the size of the RROI. A comparison of the energy measure of different components shows that the most sensitive component appears to be the horizontal low and vertical high frequency component (VHFC). It can be justified by looking at the structure of the developed epiphyses and metaphyses. While not being fused, their horizontal edges are included in the VHFC. The process of fusion effects

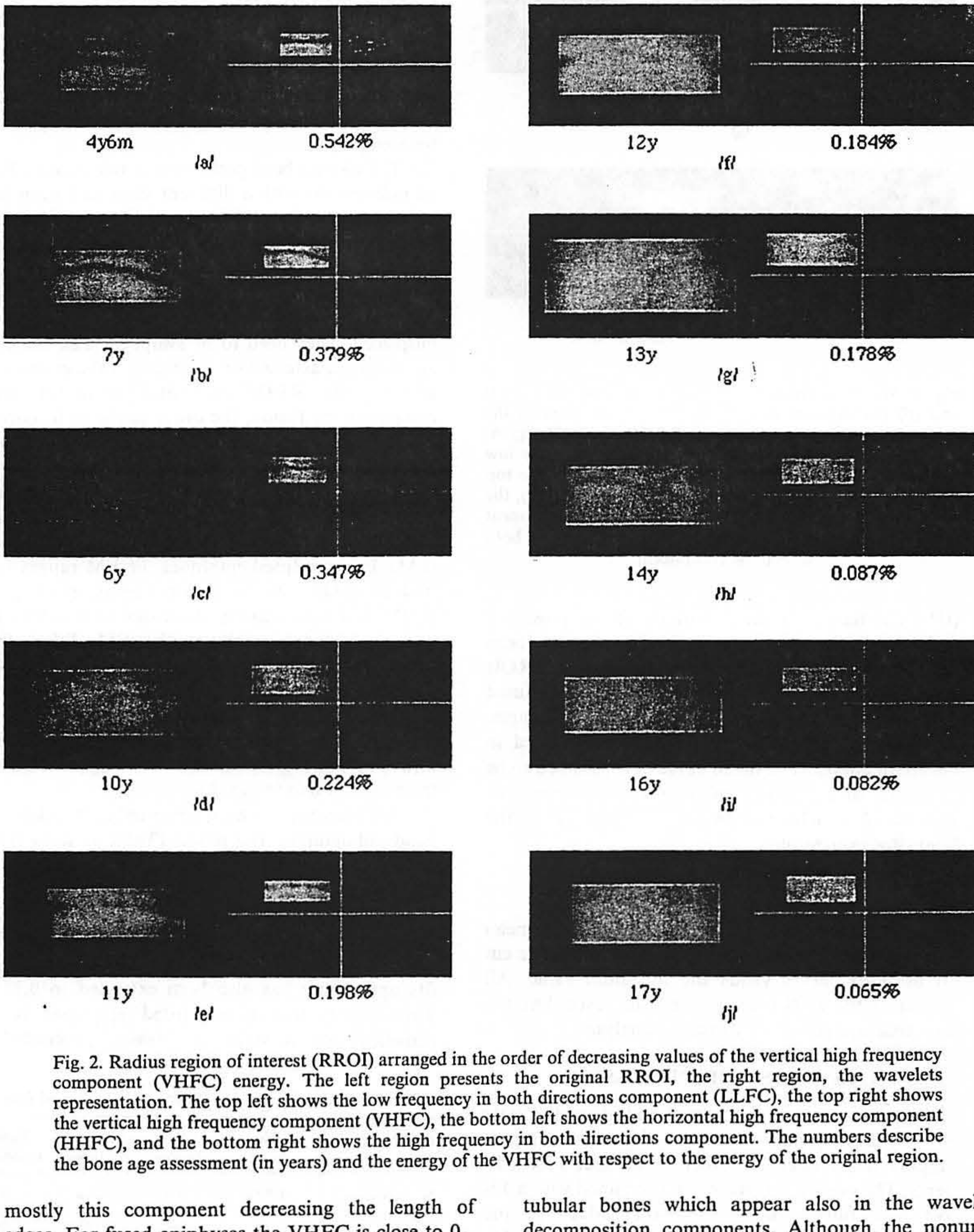

Fig. 2. Radius region of interest (RROI) arranged in the order of decreasing values of the vertical high frequency component (VHFC) energy. The left region presents the original RROI, the right region, the wavelets representation. The top left shows the low frequency in both directions component (LLFC), the top right shows the vertical high frequency component (VHFC), the bottom left shows the horizontal high frequency component (HHFC), and the bottom right shows the high frequency in both directions component. The numbers describe the bone age assessment (in years) and the energy of the VHFC with respect to the energy of the original region.

mostly this component decreasing the length of edges. For fused epiphyses the VHFC is close to 0.

Since the wavelets decomposition reflects the bony structure of the image, it appears to be sensitive to the radiographic exposure (Fig. 3). An over-exposed image (Fig. 3b) enhances the structure of the tubular bones which appear also in the wavelet decomposition components. Although the nonuniformity of the bony structure is included in all components leading to a significant increase of the energy measure, the largest difference has been noticed in the horizontal high frequency component

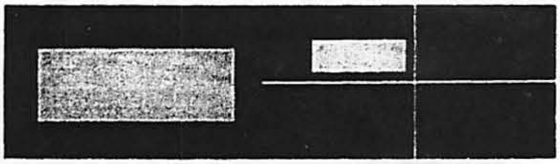

/a/

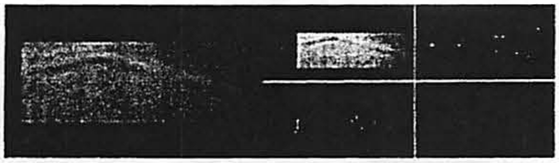

/b/

Fig. 3. Wavelets decomposition performed on (a) normal and (b) overexposed image. The left region presents the original radius region of interest (RROI), the right region, the wavelets representation. The top left shows the low frequency in both directions component (LLFC), the top right, the vertical high frequency component (VHFC), the bottom left, the horizontal high frequency component (HHFC), and the bottom right, the high frequency in both directions component.

(HHFC). Based on the sensitivity of the presented fusion analysis method, a threshold value has been found by comparing the energy measure of RROIs which have the highest energy value (non-fused epiphyses) and the RROIs of overexposed images. Both sets of energy measures have been fitted in Gaussian curves. The mean value m is assumed to be the center of the corresponding cluster, whereas, the variance δ is adjusted by minimizing over δ the following expression:

$$\sum_i [y_i - y(x_i;\ m,\ \delta)]^2$$

where $y()$ is the Gaussian distribution, m is the mean value, d is the variance and y_i are measures. The cut off of both curves yields the threshold value. All images of the HHFC energy measure exceeding the threshold are subjected to fusion analysis.

4. RESULTS AND DISCUSSION

The automatically extracted and aligned RROIs have been subjected to the wavelets with compact support using filters of different number of coefficients. The best results have been obtained with a 13-coefficient filter. Due to the noise added by the structural nonuniformity of metaphyses, the 11-coefficient filter yields worse results for all groups of fusion. The 15-coefficient filter gives comparable results for non-fused and early fusion groups. Later, the energies of the VHFC overlap and are not able to separate the "advanced fusion" from the "fusion completed" stages. Thus, using this type of wavelet bases the 13-coefficient filter matches the best the structure of the fusing epiphyses. As a criterion tested in this approach the correct classification rate has been employed.

The test has been performed in two phases. First, 10 radiographs with a different stage of fusion have been chosen. After subjecting them to the wavelets decomposition analysis, they have been arranged in an order of decreasing energy of the VHFC (Fig. 2). While comparing the radiologically assessed bone age, two images (b and c in Fig. 2) have been misplaced. They need to be swapped. Yet, the bone age has been assessed on the basis of the entire wrist and not the RROI itself and, moreover, while comparing the fusion, the order seems to be correct.

In the second phase radiographs have been grouped initially into three classes: epiphysis not fused (a–c in Fig. 2), fusion proceeds (d–h) and fusion completed (i and j). This results in obtaining the following values of the VHFC energy measure (EM). For non-fused epiphyses the EM ranges from 0.54 to 0.34%. While fusion begins, it drops to 0.22% and continuously decreases to 0.085%. For completely fused epiphyses the EM differs from 0.085% to 0.06%. Then, the interval of 0.23% to 0.085% has been divided into two classes which are considered as early and advanced stage of fusion. In the early stage of fusion the EM ranges from 0.28 to 0.18% (d–f in Fig. 3) whereas in the advanced stage, from 0.18 to 0.085% (g, h).

The classifier has been subjected to 90 additional hand radiographs. The results (Table 1) show that a non-fused region is unambiguously separated from the regions in which the fusion has begun. The interval of the EM of this class, although needed to be extended to 0.32%, is still separated from the EM of epiphyses in which the fusion has already begun (its upper limit has also been extended to 0.27%). This means, that a non-fused epiphysis is not classified into a stage of "fusion proceeds" or

Table 1. Classification results for four stages of fusion

Results/ Truth	No fusion	Early fusion	Advanced fusion	Fusion completed
No fusion	100%	0%	0%	0%
Early fusion	8%	92%	0%	0%
Advanced fusion	0%	14%	86%	0%
Fusion completed	0%	0%	0%	100%

"fusion completed". A similar situation can be noticed while epiphyses are completely fused. However, due to difference in exposure, in early stage of fusion, an epiphysis can be classified as not fused. An overexposed image exhibits a structural nonuniformity of bones (particularly the metaphysis). While being subjected to the wavelets decomposition procedure, the resulting wavelet coefficients of both types (fusion and bone nonuniformity) overlap and its separation is impossible. A significant overexposure (Fig. 3b) effects the energy of the HHFC, permitting the image to be rejected automatically. However, a moderate overexposure may not change the measure significantly enough to restrain the image from being subjected to the analysis, yet, increases the VHFC energy and leads to a misclassification.

The general evaluation shows that 10% of images have been considered as overexposed and rejected. If not imposing the quality condition, all of them would be classified as non-fused (due to a high energy of the VHFC). The next 6.7% are misclassified. This gives a result of 83.3% of correct classification. While improving the quality of radiographs, the accuracy will reach 90%.

The results show that some components of the wavelets representation can efficiently be used for the classification of epiphyseal fusion. However, they seem to be sensitive to the exposure of the radiographs, particularly if this effects the tissue structure that appears on the radiograph. Secondly, the size of the filters has to be adjusted to suppress the noise and extract the features to be considered in the classification procedure (13).

In this study, the wavelets with compact support have been tested on the epiphyseal fusion of the radius. However, this algorithm can also be applied to the assessment of epiphyseal fusion of other bones. As an addition example, the phalanges can be mentioned. The automated extraction of the region of interest is described in (8, 14). After the alignment of the region, the algorithm, as presented above, can be applied.

SUMMARY

This paper presents an analysis of epiphyseal fusion based on the wavelets decomposition approach. The procedure has been applied to an automatically extracted region of interest limited by the diameters of the epiphysis and metaphysis. After subjecting the region to a wavelets decomposition procedure four components are derived. Components enhancing the horizontal (VHFC) and vertical (HHFC) edges are employed in the analysis. As a quantitative parameter, the percentage of energy of the component calculated versus the energy of the original region and divided by the size of the region is used. Based on the energy measure derived from the VHFC the fusion is classified to one of four stages: no fusion, early fusion, advanced fusion, fusion completed. The rate of correct classification has reached 83%. An employment of a quality control test (HHFC analysis) restraining overexposed images from being subjected to the analysis increases the accuracy to 90%.

REFERENCES

1. Greulich, W.W. Radiographic Atlas of Skeletal Development of the Hand and Wrist. Stanford University Press, California; 1959.
2. Tanner, J.M.; Whitehouse, R.H.; Marshall, W.A.; Healy, M.J.R.; Goldstein, H. Assessment of Skeletal Maturity and Prediction of Adult Height (TW2). London: Academic Press; 1975.
3. Kosowicz, J. The roentgen appearance of the hand and wrist in gonadal dysgenesis. Radiology 92:354–361; 1965.
4. Kronland-Martinet, R.; Morlet, J.; Grossman, A. Analysis of sound patterns through wavelet transform. Int. J. Pattern Recog. Artificial Intell.; 1988.
5. Adelson, E.; Simoncelli, E. Orthogonal pyramid transform for image coding. Proc. SPIE, Visual Commun. Image Proc.; 1987.
6. Mallat, S.G. A theory for multiresolution signal decomposition: the wavelet representation. IEEE Trans. Pattern Anal. Machin Intell. 11:674–693; 1989.
7. Pietka, E.; Kaabi, L.; Kuo, H.K.; Huang, H.K. Feature extraction in carpal bone analysis. IEEE Trans. Medical Imaging 12:44–49; 1993.
8. Pietka, E.; McNitt-Gray, M.; Hall, T.; Huang, H.K. Computerized bone analysis of hand radiographs. Proc. SPIE 1652:522–528; 1992.
9. Daubechies, I. Orthonormal bases of compactly supported wavelets. Comm. Pure Applied Math. 41:909–996; 1988.
10. Mallat, S.G. Multiresolution approximation and wavelet orthonormal basis of L^2(R). Trans. Am. Math. Society 315:69–87; 1989.
11. Battle, G. A block spin construction of wavelets. Part 1: Lemarie functions. Commun. Math. Phys. 110:601–615; 1987.
12. Serra, J. Image Analysis and Mathematical Morphology. London: Academic Press; 1988.
13. Pietka, E. Computer-assisted bone age assessment based on features automatically extracted from a hand radiograph. Computerized Medical Imaging Graphics 19:251–259; 1995.
14. Pietka, E.; McNitt-Gray, M.; Kuo, M.L.; Huang, H.K. Computer-assisted phalangeal analysis in skeletal age assessment. IEEE Trans. Medical Imaging 10:616–620; 1991.

About the Author—Ewa Pietka, Ph.D., received her doctoral degree in Electronics from the Technical University of Silesia, Gliwice, Poland, and was an Assistant Professor in the Department of Electronics, Technical University of Silesia, Gliwice, Poland. She joined the Medical Imaging Division, Department of Radiological Sciences, UCLA, as a Postdoctoral Fellow in 1989 and was promoted to Visiting Assistant Professor in 1991. From 1992 to 1995 Dr Pietka was with the University Hospital of Geneva. Currently, she is a Visiting Assistant Professor at the University of California, San Francisco. Her research interests involve pattern recognition, image processing, and PACS.

About the Author—H.K. HUANG, D.Sc., FRCR(Hon.), Professor and Vice Chairman, Director of Radiological Informatics Laboratory, Department of Radiology, UCSF. Dr Huang has over 25 years experience in digital image processing research. He established the PACS research program and the Medical Imaging training program at UCLA. The UCLA PACS has been in clinical operation since 1992. He has been the recipient of numerous PACS related NIH grants including the Program Project Grant: "PACS in Radiology" as well as private industry-supported projects. He joined UCSF with a joint appointment in the UCSF/UC Berkeley Bioengineering Graduate Program, October 1992. He is now implementing a second generation PACS as well as doing research in medical multimedia at UCSF. Currently, he is the PI of several grants from the CalREN on ATM networking, National Library of Medicine sponsored HPCC Program on WAN Neuro-Imaging, NASA ACTS on satellite communication in medical images, NIH on Image Compression, California State Breast Cancer Research Program in Real-time telemammography.

APPENDIX

Mallat (6) reconstruction and decomposition algorithm uses the multiresolution analysis while computing the filter operators. Following Lemarie's definition of the scaling function

$$\phi(\omega) = \frac{1}{\omega^n \sqrt{\Sigma_{2n}(\omega)}}$$

and

$$\Sigma_n(\omega) = \sum_{k=-\infty}^{\infty} \frac{1}{(\omega + 2\pi)^n}$$

the multiresolution approximation is based on cubic splines obtained by computing the 6th derivative of

$$\Sigma_2(\omega) = \frac{1}{4\sin^2(\omega/2)}$$

Since

$$\phi(2\omega) = H(\omega)\phi(\omega)$$

$H(\omega)$ can be obtained as

$$H(\omega) = \sqrt{\frac{\Sigma_{2n}(\omega)}{2^{2n}\Sigma_{2n}(\omega)}}$$

The Fourier transform of the corresponding orthonormal wavelet can be derived from

$$\psi(2\omega) = G(\omega)\phi(\omega)$$

and is given by

$$\psi(\omega) = \frac{e^{-i\omega/2}}{\omega^n}\sqrt{\frac{\Sigma_{2n}(\omega/2+\pi)}{\Sigma_{2n}(\omega)\Sigma_{2n}(\omega/2)}}$$

The coefficients of the impulse response $h(n)$ are computed from the transfer function. The impulse response $g(n)$ is given by

$$g(n) = (-1)^{1-n}h(1-n)$$

Daubechies (9) has extracted the properties of the filter operator without reference to the multiresolution analysis. This permits the following set of conditions to be defined.

(i) Since

$$\sum_n |h(n)| < \infty$$
$$\sum_n |g(n)| < \infty$$

the operators

$$(Ha)_k = \sum_n h(n-2k)a_n$$
$$(Ga)_k = \sum_n g(n-2k)a_n$$

are bounded.

(ii) The reconstruction and decomposition scheme will work if $H*H+G*G=1$.

(iii) The orthogonality of subspaces requires that $HG^* = 0$.

(iv) The final condition identifies G as a difference operator which corresponds to a band pass filter and H as an averaging operator which corresponds to a low pass filter. Thus, we require

$$\sum_n h(n) = C$$
$$\sum_n g(n) = 0$$

It can be proven that $C = \sqrt{2}$.

If a sequence has finite length, then the corresponding basic wavelet has compact support. This means that there are values N_- and N_+ for which $h(n) = 0$ if $n < N_-$ or $n > N_+$.

Conditions 1–4 imply the following equation (9):

$$|m_N(v)|^2 + |m_N(v+\pi)|^2 = 1$$

with the following structure on m

$$m_N(v) = [0.5(1+e^{iv})]^N Q_N(e^{iv})$$

where Q is a polynomial such that

$$|Q_N(e^{iv})|^2 = \sum_{k=0}^{N-1}\binom{N+k-1}{k}\sin^{2k}\frac{v}{2} + \left[\sin^{2k}\frac{v}{2}\right]R\left(\frac{1}{2}\cos v\right)$$

and R is an add polynomial. The above equation is solved by a polynomial P_N of order $N-1$

$$P_N(z) = \sum_{j=0}^{N-1}\binom{N-1+j}{j}z^j$$

where $z = \cos^2 v/2$.

In our application Q of minimal order has been chosen. This means that

$$R \equiv 0 \quad \text{and} \quad |Q_N(e^{iv})|^2 = P_N \sin^{2k}\frac{v}{2}$$

In order to find $Q_N(e^{iv})$ the following Riesz lemma is used. Let A be a positive trigonometric polynomial containing only cosines, $A(v) = \sum_{n=0}^{N} a_n \cos(nv)$. Then, there exists a trigonometric polynomial $B(v) = \sum_{n=0}^{N} b_n e^{inv}$ such that $|B(v)|^2 = A(v)$. The proof can be found in (9). This defines

$$Q_N(e^{iv}) = \sum_{n=0}^{N-1} q_n e^{inv}$$

and

$$m_n = \left[\frac{1}{2}(1 + e^{iv})\right]^N \sum_{n=0}^{N-1} q_n(n) e^{inv} = 2^{-1/2} \sum_{n=0}^{N-1} h_N(n) e^{inv}$$

Medical Image Compression by Using Three-Dimensional Wavelet Transformation

Jun Wang and H. K. Huang,* *IEEE, Senior Member*

***Abstract*—This paper proposes a three-dimensional (3-D) medical image compression method for computed tomography (CT) and magnetic resonance (MR) that uses a separable nonuniform 3-D wavelet transform. The separable wavelet transform employs one filter bank within two-dimensional (2-D) slices and then a second filter bank on the slice direction. CT and MR image sets normally have different resolutions within a slice and between slices. The pixel distances within a slice are normally less than 1 mm and the distance between slices can vary from 1 mm to 10 mm. To find the best filter bank in the slice direction, we use the various filter banks in the slice direction and compare the compression results. The results from the 12 selected MR and CT image sets at various slice thickness show that the Haar transform in the slice direction gives the optimum performance for most image sets, except for a CT image set which has 1 mm slice distance. Compared with 2-D wavelet compression, compression ratios of the 3-D method are about 70% higher for CT and 35% higher for MR image sets at a peak signal to noise ratio (PSNR) of 50 dB. In general, the smaller the slice distance, the better the 3-D compression performance.**

I. Introduction

The demands on image compression in radiology are increasing as the number of digital modalities increases and the management of digital imaging becomes an important issue. Picture archiving and communication system (PACS) and teleradiology are the two major applications of image compression. PACS is an integrated digital system which archives and distributes digital images throughout a hospital. Such system requires a large storage space for long term archival and fast networks to distribute the images. Applying image compression reduces the storage requirements, reduces network traffic, and therefore improves efficiency. Teleradiology is radiology practice over a long distance for the purpose of consultation and second opinions. Teleradiology requires sending digital images to remote sites through digital communication lines. Applying compression reduces the image transfer time and therefore reduces the cost.

Manuscript received July 13, 1995; revised April 5, 1996. This work was supported in part by U.S. Army Medical Research Acquisition Activity Fellowship under Grant DAMD17-94-J-4196. The Associate Editor responsible for coordinating the review of this paper and recommending its publication was C. Roux. *Asterisk indicates corresponding author.*

J. Wang is with the Biomedical Physics Graduate Program, Department of Radiological Sciences, University of Claifornia and Los Angeles School of Medicine, Los Angeles, CA 90095-1721 USA. She is also with the Laboratory for Radiological Informatics, Department of Radiology, University of California at San Francisco, School of Medicine, San Francisco, CA 94143-0628 USA.

*H. K. Huang is with the Laboratory for Radiological Informatics, Department of Radiology, University of California at San Francisco, School of Medicine, San Francisco, CA 94143-0628 USA (e-mail: bernie_huang@radmac1.ucsf.edu).

Publisher Item Identifier S 0278-0062(96)05747-3.

Compressing an image set with multiple slices is very important in radiology because the most commonly used digital modalities, including magnetic resonance (MR), computed tomography (CT), positron emission tomography (PET), and single photon emission computed tomography (SPECT), generate multiple slices in a single examination. One slice is normally a cross section of the body part. Its adjacent slices are cross sections parallel to the slice under consideration. Multiple slices generated this way are normally anatomically or physiologically correlated to each other. In other words, there are some image structural similarities between adjacent slices. Although it is possible to compress an image set slice by slice, more efficient compression can be achieved by exploring the correlation between slices.

Methods to remove slice correlation for three-dimensional (3-D) compression include prediction methods and 3-D transformations [1]–[4]. In a prediction method, a discrete cosine transform (DCT) or a wavelet transform is first applied to two-dimensional (2-D) slices. Adjacent slices are then compared and only the differences are coded. This method requires dividing the image slices into small blocks and finding the best matching blocks between slices. The prediction method will produce the best compression result only if neighbor slices have common objects and such objects change position slightly in each slice, such as in a motion picture. However, most of medical image sets do not have this property and the prediction method may not yield the best result. A further drawback of the prediction procedure is that it is normally computationally expensive and create block artifacts. In this paper, we will focus on 3-D transformation methods.

In 3-D transformation methods, a set of slices is grouped into one 3-D block and a 3-D transformation is applied to the block data to remove inter-slice redundancy. Wavelet transformation has been proven to be very efficient for 2-D image coding [5], [6]. Compared with the popular DCT, wavelet transform yields not only frequency information, but also spatial information.

Several research efforts applied the 3-D wavelet transform to 3-D medical image compression [7]–[9]. The basic idea of those methods is to apply a separable 3-D wavelet transform to an image set or a group of slices to remove inter-slice redundancy. The separable 3-D wavelet transform employs a one-dimensional (1-D) wavelet filter bank in all three dimensions. However, a uniform 3-D wavelet transform may not have the best performance because the correlation of pixels within a slice is very different from that between slices. Typically, the distance of adjacent pixels within a slice varies from 0.3–1 mm, whereas the distance between

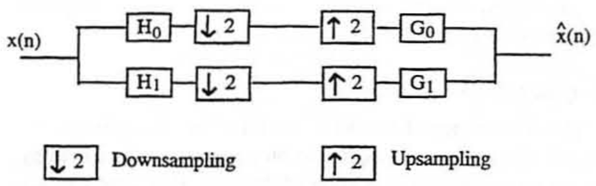

Fig. 1. Two-channel PR filter bank.

slices varies from 1–10 mm for MR or CT. The correlation within a slice is in general better than the correlation between slices. Hence, applying a second wavelet function in the slice direction adjusted to the distance characteristics may give better compression results. In this paper, a separable 3-D wavelet transform with two wavelet banks is applied to an image set. We use the same filter bank in each slice for all image sets. The wavelet filter bank used in the slice direction is selected for each image set at various slice distances according to the best compression result.

This paper is organized as follows. Section II briefly introduces the concept of the wavelet transform and its implementation for 1-D signals. Section III describes our 3-D wavelet compression algorithm. Section IV discusses the compression results obtained from the 3-D wavelet compression by using different wavelet filter banks in the slice direction and compares the results obtained with the 3-D wavelet compression and a 2-D slice by slice compression. Section V presents conclusions.

II. Wavelet Transformation

The basic idea of wavelet transformation is to represent any arbitrary function as a superposition of a wavelet basis [10], [11]. The coefficients of the basis can be used to reconstruct the original function exactly. The wavelet basis is formed by dilation and translation of a special function, which is called the mother wavelet. The wavelet transform gives a spatial and frequency representation of signals. The application of the wavelet transform to image compression has shown promising results [5], [6].

The wavelet transform can be implemented by a two-channel perfect reconstruction (PR) filter bank [12]. A filter bank is a set of filters, which are connected by sampling operators. Fig. 1 shows an example of a two-channel filter bank applied to a 1-D signal. $x(n)$ is an input signal. H_0 and H_1 are analysis filters and G_0 and G_1 are synthesis filters. H_0 is a low-pass filter and H_1 is a high-pass filter. If the output $\hat{x}(n) = x(n - l)$, where l is a delay, then the two-channel filter bank is called a PR filter bank.

The wavelet transform of a signal can be obtained by repeatedly applying a PR filter bank to the signal in a pyramidal scheme [11]. In a 1-D case, the decomposition process can be described by the following equations:

$$f_{m+1}(n) = \sum_k h_0(2n-k) f_m(k) \tag{1a}$$

$$f'_{m+1}(n) = \sum_k h_1(2n-k) f_m(k) \tag{1b}$$

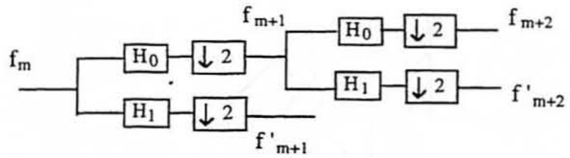

Fig. 2. Two levels of 1-D wavelet decomposition.

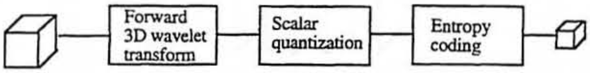

Fig. 3. Three-dimensional wavelet compression process.

where $f_{m+1}(n)$ is the smooth signal and $f'_{m+1}(n)$ is the detailed signal at the resolution level $m+1$.

Fig. 2 shows the implementation of (1). H_0 and H_1 are the frequency response of h_0 and h_1, respectively. The signal f_m is convoluted with filters H_0 and H_1, respectively, and then sampled at every other pixel. Because H_0 is a low-pass filter, and H_1 is a high-pass filter the resulting signals are a smooth signal f_{m+1}, and a detailed signal f'_{m+1}, respectively. The smooth signal f_{m+1} is again convoluted with filters H_0 and H_1, respectively, sampled at every other pixel, creating f_{m+2} and f'_{m+2}. The same process can be continued until the desired level is reached. The result of the two level decomposition (Fig. 2) contains f_{m+2}, f'_{m+2}, and f'_{m+1}. f_{m+2} is the smooth signal and f'_{m+2} and f'_{m+1} are detailed signals in the different frequency bands.

A wavelet transform decomposes a signal into a series of smooth signals and their associated detailed signals at different resolution levels. At each level, the smooth signal and associated detailed signal have all the information necessary to reconstruct the smooth signal at the next higher resolution level. The transformed signal has both spatial and frequency information from the original signal and it provides a good representation for coding.

III. Three-Dimensional Wavelet Compression

This section describes a multiple slice compression method using a 3-D wavelet transform. Fig. 3 shows a block diagram of this 3-D wavelet compression method. In the compression process, a separable 3-D wavelet transform is first applied to the 3-D image data resulting in a 3-D multiresolution representation of the image. The wavelet coefficients are then quantized using scalar quantization. Finally, run-length and Huffman coding are used to code the quantized data.

A. Three–Dimensional Wavelet Transform

A 3-D wavelet decomposes a 3-D image set into a number of blocks, with one small block containing most of the energy and rest of the blocks containing information in various frequency bands. The decomposed image provides an excellent representation for further quantization and coding.

A separable 3-D wavelet transform can be computed by extending the 1-D pyramidal algorithm. As we mentioned before, multiple slice medical image sets can have various slice thicknesses. The pixel correlation within a slice is normally

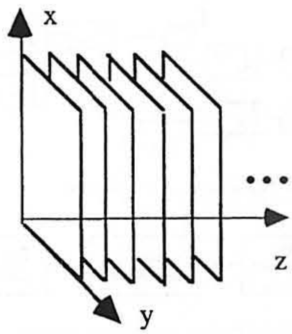

Fig. 4. The coordinates of a multiple slice image set.

much better than between slices. Our 3-D wavelet transform algorithm takes advantage of this property by using two sets of wavelet filters instead of only one wavelet filter.

Suppose we label the x and y directions in the image plane and the z direction in the slice direction (Fig. 4). The implementation of a one level 3-D wavelet transform is shown in Fig. 5.

We first convolute each line in the x-direction with filters H_0 and H_1, respectively, followed by subsampling every other pixel. We then convolute the resulting signals with H_0 and H_1 in the y-direction, followed by subsampling. Finally we apply a second sets of wavelet filters H_0' and H_1' in the z-direction and followed by subsampling.

The resulting signal has eight components. f_{m+1} contains low-frequency information, because it is obtained by convolution with only low-pass filters H_0 and H_0'. The remaining components are obtained by convolution with at least one high-pass filter, H_1 or H_1', and therefore contain the detailed signal in the x, y, and z directions and various diagonal directions. The same process can be repeated for the low-frequency signal, f_{m+1}, until the desired level is reached.

Fig. 6 shows two levels of 3-D wavelet transform on a volume of data. The first level decomposes the data into eight blocks. Three letter labels are used for each block of data, which stands for the filter type in the x, y, and z directions. L means low-pass filter and H means high-pass filter. The top left corner block is the low-frequency portion of the image data, and other remaining blocks are filtered at least once with a high-pass filter and therefore contain high-frequency components in one of the directions. The low-frequency block can be further decomposed into eight more blocks. The blocks on the second level contain higher frequency components than those of the first level.

In our case, the low-frequency component of the wavelet transform is about $1/2^{3M}$ of the original image size, but contains about 90% of the total energy, where M is the level of the decomposition. The high-frequency components are separated into different resolution levels. At a particular resolution level, each block contains the high-frequency information in certain directions. Blocks at different levels contain similar structure but different frequency band information.

The wavelet transform yields a good representation of the original image for compression purposes. Different levels of resolution can be coded in different ways to improve compression results.

B. Quantization

The second step of the 3-D wavelet compression is quantization. The purpose of quantization is to reduce data entropy by compromising the precision of the data. Reducing entropy allows more compression. The quantization step maps a large number of input values into a smaller set of output values. The original data cannot be recovered exactly after quantization. It is therefore very important to design a quantization strategy which selectively quantizes the wavelet coefficients and preserves the image quality.

Wavelet transformed data is represented by floating point values and consists of two types of data: a single low-resolution component which contains most of the energy; and multiple high-resolution components which contain the information of sharp edges. Since the low-resolution component has most of the energy, we want to keep that data as it is. To minimize the data loss in this portion, we map each floating point value to its nearest integer.

The high-resolution components contain mostly high-frequency information. Since smooth areas in the original image have less high-frequency information, high-resolution components in those areas are dominated by small amplitude coefficients. These coefficients contain very little energy. We can eliminate those coefficients without creating significant distortion in the reconstructed image. A threshold number T_m is chosen so that any coefficients less than T_m will be set to zero. Above T_m, uniform scalar quantization is used to map a range of floating point values into a single integer.

C. Entropy Coding

In the third step, run-length coding followed by Huffman coding is applied to the quantized data. Run-length coding is effective when there is more than one pixel with the same gray level in a sequence. This method uses two integers to represent a sequence of the same gray level. The first integer represents the length of the sequence, and the second integer represents the gray level of the sequence. The longer is a sequence, the more efficient the run-length coding. Since thresholding of the high-resolution components results in a large number of zeros, run-length can be expected to significantly reduce the data.

We apply Huffman coding to the run-length encoded data. Huffman coding is a minimum redundancy coding. It assigns fewer bits to the values with higher frequency of occurrence and more bits to the values with lesser frequency of occurrence. By first finding the frequency of occurrence of each gray level, Huffman coding will allow us to re-represent the data in less space than the original data.

IV. Results

We selected MR and CT image sets with various pixel sizes and slice distances. Pixel size is the distance between two adjacent pixels within a slice. Slice distance is the distance between two adjacent slices. The MR data sets have dimensions of 256×256 with 12 bits per pixel. The CT data sets

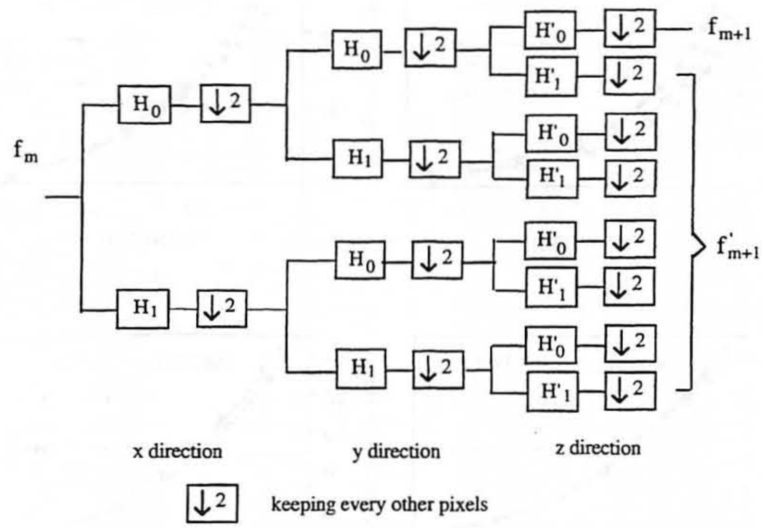

Fig. 5. The implementation of a one level 3-D wavelet decomposition. H_0 and H_1 and H_0' and H_1' are two different sets of filter banks.

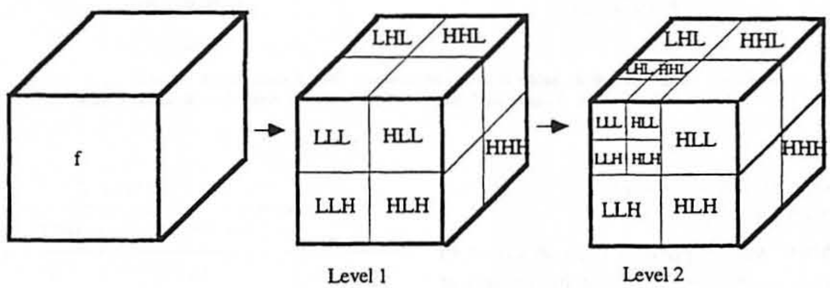

Fig. 6. The result of the two level of 3-D wavelet decomposition.

have dimensions of 512×512 with 12 bits per pixel. Table I lists 12 CT and MR test image sets selected from University of California at San Francisco image archive database. The first column is the name for each image set. The first two letters of the each name represent the image modality. The next two letters represent the anatomy. The number represents the slice distance in mm. The last letter a or c in MR sets stands for axial or coronal. In the following results, we will use the name to refer to each image set. All image sets were from different scans, but they may came from the same patient. Column six is the number of slices in each image set. To reduce the compression time and without affecting the final result, we only compressed the first 24 slices.

The decompressed image quality is measured by the peak signal-to-noise ratio (PSNR) defined as

$$\mathrm{PSNR} = 20 \log \frac{f_{\max}}{\dfrac{\left\{\sum [f(x, y, z) - f_c(x, y, z)]^2\right\}^{1/2}}{N}} \tag{2}$$

where $f_{\max}$ is the maximum gray level of the image set, N is total number of pixels, $f(x, y, z)$ is the original image, and $f_c(x, y, z)$ is the decompressed image. The denominator is the root mean square (rms) error of the decompressed image. The larger the PSNR, the better the decompressed image quality is.

TABLE I
THE DESCRIPTION OF IMAGE SETS

Image*	Modality	Anatomy	Slice distance (mm)	Pixel distance (mm)	# of slices
CTBR1	CT	Brain	1	0.41	51
CTKE1	CT	Knee	1	0.43	31
CTBR3	CT	Brain	3	0.49	25
CTSP3	CT	Spine	3	0.39	69
CTBR5	CT	Brain	5	0.41	24
CTKE5	CT	Knee	5	0.43	151
CTCH7	CT	Chest	7	0.74	43
MRBR1-a	MR	Brain-axial	1.5	1.02	124
MRBR3-a	MR	Brain-axial	3	1.17	47
MRBR6-a	MR	Brain-axial	6	0.78	26
MRBR4-c	MR	Brain-coronal	4	1.17	45
MRBR6-c	MR	Brain-coronal	6	0.78	28

*Each image set is from different scan.

The compression performance is measured by compression ratio (CR) which is defined as

$$\mathrm{CR} = \frac{\text{Original bits per pixel}}{\text{Compressed bits per pixel}}. \tag{3}$$

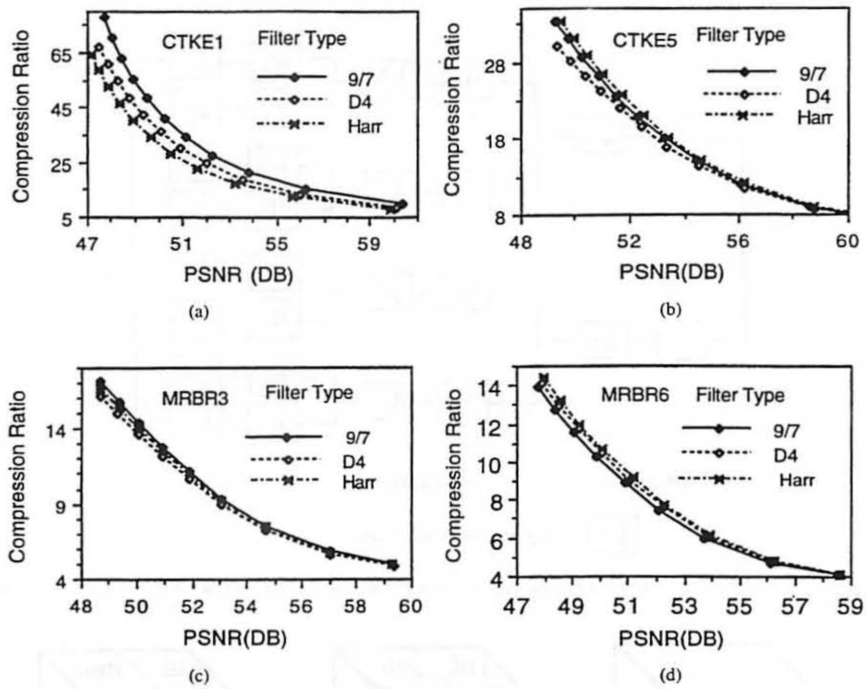

Fig. 7. Compression ration versus PSNR for different filter banks in the slice direction. (a) CT knee image set with 1-mm slice distance. (b) CT knee image set with 5-mm slice distance. (c) MR brain set with slice distance of 3 mm. (d) MR brain set with slice distance 6 mm.

A. Comparison Between Different Wavelet Filters in the Slice Direction

Different wavelet filters were applied to the z-direction in order to select an optimum wavelet filter for image sets at various slice thicknesses. The wavelet filters H_0 and H_1 used in the x and the y direction were fixed to be the 9/7 tap filter bank [13], which has been recognized as one of the best filters for the purpose of image compression. We only varied the wavelet filter H_0' and H_1' for the z direction. The selected candidates were the 9/7, the Daubechies_4 (D4) [10], and the Haar [14]. The reasons to consider these three filter banks were: the 9/7 filter bank gives a uniform 3-D wavelet transformation, and the Daubechies_4 (D4) and the Haar filter banks are representative of short filter banks. Image sets were compressed with the 3-D wavelet method using each filter bank for the z-direction. Three level wavelet decomposition was used in all cases.

Fig. 7(a) and (b) shows the compression results for two different CT knee image sets at 1 and 5-mm slice distances. The two image sets were from the same patient, but two different studies. The solid lines are the results of using the 9/7 filter in the slice direction, the dotted lines are the results of using the D4 filter, and the dash lines are the results of using the Haar filter. The compression ratios from applying the 9/7 filter to a 1-mm slice distance image set are much better than those of the D4 and Haar filters: approximately 10–50% higher in the PSNR range of 47–59 dB [Fig. 7(a)]. In contrast, the Haar filter performs better for image sets with 5-mm slice distances [Fig. 7(b)].

TABLE II
COMPARISON OF THE COMPRESSION RESULTS OBTAINED WITH THREE FILTER BANKS IN THE SLICE DIRECTION

Image Set	Harr	D4	9/7
CTBR1	Middle	Middle	Best
CTKE1	Worst	Middle	Best
CTBR3	Best	Worst	Middle
CTSP3	Best	Middle	Worst
CTBR5	Best	Worst	Middle
CTKE5	Best	Worst	Middle
CTCH7	Best	Worst	Middle
MRBR1-a	Worst	Middle	Best
MRBR3-a	Middle	Worst	Best
MRBR4-c	Best	Worst	Middle
MRBR6-a	Best	Middle	Worst
MRBR6-c	Best	Middle	Worst

Fig. 7(c) and (d) shows the results for two different MR brain image sets. For the image set with a 3-mm slice distance, the 9/7 filter performs better [Fig. 7(c)], but the improvement of the 9/7 filter is only slight. For the image set with a 6-mm slice distance, the Haar filter performs better [Fig. 7(d)]. Since the Haar filter has two coefficients, D4 has four coefficients, and the 9/7 has eight coefficients in average, the total compression time of using the 9/7 filter in the slice direction is consistently about 20% longer than that of using the Haar filter in the slice direction.

Table II summarizes the results of applying different filters in the z direction for all test image sets. The first column of the table describes the image sets. The second, third and

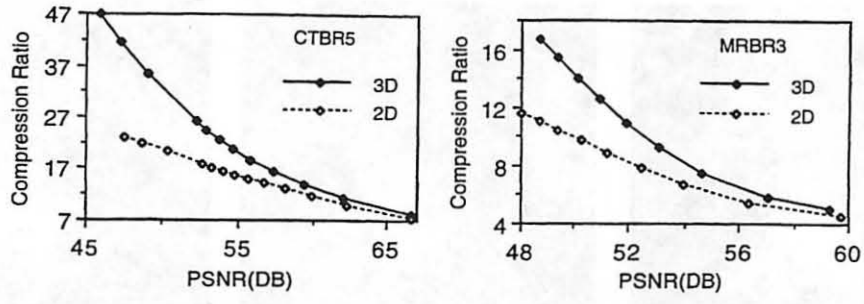

Fig. 8. The 3-D versus 2-D wavelet compression for an MR and a CT image set. (a) CT brain image set with 5-mm slice distance. (b) MR brain image set with 3-mm slice distance.

fourth columns are the compression performance. We use best, middle and worst to describe the performance of each filter. In general, the 9/7 filter has the best performance for image sets with slice distance less than or equal to 3 mm, and the Haar filter has the best performance for image sets with slice distances greater than 3 mm.

B. Comparison Between 2-D and 3-D Wavelet Transform

The image sets were also compressed with the 3-D wavelet compression method and a 2-D wavelet compression method. In the 3-D compression method, the Haar filter was used in the z direction. The 2-D compression algorithm was similar to the 3-D compression algorithm except that a 2-D wavelet transform was applied to each slice. Multiple slices are simply compressed slice by slice with the 2-D method and the final compression ratio is obtained by averaging whole set of 3-D data. Both methods used three levels of wavelet decomposition.

Fig. 8(a) and (b) shows the compression ratios versus PSNR of the 3-D and 2-D methods for the CTBR5 and the MRBR3 image sets, respectively. The horizontal axis is PSNR, and the vertical axis represents compression ratio. The solid line is the 3-D compression result and the dotted line is the 2-D compression result. The compression ratio of the 3-D method is higher than that of the 2-D at the same PSNR. We only show the result of one set of MR and CT images here. The rest of the MR and CT image sets have similar results.

To compare the increases in compression performance of the 3-D method over the 2-D method, we define the percentage increase in compression ratio as

$$\% \text{ Increase} = \frac{\text{CR(3-D)} - \text{CR(2-D)}}{\text{CR(2-D)}}. \quad (4)$$

Fig. 9 shows the percentage increase in compression ratios for MR and CT image sets at various slice distances. The performance of the 3-D wavelet method for CT image sets depends on the slice distance shown in Fig. 9(a). The general trend is that the smaller the distance between slices, the better the 3-D compression performance. This can be explained as follow: the image sets with smaller slice distances have better correlation between slices. Better correlation means that the signal is smoother in the slice direction and therefore has less higher frequency components in the slice direction. The 3-D wavelet transform decomposes the 3-D data into different frequency bands. The smoother the signal is and the better the energy concentration for the transformed data, the better the compression result.

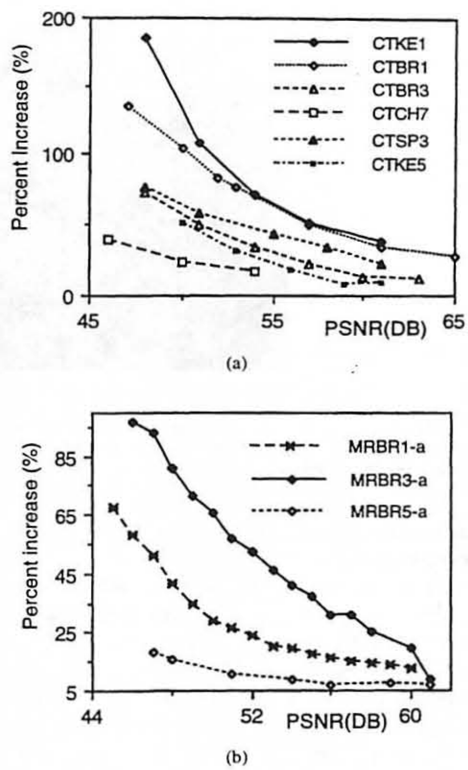

Fig. 9. The percentage increase of 3-D compression versus 2-D compression result. (a) CT image sets. (b) MR image sets.

For MR image sets, the relationship between the percentage increase in compression ratio and the slice distance is more complex than CT image sets. The performance of 3-D not only depends on the slice distance, but also depends on imaging techniques and pulse sequences. If two image sets acquired at the same technique and the same pulse sequence, the performance of 3-D is better for smaller slice distances. Fig. 9(b) shows results from three MR image sets at slice distances of 1.5, 3, and 5 mm. They are all T1-weighted brain axial sections, but from different patients. The results show

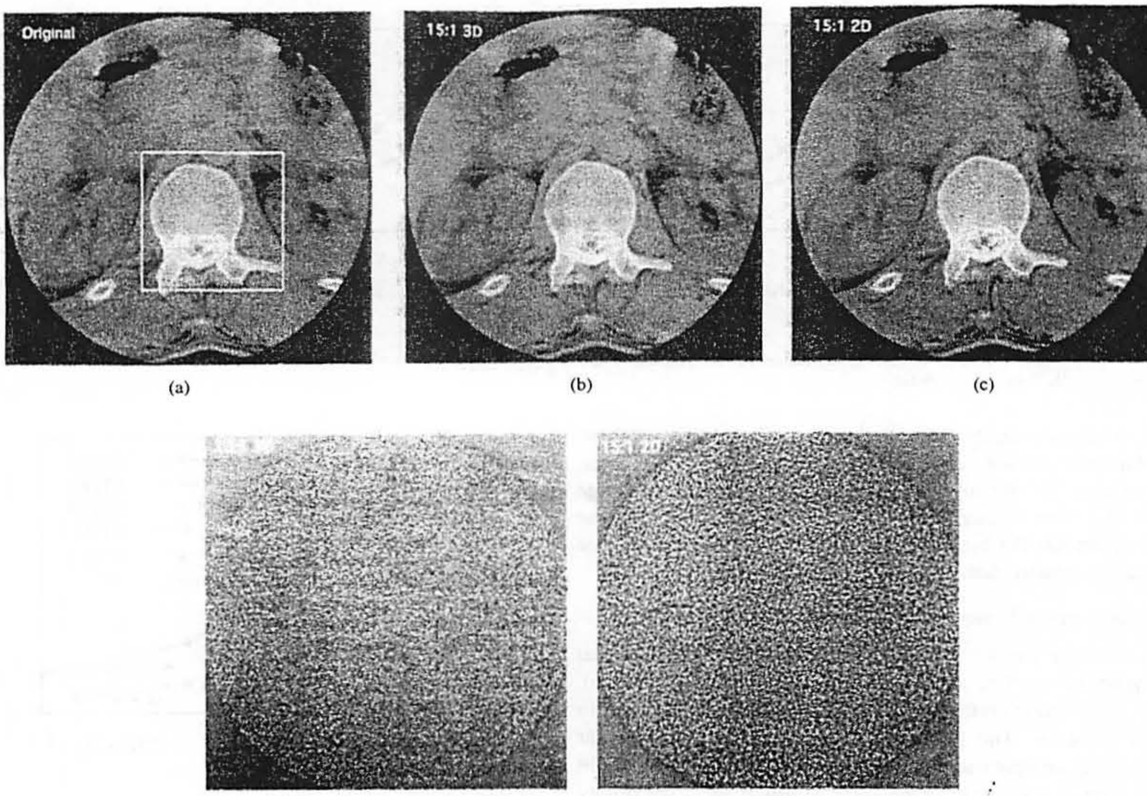

Fig. 10. One slice of a CT volume image data compressed at compression ratio of 15 : 1 using 3-D wavelet and 2-D wavelet algorithms. (a) original image, (b) image compressed with the 3-D wavelet method, (c) image compressed with the 2-D wavelet method, (d) the difference image between (b) and (a), and (e) the difference image between (c) and (a).

that the smaller the slice distance, the better the 3-D wavelet compression performs.

Overall, the benefit of 3-D wavelet compression for the CT image sets is larger than that for the MR image sets. At a PSNR of 55 dB, the percent increase in 3-D compression ratio is about 25–75% for CT, and only 5–40% for MR. The smaller improvement for MR is probably due to more noise in the MR image sets.

Finally, we present the original and decompressed images of a CT spine (CTSP3) compressed at a 15 : 1 ratio using the 2-D and the 3-D wavelet methods. Fig. 10(a) is the original image; Fig. 10(b) and (c) are the image compressed at ratio of 15 : 1 using the 3-D and 2-D wavelet methods, respectively; Fig. 10(d) and (e) shows the difference images between the original image and the decompressed image of the 3-D and 2-D, respectively. At the same compression ratio, image Fig. 10(d) shows that there is very little difference between the 3-D wavelet decompressed image and the original, whereas, image Fig. 10(e) clearly shows the difference between the 2-D wavelet decompressed image and the original image.

C. Comparison Between 3-D Wavelet Transform and DCT Based Compression

We also compare our 3-D wavelet method with the Joint Photographic Expert Group (JPEG) compression method [15]. JPEG is an industrial standard compression algorithm which is based on a block DCT transform. The CTSP3 is compressed slice by slice using the JPEG algorithm. The PSNR of the JPEG compressed image set is 49.4 dB at the compression ratio of 15 : 1. The PSNR of 3-D wavelet compressed image set is 54.4 dB at the same compression ratio. The PSNR of the 2-D wavelet compressed image set is 49.4 dB which is the same as for JPEG.

Fig. 11 shows the difference images of the JPEG and 3-D wavelet compression at the compression ratio of 15 : 1. In order to emphasize the differences, we have selected a window in the spine region [Fig. 10(a)] and zoomed it at 2 : 1 ratio. The JPEG compressed image [Fig. 11(b)] has larger errors in high-frequency regions than does the 3-D wavelet compressed image. Also, the JPEG difference image clearly shows blocky artifacts. The difference image for the 3-D wavelet compressed looks more like granular noise.

V. Conclusions

We have developed a 3-D image compression method that uses a separable nonuniform 3-D wavelet transform. The nonuniform 3-D transform applies one wavelet filter bank in the x and y directions, and a second wavelet filter bank in the z-direction. The second wavelet filter bank is selected for

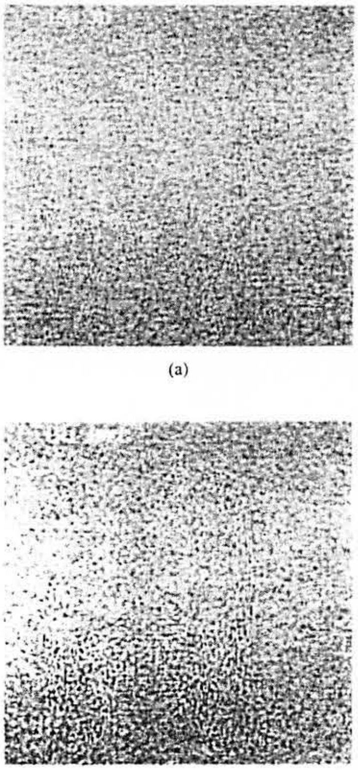

(a)

(b)

Fig. 11. A portion of the difference images that have been compressed using (a) the 3-D wavelet compression and (b) the JPEG compression. The original image is shown in Fig. 10(a).

image sets at various slice distances according to the best compression performance.

The results show that the Haar transform in the slice direction gives the optimum results in the majority of cases, except for the CT image set with 1-mm slice distances. In general, the Haar transform in the slice direction produces better results for image sets with slice distances greater than 3 mm. The 9/7 filter generally produces better compression results for image sets with slice distances less than 3 mm. However, the increase in compression ratio using the 9/7 filter in the slice direction is only less than 5% for most of the MR image sets and yet the compression time is about 20% longer than using the Haar transform. Therefore, it may not be worth the effort to use a 9/7 filter in the slice direction. The only exception is for the CT image set with 1-mm slice distance, the increase in the compression ratio is about 10–50% with the 9/7 filter. In this case, it is worth to use the 9/7 filter.

Three-dimensional wavelet compression achieves better results than 2-D wavelet compression. The increase in compression ratio for 3-D is about 70% over that of 2-D for CT image sets and 35% higher for MR image sets at a PSNR of 50 dB. The benefit of 3-D compression depends on the slice distance of an image set. The smaller the slice distance, the better the correlation in the slice direction, and the better the compression performance.

REFERENCES

[1] J. I. Koo, H. S. Lee, and Y. Kim, "Applications of 2-D and 3-D compression algorithms to ultrasound images," *SPIE Image Capture, Formatting, and Display*, vol. 1653, pp. 434–439, 1992.
[2] H. Lee, Y. Kim, A. H. Rowberg, and E. A. Riskin, "Statistical distributions of DCT coefficients and their application to an interframe compression algorithm for 3d medical images," *IEEE Trans. Med. Imag.*, vol. 12, no. 3, pp. 478–485, Sept. 1993.
[3] K. K. Chan, C. C. Lau, S. L. Lou, A. Hayrapetian, B. K. T. Ho, and H. K. Huang, "Three-dimensional transform compression of images from dynamic studies," *SPIE med. Imag. IV: Image Capture and Display*, vol. 1232, pp. 322–326, 1990.
[4] K. K. Chan, C. C. Lau, K. Chuang, and C. A. Morioka, "Visualization and volumetric compression," *SPIE Med. Imag. IV: Image Capture and Display*, vol. 1444, pp. 250–256, 1991.
[5] M. Ohta, M. Yano, and T. Nishitani, "Wavelet picture coding with transform coding approach," *IEICE Trans. Fundamentals*, vol. E75-A, no. 7, pp. 776–785, 1992.
[6] J. N. Bradley and M. Brislawn, "The wavelet/scalar quantization compression standard for digital fingerprint images," in *Proc. IEEE ISCA-94*, London.
[7] J. Wang and H. K. Huang, "Three-dimensional medical image compression using a wavelet transform with parallel computing," *SPIE Med. Imag. 95*, vol. 2431, pp. 162–172.
[8] A. Baskuet, H. Benoit-Cattin, and C. Odet, "On a 3-D medical image coding method using a separable 3-D wavelet transform," *SPIE Med. Imag. 95*, vol. 2431, pp. 173–183.
[9] J. Wei, P. Saipetch, R. Panwar, D. Chen, and B. K. T. Ho, "Volumetric image compression by 3-D discrete wavelet transform," *SPIE Med. Imag. 95*, vol. 2431, pp. 184–194.
[10] I. Daubechies, "Orthonormal bases of compactly supported wavelets," *Comm. Pure Appl. Math.*, vol. 41, pp. 909–996, 1988.
[11] S. G. Mallat, "A theory for multiresolution signal decomposition: the wavelet representation," *IEEE Trans. Pattern Anal. Machine Intell.*, vol. 11, no. 7, pp. 674–693, June 1989.
[12] M. Vetterli and C. Herley, "Wavelets and filter banks: Theory and design," *IEEE Trans. Signal Processing*, vol. 40, pp. 2207–2232, 1992.
[13] M. Antonini, M. Barlaud, P. Mathieu, and I. Daubechies, "Image coding using wavelet transform," *IEEE Trans. Image Processing*, vol. 1, no. 2, 1992.
[14] M. G. Albanesi and I. De Lotto, "Image compression by the wavelet decomposition," *Signal Processing*, vol. 3, no. 3, pp. 265–274, 1992.
[15] FTP: havefun.stanford.edu

Cost-Effectiveness of Radiology Information Systems

Cost Benefits of Picture Archiving and Communications Systems

Ronald L. Arenson, MD, Elizabeth S. Burnside, MD, David E. Avrin, MD, PhD, Robert G. Gould, ScD, H. K. Huang, ScD, Robert P. Marco, MBA

With the rapid onslaught of managed care, radiology departments are increasingly being viewed by medical centers as expensive cost centers rather than as sources of revenue. Hospital administrators are placing pressure on radiology departments to reduce their operating and capital costs. In the past decade, a number of leaders in radiology have stated that picture archiving and communications systems (PACS) would make radiology departments more efficient and cost-effective. By eliminating film, thereby reducing personnel required to manage film images, the department should be able to reduce its operating costs (Seshadri SB et al., presented at the Conference on Computer Applications, June 1988). However, few studies have been published that substantiate such claims [1, 2].

The opportunities for savings in the radiology department can be divided into several major categories: personnel, supplies, equipment, and maintenance. Because personnel represent the majority of direct expense in the department, reductions in personnel are essential to realize sufficient savings to offset the added expense of PACS equipment.

Personnel who may be replaced by PACS include the staff associated with handling film—specifically film librarians, darkroom aides, and technologists required for computed tomography (CT) scanning or magnetic resonance (MR) imaging. The supplies that could be eliminated include film, processing chemicals, and other film-related costs such as film jackets. The equipment expenses that could be avoided by PACS include film processors, multiviewers and view boxes, and format cameras or laser imagers. Some equipment associated with the radiology information system also can be eliminated, such as bar-code light pens for tracking films and a number of terminals or personal computers in the film library.

Space savings can be realized if film libraries can be substantially reduced. In addition, darkrooms and spaces for laser imagers can be used for more patient-oriented tasks. Maintenance costs for the equipment eliminated also are saved. However, as we point out, the maintenance cost for PACS can be substantial.

The expenses for PACS are primarily in equipment and associated maintenance. The equipment can be divided into acquisition devices—inter-

From the Department of Radiology, University of California, San Francisco.

Address reprint requests to R. L. Arenson, MD, Department of Radiology, University of California, 505 Parnassus Ave., M-391, San Francisco, CA 94143-0628.

Acad Radiol 1996;3:S72–S74

faces, archive systems, display workstations, and networks—and hard-copy devices (which will always be needed to some extent).

The supplies required for PACS include optical platters for on-line archiving and phosphor plates for computed radiography (CR). A relatively small amount of space is required to house the needed computers and archive equipment and to provide space for CR. Some added personnel are needed to support the PACS. However, some of these tasks can be done by current employees, such as the systems personnel supporting the radiology and the hospital information systems.

Because of the high cost of the equipment associated with a departmentwide PACS, careful analysis of more limited implementations is needed. Although useful for producing high-quality portable chest images with few retakes, CR equipment is expensive and has high maintenance costs. Also, the phosphor plates have a finite life span, which is often much less than the manufacturers claim. Certainly, CR is not cost-effective if film is produced for interpretation rather than using soft-copy interpretation on digital workstations.

The areas in the department best suited for the implementation of PACS modules include sonography, CT scanning, MR imaging, nuclear medicine, CR for the intensive care unit (ICU), and gastrointestinal or genitourinary fluoroscopy. The primary areas excluded are mammography and plain films for chests or musculoskeletal work. Departments also may have their own specific opportunities for using CR or digitized films, for example, receiving information from a remote emergency department or a remote orthopedic clinic. Such special cases were not considered in this article. In addition, certain advantages of PACS, such as more rapid communication of image results to referring physicians, reduction in lost or misplaced films, and image enhancement for detection of lines or tubes, were not considered in the analysis.

For the purposes of this discussion, two scenarios are examined. The first focuses on the additional costs of adding a section to an existing PACS that is already supporting the infrastructure. The only network costs will be the hardware and wires or fiber needed to extend to the section. The only archive costs will be for platters. The second scenario also will consider the prorated costs for all components as if starting from scratch.

The nuclear medicine section was examined as an example for our analysis. At present, the nuclear medicine section uses one full-time equivalent (FTE) film clerk, and each technologist does filming tasks estimated to equal one FTE. The pertinent equipment, supplies, and personnel are indicated in Table 1.

The PACS expenses for the nuclear medicine section, also shown in Table 1, include acquisition interfaces, display workstations, portions of the archive and network, and other "infrastructure costs." Both scenarios are included, and the differences between the film system and the PACS system also are shown.

As can be seen in Table 1, a mini-PACS for the nuclear medicine section is cost-effective even if the infrastructure costs are included. The proportion of infrastructure costs allocated to the section was determined by the size and volume of images in that section compared with the rest of the department. These savings can be realized only if the personnel reductions are achieved and if film is not created. Without the salary savings, the PACS implementation will still be cost-effective, but not by a large margin for the nuclear medicine section. If film is required to provide referring physicians with images outside of the radiology department, the film savings will be reduced as well.

Implementation of PACS in other sections, such as sonography, abdominal imaging (gastrointestinal and genitourinary), and neuroradiology, also is cost-effective. The chest and musculoskeletal sections are more problematic because of the cost of CR. CR is useful in reducing retakes for portable chest films because it is so forgiving of radiologic technique. Even though the early claims of reduced radiation have not been realized to any significant extent, CR in conjunction with PACS including filmless interpretations serves a few very important functions. CR and PACS provide immediate viewing of images in both the ICU and the radiology department. This simultaneous viewing allows faster action on patients in the ICU based on the information in the images as well as rapid interpretation by the radiologist. Immediate remote consultations are also possible.

Even with proven cost-effectiveness, PACS will not gain wide implementation until several problems are overcome. The current technology has significant spatial and contrast limitations, especially on the display side. These limitations are particularly problematic in mammography and to a lesser extent, for plain films of the extremities and chest. An even more important deficiency is related to the software design on commercial workstations for physicians. The concepts of a folder manager (including advance fetching of previous comparison images, autorouting images to the appropriate

TABLE 1: Cost-Effectiveness of Picture Archiving and Communication Systems (PACS)

Description	Item Cost	Quantity	Depreciation (Years)	Annual Cost
		Nuclear medicine		
Savings from film system				
Film library clerk	$40,000	1		$40,000
Filming technologist	50,000	1		50,000
Film and chemicals	48,000	1	1	48,000
Processor	18,000	2	10	3,600
Multiformat camera	12,000	2	7	3,429
Maintenance	1,800	1	1	1,800
Multiviewers	20,000	2	15	2,667
Total savings				$149,496
PACS expenses				
Acquisition devices	$12,000	1	6	$2,000
Network components	3,000	1	5	600
Display workstations	36,000	2	6	12,000
Maintenance	5,100	1	1	5,100
Systems personnel	65,000	0		
Optical platters	500	4	1	2,000
Total costs				$21,700
		Infrastructure costs		
Archive devices	$398,000	1	6	$66,333
Network components	282,000	1	5	56,400
Display workstations	36,000	2	6	12,000
Maintenance	71,600	1	1	71,600
Systems personnel	65,000	3		195,000
Optical platters	500	10	1	5,000
Air conditioning and uninterrupted power supply	100,000	1	18	5,556
Total costs				$411,889
Nuclear medicine section's share				20,594
Realized savings/year without infrastructure				$127,796
Realized savings/year with infrastructure				107,202

workstation, and autosequencing of images on display) and presets for window and level are often missing [3]. Without these features, the radiologist at the workstation must serve as filming technician and film library clerk, in addition to doing the usual interpretation functions. Thus, radiologists are hampered in performing their tasks and resist the PACS.

In summary, PACS is cost-effective for selected portions of the radiology department and can be phased in as needs require. Several obstacles still prevent more widespread implementation, including the high cost for CR, the need for access to images outside the radiology department, and poor commercial design (lack of folder manager concepts) of physicians' workstations.

REFERENCES

1. Langlotz CP, Even-Shoshan O, Seshadri SS, et al. A methodology for the economic assessment of picture archiving and communication systems. *J Digit Imaging* 1995;8:95–102.
2. Becker SH, Arenson RL. Costs and benefits of picture archiving and communication systems. *J Am Med Informatics Assn* 1994;1:361–371.
3. Arenson RL, Avrin DE, Wong A, Gould RG, Huang HK. Second generation folder manager for PACS. In: *SCAR: computer applications to assist radiology*. Carlsbad, CA: Symposia Foundation, 1994:601–605.

Journal of Digital Imaging

VOL 9, NO 2 MAY 1996

Design and Implementation of a Picture Archiving and Communication System: The Second Time

H.K. Huang, Katherine Andriole, Todd Bazzill, S.L. Lou, Albert W.K. Wong, and Ronald L. Arenson

This report describes the authors' experience in the design and implementation of two large scale picture archiving and communication systems (PACS) during the past 10 years. The first system, which is in daily clinical operation was developed at University of California, Los Angeles from 1983 to 1992. The second system, which continues evolving, has been in development at University of California, San Francisco (UCSF) since 1992. The report highlights the differences between the two systems and points out the gradual change in the PACS design concept during the past 10 years from a closed architecture to an open hospital-integrated system. Both systems focus on system reliability and data integrity, with 24-hour on-line service and no loss of images. The major difference between the two systems is that the UCSF PACS infrastructure design is a completely open architecture and the system implementation uses more advanced technologies in computer software, digital communication, system interface, and stable industry standards. Such a PACS can withstand future technology changes without rendering the system obsolete, an essential criterion in any PACS design.

KEY WORDS: picture archiving and communication system (PACS), communication networks, infrastructure design, open architecture, display workstation.

THERE ARE generally three methods of approach to design and implementation of a picture archiving and communication system (PACS).[1] In the first approach, systems integration, a multidisciplinary team with technical know-how is assembled by the radiology department or the hospital. The team becomes a system integrator, selecting PACS components from various manufacturers. The team develops system interfaces and writes the PACS software according to the clinical requirements of the hospital. In the second approach, requirements specification and contracting, a team of experts, from both outside and inside the hospital, is assembled to write detailed specifications for the PACS for a certain clinical environment. A manufacturer is contracted to implement the system. In the third, or turnkey approach, the manufacturer develops a turnkey PACS and installs it in a department for clinical use. Each of these approaches has advantages and disadvantages. One advantage of the first, or systems integration approach, is that the research team can continuously upgrade the system with state-of-the-art components and therefore, the system will not become obsolete. The system so designed is tailored to the clinical environment and can be upgraded without depending on the schedule of the manufacturer. One disadvantage is that it requires a substantial commitment by the hospital to assemble a multidisciplinary team. In addition, the system developed will be one of a kind, and therefore, service and maintenance will be difficult because it consists of components from different manufacturers.

The primary advantage of the second approach (requirements specification and contracting) is that the PACS specifications are tailored to a certain clinical environment, yet the responsibility for implementing the PACS is delegated to the manufacturer. The department acts as a purchasing agent and does not have to be

From the Laboratory for Radiological Informatics, Department of Radiology, University of California, San Francisco 94143-0628.

Partially supported by PHS grant RO1 CA 51198, National Library of Medicine contract NO1-LM-4-3508, Cal REN grant ATMN-007, Fuji Medical Systems USA, Lumisys, and Abe Sekkei.

Address reprint requests to H.K. Huang, DSc, Laboratory for Radiological Informatics, Department of Radiology, University of California, San Francisco, CA 94143-0628.

R.L.A. contributes to the design of the UCSF PACS.

0897-1889/96/0902-0001$3.00/0

concerned with the installation. The disadvantages are that the specifications tend to be overly ambitious. The experts may not be familiar with the clinical environment, and they may underestimate the technical and operational difficulty. The designated manufacturer, who may lack clinical experience, tends to overestimate the performance of each PACS component. As a result, the completed PACS may not meet the overall specifications. The cost of contracting the manufacturer to develop a specified PACS is also high because of the manufacturer's narrow profit margin in building only one system.

The advantage of the third or turnkey approach is that it is a generalized production system, therefore, the cost tends to be lower. However, in this approach, the manufacturer needs a couple of years to complete the production cycle. By the time the system is commercially available, some components may have already become obsolete because of the fast moving computer and communication technologies. Also, it is doubtful whether a generalized PACS can be used by every specialty in a department and by every radiology department. In the past several years, these three approaches gradually merge as additional clinical data in PACS become available. As a result, the distinction among them has become blurred.

This report describes the authors' experience of design and implementation of two PACS, one at University of California at Los Angeles (UCLA) and the other at University of California at San Francisco (UCSF) during the past 10 years. The first system was based on the first approach and the second was based on combining the first and second approaches. Sections 2 and 3 describe the UCLA and the UCSF PACS, respectively. Section 4 compares the differences between these two systems.

THE FIRST PACS SYSTEM AT UCLA

We began the design of the UCLA PACS in 1983.[2] Its implementation went through three phases. Phase 1, from 1984 to 1990, encompassed the demonstration of the concept of PACS and the design of the PACS infrastructure. Phase 2, from 1990 to 1991, comprised clinical implementation of several PACS modules. Phase 3, from 1992 on, included the system's refinement, maintenance, and applications. This PACS was designed for the radiology department operation without consideration of a hospital integrated PACS.

Phase 1: Demonstration of Concept and Design of PACS Infrastructure

To show the concept of PACS to physicians, in 1987 we implemented two PACS modules; one in the pediatric radiology section within the department,[3] and the other in the coronary care unit.[4] The pediatric radiology section was selected because it operates independently from other radiology specialties and resembles a mini radiology department. It is an excellent model to study the implementation of a PACS for the entire radiology department. In this module, images were displayed on two 2,048-line monitors. The module was used for daily conferences and case reviews. The coronary care unit was chosen for the second PACS module because it explored the application of PACS outside of the radiology department. In this module, images were displayed on three 1,024-line monitors. Both modules were in clinical operation 24 hours a day, 7 days a week. The reactions from both radiologists and clinicians who used these two systems was very positive.

From 1988 to 1990,[5] we concentrated on the design of the PACS infrastructure. The critical components in the infrastructure were the communication system, PACS controllers, data base design, fault tolerance consideration, and system integration software. This infrastructure supported a digital-based radiology operation.

The infrastructure was implemented from 1990 to 1991.[6] There were 64 multimode and 48 single-mode fiber optic cables connecting the three buildings (Center for the Health Sciences [CHS], Medical Plaza, and Taper Building) housing the radiology department. There were two PACS controllers, one at the CHS and one at the Medical Plaza. The infrastructure was on-line in the beginning of 1991.

Communication system. We designed a three-tiered fiber optic communication system with Ethernet, FDDI (fiber distributed data interface), and Ultranet (a proprietary 1 gbit/sec network).[7] Ethernet was used to transmit images from acquisition devices to the acquisition computer. Because the acquisition device was slow in generating images, the transmission speed between these two nodes was not crucial. Images were reformatted at the acquisition computer and sent to the PACS controller by means of FDDI. Images were archived onto optical disks and distributed to the image display stations with the Ultranet. The three communication networks were coexistent in the infrastructure and served as backups for each other.

PACS controllers. There were two PACS controllers in the infrastructure.[8] Each controller was composed of an image server (4/490 SPARC; Sun Microsystems, Mountain View, CA) with 4-Gbyte magnetic disk storage, a 1-Tbyte optical disk library with write once read many (WORM) disks for archiving images, and a Sun 4/490 SPARC server running the data base (Sybase, Emeryville, CA) for patient directory and text information. The architecture of each controller was identical and could be used as the backup for the other. The PACS controllers were connected with the Ultranet. Images could be transmitted between the PACS controllers and display workstations at 4 to 8 Mbytes/sec.

Data base. Two identical Sybase data bases existed in each PACS controller and served as a mirrored system. Current patient image information was updated continuously on the data base of each controller.

Fault tolerance consideration. In the infrastructure, every critical component had a backup. There were two identical data bases one in each PACS controller. Each PACS controller was located in a separate building to avoid potential disaster. The three communication networks backed up each other, and all active fiber optic cables had spares. Each PACS controller was powered by an uninterruptable power supply with up to 20 minutes of uninterrupted power.

Systems integration software. The previously described components were integrated as the PACS infrastructure by means of an elaborate system software. The system software was written in C programming language and ran under the UNIX operating system.

Phase 2: Implementation of PACS Modules

To implement PACS modules in the clinical environment, two additional tasks were needed. The first task, completed in Phase 2, was to connect image acquisition devices to the PACS controller through the infrastructure. The second was to design and implement display workstations in the department and clinics in the third phase. In image acquisition, we connected three computed tomography (CT) and three magnetic resonance (MR) scanners with direct digital interfaces, as well as three computed radiography (CR) units and two film digitizers to the infrastructure.

Phase 3: Systems Refinement, Training, Maintenance, and Applications

Phase 3 was comprised in two stages.[9] Stage 1 was the development of display workstations and their clinical implementation. Stage 2 consisted of refining the PACS; upgrading the display workstation software; and establishing training, maintenance, and service.

Stage 1: Display stations and clinical implementation. In this stage, four stations, each with two 2,048-line monitors, were deployed in the pediatric radiology (two stations), neuroradiology, and genitourinary radiology section. Also, one laser imager printing station was installed as a hardcopy device. In addition, two three-monitor stations with 1K monitors were installed in the coronary care unit and pediatric intensive care unit (ICU). Figure 1 shows the UCLA PACS infrastructure and image acquisition and display stations as of October 1992.

Stage 2: Systems refinement and training, maintenance, and service. During clinical implementation, we set up procedures for training, system maintenance, and service. Three groups of personnel were trained. The first group was radiologists and clinicians to use the display stations. The second group included the PACS coordinator, technologists, and clerical personnel. This training was extensive and covered image quality assurance, updating the patient directory, and first-line troubleshooting. The third group was the PACS engineers. This training was most elaborate. It included all operational aspects of the PACS.

In September 1992, the authors transferred the responsibility of daily operation to a new PACS management team at UCLA, and we relocated to UCSF to develop a second generation PACS. This report only summarizes the

A

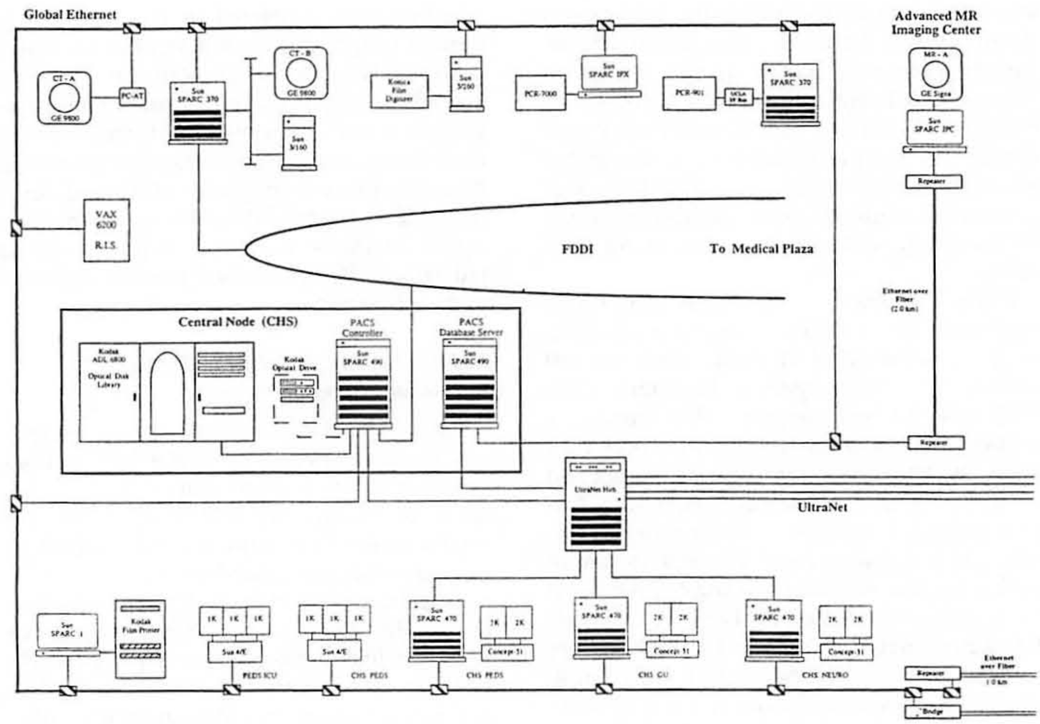
Global Ethernet
Advanced MR
Imaging Center
CT - A
GE 9800
PC-AT
Sun
SPARC 370
CT - B
GE 9800
Sun
3/160
Konica
Film
Digitizer
Sun
3/260
PCR-7000
Sun
SPARC IPX
PCR-901
Sun
SPARC 370
MR - A
GE Signa
Sun
SPARC IPC
Repeater
VAX
6200
R.I.S.
FDDI
To Medical Plaza
Ethernet over
Fiber
(2.0 km)
Central Node (CHS)
Kodak
ADL 6800
Optical Disk
Library
Kodak
Optical Drive
PACS
Controller
Sun
SPARC 490
PACS
Database Server
Sun
SPARC 490
Repeater
UltraNet Hub
UltraNet
Sun
SPARC 1
Kodak
Film Printer
1K
1K
1K
Sun 4/E
PEDS ICU
1K
1K
1K
Sun 4/E
CHS PEDS
Sun
SPARC 470
2K
2K
Concept-51
CHS PEDS
Sun
SPARC 470
2K
2K
Concept-51
CHS GU
Sun
SPARC 470
2K
2K
Concept-51
CHS NEURO
Repeater
Bridge
Ethernet
over Fiber
1.0 km

B

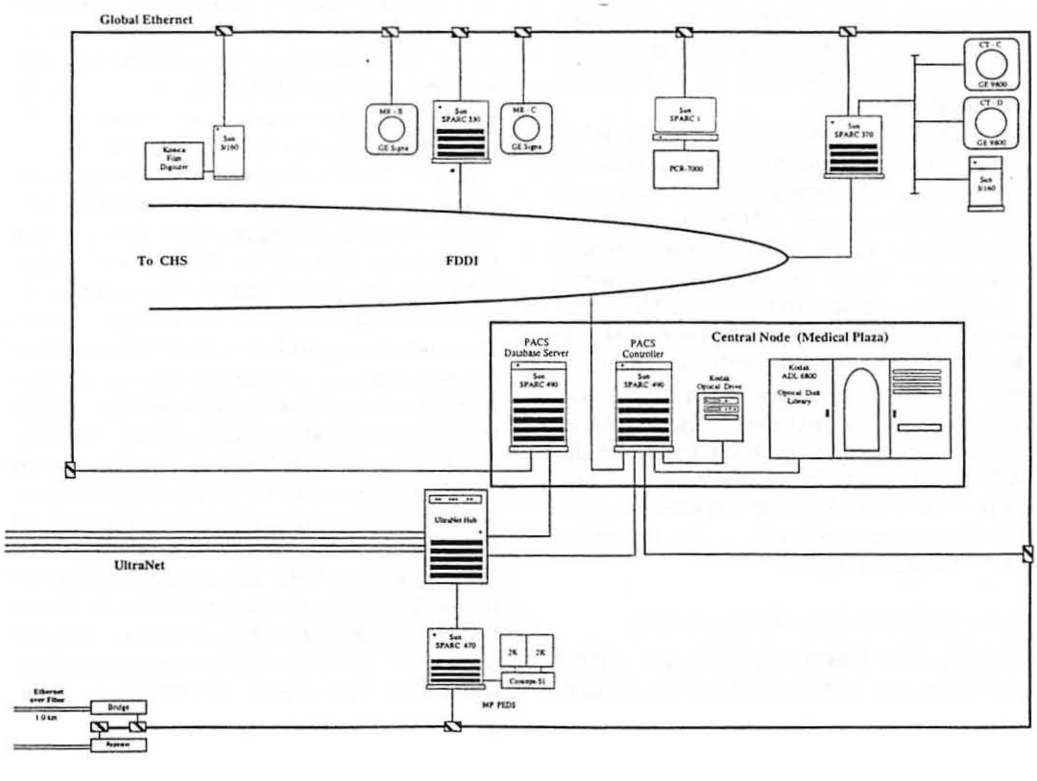
Global Ethernet
Konica
Film
Digitizer
Sun
3/160
MR - B
GE Signa
Sun
SPARC 330
MR - C
GE Signa
Sun
SPARC 1
PCR-7000
Sun
SPARC 370
CT - C
GE 9800
CT - D
GE 9800
Sun
3/160
To CHS
FDDI
Central Node (Medical Plaza)
PACS
Database Server
Sun
SPARC 490
PACS
Controller
Sun
SPARC 490
Kodak
Optical Drive
Kodak
ADL 6800
Optical Disk
Library
UltraNet Hub
UltraNet
Sun
SPARC 470
2K
2K
Concept-51
MP PEDS
Ethernet
over Fiber
1.0 km
Bridge
Repeater

UCLA system up to September 1992. Further development of the UCLA system has since been done by the new management team.

THE SECOND TIME, UCSF

We started to plan the second generation PACS at UCSF in October 1992. In addition to following our previous PACS design philosophy at UCLA, we have redesigned the PACS as a hospital-integrated system,[10] and built the framework in the infrastructure for future PACS-based radiology research.[11]

There are several major differences between the UCSF and the previous UCLA PACS design, among them intelligent image archiving and distribution; integration of hospital information system (HIS), radiology information system (RIS),[12] and other manufacturer's PACS components; new network architecture and technology; and collaboration with manufacturers to develop new display workstations. This section describes these major features.

Intelligent Image Archive and Distribution

The UCLA PACS was designed with focus on system reliability and data integrity, promising 24-hour on-line service and no loss of images. Images were managed in the individual PACS component on a first come-first serve basis, which resulted in inefficient image distribution and retrieval.

The second generation UCSF PACS design includes more intelligent and thereby minimizes access time for both current and historical images. The system is hospital-integrated and based on a composite staging mechanism using multiple storage media, HIS and RIS, and the client server concept.

Two major aspects are considered in the implementation of the second-generation UCSF PACS: data integrity, which promises no loss of images once the PACS receives the images from the radiologic imaging system and system efficiency, which minimizes access time for images at the display stations. The following describes some major components.

Local storage management via PACS intercomponent communication. To ensure data integrity, the UCSF PACS always retains two copies of an individual image on separate storage devices until a successful archive of the image to the long-term optical disk library has been made. This backup scheme is achieved via the PACS intercomponent communication:

(1) At the radiologic imaging system: Images are not deleted from the imaging devices unless technologists have verified the successful archiving of individual images via the PACS terminals. Should any failure of the acquisition process or the archival process occur, images can be resent from these imaging systems to the PACS; (2) At the acquisition subsystem: Images acquired in the acquisition subsystem remain on its local magnetic disks until the archive subsystem acknowledges back to the acquisition subsystem a successful archive. These images are then deleted from the magnetic disks so that storage space from these disks can be reclaimed; (3) At the archive subsystem: Images received in the archive server from various acquisition nodes are not deleted before their successful archiving to the optical storage. On the other hand, all archived images are stacked in the archive server's cache magnetic disks and will be deleted based on their aging criteria (eg, number of days an examination is performed, discharge or transfer of a patient, etc).

Multiple storage media. The storage management system features three levels of user-accessible storage media: (1) redundant array of inexpensive disks (RAID) in the display station for immediate access for current images; (2) magnetic disks in the archive server for fast retrieval of cached images; and (3) erasable magneto-optical disks and WORM disks in the optical disk library for retrieval of any historical images. On the other hand, all local magnetic disks in the radiologic imaging systems and the acquisition subsystem are used for storing newly acquired images. These images are deleted once they have been successfully archived to the optical disks. Table 1 illustrates the configuration of these multiple level storage media.

Fig 1. (A) UCLA PACS network at the Center for Health Sciences, and remote MR site. (B) UCLA PACS network at Medical Plaza. They are connected together. CHS, Center for the Health Sciences; GenUn, genitourinary radiology; PCR, Philips computed radiography; Peds, pediatric radiology; RIS, radiology information system (Reprinted from Computerized Medical Imaging & Graphics, Vol 17, Huang HK, Taira RK, Lou SL, et al, Implementation of a large scale picture archiving and communication system, pp 1-11, 1993, with permission from Elsevier Science Ltd, The Boulevard, Langford Lane, Kidlington OX5 1GB, UK. 9)

Table 1. Multiple Storage Devices for Images in the Storage Management System

	Storage Media	Location	Purpose
Level 1	Redundant array of inexpensive disks (temporary storage)	Display subsystem (display host)	Provides immediate access to both current and selected historical images
Level 2	Magnetic disks (temporary storage)	Archive subsystem (archive server)	Provides fast retrieval of current images
Level 3	Magneto-optical disks (longer-term storage)	Archive subsystem (optical disk library)	Provides retrieval of historical images
	WORM disks (permanent storage)	Archive subsystem (optical disk library)	Provides retrieval of historical images

RAID technology applied to PACS storage. All high-resolution (2,048 × 2,048 pixels) display stations in the UCSF PACS are configured with 5-Gbyte high-performance RAID. With this configuration, a 2,048 × 2,048 × 10-bit (8-Mbyte) CR image can be displayed in less than 2 seconds.

Folder manager. The storage management system is characterized by its on-line patient folder management.[13] When the first radiological examination is scheduled, a patient folder is created in the PACS controller for the given patient. During the patient's hospital stay, this folder remains in the display station(s) for immediate access until the patient is discharged, transferred, or other aging criterion (eg, two days after an out-patient visit) is met. The patient's admission, discharge, and transfer (ADT) information is obtained directly from the HIS and RIS. Images and associated data from any new examinations of the patient are continually added to the existing folder so that no redundant prefetching procedures will be performed. By applying the folder manager concept, the prefetch mechanism is only performed once per hospital stay of an individual patient.

Implementation of the Intelligent Archive Server

HIS/RIS/PACS interfacing. Interfacing the HIS allows the storage management system to receive patient ADT messages. Interfacing the RIS, on the other hand, allows the storage management system to receive information such as patient arrival, examination scheduling, examination cancellation, examination completion, etc. These events trigger the storage management system to perform the prefetch, studies grouping, and platter management mechanisms. Exchange of messages among these heterogeneous computer systems is conducted in the Health Level Seven (HL7) standard data format[14] with the use of Transmission Control Protocol/Internet Protocol (TCP/IP) protocols on a client/server basis.

Integration with other manufacturer's PACS components. The UCSF second generation PACS can integrate with other manufacturer's PACS components using the Digital Imaging and Communications in Medicine (DICOM) 3.0 standard. An example is the Aegis ultrasound PACS (Acuson, Mountain View, CA).[15] In this case, PACS treats the Aegis as a PACS acquisition device and coordinates the US images the same way as CT and MR images in the patient's image folder.

Image routing. Before successful archiving to long-term optical storage, all current images arrived at the archive server from various acquisition nodes are immediately routed to their destination display station(s). This routing mechanism minimizes access time for current images at the display stations. The routing process is driven by a predefined routing table composed of parameters including examination type, display station site, radiologist, and referring physician. The routing algorithm performs table look-up based on these parameters and determines where an image should go.

Image stacking. Stacking current images in the archive server's cache magnetic disks allows these images to be retrieved from the high-speed magnetic disks instead of the low-speed optical disks. The archive server holds as many images in its magnetic disks as possible and manages these images on the basis of their aging criteria. During a hospital stay, for example, images belonging to a given patient remain on the magnetic disks of the archive server until the patient is discharged or transferred.

Image aging. Aging criteria such as number of days since an examination was performed, discharge or transfer of a patient, or class of the patient (in-patient or out-patient) are used by the storage management system to control the migration of images from one storage device to another (eg, from a magneto-optical disk to a WORM disk) or the deletion of images from their resident storage devices.

Image prefetching. The prefetching mechanism[16] is triggered by means of a patient arrival message from the RIS. Selected historical images are retrieved from the long-term optical storage. These images are then distributed to the destination display station(s) before completion of the patient's current examination. Prefetching historical images to the display stations minimizes on-line image retrieval, hence relieving peak-hour workload of the archive subsystem and the networks. The prefetch algorithm is based on predefined parameters such as examination type, disease category, radiologist, referring physician, location of display station, and the number and age of the patient's archived images. These parameters determine which historical images should be retrieved from the long-term archive.

Studies grouping. During a hospital stay, a patient may undergo different examinations on different days. Images from these examinations are archived to the erasable magneto-optical disks, where they are scattered across different platters. When a patient is discharged or transferred, these images are then grouped from the magneto-optical disks and copied contiguously to a single WORM disk or to consecutive WORM disks for permanent storage. Once these images have been archived permanently, they are removed from the magneto-optical disks so that storage space in the magneto-optical disks can be reclaimed. Studies grouping allows all images from a patient during a hospital stay to be archived contiguously to optical disk(s), hence optimizing future retrieval of a patient's images from multiple examinations.

Platter management. Platter management allocates the storage space reserved in the WORM disks for future images in case a patient revisits or is readmitted to the hospital. In this way, images of a patient from multiple hospital visits can be accumulated in a single WORM disk or in consecutive disks, reducing excess disk swapping and consequently minimizing retrieval time for these images. However, preallocating storage space in an optical disk for a particular patient is expensive. Logically grouping consecutive optical disks into one volume, on the other hand, can reduce disk swapping time and hence minimizes the retrieval time for images stored in different disks within the same volume.

Networking

One distinct difference in networking between the UCSF and the UCLA PACS is the availability of asynchronous transfer mode (ATM) technology in the UCSF system. The UCLA networks were mainly a local area network (LAN) with Ethernet, FDDI, and Ultranet. In the UCSF PACS networks, ATM is used both in wide area network (WAN) and LAN with the conventional T-1 and Ethernet as back-up, respectively.[17] Figure 2 shows the logical network connection and Fig 3 shows the physical ATM connection.

Image Display

The UCSF PACS image display system is based on three implementation methods: using existing in-house workstations, working with manufacturers to develop new workstations, and distributing images and patient textual data to existing low-end desk top Macintosh computers (Apple Computers, Cupertino, CA). In the first type, we modified the two-monitor 2K display workstations developed at UCLA by adding the HIS/RIS interface and some extra display functions. An example is the Montage function that allows the assembly of images from different examinations into one file. These workstations are used in the neuroradiology and pediatric radiology sections. Second, we worked

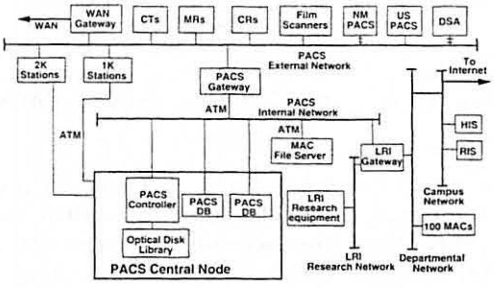

Fig 2. Department of Radiology, UCSF Logical Network Architecture, which includes WAN and LAN. The external network is open whereas the internal network has a firewall protection.

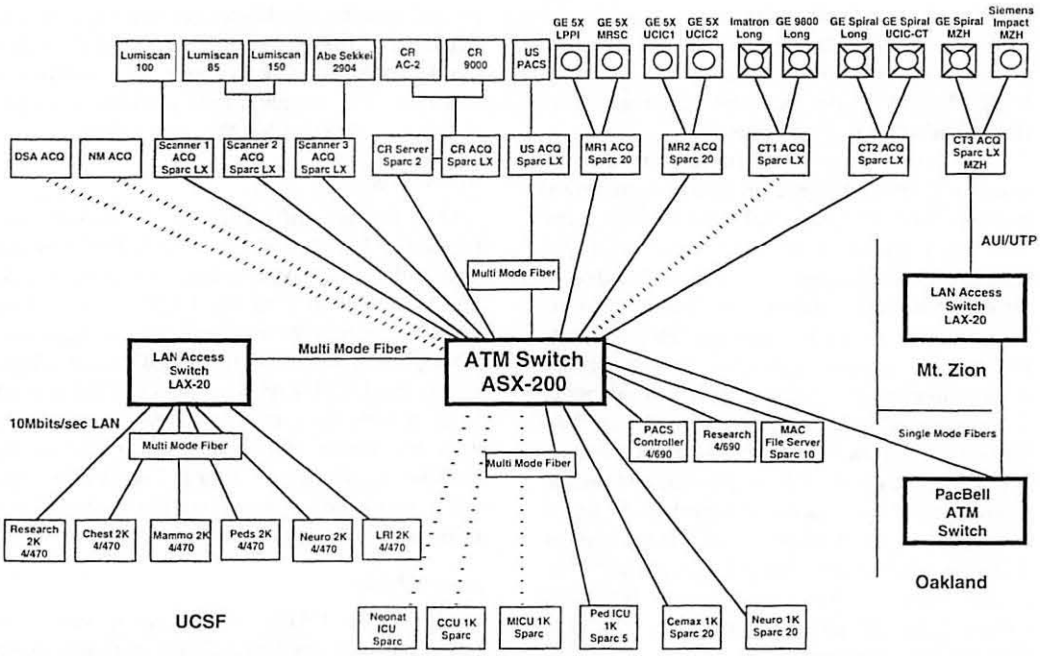

Fig 3. First phase ATM connection between UCSF and Mt Zion Hospital; (—) completed, (------) second phase. WAN and LAN ATM (155 mbits/sec) Network Physical Connection at UCSF. For those older components that do not support ATM, an ATM to LAN switch is used which supports 10 mbits/sec for every node connected to the switch.

with ISG Technologies Inc (Toronto, Ontario, Canada) to develop the two-monitor 1,600-line display stations for ICU applications. Figure 4 shows such a workstation.

The third method is to develop a file server to distribute integrated PACS images and textual data to the Macintosh desk top computers for individual review, teaching, and research.[18] Figure 5 shows the distributed network and Fig 6 depicts a page on the Macintosh screen.

MAJOR DIFFERENCES BETWEEN THE UCSF AND THE UCLA PACS

This section summarizes some major differences between the UCSF and the UCLA PACS.

PACS Controller

The PACS controller is an intelligent machine that controls the flow of data within the entire PACS from acquisition (data input) to archiving (long-term and short-term storage) and display (data output). The primary functions of the PACS controller include: (1) accepting images from acquisition nodes; (2) accepting HIS/RIS data; (3) updating global PACS data base; (4) archiving images to optical disks; (5) routing images and HIS/RIS data to display workstations; (6) handling retrieval requests from display stations.

The PACS controller implemented in the UCLA PACS was a single-processor Sun SPARCserver 490 computer, from which a one terabyte optical disk library based on 14 inch platters was attached. A three-tiered communication network comprising Ethernet, FDDI, and the proprietary fiber-optic UltraNet network was used to provide independent paths for data transmission between the PACS controller and other PACS computers. Images acquired from radiologic imaging devices were transferred from various acquisition nodes to the PACS controller, where they were then routed to destination display stations and were archived chronologically on WORM optical disks. With its fault-tolerant design, the PACS controller focused on system reliability and data integrity, promising 24-hour on-line service and no loss of images.

The PACS controller developed at UCSF includes more intelligence and thereby minimizes access time for both current and previous imaging studies. The computer system is based

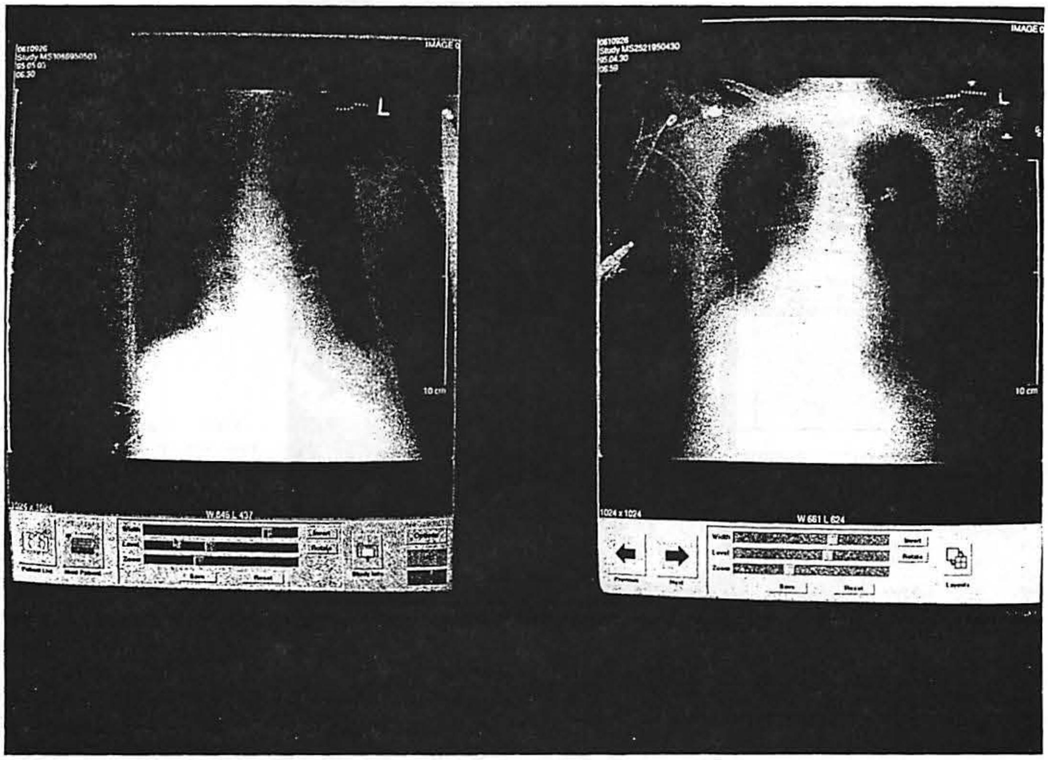

Fig 4. A 1,600-line two monitor workstation for ICUs. This station consists of a SPARC 20 with 128 Mbytes memory and two TurboGXplus cards, all off-the-shelf components. The display software was developed by ISG Technologies Inc based on UCSF specifications. The communication interface between workstations and the PACS controller was codeveloped by both parties based on the DICOM standard.

on the SUN 690 (Sun Microsystems) with four central processing units (CPUs), which allows multiple processes to run simultaneously with minimal shared CPU time. Two standard network interfaces, the Ethernet and the 155-bit/

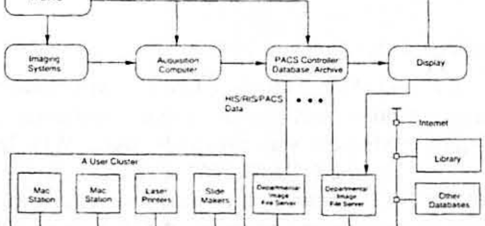

Fig 5. Distributed image file servers connected to the PACS controller. Each server provides specific applications for a given cluster of users. One of this clusters is to serve the Macintosh users in the department to access PACS data.

sec bandwidth ATM, OC 3 networks, are used for receiving and distributing images. The optical disk library attached to the PACS controller supports both erasable magneto-optical disks and WORM disks. A composite staging mechanism is implemented in the PACS controller to manage images stored in its multiple storage media: magnetic disks (immediate-access temporary storage), erasable magneto-optical disks (longer-term archive data cache), and WORM disks (permanent storage). This second-generation PACS controller differs from the first-generation system in several of its new features: multiple storage media, image stacking, automated image prefetching, studies grouping, platter management, and HIS/RIS/PACS interfacing. Table 2 shows the major differences in the infrastructure design between the two systems.

In Table 2 there are several items that were not considered in the original UCLA design, for example, integration to the HIS/RIS and other

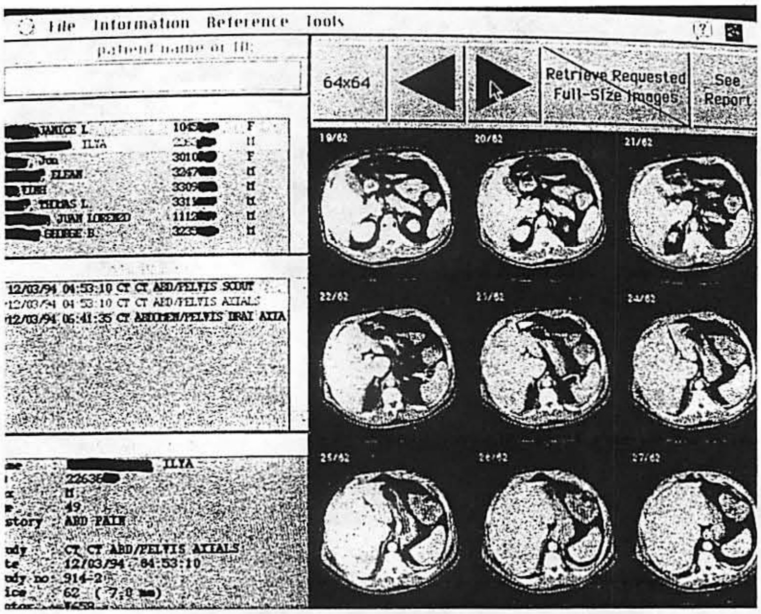

Fig 6. A page on the Macintosh screen. The user can directly access both images and textual information including diagnostic reports from PACS. The "Tools" kit allows user to manipulate individual images which includes programs like National Institutes of Health Image, etc.

vendor's PACS. The reason was because the hospital-integrated concept was not introduced until 1992. Also, the American College of Radiology-National Electrical Manufacturers Association (ACR-NEMA) and DICOM were not ready for implementation in 1991. On the other hand, the UCSF PACS does not have a duplicate PACS controller and all archiving is done within one site are because of limited space and financial resource.

Table 2. Differences in the Infrastructure Design

	UCLA (as of September 1992)	UCSF
Open architecture	limited	Y
Connectivity	limited	Y
Standardization		
ACR-NEMA, DICOM	N	Y
HL 7	N	Y
TCP/IP	Y	Y
Interface to HIS/RIS	N	Y
Interface to other vendor PACS modules	N	Y
Mirrored data base	Y	Y
Duplicate PACS control and archiving	Y	N
Different sites for archiving	Y	N
Auto routing	Y	Y
Image prefetching	N	Y
Image sequencing	N	in progress

Abbreviations: Y, Yes; N, No.

Networking

Table 3 shows the major differences in network design between these two systems. The UCLA network was mainly a LAN with very long fiber optic cable connections between buildings, whereas the UCSF system includes both WAN and LAN.

It is seen in Table 3 that the UCSF network design is more sophisticated with up-to-date network technology. On the other hand, the UCLA system had the higher speed proprietary Ultranet for high speed image communications. The UCLA system had no firewall protection for data integrity and security, which was a main draw-back in network design.

Image Acquisition Component

CT and MR. The UCLA CT/MR image acquisition systems were all made by General Electric Medical Systems (Milwaukee, WI). In this regard, the GE 9,800 CT scanners used GE IDNET-1 configuration for interfacing, and the image acquisition processes of GE high-speed CT scanners and Signa 5× MR scanners were based on GE proprietary communication protocols. The acquisition processes in the PACS did not have patient ID verification algorithm, no automatic process recovery mechanism, and no

Table 3. Differences Between the Two Networks

UCLA*	UCSF
• Fibers were used to connect remote buildings, but the backbone primarily consisted of Thicknet Ethernet (copper) that stretched through multiple buildings and levels. • Clinical acquisition, Research, and Distribution networks were all physically connected to the same subnet. Ultranet used for 2K distribution only. • AUI cables were connected directly to the backbone as opposed to CAT 5 UTP cables. Radiology Dept did not have a direct connection to the Internet. • Ultranet was used for transfer of images from the PACS Controller to the 2K display stations at a rate of 125 Mb/s. The transfer of information between the two Ultranet hubs in CHS and Medical Plaza was striped between four 250 Mb/s fibers giving a total transfer rate of 1,000 Mb/s or 1 Gb/s. • No routers or firewalls were used. • No WAN connections. • Only Med Plaza had a UPS.	• The backbone consists of primarily fiber optics, but CAT 5 UTP is the media used for station connections. • ATM via fiber used for acquisition and distribution. • The design is a distributed star configuration with multiple subnets. For examples, Genesis network is used to connect the digital modalities ie, CT, MR to the PACS controller. The departmental network is used to distribute images to Macintosh's users, etc. • PACS External network is used for transferring image data from the imaging modalities to the acquisition computers. The internal network, with a firewall protection is used to transfer data from the acquisition computers to the PACS Controller. • The External network is also used as a backup network for the display systems. • Distribution to the 1K stations is done via ATM, which uses a dedicated 155 MB/s fiber optic connection directly to the PACS Controller. • Distribution to the 2K systems is done through an ATM to Ethernet switch, which has dedicated 10 Mb/s connections to each station. • Radiology has direct connections to the Internet via the departmental network which has over 100 connections to faculty and staff offices. • Routers and gateways are used to divide subnets and insure security among the networks. • The network has T1 and ATM WAN connections to two affiliated hospitals. Network hubs are backed up by UPS's.

*As of September 1992.
Abbreviations: AUI, attachment unit interface; CAT UTP, category 5 unshielded twist pair; UPS, uninterrupted power supply.

automatic paging system for engineering service. The image header format was based on a UCLA internal design and was not standard.

The UCSF CT/MR image acquisition systems consist of multivendor equipment including GE, Siemens (Erlangen, Germany), and Imatron (South San Francisco, CA). The GE 9800 CT scanner uses GE IDNET-II configuration for interfacing, and image acquisition processes of GE spiral CT scanners and Signa 5× MR scanners are based on DICOM standard communication protocol (upper level for TCP/IP). The Siemens and Imatron use their own proprietary interface protocols.

The PACS acquisition computers have a patient ID verification algorithm to correct typographical errors by imaging modality technicians, a mechanism to automatically recover image acquisition processes, and a central paging scheme to automatically page service engineers for system fatal errors. The PACS uses both ACR/NEMA 2.0 as well as DICOM 3.0 header information format.

CR. The UCLA PACS used earlier versions of CR technology: Philips 901 and two Philips 7000 laser plate readers (Philips Medical Systems, Shelton, CT), and ST-III type photostimulable phosphor plates; while the UCSF PACS incorporates the latest in CR technology: Fuji FCR AC2 and FCR 9,000 plate readers (Stamford, CT), and ST-V (standard) and HR-V (high-resolution) photostimulable phosphor plates. The interfacing of the CR devices to PACS required three different methods: two different methods for the two different models of Philips CRs and one method compatible with both Fuji CRs. The Philips 901 digital interface consisted of a RS-422 connection to a Data Interception Circuitry (buffer) board and a DR-11W link over which the image data was transmitted to the SUN acquisition computer; textual information (demographic and image header data) came over an RS-232 cable connection. The Philips 7,000 interface device included a PCR interface processor (PIP) which contained an auto data transfer board, memory buffer board and Ethernet board and transmitted both images and text to the SUN acquisition computer over Ethernet. The digital interface to PACS for both the Fuji AC2 and the 9,000 consists of a DMS Bus with a RS-485 cable (which is a combination RS-232 serial bus for messages and textual information and an RS-422 parallel bus for image data) connection to the data acquisition system manager (DASM). The DASM is basically a ring-buffered small computer system interface (SCSI) disk that transmits both textual and image data to the SUN acquisition computer over SCSI cable. Table 4 summarizes the differences in CR between these two PACS systems.

The Display Component

The UCLA PACS display component consisted of the 2K display stations, 1K display stations, and a film printing station. The UCSF display component is comprised of 2K display stations, 1K display stations, and Macintosh stations. Both 2K stations in the UCLA and UCSF PACS are of the same hardware platform. We developed the software in-house at UCLA, and carried it over to UCSF. Certain enhancements have been added to the software at UCSF based on users' feed-back. In particular, there is a local montage feature for users to select images from different files for display. A feature with 1 on 1 for current images and 4 on 1 for historical images was specifically designed for pediatric CR image viewing. The study list automatic update feature alerts users that the active (selected) patient has a new image file just arrived. Another new feature is a workstation usage statistic software package to track system usage. This package allows refinement of workstation software based on users' working habits.

The UCLA 1K system was developed based on an in-house designed display board which supported three 1,024 monitors. The UCSF 1K system is developed in collaboration with ISG Technologies Inc based on off-the-shelf components. This 1K system can support either 2, 3, or 4 1,600 line monitors, and has very easy to use user interface.

The UCSF system currently does not support a film printing station, instead, it supports over 100 Macintosh users to retrieve images and related PACS data for research, teaching, and case review. From these Macintosh computers, the users can select other printing resources in the department for hardcopy output. Table 5 summarizes the major differences in the display components between these two PAC systems.

Table 4. Differences Between the CR Acquisition Components

	UCLA*	UCSF
Devices	Philips 901 Philips 7,000 (two)	Fuji AC2 Fuji 9,000
Phosphor plate type	ST-III	ST-V, HR-V
Interface	DR-11W board to 901 PIP to 7,000	DASM to AC2 and 9,000

*As of September 1992.

Table 5. Major Differences in the Display Component Between the Two PAC Systems

Types of Workstation	UCLA*	UCSF
2K	SUN 4/470, Megascan display boards with two monitors (4)	Same with new enhancement software (4)
1K	SUN 4, in-house display board with three 1,024 monitors (2)	SPARC 20, Tubor GX+ boards supporting 2, 3, or 4 monitors (5)
Film printing	Y	N
PC station	N	100

*As of September 1996.

DISCUSSION

Both the UCLA and the UCSF PACS are designed in-house based on the SUN workstation platform. Because of the evolution of the PACS concept, the UCSF system is designed as a hospital-integrated PACS with the ACR-NEMA and DICOM and HL7 standards. Relevant data from HIS and RIS is automatically incorporated in the PACS. Other manufacturer's PACS components that conform with these standards can be easily integrated into the system. The UCSF system also takes advantage of newer communication, storage, and software technologies in ATM, multiple storage media, and automatic programming for a better cost-performance system.

The new concepts of auto-routing, prefetching, and auto-sequencing have influenced our design in the UCSF PACS controller, which is quite a drastic difference from the UCLA PACS controller. With the client-server concept, we are able to implement the Macintosh server to distribute PACS images and patient textual data to every Macintosh user in the department. This feature was not available in the UCLA system because of a lack of such knowledge on our part as well as not understanding the importance of data distribution to every radiologist and clinician at that time.

To our disappointment we have not seen any improvement in the 2K display technology in 5 years. Both the UCLA and UCSF 2K display systems are practically the same in terms of hardware platform and display software. On the other hand, 1K display has improved in both performance and cost.

The UCSF hospital integrated PACS has been developed to such a stage that the infrastructure will not become obsolete and it can support any new PACS components as well as additional acquisition modalities and display workstations. PACS system refinement will continue evolving for higher reliability, better performance, and new application functions as its development is a continuous dynamic process.

REFERENCES

1. Huang HK: Three methods of PACS research, development, and implementation. Radiographics 12:131-139, 1992

2. Huang HK, Mankovich NJ, Barbaric Z, et al: Design and implementation of multiple digital viewing stations. *Proceedings of the Society of Photo-Optical Instrumentation Engineers Second International Conference on Picture Archiving and Communication Systems for Medical Applications (PACS II)*, vol 418. 1983, pp 189-198

3. Taira RK, Mankovich NJ, Boechat MI, et al: Design and implementation of a picture archiving and communication system (PACS) for pediatric radiology. Am J Roentgenol 150:1117-1121, 1988

4. Cho PS, Huang HK, Tillisch J, et al: Clinical evaluation of a radiologic picture archiving and communication system for coronary care unit. Am J Roentgenol 151:823-827, 1988

5. Huang HK, Kangarloo H, Cho PS, et al: Planning a totally digital radiology department. Am J Roentgenol 154:635-639, 1990

6. Huang HK, Taira R: Infrastructure design of a PACS. Am J Roentgenol 158:743-749, 1992

7. Huang HK, Wong WK, Lou SL, et al: Architecture of a comprehensive radiologic imaging network. IEEE JSA Comm 10:1118-1196, 1992

8. Wong WK, Taira RK, Huang HK: Digital archive center: Implementation for a radiology department. Am J Roentgenol 159:1101-1105, 1992

9. Huang HK, Taira RK, Lou SL, et al: Implementation of a large scale picture archiving and communication system. Comp Med Imaging & Graphics. 17:1-11, 1993

10. Osteaux M: A Second Generation PACS Concept. Berlin, Germany, Springer-Verlag, 1992, pp 1-322

11. Huang HK, Arenson RL, et al: Multimedia in the radiology environment: Current concept. Comp Med Imaging & Graphics 18:1-10, 1994

12. Breant CM, Taira RK, Huang HK: Interfacing Aspects Between the PACS, RIS, and HIS. J Digit Imaging 6:88-94, 1993

13. Arenson RL, Avrin DE, Wong AWK, et al: Second Generation Folder Manager for PACS, in: Boehme JM, Rowberg AH, Wolfman NT (eds), Proc 12th Comp Appl to Assist Radiol, SCAR 94:601-605, 1994

14. Health Level Seven: An Application Protocol for Electronic Data Exchange in Healthcare Environments. Ann Arbor, MI, Health Level Seven Inc, 1991

15. Moskowitz M, Gould RG, Huang HK, et al: Initial Clinical Experience with Ultrasound PACS. Proc SPIE Med Imaging. 2435:246-251, 1995

16. Wong AWK, Huang HK, Arenson RL, et al: Multimedia Archive System for Radiologic Images. Radiographics 14:1119-1126, 1994

17. Huang HK, Arenson RL, Dillon WP, et al: Asynchronous transfer mode (ATM) technology for radiologic communication. Am J Roentgenol 164:1533-1536, 1995

18. Ramaswamy MR, Wong AWK, Lee JK, et al: Accessing a PACS's text and image information through personal computers. Am J Roentgenol 163:1239-1243, 1994

Journal of Digital Imaging

VOL 9, NO 4 NOVEMBER 1996

Clinical Experience With a Second-Generation Hospital-Integrated Picture Archiving and Communication System

H.K. Huang, Albert W.K. Wong, Andrew S.L. Lou, Todd M. Bazzill, Katherine Andriole, Jianguo Zhang, Jun Wang, and Joseph K. Lee

In a previous report we described a second-generation hospital-integrated picture archiving and communication system (HI-PACS) developed in-house. This HI-PACS had four unique features not found in other PAC systems. In this report, we will share some of our clinical experiences pertaining to these features during the past 12 months. We first describe the usage characteristics of two 2,000-line workstations (WSs), one in the in-patient and the second in the out-patient neuroradiology reading area. These two WSs can access neuro-images from 10 computed tomographic and magnetic resonance scanners located at two medical centers through an asynchronous transfer mode network connection. The second unique feature of the system is an intensive care unit (ICU) server, which supports three WSs in the pediatric, medical surgery, and cardiac ICUs. The users' experiences and requests for refinement of the WSs are given. Another feature is physician desk-top access of PACS data. The HI-PACS provides a server connected to more than 100 Macintosh users for direct access of PACS data from their offices. The server's performance and user critiques are described. The last feature is a digital imaging and communication in medicine (DICOM) connection of the HI-PACS to a manufacturer's ultrasound PACS module. The authors then outline the interfacing process and summarize some of the difficulties encountered. Developing an in-house PACS has many advantages but also some drawbacks. Based on experience, the authors have formulated three axioms as a guide for in-house PACS development.

KEY WORDS: picture archiving and communication system (PACS), system implementation, clinical experience, infrastructure design, open architecture, display workstation.

THE UNIVERSITY of California at San Francisco (UCSF) is a health sciences campus located in the San Francisco Bay area comprising two medical centers. The distance between the main campus (UCSF Medical Center) and the Mt. Zion Medical Center (MZH) is 2 km. Table 1 shows some statistics of the two campuses. In addition, UCSF also affiliates with the San Francisco VA Medical Center (SF-VAMC). The HI-PACS at UCSF was designed to connect all three medical centers.

The design concept of the HI-PACS at UCSF is based on standardization and open architecture.[1] The concept of open architecture design means that system software and hardware components in the system can be replaced and upgraded without affecting the system operation. Any change in the hardware platform or the software operating system (OS) requires only the development of an adapter (software layer) between the existing application software and the new operating system. The application software remains intact. This design philosophy minimizes the software development cost that remains a major obstacle in PACS implementation. Table 2 summarizes some industry standards used in the system.

The system infrastructure implementation is based on in-house development. The worksta-

From the Laboratory for Radiological Informatics, Department of Radiology, University of California, San Francisco, CA.

Partially supported by IBM Research Center, PHS grant PO1 CA 51198, NLM contract NO1-LM-4-3508, NCHS BPA 50257C-95, National Center for Health Statistics, CalREN grant ATMN-007, Pacific Bell, US Army Medical R&D DAMD 17-94-J-4196, US Army Medical R&D DAMD 17-94-J-4338, Lumisys (equipment), Fuji Medical Systems USA, Inc (equipment), Abe Sekkei, Japan (equipment), Polaroid, and California Breast Research Program.

Address reprint requests to H.K. Huang, DSc, Laboratory for Radiological Informatics, Department of Radiology, University of California, San Francisco, CA 94143-0628.

0897-1889/96/0904/0001$3.00/0

Table 1. The University of California at San Francisco Medical Center Statistics (Annual)*

Parnassus Campus	Mt. Zion Campus
560 beds with 76% occupancy	230 beds with 61% occupancy
22,200 admissions	6,800 admissions
7.1-day average length of stay	7.9-day average length of stay
289,000 patient visits	29,500 patient visits
23,000 emergency room visits	17,500 emergency room visits

*From 1993 survey.

tion (WS) design and interface with other manufacturer's PACS modules are accomplished through a close collaboration with private industry. In the following, the authors first describe the system of today and its estimated costs. They then highlight certain features that are unique in this system compared with other PACS systems.

The authors describe their clinical experience in four areas: neuroradiology WS usage characteristics, ICU WS user preference, physician desk-top image/report access, and connection of a manufacturer's ultrasound (US) PACS module to the authors' PACS infrastructure. In the last section, the authors formulate three axioms as a guide for in-house PACS implementation.

SYSTEM DESCRIPTION

Overall Architecture and Component Connections

The second-generation PACS at UCSF has been described elsewhere.[2] For completeness, the authors summarize its main features briefly here. The complete system architecture is shown in Fig 1.

The system uses state-of-the-art communication, storage, and software technologies in asynchronous transfer mode (ATM), multiple storage media, automatic programming, and multilevel process control for a better cost-performance system. The primary PACS local area network is the 155 Mbits/sec OC3 ATM[3] with the Ethernet as the back-up. The system also connects MZH and SFVAMC via an ATM wide area network with a T-1 line as the back-up. Relevant data from the hospital information system (HIS) and radiology information system (RIS) is automatically incorporated into the PACS using Health Level 7 data format[4] and Transmission Control Protocol/Internet Protocol (TCP/IP) communication protocol.

Table 2. Standards Used in the UCSF HI-PACS

• Image format	DICOM 3.0 (ACR/NEMA 2.0)
• Data format	Health Level 7
• Computer operating system and language	UNIX Operating System C Programming Language X-Window User Interface
• Communication protocol	TCP/IP
• Data base query	SQL Structured Query Language

Image Acquisition

Currently, five magnetic resonance (MR) and five computed tomographic (CT) scanners from multiple sites, two computed radiography systems, two film digitizers, one US PACS module, the hospital HIS, and the department RIS have been connected to the PACS network. The imaging acquisition components are described subsequently.

CT and MR. The network is connected to 10 CT/MR scanners located at both UCSF and MZH (CT: 3 GE spiral, 1 GE 9800 Quick [Milwaukee, WI], and 1 Imatron [South San Francisco, CA]; MR: 4 GE Signa 5 and 1 Siemens Vision [Erlangen, Germany]). The GE 9800 CT scanner uses GE IDNET-II configuration for interfacing and image acquisition processes. GE spiral CT scanners and Signa 5X MR scanners are based on DICOM standard communication protocol (upper level for TCP/IP). The Siemens and Imatron use their own proprietary interface protocols.

The PACS acquisition computers have a patient identification (ID) verification algorithm to correct typographical errors by imaging modality technicians, a mechanism to recover image acquisition processes automatically, and a central paging scheme to page service engineers automatically for fatal system errors.[5] The PACS uses both the American College of Radiology/National Electrical Manufacturers' Association (ACR/NEMA) 2.0 as well as the digital imaging and communication in medicine (DICOM) 3.0 header information format.[6,7]

Computed radiography (CR). The UCSF PACS connects to one FCR AC2 (Fuji Medical Systems, Tokyo, Japan) and one FCR 9000 system. Both systems use ST-V (standard) and HR-V (high-resolution) photostimulable phosphor plates. The digital interface to PACS for

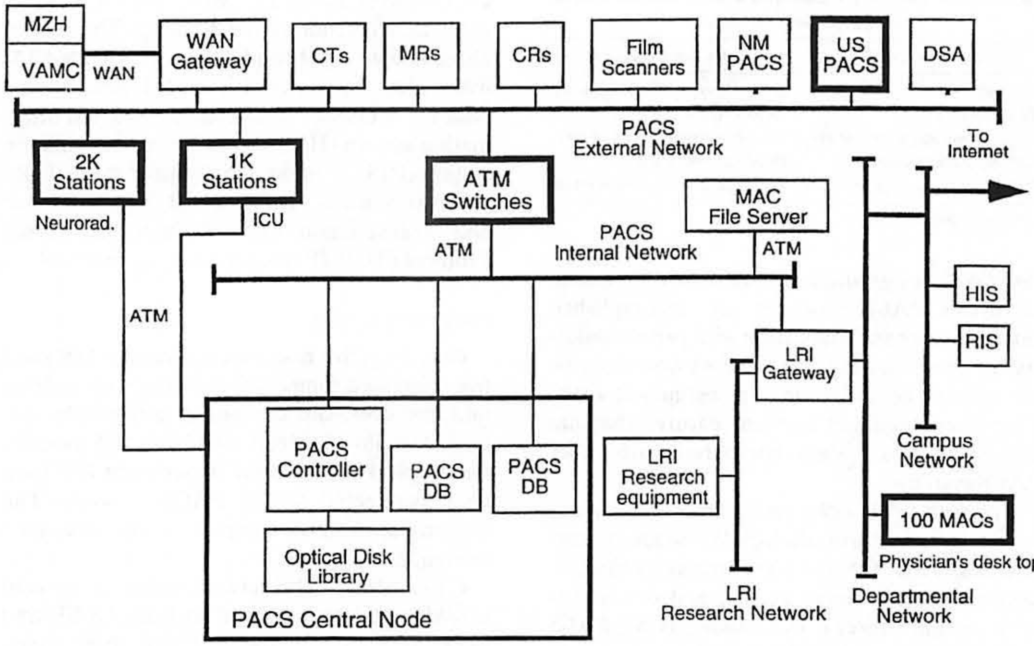

Fig 1. Department of Radiology, UCSF network architecture. The bold rectangles are the components unique to this HI-PACS.

both systems uses a direct memory access Bus with a RS-485 cable (a combination of RS-232 serial bus for messages and textual information, and a RS-422 parallel bus for image data) connection to the data acquisition system manager (DASM). The DASM is basically a ring-buffered small computer systems interface (SCSI) disk that transmits both textual and image data from the CR to the SUN acquisition computer (Mountain View, CA) over a SCSI cable. All intensive care unit (ICU) portable, pediatrics, and newborn radiographic examinations use the CRs.

Two important features developed for automatic CR image acquisition are automatic background recognition and removal, and multilayer adaptive process control. The former allows the automatic background removal from CR, allowing a high percentage of correct automatic rotation and look-up table setting.[8] The multilayer adaptive process control guarantees no loss of CR images from the CR to the acquisition computer.[9]

Display WS

The authors use three types of display WSs: 2,000-line (2K), 1,600-line (1K), and Macintosh computers. The description of the 2K station is given by Huang et al.[10] A feature in the 2K station is a WS usage statistic software package that tracks system usage. This package allows refinement of WS software based on users' working habits.

The 1K system was developed in collaboration with ISG Technologies, Inc (Ontario, Canada) based on off-the-shelf hardware components. This 1K WS can support two to four 1,600-line monitors and has a user-friendly interface. Figure 2 shows the schematic of the ICU 1K WS.

The PACS also supports more than 100 desk-top Macintosh users for images and related PACS data retrieval for research, teaching, and case review. From these Macintosh computers, radiologists can select other printing resources in the department for hard-copy output. Table 3 summarizes the specifications of these three types of image display WSs.

Networking

A unique feature in our PACS network is a two-tier system with ATM as the primary network,[2] and Ethernet and T-1 as the secondary.

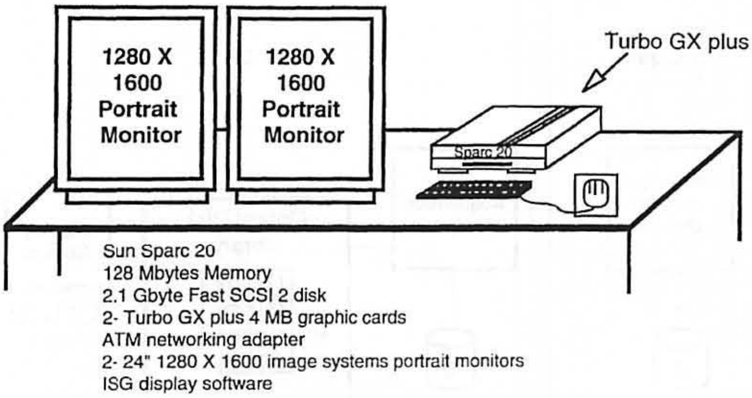

Fig 2. Schematic of the 1K WS used in ICU.

Table 4 shows the characteristics of the PACS network.

Storage Management

To ensure that no images are lost once they are acquired from an imaging modality, two copies of the same image are always retained in the PACS until it is archived in the optical disk library (Fig 3D). Figure 3 shows the four-level image storage scheme in which the same image always resides in two of the four intermediate disk systems A to C or E. The image data in the 1.3-Tbyte optical disk library (ODL) is managed by a mirrored database (Sybase, Emeryville, CA). The system acquires 2.5-Gbytes digital data daily.

Cost Estimate

Table 5 shows the cost estimate of the UCSF HI-PACS as of today. This cost estimate does not include personnel. The PACS infrastructure development involves about seven to eight full-time equivalents (FTEs) per year for years 1 and 2, and about five to six during year 3.

Equipment in Table 5 includes the cost for all infrastructure components described here and by Huang et al[2] consisting of two CRs, two

Table 3. Specifications of Three Types of Display WSs

WS Types	Specifications (No. of WSs)
2K	SUN 4/470, Megascan display boards with two monitors (four WSs in Neuroradiology and Pediatric Radiology)
1K	SPARC 20, Turbo GX+ boards supporting two monitors (five WSs in ICUs, quality assurance, and ICU server)
Physician desk-top	Macintosh (100)

Table 4. Characteristics of the UCSF HI-PACS Network

Function	Description
Media	The network backbone consists of primarily fiber optic cables. Category (CAT) 5 unshielded twisted pair (UTP) is used for some WS connections.
Router/gateway/hub	Routers and gateways are used to divide subnets and ensure security among the networks. The design is a distributed hub configuration with multiple subnets. For example, Genesis network by GE is used to connect the digital modalities (ie, CT/MR) to the PACS controller. The departmental network uses routers to distribute images to Macintosh users, etc.
Communications technologies	ATM and Ethernet WAN and LAN via fiber and UTP are used for image acquisition and distribution. Ethernet and T-1 are used for back-up.
Image acquisition	PACS external Ethernet network is used for transferring image data from the imaging modalities to the acquisition computers. The ATM network with firewall protection is used to transfer data from the acquisition computers to the PACS controller.
Image distribution	Image distribution to the 1K WSs from the PACS controller is transmitted via the 155 Mbits/sec ATM network. Image distribution to the 2K WSs is transmitted through an ATM to an Ethernet switch, which has dedicated 10 Mbits/sec connections to each WS.
Connection to the outside world	T1 and ATM WAN are used to connect two affiliated medical centers. Departmental Ethernet is used to connect to the Internet and to more than 100 Macintosh computers in the department.

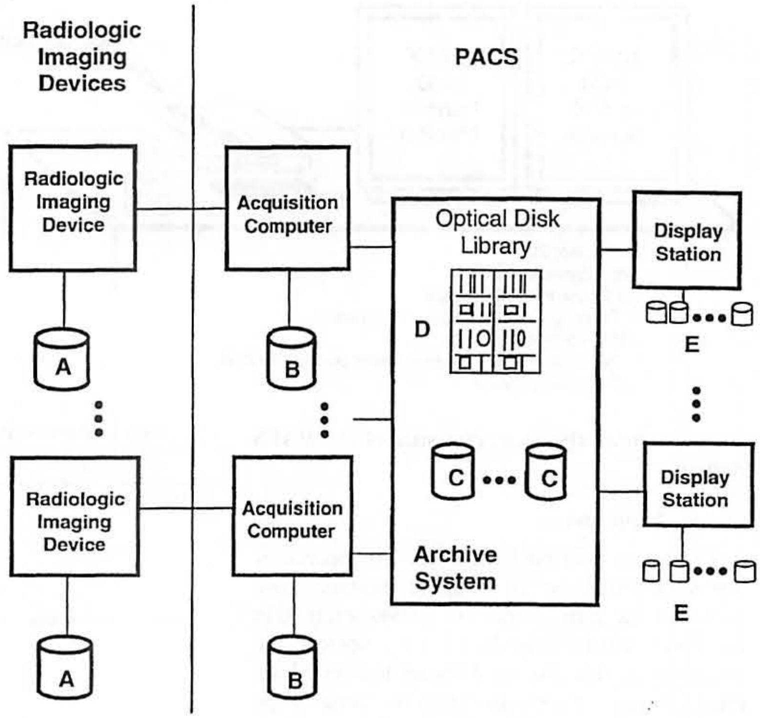

Fig 3. Four-level image storage scheme to assure no images lost (see text for explanation).

digitizers, one US PACS module, one ODL, one fiber optic broadband system, ATM switches, fiber optic cables and routers, a mirrored database, and four 2K and three 1K WSs. The actual cost is after the manufacturer's discount. The research and development (R&D) contributions are from research grants and contracts, and funds generated by the authors' laboratory. Maintenance and consumables are annual costs paid by the hospital.

CLINICAL EXPERIENCE

In this section, the authors describe their clinical experience in four areas: neuroradiology WSs for teleradiology applications, ICU WS use, physician desk-top image and report access, and connection of US PACS module to the infrastructure. These four areas are unique in the authors' PACS compared with other PAC systems currently in clinical operation.

Table 5. UCSF Hospital Integrated PACS Infrastructure Costs (Approximate) (April 1995)

	Actual Cost ($)	R & D Contributions ($)	Cost to UCSF ($)	Annual Maintenance and Consumables*
Equipment only	2,300K	800K	1,500K	360K

*Maintenance includes US PACS module and two CRs. Consumables includes optical disks for long-term archive.

Neuroradiology

Distinctive features in the neuroradiology application are the two WSs and their remote reading feature. The neuroradiology section at UCSF manages and supervises all neuroradiology cases at UCSF and MZH. Beginning in May 1995, we placed two 2K-line, two-monitor WSs in the in-patient and out-patient neuroradiology reading areas at two separate buildings in UCSF. Both stations have an identical image database each with a capacity of storing more than 1-week of current neuro CT/MR examinations and some with historical images. The neuroradiology section is currently still running a dual display system with both film and soft copy. Neuroradiologists are free to use either display mode or both for their daily clinical practice.

Table 6 shows a 4-month summary from May 1995 to August 1995 of the total neuro-CT/MR procedures performed at both UCSF and MZH and the soft-copy reading statistics. To interpret the statistical data, the user first considers the

Table 6. Number of Neuro-CT/MR Examinations and WS Soft-Copy Reading Statistics

	1995			
	May	June	July	August
Total no. neuro-CT/MR examinations at				
UCSF	1,028	996	938	1,022
MZH	268	283	283	309
Patient select				
In WS*	480	585	444	612
Out WS†	131	73	216	175
Utility of WS (%)‡	47	51	54	59
Library search				
In WS	148	196	281	292
Out WS	182	84	249	172
Find patient				
In WS	32	70	54	45
Out WS	32	9	27	24

*In-patient workstation, no. of requests.
†Out-patient workstation, no. of requests.
‡"Patient select" "total number of examinations."

2K WS patient monitor directory, which shows all current patient examinations by patient name and ID in the local parallel transfer disks. Scroll to the selected patient, and click the mouse constituting one "patient select" request (second row). After a patient is selected and if some older images required for comparison are not in the local disk, clicking the "Lib Search" (library research, fourth row) button allows the user to find out if this patient has older images from the global data base in the ODL.

If the user wants to select a patient who is not in the local disk, then "Find Patient" (fifth row) is the proper command. After the patient is selected, it takes about 1 to 1.5 seconds to display the images on the 2K monitor if they are in the local disk and about 45 seconds if they are in the ODL. Table 6 shows that in August 1995, about 59% ([612 + 175)/(1,022 + 309]) of all neuro-examinations were read with the soft-copy method, assuming that each patient was only read one time at the station. We define this percentage as the "utilization of the WS/exam." Also in August, about 59% ([172 + 292]/[612 + 175]) of the time the user wanted to see if a selected patient had previous examinations. Our log indicates that the "utility of the WS/exam," shows a steady increase to about 80% in January 1996, demonstrating that soft-copy reading is gaining acceptance in neuro-imaging. The request to see if a patient has previous examinations remains steady at about 61%.

One unique feature in the neuroradiology PACS application is that all CT/MR images from MZH are transmitted directly to UCSF through the ATM network. For these images, although a neuroradiology fellow may be at MZH interpreting them with films, all readings are verified at UCSF through the two 2K WSs (ie, all 309 examinations done in MZH in August were reviewed or primarily read on the WSs).

We will describe here the similarity and differences of the in-patient and out-patient neuro-WS use. Figure 4 shows the in-patient and the out-patient WS usage by hour in August 1995. The in-patient WS was used almost hourly with a bimodal distribution with two peaks at 8 to 10 AM and 4 to 5 PM. The out-patient WS usage was different. It was used from 8 AM to 6 PM with two peaks at 10 AM and 12 PM. Figure 5 shows the duration of WS use after a patient selection. Both WSs exhibit similar trends with duration from 0 to 4 minutes. More than 20 minutes' duration means there were no other activities with the WS during the next 20 minutes after the last usage. Table 7 shows the in-patient and out-patient WS usage by function. The end numerals 1 and 2 in some functions (eg, IMAGE_SELECT1 and IMAGE_SELCT2) represent monitors 1 and 2, respectively. The functions most commonly used were patient select, library search, image select, cine mode, window level, and find patient. Image select is used when an examination has more than one study (sequence). To the authors' surprise, even though reports were available at the WS through an RIS interface with instant retrieval, its (REPORT_SELECT) usage was almost negligible. The last function, WS_MAIN_STARTUP, means that during that month the in-patient workstation somehow crashed and rebooted itself eight times. We found similar trends in WS usage in other months.

ICU WSs

ICU server. The PACS infrastructure includes an ICU server based on the client/server principle shown in Fig 6.[11] Currently, the authors' ICU server is serving three units, which

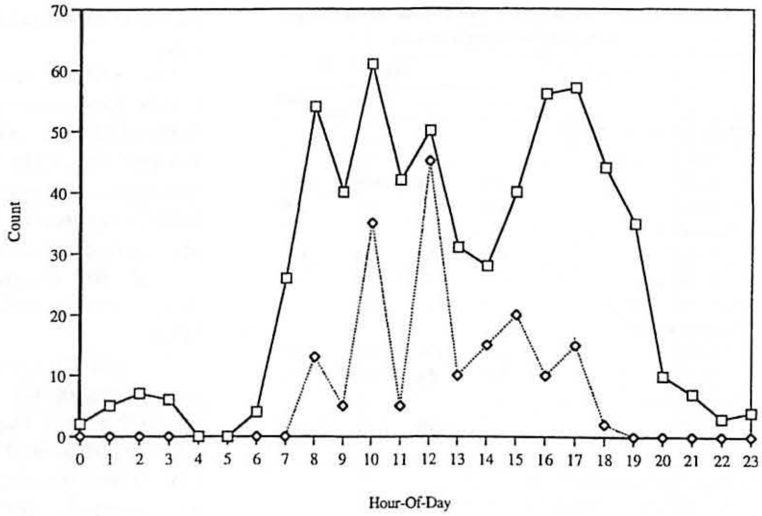

Fig 4. Neuroradiology workstation image usage by hours of the day—selection (August 1995). —□—, inpatient; ---◇---, outpatient.

include the pediatric (16 beds), medical surgery (16 beds), and cardiac care (14 beds). Three WSs, one at each ICU, were installed sequentially during a 1-month period in 1995. The ICU server, containing 30-Gbyte redundant array of inexpensive disks (RAID), can be easily expanded as needed. Instead of configuring a large global data base, which can bring all three ICU applications to a halt should the global data base become inoperable, the ICU server maintains a separate data base for each ICU WS. In other words, images are stored centrally yet managed in a distributed data base environment.

A local directory containing all the current patients of that ICU is maintained. A user can request images of a patient by first selecting the patient ID from the patient directory. On receiving the request, the ICU server routes the patient's images and demographic data back to the ICU WS through an ATM network.[11] Images are transferred in their original size to the WS's memory cache but are interpolated to 1,600 × 1,200 for the two display monitors.

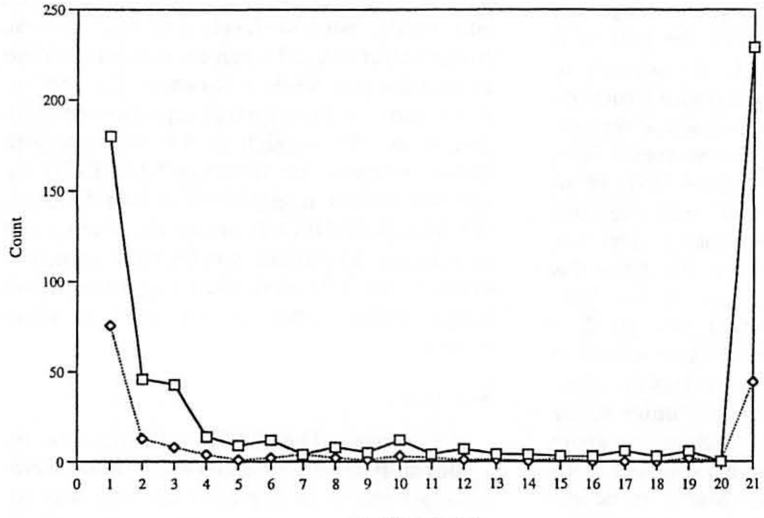

Fig 5. Duration of the neuroradiology WS in use after a patient selection (August 1995). —□—, inpatient; ---◇---, outpatient.

Table 7. Neuroradiology WS Usage by Function (August 1995)

Function	In-Patient	Out-Patient
Patient Select	612	175
Sort Mode	110	29
Library Search	292	172
Report Select	9	4
Patient Search	45	24
Image Select 1	562	76
Image Select 2	906	176
Cine 1	357	54
Cine 2	603	101
Zoom/Scroll 1	37	2
Zoom/Scroll 2	107	9
Measure 1	9	
Measure 2	12	
Region of Interest (ROI) 1	7	
ROI 2	5	
Slice Select 1	1	8
Slice Select 2	3	3
Window/Level 1	175	24
Window/Level 2	435	49
CT brain	2	
CT liver	1	2
Bone	34	10
Lung	1	
Soft tissue	28	8
Look-up Table (LUT) defaults	20	2
Negative	2	2
Globalize	22	13
Montage	5	1
WS Main Start-Up	8	9

While one monitor maintains the most current image, the other monitor can be used to review the set of remaining images.

To manipulate images, many user-friendly, easy-to-use functions are available. Some of the most frequently used features include window and level, zoom, rotation, and image layouts. Through a pop-up window, a patient's demographic data and study information can be obtained. Real-time access to historical images and diagnostic reports is also available. The image retrieval icon allows a user to retrieve images from the PACS archive that are not in the ICU server. The report icon allows instantaneous access to the Sybase data base, which stores all the diagnostic reports obtained from the RIS. When a report request is initiated, a report window will open, and a user can browse through the directory of all available reports. Because of direct access, historical images and diagnostic reports can be forwarded from the PACS to an ICU workstation without severely affecting the performance of the ICU server.

The image acquisition process is through a FCR-9000 and a FCR AC-II CR System. The technologist enters a two-letter code designating a particular ICU when the CR reads the imaging plate. During the acquisition process, the CR image is first converted to DICOM 3.0 format. The patient ID is then validated, and special utility is run to remove any white background[8] and to send the image to the PACS. On receiving the CR image, the PACS archives the image onto the ODL, updates the mirrored Sybase data bases, and routes a copy of the image to the ICU server. An acknowledgment is

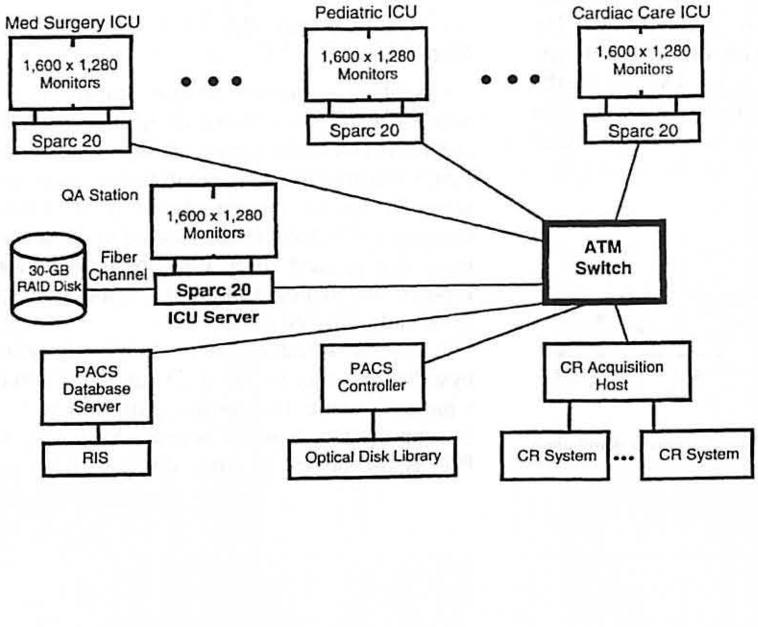

Fig 6. An ATM distributed PACS server for ICUs.

also sent back to the acquisition computer so that the local image there can be purged (see Fig 3).

Clinical experience. The ICU WS performance has been exceptional during the past 6 months without any interruption from hardware, software, or the ATM network. Physicians, on average, are able to request and review the first image within 1.5 to 2.0 seconds. Figure 7 shows a typical 24-hour viewing activity distribution in the medical surgery ICU. The WS was accessed at almost every hour of the day with two peaks during premorning and sign-out rounds. Based on the authors' 6 months of clinical experience with these three ICU WSs, we conclude the following:

1. *Robustness.* We have not experienced any down time in these three WSs during the past 6 months. They believe it is due to a combination of robustness in both hardware components and software design. All hardware components are off the shelf; therefore, the maintenance and service requirement is minimal. The software was developed jointly by ISG Technologies, Inc (Toronto, Canada) and the authors' laboratory. It went through three revisions with input from clinicians before the WSs were installed. The software is user friendly and easy to use.

2. *Physicians' reaction.* The physicians at the ICUs accepted the system the first day it was installed, and it has become an integral part of their daily clinical operation. The viewing time of a patient image is usually less than 1 minute. The location of these three WSs in the ICUs are different. In the medical/surgical ICU (MICU), the WS is side by side with other monitoring systems at the nursing station. The WS in the cardiac ICU is located in the conference area with a large window. Because of the ambient light, the image quality on the monitors is suboptimal. In the pediatric ICU, it is at the entrance of the unit. Regarding WS usage, although reports from RIS are usually available within 6 to 12 hours, they are seldom requested. According to the clinicians, for easy cases they can interpret them themselves; for difficult cases, they would have already consulted with the radiologist; in either situation, a report delayed 6 hours adds little value if any.

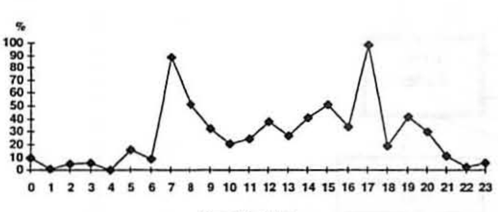

Fig 7. Medical ICU display WS viewing activity distribution over a typical 24-hour period.

Two requests from these ICUs surprised us. In the pediatric ICU, because the WS is at the entrance of the unit, the staff asked to have a screen-saver program added with a short (1-minute) time-out so that images would disappear from the screen if no action is taken for 1 minute. The rationale behind this was that the physicians do not want relatives or visitors of ICU patients seeing those images when they walk into the unit, whereas in the MICU and cardiac ICU no such request was made. The WSs have a patient image retrieval icon so that any images from the PACS archive can be retrieved when requested. A couple of months after the WSs were installed, MICU requested the button be removed. The reason was that house staff rotating through other ICUs that do not have WSs learned how to retrieve their patients' images from the MICU workstation. The MICU felt that such activity interfered with their daily clinical work progress and also accumulated patients in the local data base directory who did not belong to the MICU.

Access of Multimedia PACS Information from a Macintosh-Based WS

Operation. Another unique feature in the authors' PACS is a server designated to allow clinicians and radiologists access to multimedia PACS information for research, teaching, and review from his or her desk-top Macintosh computer.[12,13] Once it is connected to the server, users can request three types of information: reports and demographic data, thumbnail images, and full-sized images.

A user can retrieve patient study information by either entering a patient ID number (PID) or a patient's name. In addition, pattern matching is supported in a name search. Searching by PID is the fastest because the data base has maintained an index on the PID, whereas searching by a patient's name can take longer. If the retrieval is successful, vital textual information concerning the studies of the patient will be displayed in the study windows (see Fig 6 in Huang et al).[2]

Users can click on any study to retrieve the thumbnail sketch. When the thumbnail sketch arrives, a user can page through the entire set or click the report button to see the diagnostic report associated with the study. The resolution of thumbnail images are 128×128. Any of the individual thumbnail images, however, can be magnified up to 256×256 resolutions for better viewing. Also, NIH Image, a public domain Freeware from National Institutes of Health, can be launched to provide window and level adjustments while reviewing the thumbnail sketch. After examining the thumbnail, users can request one or more full-resolution images. The full-sized images have a standard 8-bit picture (PICT) format or 12-bit full-resolution raw image format.

Users can name these full-resolution images and store them in their image folder in the Macintosh. In general, these images have been windowed and leveled to a default setting according to the type of image before they arrive on the Macintosh. The PICT format images can be easily manipulated by various popular Macintosh-compatible software, such as Photoshop or Powerpoint. These off-the-shelf programs have some excellent tools for image annotation, editing, filtering, window and level adjustment, printing, and making slides.

Within the application, a user can connect to other medical informational resources without leaving or interrupting the client application. These resources include HIS, RIS, Medline, and UCSF library on-line catalog.

System usage. More than 100 Macintosh computers in our department have been connected to the server for PACS information access, but only 10 to 15 are active. Most clinicians use them to access particular images from an interesting case, mostly in MR or CT. Several sections trained their administrative assistants to retrieve cases for research projects. The availability of raw images from the past 2 years at their desk-top is a quantum leap from the traditional method of getting raw images from tapes or disks in the CT or MR scanner rooms.

Performance and reliability. The connection of the Macintosh computer to the server is through conventional Ethernet. The response time to retrieve demographic and historical text data from the PACS data base through the Macintosh, using the PID as the search key, ranges from less than 2 to 5 seconds. However, when the patient name is used as the search key, the response time can vary between 4 to 15 seconds because of the nonindexed search.

The response of the thumbnail sketch request also varies and depends on the size of the study. In general, if the retrieval is successful, it takes between 5 to 45 seconds. The performance is significantly better in the evening than during the peak hours of the day because of lesser network contention.

Once the thumbnail sketch is received, the response time to request full-resolution images is fast. Because the server retains a copy of the original full-sized images after sending the thumbnail set, requesting full-resolution images can bypass the PACS central archive and the PACS data base resulting in an impressive response time. The average time to receive a single CT slice is less than 2 seconds, and multiple-slice requests may take slightly longer. However, performance can be degraded tremendously during peak traffic hours because of the large file size of the image.

System availability is considered satisfactory. It operates on a 24 hours per day, 7 days per week basis. The server machine has been running without interruption for a 5-month period. The system requires little operator intervention and maintenance. The required system administration routine is to maintain users' log-in accounts and the Internet addresses of the client machines.

Users' feedback. Users, in general, are happy about this feature in the PACS because it allows them access to both images and text at their desk-top with minimal effort. However, there are several criticisms to be considered in revising the next system design.

In the infrastructure design, accessing PACS information from a physician desk-top computer is considered a low priority compared with accessing from clinical WSs. For this reason, the PACS allocates the server a maximum of 3 minutes for each request. After 3 minutes, if the retrieval is not completed, the server aborts the request automatically without requeuing. Because the communication from the Macintosh to the server is through Ethernet, retrieving a large image file like a CT body examination may exceed the 3-minute limit during peak hours. Users were usually frustrated under this circumstance. Although the authors tried to adjust the 3-minute limit to a longer one, it did not help much because of the characteristics of Ethernet protocol. Once the network transmission slows down, retrying will normally create more network collisions. A fundamental change in design, for example, would be to put the request in a dormant state once the system senses a slow-down in the transmission, notify the user, and retry again during off hours.

Because the storage capacity in the server (Sun SPARC 10 with 8 Gbytes of disk storage) is limited and must serve about 100 Macintosh computers (Cupertino, CA), we limited the retrieval program to a maximum of 32 most recent sequences (or studies) per patient. In the case of CT retrieval, this does not post a problem because a patient would seldom have more than 32 studies. However, in the case of MR, a patient can have many studies, and each study can have many sequences. This results in an inability to retrieve patient's older MR studies. This situation is especially acute in a longitudinal research protocol when the researcher has to go back several months to retrieve data from the same patient. Future designs can have larger-capacity disks but as the PACS data base grows with time, and has to support more users throughout the whole hospital, similar problems will happen again. It is a classical cost versus capacity trade-off problem.

Note that the physician desk retrieval problem is different from the PACS central archival requirement problem. The PACS archival requirement is predictable in the sense that the number of images archived can be estimated once the hospital and the Radiology Department operation environment is known. In desk-top retrieval, the user demand is variable because it depends on the number of users, research topic, user's preference, and retrieval characteristics. Because physician desk-top PACS information retrieval is a unique feature in the authors' PACS, we lack information from other sites for comparison. Therefore, the authors are still at the bottom of their learning curve.

Interfacing a Commercial PACS Module to the PACS Infrastructure

Connectivity. Another unique feature in our PACS is the open architectural design which allows a PACS module developed by a commercial company conforming with the DICOM standard[14] to be connected to the PACS infrastructure. In 1994, we acquired a stand-alone ultrasound PACS (Aegis) from Acuson (Mountain View, CA). This PACS module links seven Acuson US scanners (Fig 8A) in two buildings. This US PACS module features a network server with 1.5-Gbytes of disk storage used for short-term archiving, with images stored in a compressed format (DICOM compatible). Figure 8 shows the connectivity between the US module and the PACS infrastructure. The connectivity is provided by the US module Aegis SPARC GATE (B) and the PACS US SUN SPARC acquisition machine (C) in the infrastructure through a DICOM interface.[15]

Data flow. The data flow is in four routes. The first route is to transmit DICOM formatted compressed US images from the SPARC GATE (Fig 8B) to the ultrasound acquisition machine (Fig 8C) and to the PACS central archive ODL (Fig 8D) for long-term storage. In the PACS data base (Fig 8E) it opens a new patient folder or appends the images to an existing folder with historical US or other type images. The second route is to allow the retrieval of US images from the long-term archive through a request from any US WS (Fig 8F). The third route is the same as the second route except that, in addition, other modality images belonging to the same patient can also be retrieved with that same patient's image folder. The fourth route is to allow other WSs in the PACS to retrieve US images along with other modality images. Both routes 1 and 2 have been completed. However, we encountered great difficulties during the implementation of routes 3 and 4 as described in the next section.

In Table 8, the average time required for image archiving and retrieval are shown. On

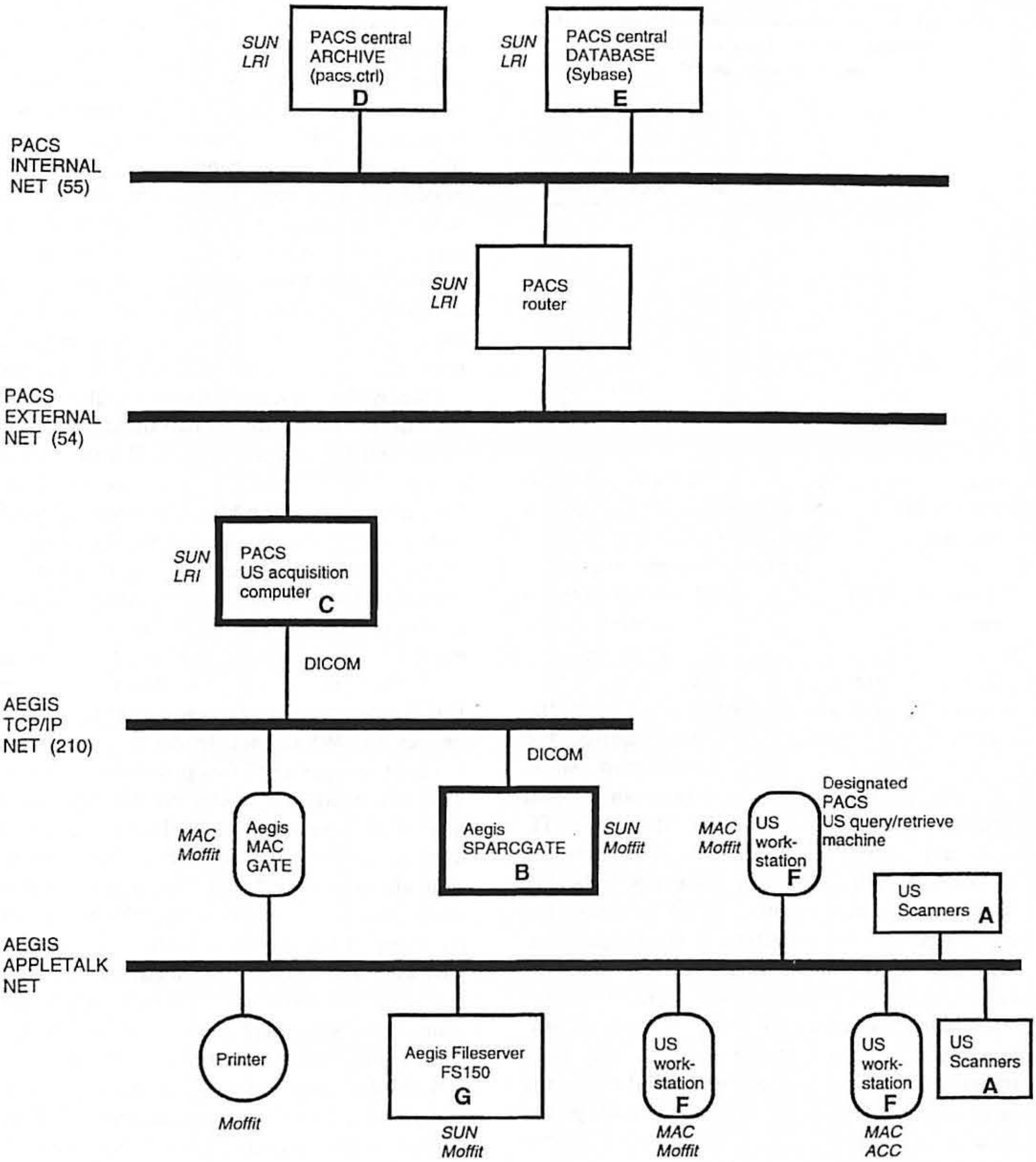

Fig 8. Connection of a US PACS module to the PACS infrastructure. The PACS infrastructure treats the US module as a single imaging device. An acquisition computer (C) in the PACS infrastructure and a SUN SPARC station (B) in the US PACS module are used as two DICOM gateway computers. Moffit, Moffit Hospital; ACC, Ambulatory Care Center; LRI, Laboratory for Radiological Informatics; SUN, SUN SPARC WS. Bold letters are component identifficators.

average, a study file stored on the Aegis SPARC 5 File Server (Fig 8G) was about 13 ± 6.7 Mbytes, on average. Based on these numbers, two study sizes were used: 25 and 66 images. The smaller study file was 7.8 to 22.8 Mbytes (compressed—uncompressed), and the larger study was 20 to 66 Mbytes.

During clinical hours, we sent these US studies back and forth between the Aegis SPARC File Server (Fig 8G) and the Aegis

Table 8. Transmission Rates Between the Ultrasound Server, the Ultrasound Gateway, and the PACS Acquisition Computer*

No. of Images	File Size (MBytes)	Compression	File Server (Fig 9G) to SPARCGATE (Fig 8B) (sec) [Fig 8B-G] (sec)	SPARCGATE (Fig 8B) to Acquisition Computer (Fig 8C) (sec) [Fig 8C to B] (sec)
25	22.8	No	415.4 ± 3.6 [290.7 ± 1.2]	74 ± 2.1 [56.5 ± 0.9]
25	7.8	Yes	202.1 ± 6.9 [161 ± 7.5]	43 ± 2.1 [24.9 ± 1]
66	60.2	No	1076.8 ± 3.5 [704.5 ± 3.5]	196.4 ± 2.9 [157 ± 2.0]
66	20.0	Yes	497.5 ± 2.5 [433 ± 1.0]	112.0 ± 2.5 [71.5 ± 1.5]

*See Fig 8.

Sparc Gate (Fig 8B), and then back and forth between the Aegis Sparc Gate to the acquisition computer (Fig 8C). The files were sent in both compressed and uncompressed formats to quantify the use of compressed images. Each transmission time was measured 5 to 10 times, with the standard deviation never being greater than 7 seconds.

Compressing/formatting/writing the individual files on the Aegis Sparc Gate from the File Serve was the process that required the most time to complete. For both study sizes, using compressed files reduced the transmission time by at least a factor of 2. The SPARC GATE acquisition computer transmission rate over the dedicated Ethernet fiber was measured to be 179 Kbytes/sec, on average, in the US PACS direction and 296 Kbytes/sec for return. If the images were sent uncompressed, the rates were 307 and 393 Kbytes/sec, respectively, each way, server to server.

Clinical experience. The US section is filmless now in the sense that it acquires and stores images digitally, and radiologists and clinicians read from soft copy. The US section prints several selected images from each study on films and inserts them in the patient's record. Currently, it still keeps separate erasable optical disks (ODs) until routes 3 and 4 are completely installed. At that time, these ODs can be erased and recycled in the ODL in the PACS because both archives use a similar type OD.

The current design of the US PACS module is crude. During each transfer, the image file has to go through the US internal networks (Appletalk and Aegis TCP/IP net) at least four times before it goes out to the PACS infrastructure's acquisition computer. The handshaking between computers (especially Apple Computer [Cupertino, CA]) during the transfer becomes tedious and creates some network bottleneck problems. Our original plan to complete routes 1 and 2 in-house was 3 months; it ended up taking more than 1 year, during which both the manufacturer and the authors' laboratory had personnel changes that complicated the issues. Fortunately, both parties were committed to the project and that eventually led to the completion of routes 1 and 2. The manufacturer has been cooperative during this venture.

During the implementation of routes 3 and 4, the authors encountered two difficulties. First, in the third route, after a US WS successfully receives a patient image folder from the PACS long-term archive the Macintosh-based Quadra computer (Apple) does not have the capability of displaying other modalities even though they are in DICOM format, and any attempt to do so results in a crash. This is a fundamental problem that can be resolved by only the manufacturer. Second, in route 4, when an existing PACS WS retrieves a patient folder that has US images, the WS cannot display the compressed US color images until two problems are solved. The WS needs a decoder to decompress the images and a color monitor. The decoder problem can be resolved easily because the compression algorithm used is in the public domain. However, to add the color capability for displaying Doppler US images requires both extensive hardware and software modifications in existing gray-scale monitors. An easy but not desirable solution is just to display colors in gray scale.

To resolve the network problem and the US WS display capability, the manufacturer has made a commitment to introduce a new US PACS module architecture based on a SUN SPARC WS. For this reason, the developmental effort of completing routes 3 and 4 was temporarily stopped until the new PACS US module is installed.

DISCUSSION

Developing an in-house second-generation HI-PACS system has many advantages including designing a system tailored to the user's specific needs, adopting an open architecture design for future expansion, using state-of-the-art technology, providing a faster turnaround time for system upgrade, and potentially possessing a lower total system cost. Conversely, there are also some drawbacks. The following are some of the authors' experiences.

Importance of Securing and Maintaining Sufficient Resources

The resources required for developing an in-house PACS are tremendous. It is advisable to secure enough resources both in terms of personnel and capital for each phase of the implementation before it starts.

In our case, the first phase was the infrastructure design and implementation, which was completed at the end of year 2 after the project started. The goals of the second phase were to place WSs in neuroradiology and pediatrics, install the ICU module, link the US PACS module to the infrastructure, and connect all departmental Macintosh computers on-line to the PACS Macintosh server. The authors wanted to accomplish these goals in the second phase because they had extramural support from the High Performance Computing and Communication Research Program for neuroradiology, we had past experience in installing a pediatric radiology PACS, an ICU server would demonstrate a true HI-PACS that would provide PACS visibility at the medical centers, US PACS would show the first filmless section, and physician desk-top access of PACS data would allow every radiologist and potentially every clinician to have access to the PACS. Unfortunately, at the end of year 2 while the authors were installing PACS workstations, the managed care problem hit California. The capital budget originally allocated for WS implementation for phases 2 and 3 was frozen by the hospital administration. We faced the problem of whether they should continue or stop the WS installation. If we stopped, all the promises made would be broken. The infrastructure alone could not demonstrate the existence of a PACS. It was a critical moment in our PACS R&D program. Finally, completing the goals set forth in the second phase prevailed, and the authors decided to use extramural funding sources from other research and development programs to subsidize the continuing PACS implementation. Since year 2, two full-time engineers and all clinical PACS-related equipment maintenance were paid by the hospital's annual operating budget. In addition, a two-thirds FTE was paid by the departmental budget. All other PACS continuous implementation costs, including personnel and equipment purchases, were provided by the laboratory's own extramural R&D funds. Consequently, we were fortunate to have completed the second-phase efforts.

Users' Demands

During the second phase, while we were installing WSs, they received many requests for help in connecting to the PACS from colleagues both in the department and the hospital who were not on the list for WS installations. They had requests for connecting digital subtraction angiography system and Nuclear Medicine to the PACS, WSs in other radiology sections, and in the Oncology Department. These connections were planned in phase 3 within the authors' originally allocated budget. While they were grappling for sufficient resources to complete phase 2, the authors had no energy left to satisfy these needs. This unfortunate situation created much disappointment. Fortunately, the authors' infrastructure design has been completed, and connection protocols have been developed. Future connections will become routine and will require only a small budget for each connection.

After WSs were installed, users would occasionally request some customized modifications to facilitate their clinical needs. The authors did these modifications whenever possible. Some of these requests were simple changes, but some required much effort. If the system was installed by a manufacturer, normally they would handle these requests by offering to consider making the changes during the next software or hardware release. This meant it would never happen or would take months. However, we could not use this strategy because the users are colleagues with whom we interact daily. Furthermore, we developed the system and wanted it to be perfect and to make every user happy. As a result, much energy has been spent in customization after the WS installation. In the business sector, too much customization translates to bad business. In an R&D team, it means decreasing future research development.

R&D Staff Members Do Not Like to Do Quality Assurance, Service, and Maintenance

After WSs had been installed and used, they needed to undergo quality assurance (QA) monitoring and maintenance. The team we assembled to implement the PACS was mostly faculty, postdoctoral fellows, graduate students, and R&D engineers. A group with this background and experience normally is good in R&D, but weak in service and maintenance. We had requested departmental support to provide a category of personnel to maintain the system for more than a year without success. The department was also in financial difficulty because of the managed care problem. Therefore, the team reluctantly assumed this responsibility. In our experience, it has been most difficult arranging on-call schedules during weekends, holidays, and national meetings of the Radiological Society of North America and the International Society of Optical Engineers. If a PACS had been purchased from a manufacturer, it would have required that a maintenance program be included in the purchase order providing sufficient personnel to service the system.

AXIOMS

Based on our experience, we would like to offer the following three axioms as a guide for in-house PACS implementation:

Axiom 1: PACS Is a Black Hole

PACS is an evolving system integration process; once it starts, it continues. By the time a perfect system integration scheme is developed and implemented, technology will have changed. One should prepare for continuous system modifications and upgrades. A definitive resource and commitment from the institution is absolutely required during each phase of implementation and upgrade.

Axiom 2: User's Need is Difficult to Satisfy

If a system is not well designed, nobody will use it. Conversely, if it is a good system, everybody wants a connection and a WS. In a sense, one is penalized by his or her own success. In addition, every user wants his or her own customization. One should prepare how to handle this situation gracefully.

Axiom 3: R&D Team is Not Good for Maintaining the System

Your team is good for R&D. The R&D team is qualified but may not be good at maintaining a system. Once the system is installed and stabilized, train a new team and then transfer the QA, and service and maintenance responsibility to them. This will free your R&D team to move on to next project.

SUMMARY

In this report, we briefly describe an in-house developed second-generation HI-PACS. The four unique features in this HI-PACS compared with other PAC systems are the 2K neuroradiology WSs, the ICU server, physician desk-top access of PACS data, and connection of a manufacturer's US PACS module to the PACS infrastructure. The authors describe their clinical experience with respect to these four unique features. There are many advantages of developing an in-house HI-PACS but also some drawbacks. Among the drawbacks are the resource requirement, user's demands, system quality assurance, and maintenance and service. We have formulated three axioms as a guide for in-house HI-PACS implementation. To follow Axiom 3, the R&D team has transferred the clinical PACS responsibility to a new team for the day-to-day operation.

ACKNOWLEDGMENT

We thank the neuroradiology, pediatric, and US sections from our department; and the pediatric, medical surgery, and cardiac ICUs, as well as colleagues who use the physician desk-top access for their clinical input.

REFERENCES

1. Huang HK, Arenson RL, Lou SL, et al: Second generation picture archiving and communication systems. Proc SPIE Med Imaging 2165:527-535, 1994

2. Huang HK, Andriole K, Bazzill T, et al: Design and implementation of a PACS: The second time. J Digit Imaging 9:1-14, 1996

3. Huang HK, Arenson RL, Dillon WP, et al: Asynchronous transfer mode (ATM) technology for radiologic communication. Am J Roentgenol 164:1533-1536, 1995

4. Health Level Seven (HL7): An Application Protocol for Electronic Data Exchange in Health Care Environments, version 2.1. Ann Arbor, MI, Health Level Seven, 1991

5. Lou SL, Wang J, Moskowitz M, et al: Methods of automatically acquiring images from digital medical systems. J Comp Med Imaging Graphics 19:369-376, 1995

6. ACR/NEMA Digital Imaging and Communication Standard Committee: Digital Imaging and Communications (ACR-NEMA 300-1988). Washington, DC, National Electrical Manufacturers Association, 1989

7. Wong AWK, Huang HK, Arenson RL, et al: Multimedia archive system for radiologic images. Radiographics 14:1119-1126, 1994

8. Zhang J, Huang HK: Automatic background recognition and removal of computed radiography images. IEEE Trans Med Imaging (submitted for publication)

9. Zhang J, Wong STC, Andriole KP, et al: Real time multi level process monitoring and control of CR image acquisition and preprocessing for PACS and ICU. Proc SPIE Med Imaging 2711:290-297, 1996

10. Huang HK, Taira R, Lou SL, et al: Implementation of a large scale picture archiving and communication system. J Comp Med Imaging Graphics 17:1-11, 1993

11. Huang HK, Wong AWK, Bazzill TM, et al: Asynchronous transfer mode-distributed PACS server for intensive care unit applications. Radiology 197: p 247, 1995

12. Ramaswamy MR, Wong AWK, Lee JK, et al: Accessing a PACS' text and image information through personal computers. Am J Roentgenol 163:1239-1243, 1994

13. Lee JK, Wong SWK, Ramaswamy M, et al: Access to multimedia PACS information from a MAC-based workstation. Proc SPIE Med Imaging 2435:33-42, 1995

14. Digital Imaging and Communications in Medicine (DICOM). V. Addendum: Data structures and encoding extensions. Committee Draft Version 0.5, December 21, 1994, pp. 36-43

15. Moskowitz M, Gould RG, Huang HK, et al: Initial clinical experience with ultrasound PACS. Proc SPIE Med Imaging 2435:246-251, 1995

Chapter 8

Some Aspects of Medical Imaging

H.K. HUANG

Principles of Medical Biology, Volume 4
Cell Chemistry and Physiology: Part III, pages 211–239.

ISBN: 1-55938-807-2

INTRODUCTION

Medical imaging is the study of human functions and anatomy through pictorial information. In order to generate this pictoral information, multidisciplinary knowledge, including biology, anatomy, physiology, chemistry, computer science, optical science, radiological science, electrical engineering, mathematics, and physics are required (Huang, 1993a). Generally speaking, medical imaging investigates methods and procedures of:

1. Converting a conventional medical image, or synthesizing some biological, anatomical, or physiological information, to a digital image.
2. Analyzing the digital image according to a specific application or clinical need.
3. Extracting key results and casting them into a format suitable for presentation, archiving, and decision making.

Some successful medical imaging applications in the early 1970s were the blood cell analyzer (Pressman and Wied, 1979) and the gamma camera in nuclear medicine (NM). The development of the computed tomography (CT) scanner resulted in the award of the Nobel Prize in Medicine to Allan M. Cormack and Godfrey N. Hounsfield in 1979. Major medical imaging developments in the 1980s were electron microscopy (EM), laser microscopy (LM), digital subtraction angiography (DSA), magnetic resonance imaging (MRI), positron emission tomography (PET), computed radiography (CR), Doppler ultrasound, and picture archiving and communication systems (PACS) (Huang, 1981a; Huang et al., 1990). EM can reveal minute details in biological infrastructures as small as a few angstroms in

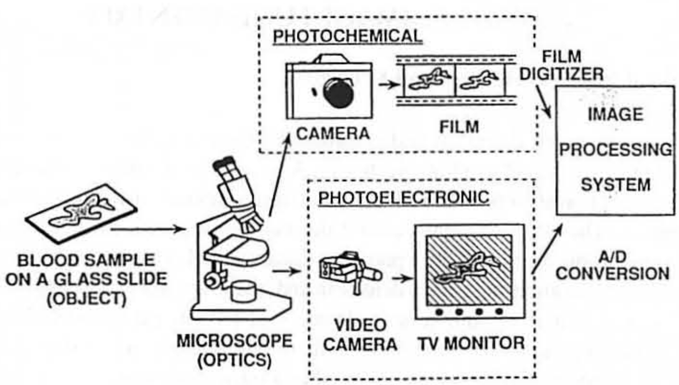

Figure 1. An example of biomedical image detectors and recorders.

size. LM yields thin serial images providing three-dimensional morphology of living cells. DSA allows real-time subtraction to enhance the vascularities in millimeters. Without the use of ionizing radiation, MRI reveals high-contrast images of anatomical structures in any plane of the body. MRI is the method of choice for neuroradiological, vascular, and musculoskeletal diagnosis.

PET provides chemical and physiological images of the human body that complement anatomical images obtained using MRI and CT (Hawkins et al., 1992). The registration of MRI or CT with PET head images provides an insight into the specific function of various parts of the brain (Valentino et al., 1991). CR allows an X-ray image to be recorded directly as a digital image, opening new avenues for using digital image processing as an aid in medical diagnosis (Kangarloo et al., 1988).

PACS is a novel concept for medical image management and communication (Huang et al., 1988). When fully implemented, the system will revolutionize medical practice (Huang et al., 1993b). PACS storage technology includes parallel transfer disks and optical disk libraries. In the former, a conventional X-ray image of 8 megabytes can be stored or retrieved from the parallel transfer disks within one second. In the latter, an optical disk library that occupies a footprint of no more than 3 × 6 feet allows the storage of one terabyte of information, equivalent to about two years worth of all MR and CT examinations conducted in a large teaching hospital.

In communication components, fiber optic systems with specially designed fiber optic transmitters and receivers can transmit images at a rate up to 1 gigabit per second. A conventional 8-megabyte X-ray image can be transmitted between two points in about one second (Huang et al., 1992). For display, 2,000 × 2,000 pixel monitors are readily available that display a conventional X-ray image without loss of diagnostic quality (Huang et al., 1993b). Three-dimensional display stations are used in various clinical applications (Udupa et al., 1993).

MEDICAL IMAGE FUNDAMENTALS

Medical Image Detectors and Recorders

Medical image detection and recording methods can be categorized as being either photochemical or photoelectronic. An example of a photochemical method is the phosphorous screen and silver halide film combination system used for X-ray detection. The television camera and display monitor used in fluorography is a photoelectronic technique. The photochemical method is a direct process; it has the advantage of combining image detection and image recording in a single step. The screen/film system simultaneously detects and records the attenuated X-rays. A photoelectronic system, on the other hand, usually involves a two-step process; the image is detected first and then recorded in a subsequent step.

In the case of DSA, an image intensifier tube (II) is used as the X-ray detector instead of a screen/film combination. The detected X-rays are converted first into light photons and then into electronic signals that are recorded by a video camera. The images from the video camera can be displayed on a television monitor, and the video signal can be digitized to form a digital image. The photoelectronic system, while clearly more complicated, has one important advantage: the output information can be converted to digital format for image processing.

Figure 1 shows an example of medical image detectors and recorders. In this case, an image of blood cells from a blood sample on a glass slide is to be recorded. The glass slide is first placed under the microscope. If a 35 mm camera is attached to the microscope, the image of the blood cells can be recorded on film. On the other hand, if a television or CCD (charge couple device) camera is attached to the microscope, then the blood cells are seen as an electronic image on a television monitor. In either case, the recorded image is in analog form. For a digital computer to process these images, they must first be converted to digital form, a step called analog to digital conversion.

Digital Images

A digital image $P(x,y)$ is defined as an integer function of two variables x,y such that

$$0 \leq P(x,y) \leq N \text{ where } 1 \leq x \leq m,\ 1 \leq y \leq n$$

and x, y, m, n, and N are positive integers. For simplicity, we let $m = n$ (i.e., $P(x,y)$ is a square image). Given (x,y), $P(x,y)$ is called a picture element, or *pixel*. The computer memory requirement for storing image $P(x,y)$ is $n \times n \times k$ bits where $k = \log_2 (N + 1)$. Thus, $n \times n \times k$ means that the image has n lines, each line has n pixels, and each pixel can have a discrete gray-level value that ranges from 0 to $2^k - 1$ (Udupa et al., 1993). A typical microscopic digital image has 512×512 pixels and each pixel can have values from 0 to 255.

Spatial and Density Resolution

Once an object of interest has been digitally recorded, we would like to know the image quality. Image quality is characterized by three parameters: spatial resolution, density resolution, and signal to noise ratio. Spatial resolution is a measure of the number of pixels used to represent the object, and density resolution is the total number of discrete gray level values in the digital image. It is apparent that n and N are proportional to spatial resolution and density resolution, respectively. A high signal-to-noise ratio means that the image is very pleasing to the eye and hence is a better quality image. Figure 2 demonstrates the concept of spatial and density resolution of a digital image of a lymphocyte. The left-hand column in

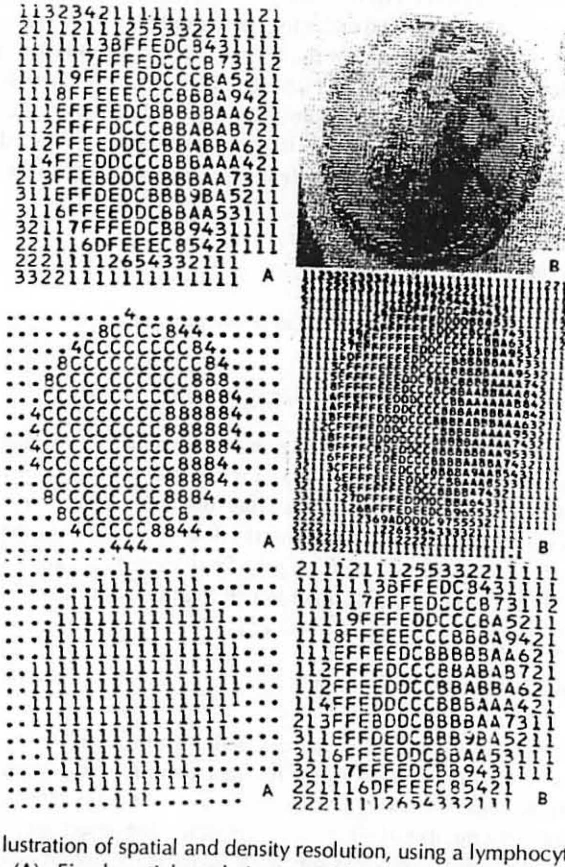

Figure 2. Illustration of spatial and density resolution, using a lymphocyte image as an example. **(A)** Fixed spatial resolution, variable density resolution: 16, 4, and 2 grey levels. **(B)** Fixed density resolution (16 levels), variable spatial resolutions. The 16 levels are represented by: •, 1, 2, 3, 4, 5, 6, 7, 8, 9, A, B, C, D, E, and F.

215

Figure 2 shows digitized images of the lymphocyte with a fixed spatial resolution (21 × 15) and variable density resolutions (from top to bottom: 16, 4, and 2 gray levels). The right-hand column depicts the digital representation of the same analog image with a fixed density resolution (16) and variable spatial resolutions (from top to bottom: high, medium, low). It is clear from this example that the upper right corner digital image has the best quality (highest spatial and density resolutions), whereas the lower left corner image has the lowest spatial and density resolutions. Depending on the application requirement, the spatial resolution, density resolution, and signal-to-noise ratio of the image should be adjusted properly during image acquisition. A high-resolution image requires a larger memory capacity for storage and a correspondingly longer time for image processing than a lower-resolution image.

Sources of Medical Images

By far, the richest sources of medical images is in radiology; sometimes we call those images macroscopic to differentiate them from microscopic and infrastructural images. In radiology, about 70% of the examinations, including those that involve skull, chest, abdomen, and bone, produce images that are acquired and stored on X-ray film. These images have a spatial resolution of about 5 lp/mm. Line pair per millimeter (lp/mm) is a measure of spatial resolution; one line pair represents two pixels. These films can be converted to digital format using a film digitizer. Among various types of digitizers, the laser scanning digitizer is considered superior because it can best preserve the density and spatial resolutions of the original analog image. A laser film scanner can digitize a 14" × 17" X-ray film to 4,000 × 5,000 pixels (about 5 lp/mm), with 12 bits per pixel. At this spatial and density resolution, the quality of the original analog image and the digitized image is essentially equivalent. In clinical practice, however, we digitize an X-ray film to 2,000 × 2,500 pixels. CR, which uses a laser stimulable luminescence phosphor imaging plate as a detector, is gradually replacing the screen/film combination as the image detector. In this case, a laser beam is used to scan the imaging plate that contains the latent X-ray image. The latent image is excited and emits light photons that are detected and converted to digitized electronic signals forming a direct digital X-ray image.

The other 30% of radiological examinations—those that involve CT, ultrasonography (US), MRI, PET, and DSA—produce images that are already in digital format. A CT, US, MRI, PET, and DSA image has sizes of 512 × 512 × 12, 512 × 512 × 8, 256 × 256 × 12, 128 × 128 × 12, and 512 × 512 × 8 bits, respectively. These techniques use different energy sources and detectors to generate images and are complementary in their clinical applications to each other. CT uses X-rays as an energy source and gas or scintillating crystals as detectors. US uses an ultrasonic transducer both as the energy source and detector. MR uses two energy sources, magnetic fields and radio-frequency electromagnetic waves, and a radio-frequency receiver as the detector. DSA uses X-rays as an energy source and an image intensifier tube as the detector. Conventional X-ray examinations and DSA produce a projectional image, whereas CT, US, PET, and MRI give sectional images. Sectional images can be stacked to form a three-dimensional image set which represents the true three-dimensional object. All radiologic images are monochromatic except NM, PET, and Doppler US in which pseudo colors are used as an image enhancement tool.

Other medical images sources used in anatomy, biology, and pathology are light and electron microscopes. Images from these sources are collected with a video or CCD camera and then digitized to a $512 \times 512 \times 8$ bit image. Light microscopy produces true color images, using red, green, and blue filters for color separation. Thus, a color image after digitization yields three digital images, the combination of which produces a true-color digital image encoded at 24 bits/pixel. Figure 3a–j shows some examples of these medical images.

Image Processing Systems

After a medical image is formed, it is analyzed by an image processing system. The architecture of an image processing (IP) system consists of three major components: image processor(s), image memories, and video processor(s). They are connected by internal computer buses to form an integrated system. Figure 4 shows the general block diagram of an integrated image processing system. For this particular system, only the system controller is connected to the computer host bus. The image processor is a high-speed array processor. It is composed of arithmetic-logic units, multipliers and shifters, comparators, and look-up tables. The image memories can be partitioned into various sizes for efficient storage of image data. The video processor takes the images from the image memories and selectively displays them on video monitors.

An IP system requires extensive software support. The trend in IP software development is towards portability. Figure 5 shows the general organization of IP software. Portability is preferred in the three higher levels of software so that they can be used again when the system hardware is upgraded in the future. The two lower levels are machine dependent and have to be rewritten for every new hardware architecture. IP functions include pixel, local, global, and statistical operations, and also consist of image database manipulation and image display. In the past, Fortran was used in most IP software development, but C programming language running under UNIX operation system is now standard.

In medical imaging applications, contour extraction of an object of interest is important because it leads to quantitative measurements. Despite many years of software research and development, soft-tissue segmentation in radiologic images, and differentiation of objects of interest in histology specimens, are still a very

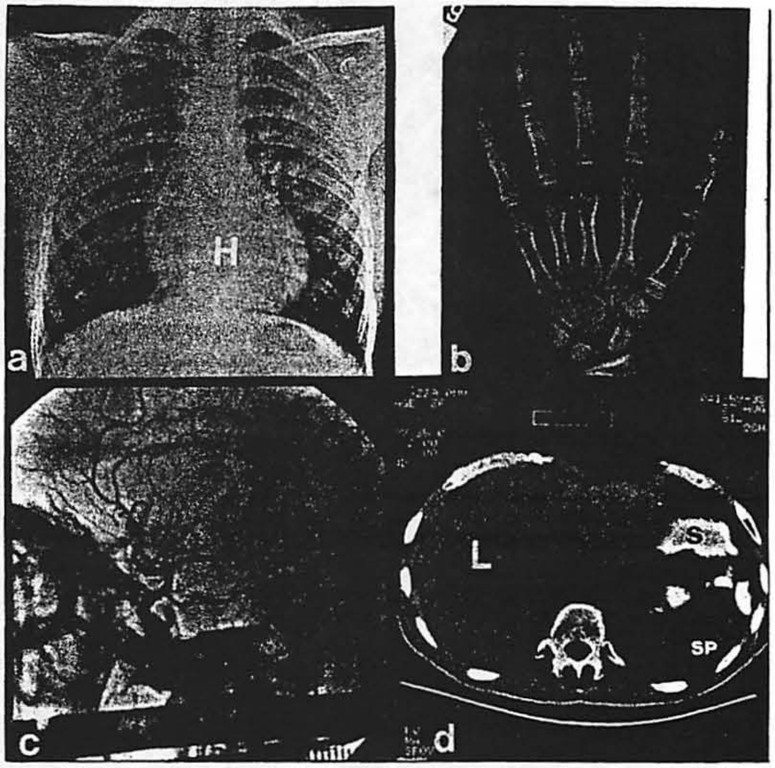

(continued)

Figure 3. Examples of medical images obtained from various sources. (**a**) CR (computed radiography) image of the chest, the image is 2,000 × 2,500 pixels and 10 bits/pixel. Excellent delineation of the blood vessels behind the heart (H). (**b**) CR image of the hand. Both soft tissue and the detail of the bones are seen very clearly. (**c**) DSA (digital subtraction angiography) of the brain showing contrast enhanced blood vessels. (Courtesy of E. Pietka.) (**d**) CT (computed tomography) image of the upper abdomen. Contrast media is shown in the stomach (S). L, liver; SP, spleen; A, descending aorta. (**e, f, g**) MR (magnetic resonance) images of the head from the same patient in the transverse, sagittal, and coronal plane. Images show fine structures of the brain. (Courtesy of S. Sinha.) (**h**) Mapping of the brain function to anatomy. The grey level image is from the MR, the color is from the PET (positron emission tomography) of the same patient. Red color shows high metabolic rates. Registration of these two images required sophisticated mathematics and computer programming. (Courtesy of D. Valentino.) (**i**) A longitudinal section Doppler ultrasound image of the abdomen. Red color shows the blood flow, arrow indicates that flow in the portal vein is hepatopetal. (Courtesy of E. Grant.) (**j**) Three-dimensional reconstruction of the lumber spine from sectional CT images.

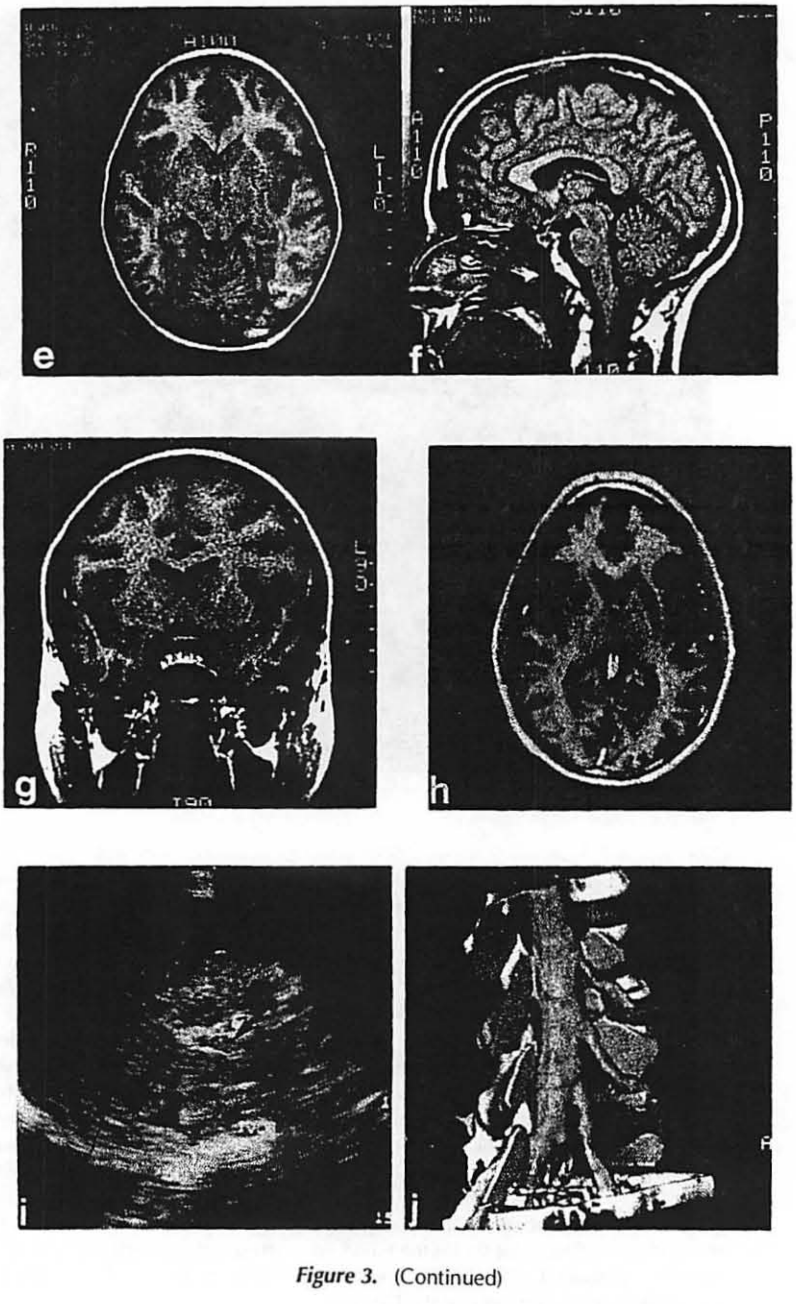

Figure 3. (Continued)

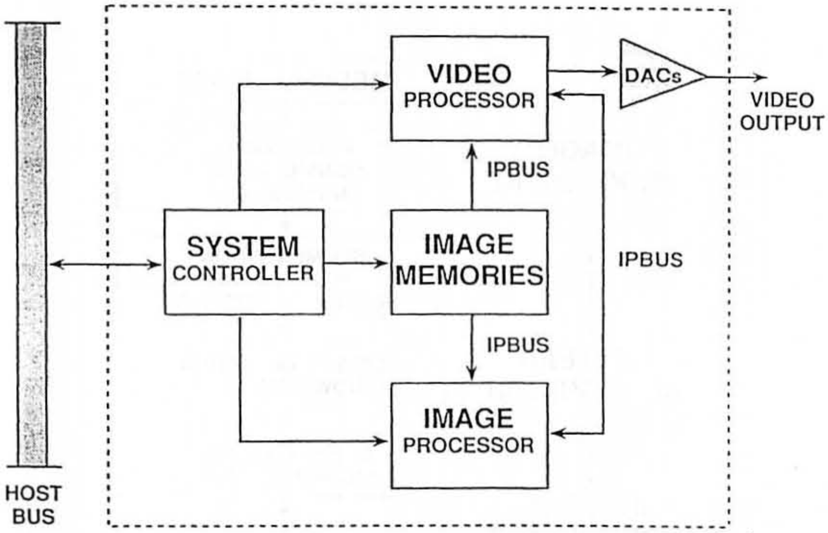

Figure 4. A general architecture of an integrated image processing system. Only the system controller is connected to the computer host bus. IP: Image Processing.

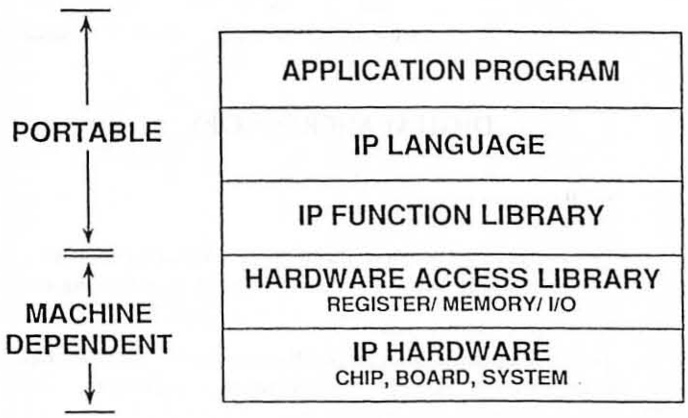

Figure 5. Organization of image processing software. The three higher-level software should be portable so that they can be used for any future hardware architecture.

220

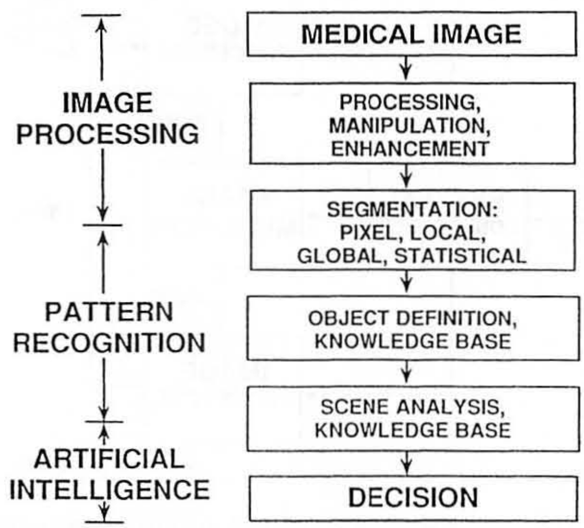

Figure 6. Levels of sophistication in medical image processing. Medical database, pattern recognition and artificial intelligence will be major research topics in the 1990s.

difficult task. Advances in medical image processing remain largely in the domain of quantization. Figure 6 shows the levels of sophistication in medical image processing.

DIGITAL MICROSCOPY

Instrumentation

Digital microscopy is used to extract quantitative information from microscopic slides. A digital microscopic imaging system consists of the following six components (Huang, 1981b):

- a compound microscope with proper illumination for specimen input,
- a vidicon (or CCD) camera for scanning microscopic images,
- TV monitors for displaying the image,
- an analog to digital (A/D) converter, and
- a computer (or image processor) to process the digital image.

Figure 7 shows the block diagram and the physical setup of the instrumentation.

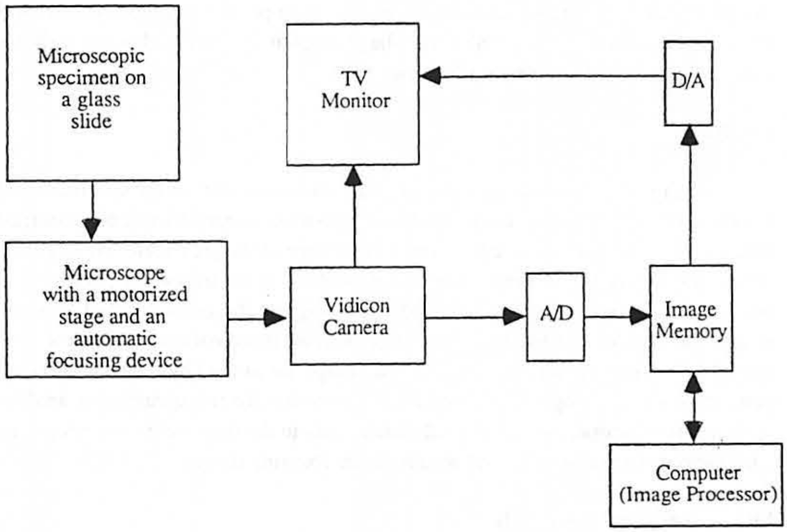

Figure 7. A block diagram showing the digital microscopy instrumentation.

Resolution

The resolution of a microscope is defined as the minimum distance between two objects in the specimen which can be resolved by the microscope. Three factors control the resolution of a microscope (Burrells, 1971; Rochow and Rochow, 1978).

1. The angle subtended by the object of interest in the specimen and the objective lens; the larger the angle, the higher the resolution.
2. The medium between the front lens and the coverslip of the glass slide; the higher the refractive index of the medium, the higher the resolution.
3. The wavelength of light employed; the shorter the wavelength, the higher the resolution.

These three factors can be combined into a single equation (Ernst Abbe 1840–1905):

$$s = \frac{\lambda}{2(NA)} = \frac{\lambda}{2n \sin i}$$

where s is the distance between two objects in the specimen that can be resolved; the smaller the s, the greater the resolution. λ is the wavelength of the light employed; n is the refractive index of the medium; i is the half-angle subtended by the object at the objective lens; and NA is the numerical aperture commonly used for defining the resolution; the larger the NA, the higher the resolution. Therefore, in order to obtain a higher resolution for a microscope, use an objective lens with an oil immersion lens (large n) with a large angular aperture and select a shorter wavelength of light source for illumination.

Contrast

Contrast is the ability to differentiate various components in the specimen with different intensity levels. There are black-and-white contrast and color contrast. Black-and-white contrast is equivalent to the range of the grey scale; the larger the range, the better the contrast. The color contrast is an important parameter in microscopic image processing: in order to bring out the color contrast from the image, various color filters have to be used with the illumination. It is clear that the spatial and density resolutions of a digital image are limited by the resolution and contrast of a microscope, respectively. In order to do effective quantitative analysis with the microscope, two additional attachments to the microscope are necessary: a motorized stage assembly and an automatic focusing device.

Motorized Stage Assembly

The purpose of a motorized stage assembly is for rapid screening and locating the exact position of objects of interest for subsequent detailed analysis. The motorized stage assembly consists of a high precision x-y stage with a specially designed holder for the slide to minimize the vibration due to transmission when the stage is moving. Two stepping motors are used for driving the stage in the x and the y directions. A typical motor step is about 2.5 micron with an accuracy and repeatability to within ±1.25 microns. The motors can move the stage in either direction with a maximum speed of 650 steps, or .165 cm, per second. The two stepping motors can either be controlled manually or automatically by the computer.

Automatic Focusing Device

The purpose of the automatic focusing device is to assure that the microscope is focusing all the time when the stage is moving from one field to another by the stepping motors. It is essential to have the microscope in focus before the vidicon camera starts to scan. Two common methods for automatic focusing are using a third stepping motor in the z-direction or an air pump. The principle of using a stepping motor in the z-direction for automatic focusing is as follows: the stage is moved up and down with respect to the objective lens by the z-direction motor. The z movements are nested in large +z and –z values initially and then gradually to smaller +z and −z values. After each movement, a video scan of the specimen through the microscope is made and some optical parameters are derived from the scan. A focused image is defined as the scan with these optical parameters above certain threshold values. Since this method requires nested upward and downward movements of the stage in the z-direction, though automatic, it is time consuming.

The use of an air pump for automatic focusing is based on the assumption that in order to have automatic focusing, the specimen lying on the upper surface of a glass slide has to be on a perfect horizontal plane with respect to the objective lens all the time. One reason why the slide is not focused is that the glass slide is not of uniform thickness. When it rests on the horizontal stage, the lower surface of the slide will form a horizontal plane with respect to the objective but not the upper surface. If an air pump is used to create a vacuum from above, such that the upper surface of the slide is suctioned from above to form a perfect horizontal plane with respect to the objective, then the slide will be focused all the time. Using an air pump for automatic focusing does not require additional time during operation; however, it requires precision machinery.

Vidicon (CCD) Camera and Scanning

Once the specimen is focused under the microscope, a vidicon or a CCD camera can be attached to the microscope tube to detect the light emitted from the specimen within the microscopic field of view. The camera scans the specimen point by point from left to right, top to bottom and forms a light image of the specimen on the photosensitive face of the camera. The brightness $B(x, y)$ of each pixel is converted into an electrical voltage (video signal) which is transmitted to the display monitor. This voltage is used to control the brightness of a corresponding spot on the fluorescent screen of the monitor. These spots reconstruct a video image of the specimen on the television screen. In order to have the camera perform satisfactorily for microscopic imaging, the following specifications should be met:

Gamma (γ) of the tube:	.65 or less
Dynamic range:	200:1
Resolution:	The MTF (modulation transfer function derived by plotting the video amplitude versus the number of lines) should be comparable to that of an ideal Gaussian Spot with diameter 1/500 of the image width.
Linearity:	± 1/2% of the image height for all pixels.

Analog to Digital Conversion

There are two methods for digitizing the microscopic image formed by the vidicon camera: the real-time digitizing with a fast A/D converter, usually in the

10 MHz range. It converts the video signal B(x, y) into a digital number P(x, y) and sends it to the (x, y) location of the image memory. A complete TV frame (512 × 512 pixels with eight bits/pixel) can be digitized in 1/30 second. Because of the high speed A/D conversion, the signal to noise ratio of the real-time digitized image tends to be low. In order to have a better signal to noise ratio, it is common to digitize the same frame many times and take the average value for each pixel. The high-resolution digitizer uses a slower but better signal-to-noise ratio A/D converter; the digital image thus obtained is of better quality. Since the A/D conversion rate is much slower than the TV scanning rate, the same microscopic field has to be scanned many times in order to have a complete digital image.

Image Memory

The purpose of the image refresh memory is for storage and display of the digitized microscopic image. Once the image is digitized and stored in the memory, it is continuously refreshed in synchronism with the video scan. The refresh memory is not a component of the main computer and should be considered as a very fast peripheral storage device. Once the image is stored, it can be accessed by the computer for image processing. The refresh memory is generally organized into memory planes, with each plane having the storage capacity to refresh a 512 × 512

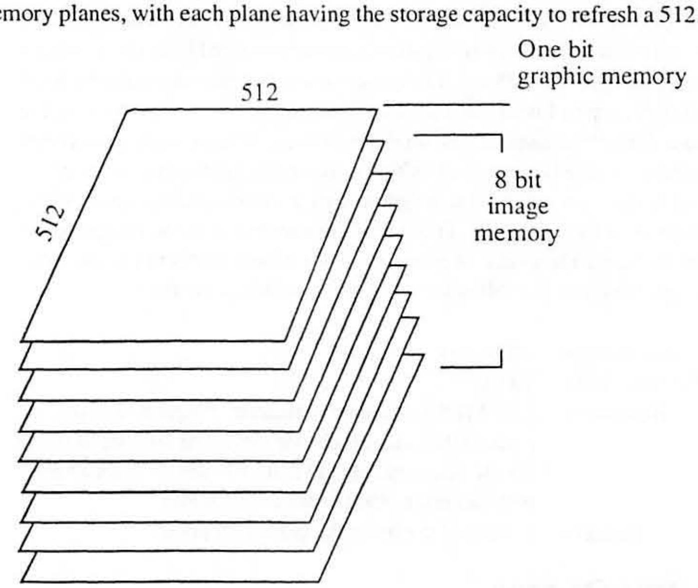

Figure 8. Organization of a 512 × 512 × 8 image memory and a 512 × 512 × 1 graphic memory. For black-and-white image processing, one eight-bit image memory is sufficient; for real color image processing, three image memories are necessary.

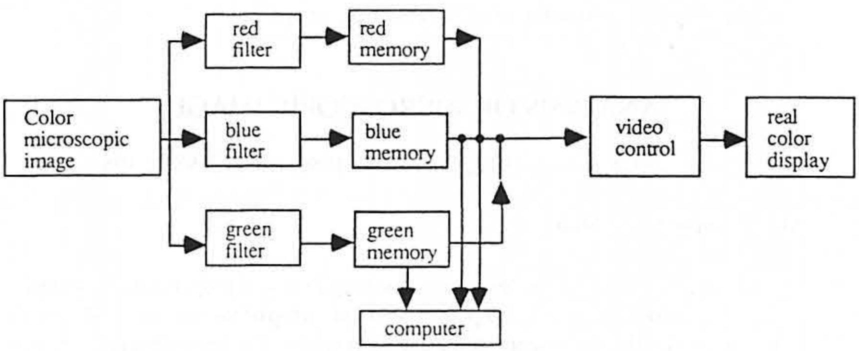

Figure 9. Color image processing block diagram. Three filters (red, blue, and green) are used to filter the image before digitization, respectively. The three digitized filtered images are stored in the red, blue, and green memories. The real color image can be displayed back on the color monitor from these three memories through the composite video control.

one-bit grey-level image. The most commonly used refresh memory for imaging has 8 or 12 memory planes which give 256 to 4,096 grey levels. In addition, there should be one extra memory plane for graphic overlay on top of the image memory for interactive image processing. Figure 8 shows the architecture of the image memory.

If real color microscopic image is used, the color specimen is generally digitized in three steps, each time with a red, blue, and green filter, respectively. The three color-filtered images are then stored separately in three refresh memories, the blue, red, and green, each of which with eight planes. The computer will treat each of the eight planes refresh memory as an individual microscopic image and process them separately. Thus, a true color image has 24 bits/pixel. The real color digital microscopic image can be displayed back on a color monitor from these three memories through a color composite video control. Figure 9 shows the block diagram of the real color microscopic imaging.

Computer

The computer, usually a personal computer with necessary peripherals, serves as a control, as well as performing image analysis in the system. The following are the major control functions:

Movement of the x-y stepping motors
Control of the automatic focusing
Control of the color filtering

Control of the digitization of the microscopic image
Image processing

ANALYSIS OF MICROSCOPIC IMAGES

For reviews, see Castleman, 1979; Onoe et al., 1980; Huang, 1981a, 1982.

Microscopic Glass Slide

The specimen under consideration is first prepared with proper staining and put on the glass slide. A thin cover slip is then placed on top of the specimen. The slide is positioned on the microscope stage and an origin is selected with respect to the motorized stage. The slide is now ready to be analyzed. For automatic analysis of the slide, the following nomenclature is commonly used (Huang, 1982). (See Figures 10 and 11 for illustration.)

The total scan area (TSA) is that portion of the slide to be scanned by the vidicon camera. The dimensions of the TSA cannot exceed the size of the cover slip (15 mm × 15 mm). For example, 10 mm × 10 mm is a commonly used dimension. A strip is a lateral (or vertical) portion of the TSA. For example, if a 20× objective lens is used, a strip would have the dimensions of about 10 mm × 200 μ. A field represents a portion of a strip; using the same example, it would have the dimensions of about 200 μ × 200 μ. This field represents a square area to be scanned by the vidicon camera and when it is digitized it will consist of 512 × 512 pixels. The

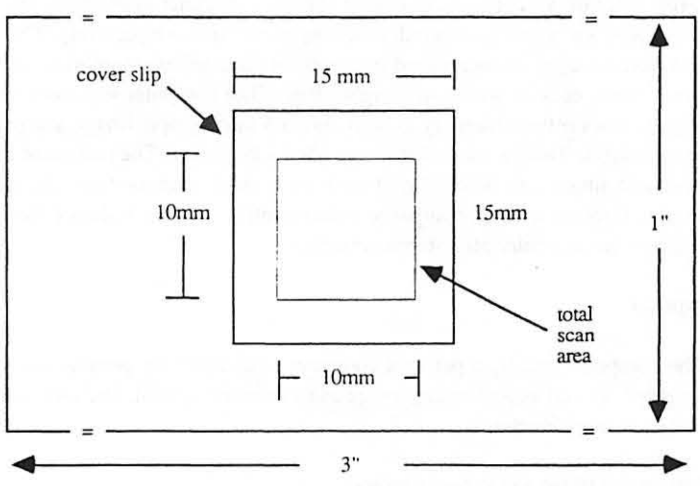

Figure 10. The dimensions of a sample glass slide.

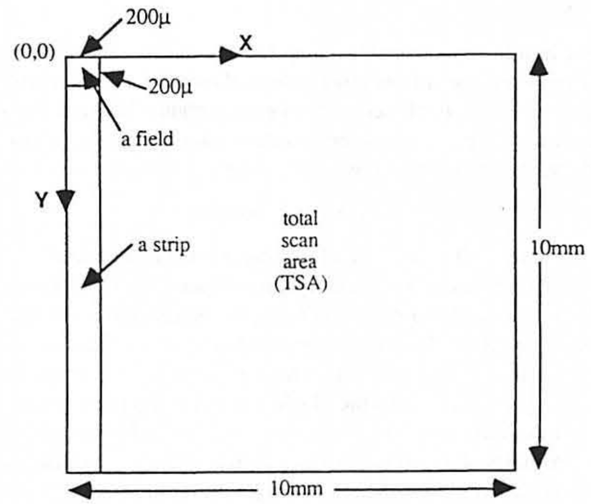

Figure 11. The subdivision of the total scan area (TSA). The numerical values used in this drawing are based on a 100× oil immersion objective lens. There is some overlapped area between adjacent fields.

origin is at the left upper corner of the TSA. The positive x-axis is taken as the line starting from the origin and extending horizontally (towards the right) along the upper edge of the TSA. The positive y-axis is taken as the line starting from the origin moving longitudinally along the left edge of the TSA. The step is the smallest increment the x, y stepping motors can advance, for example, 2.5 microns.

Search for Objects of Interest

The first step in analyzing a microscopic slide is to search for objects of interest from the TSA using a lower magnification objective lens. For example, in blood karyotyping, the objects of interest would be metaphase blood cells. Since different objects of interest have different characteristics, there is no general search algorithm for every biological specimen. However, some guidelines can be used to facilitate the search. Consider the chromosome karyotyping as an example to illustrate the search technique.

In chromosome karyotyping, the goals are to search for isolated metaphase cells under low magnification and karyotype these metaphase cells using higher magnification. The blood cell sample is first prepared with proper staining. A low magnification objective (for example, 20×) is used to scan each field in the TSA. Since only low resolution is needed to identify metaphase cells, two grey level and every other scan line from the image are sufficient. Let us define:

An object in a binary image (two grey level) consists of a string which has n consecutive ones separated from other groups of ones by at least n zeros on either side. The parameter, n, is chosen as the optimal choice between the width of a chromosome and the spacing between two chromosomes in a metaphase cell under this magnification. Thus, for example, the string

0000001 1 1 1000000

is an object with n = 4. The location of the object is the order pair consisting of the coordinates of the left most "one" and right most "one." If n is too small, the object could be dirt in the field and if n is too large, the object could be a line through a non-metaphase cell. In both cases, the object should be discarded.

A cover is a horizontal string of at least p such objects, where the distance between two neighboring objects must be less than q points (p and q are parameters typical of a metaphase cell). The starting coordinates of a cover (x_s, y_s) is the left-hand coordinates of its left most object, and the ending coordinate of this cover (x_e, y_e) is the right-hand coordinates of its right most object, and

$$s > (x_e - x_s) > \gamma$$

where γ, s are parameters typical of a metaphase cell. For example, the string

```
y = 1:      000 1 1 1 0000 1 1 1 1 00000000 1 1 1 0000
                object1    object2           object3
                  First Cover             Second Cover
```

consists of three objects, if q = 5, then object 1 and 2 form a cover with p = 2 and object 3 forms a second cover with p = 1. In the first cover, $x_s = 4$ and $x_e = 14$, and the second cover, $x_s = 23$ and $x_e = 25$.

A chromosome spread is a collection of at least two longitudinal proximate covers; its size must lie within a square of certain dimensions which is determined by the magnification. The center of the spread is determined as the arithmetic means of the minimum and maximum coordinates of all the covers.

A search algorithm can then be developed to look for chromosome spreads based on these hierarchical structures starting from objects, to cover, and to chromosome spreads. The algorithm can continue searching from field to field, strip to strip, until the complete TSA is scanned. With a carefully prepared specimen, and a 20× objective, an average of 100 good metaphase cells can be located. The center of these spreads can be recorded and the computer can move the stage back to all these centers for subsequent analysis with a higher magnification objective. Figure 12 shows the relative magnification of a partial chromosome spread using a low (20×) and a high (100×) objective. Figure 13 shows some covers and chromosome spreads found by this algorithm.

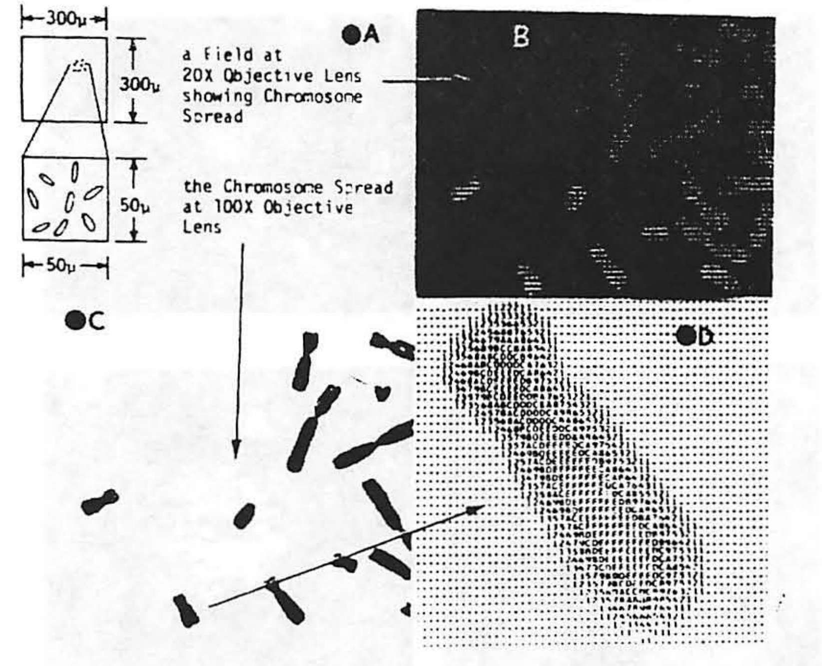

Figure 12. (A) Relative magnification of metaphase cells under a low and a high objective lens; (B) a partial chromosome spread under a low objective lens digitized in two grey-level and low resolution; (C) the same partial chromosome spread under 100× objective; (D) a chromosome spread digitized in 16 levels.

Analysis: Boundary Determination

After objects of interest have been located, a higher magnification objective lens, for example a 100× oil immersion, can be used for analysis. The first step is to find the boundary or boundaries of the objects. The simplest is the histogram method. The histogram method generates the histogram of the field which includes objects of interest as well as the background. The algorithm defines the grey-levels at the trough(s) of the histogram as the boundary cut-off level of objects. Once a cut-off grey level is known, the coordinates of the boundary of objects can be obtained by a program searching through the digital picture.

Figure 14 shows an example of the histogram technique (Huang et al., 1983). Figure 14a is a bone biopsy microradiograph obtained from a cross section of the rib of a dog. This image is as seen directly from the television monitor through the camera attached to the microscope focusing on the microradiograph. The goal of this study is to determine the total bone area, area of the trabecular bone (T), area

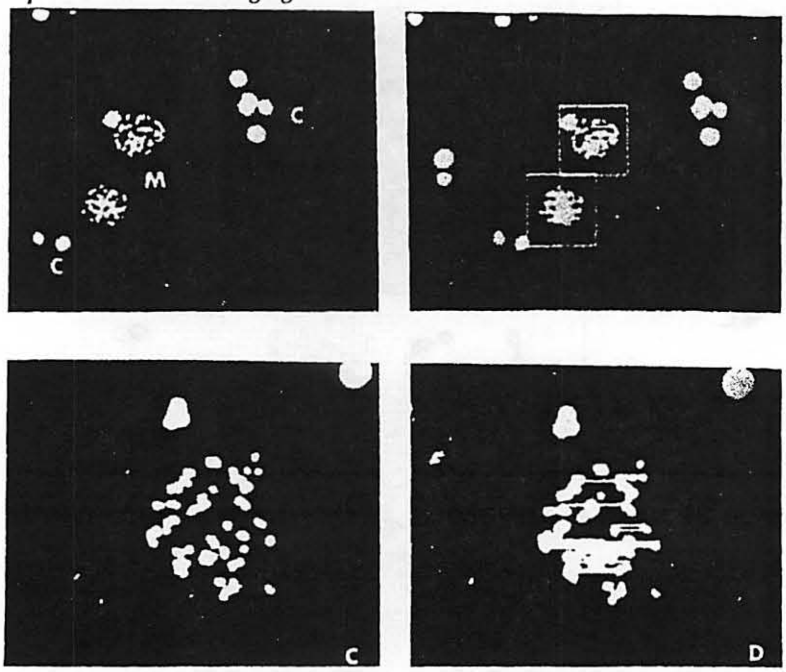

Figure 13. **(A)** A field showing two metaphase chromosome spreads (M) and some blood cells (C); **(B)** search algorithm locating the two spreads based on the hierarchal structure of objects, covers, and spreads; **(C)** another metaphase spread with a higher magnification; **(D)** horizontal lines showing the covers found during each line scan.

of marrow cavity (M), area of the cortical bone (C), and area of holes (arrows) in the cortical bone from this microradiograph. In order to extract these parameters, the boundaries of these areas must be determined first. The histogram technique is used to determine these boundaries. Figure 14b shows the histogram, h, of the complete image including the bone and the background, where

$$h = h(g) \qquad 0 \leq g \leq 255$$

where g is the grey-level value, and h is the grey-level count. Both the image and the graphic memory are used to display the result. The histogram can be smoothed by using a low pass digital filter in the frequency domain as follows: the Fourier Transform, H or h, is first performed and its spectrum |H| is shown in Figure 14c. A low pass filter, F, is used to smooth H such that

$$S = FH$$

where S is the transform of the histogram to be smoothed. The inverse transform, s of S, is then the smoothed histogram. The smoothed histogram, using a second

Figure 14. An example demonstrating the boundary detection technique. A bone biopsy microradiograph from a cross section of the rib of a dog is shown in (A). The objective is to find the boundaries of the cortical bone (c), trabecular bone (T) and holes (arrows) in the cortical bone. Histogram technique is used in the spatial domain for boundary detection. The histogram is smoothed in the frequency domain. See text for description. M, marrow.

order Butterworth low pass filter on H, is shown in Figure 14d. Compare the original histogram shown in Figure 14b with that of 14d. From this smoothed histogram, the boundary of the bone can be automatically traced by a standard boundary trace program using the grey level value at trough T (Figure 14d) as the cut-off value. The automatically traced bone boundary is shown in Figure 14e. The interface between the cortical and the trabecular bone is difficult to determine automatically since there is no clear-cut boundary between them. An interactive graphic technique has to be used which requires judgment from the operator. The interactively traced boundary between the cortical and the trabecular bone is shown in Figure 14f. The grey level value at trough B in Figure 14d is used as the cut-off value for automatically tracing the holes in the cortical bone areas; some holes are being automatically traced at the lower left corner of the bone in Figure 14g. Figure 14h shows the final result after all the holes have been traced and counted, only the graphic memory is shown in this figure to highlight the tracing. Thus, in this microscopic image, all the boundaries of objects of interest have been identified and their coordinates recorded. The next step is to perform measurements from these coordinates.

Analysis: Geometric and Density Parameters

Geometric Parameters

In black and white microscopic imaging, two types of parameters can be extracted from boundary coordinates for quantitative analysis: geometric parameters and density parameters. Geometric parameters (Huang, 1981a) only measure the size and shape of the object under consideration whereas density parameters measure both the geometry and the grey level distribution of the object.

Some commonly used descriptive geometric parameters are height, width, major diameter, minor diameter, elongation (major/minor), perimeter, convex perimeter, irregularity of outline (perimeter/convex perimeter), total area, inner area, outer area, features with holes (outer area/inner plus outer), circularity (area) (4π)/Perimeter^2), goodness of fit to square (perimeter/4·minor diameter), coil packing (perimeter/2·major diameter), orientation, location, intercept, and nearest neighbor distance. Figure 15 illustrates these features along with their definitions. Thus, the areal measurements in the microradiograph example previously described is only one of these many parameters.

Mathematically, geometric parameters can be described by using the Fourier Series in polar coordinates (ρ,θ). Thus, given a set of boundary points (x, y) from an object of interest, they can be transformed into the polar coordinates with respect to its geometric center (x, y). A curve fitting technique in polar coordinates can be used to fit this set of points into a Fourier Series such that any point $\rho(\theta)$ on this boundary can be expressed by

$$\rho(\theta) = A_o + \sum_{n=1}^{\infty} (A_n \cos n\theta + B_n \sin n\theta)$$

where A_o, A_n, and B_n, coefficients from the fitting. Each coefficient and each term in this expression has a certain meaning in terms of the shape of the boundary. For example, the plot $A_o + A_1 \cos\theta$ versus θ represents the error in locating the centroid; the A_2 term is the elongation; the A_3 term represents the triangularity; the A_4 term indicates the degree of squareness. Also, the higher the

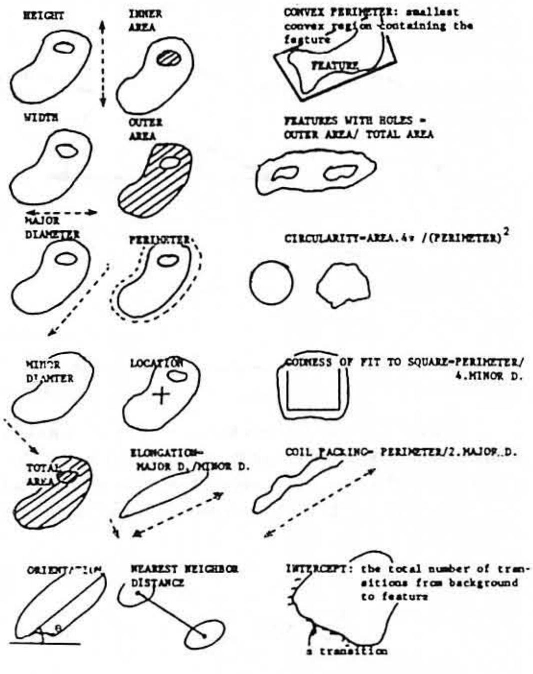

Figure 15. Some commonly used descriptive geometric parameters.

order of the term, the finer the morphological detail it represents. Figure 16 illustrates the concept of using the Fourier Series to describe geometric parameters.

Density Parameters

Density parameters take into consideration both the geometry and the density distribution within the object. Commonly used density parameters are the total mass, the center of gravity, and the second moment. Mathematically, they can be expressed as follows:

$$\text{Total mass: } M = \sum_{x,y} p(x,y)\Delta A$$

$$\text{Center of gravity: } X = \sum_{x,y} p(x,y)x \sum_{x,y} p(x,y)$$

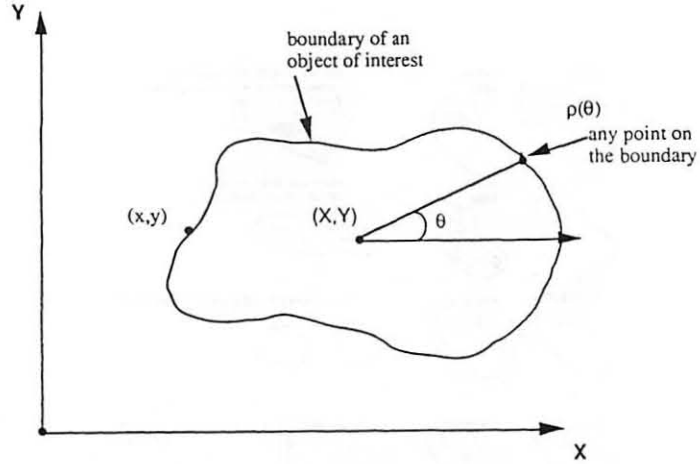

Figure 16. Concept of using a Fourier Series to represent the boundary of an object. The (x,y) coordinates of the boundary points of an object is transformed to polar coordinates. Each point on the boundary ρ(θ) can be expressed by a Fourier Series obtained from curve fitting of the boundary points. (X,Y) are the coordinates of the center of gravity.

$$Y = \sum_{x,y} p(x,y)y \sum_{x,y} p(x,y)$$

$$\text{Second moments: } I_{xx} = \sum_{x,y} p(x,y)(y - Y)^2$$

$$I_{yy} = \sum_{x,y} p(x,y)(x - X)^2$$

$$I_{xy} = \sum_{x,y} p(x,y)(x - X)(y - Y)$$

where p(x,y) is the pixel value located at (x,y), and ΔA is the size of a pixel.

Scan and Count

In some specimens, the objects of interest in a microscopic image are not well-defined. In this case, boundary detection technique will not be effective. Quantization can only be done using a scan and count technique which produces a density distribution map of the image according to some preassigned conditions,

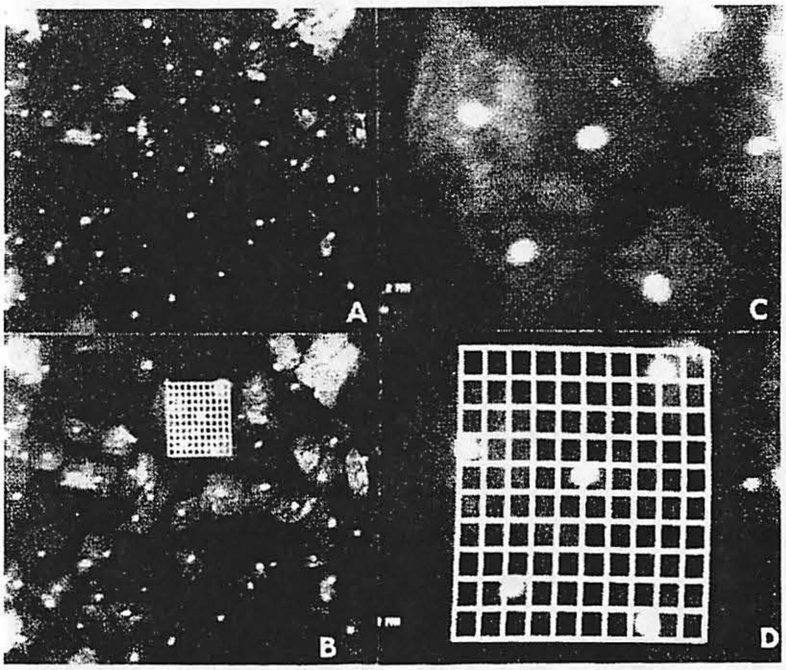

Figure 17. An example using the scan and count technique to count exfoliative cells in a Pap smear; see text for description.

for example, within a square mesh. This technique is best explained with an example. Figure 17a shows some exfoliative cells as seen in a Pap smear; bright dots are nuclei of the cells. Suppose it is required to find a quick count on the number of cells in a certain subregion. A square mesh from the graphic memory can be superimposed onto the image memory (Figure 17b) and the average density of each square can be evaluated. Since nuclei have higher density than the cytoplasm and the background, a proper choice threshold for the average density in each square will yield an approximate count of number of nuclei in the area of interest. Figure 17c and 17d are the zoom images of the corresponding area.

Color Parameters

Color parameters are extremely important in characterizing objects of interest in a microscopic slide. The method of separating the three primary colors, red, blue, and green, from a microscopic image to three image memories has been previously described. Various parametric analyses using a set of two images (red and blue, blue and green, and red and green) can be performed to isolate the color of interest, the detail of which is beyond the scope of this chapter and will not be treated here

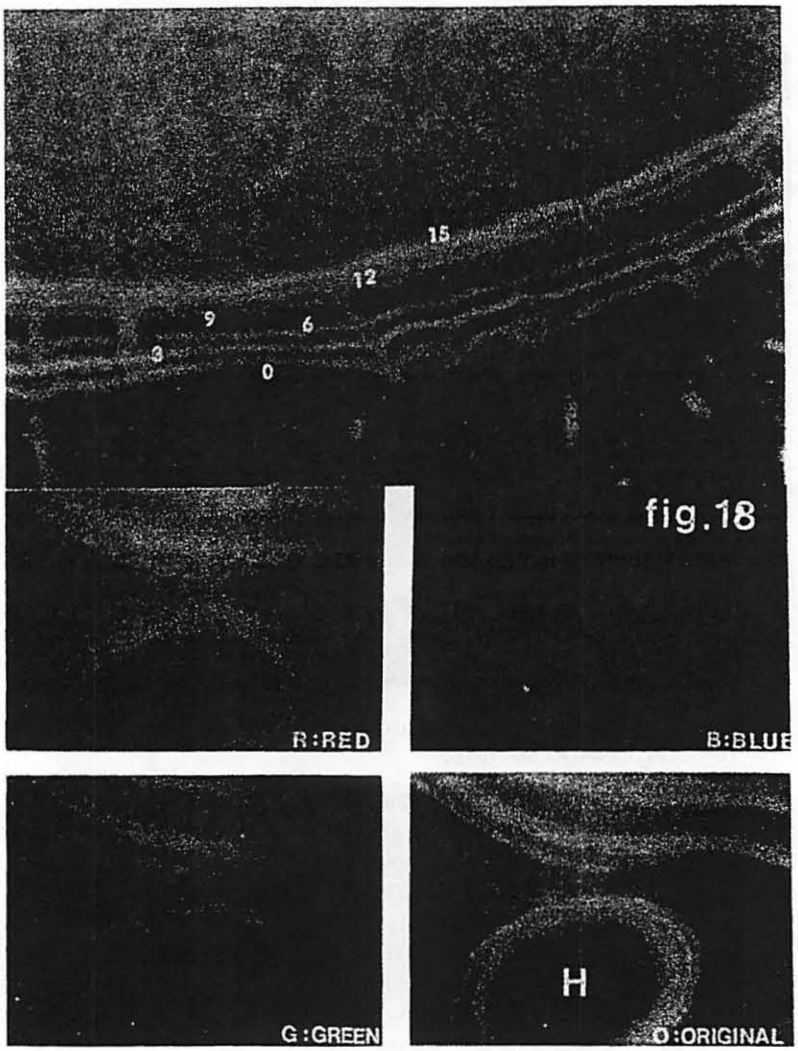

Figure 18. A bone cell in a fluorochromic image with tetracycline label shown in orange red. The objective is to quantify the tetracycline label. **a.** A fluorochromic image form the tibia of a rat bone biopsy with five different tetracycline labels. Each label has its own color characteristics: 0-day, oxytetracycline label; 3-day, DCAF; 6-day, xylenol orange, 90mg/kg; 9-day, hematoporphin, 300mg/kg (did not stain); 12-day, doxycycline; 15-day, alizarin red 5. The dose is 20 mg/kg except otherwise specified. **b.** A partial osteonal unit depicting the osteoid and the Haversian canal (H). One tetracycline label is shown in orange red, the inside ring immediately adjacent to H. The three color images (red, blue, and green) are also shown (the blue image was accidentally flipped during the photographic process).

(Huang et al., 1983). However, as an example, consider a bone cell in a fluorochromic image with tetracycline label shown in Figure 18. The objective of the study is to identify the tetracycline label (orange red) from the cell and quantify its intensity. If black-and-white imaging is used to perform the analysis, it would be extremely difficult because of the lack of its color components. However, if color parameters are used with parametric analysis, it is possible to identify the tetracycline label fairly easily. Figure 18a shows a fluorochromic image from the tibia of a rat bone biopsy with five different tetracycline labels; each label has its own color characteristic. Figure 18b depicts a fluorochromic image of a partial osteonal unit showing the osteoid and the Haversian canal. The image is decomposed to red, green, and blue images.

SUMMARY

We have discussed the fundamentals of medical imaging and have covered several matters including some definitions, image detectors and recorders, sources of medical images, and image processing systems.

The use of medical imaging in the radiological sciences is expected to increase about 40% in the next five years (Huang, 1987). New methods producing medical images will not progress drastically, but image quality from existing imaging modality will continue to improve. Traditionally, medical imaging is used only for diagnostic purposes, but we see the trend that they are also being used for therapeutic applications as well. PACS will become a vital image database management system. This will lead to the development of an image knowledge database that will require new IP hardware and software. The leading candidate in hardware design for medical image processing will be a modified parallel processing architecture that will shorten the time required for interprocessor communication. Mathematical advances may provide a new approach for image segmentation (Trambert, 1986). Fractal analysis shows promise for image feature extraction and object definition. Neutral networks may prove useful for medical pattern recognition, and other artificial intelligence techniques may bring medical imaging to the threshold of a mature science.

With regard to digital microscopic image processing, it requires fundamental knowledge of microscopy, television scanning, and digital image processing. In microscopy, specimen preparation is the most important step, since a good preparation can account for almost 50% of the success in designing a digital microscopic imaging system. The motorized x-y stage and automatic focusing are two important components for screening and quantitative analysis of microscopic images. The television camera used for scanning should have the proper specifications so that its resolution is adequate for imaging the objects of interest. In digital imaging technology, an image memory (or memories if color processing is necessary) and a graphic memory are essential in addition to the computer memory.

lens is used during the search and a high power objective with oil immersion is used for the feature extraction. The starting point in searching is using a two grey level and low resolution image. And the development of a search algorithm depends on the characteristics of the objects of interest. Three types of parameters should be considered in feature extraction: geometric, density, and color. All these parameters are essential in the success of performing quantitative microscopic imaging.

REFERENCES

Burrells, W. (1971). In: Microscope Technique. John Wiley & Sons, New York.

Castleman, K.R. (1979). In: Digital Image Processing. Prentice-Hall, New Jersey.

Hawkins, R.A., Hoh C., Glaspy, J., Choi, T., Dahlbom, M., Rege, S., Messa, C., Nietszche, E., Hoffman, E., Seeger, L., Moddahi, J. & Phelps, M.E. (1992). The role of positron emission tomography in oncology and other whole body applications. Sem. Nucl. Med., XXII (No. 4), 268–284.

Huang, H.K. (1981a). Biomedical image processing. CRC Critical Revs. Bioeng. 4, 185–271.

Huang, H.K. (1982). Introduction to digital microscopy. In: Application of Computers in Medicine (Schwarz, M. D., ed.), IEEE Engineering in Med. and Biol. TH0095–0; 177–186.

Huang, H.K. (1987). In: Elements of Digital Radiology. Prentice Hall, Englewood Cliffs, N.J.

Huang, H.K. (1993a). In: Medical Imaging Encyclopedia of Computer Sciences. 3rd ed. (Ralston, A. & Reilly, E.D. eds.), pp. 842–847, Van Norstrand, New York.

Huang, H.K., Aberle, D.R., Lufkin, R., Grant, E.G., Hanafee, W.N., & Kangarloo, H. (1990). Advances in medical imaging. Ann. Int. Med. 112, 203–220.

Huang, H.K., Mankovich, N.J., & Altmaier, J. (1981b). A macroscopic and microscopic image processing system. Proc. Fifth Ann. Symp. Comp. Applic. Med. Care, pp. 580–585, Washington, D.C.

Huang, H.K., Mankovich, N.J., Taira, R.K., Cho, P.S., Stewart, B.K. Ho, B.K.T., Chan, K.K., & Ishimitsa, Y. (1988). Picture archiving and communication systems for radiological images: State-of-the-art. CRC Critical Revs. Diagn. Imag. 28, 383–427.

Huang, H.K., Meyers, G.L., Martin, R.K., & Albright, J.P. (1983). Digital processing of microradiographic and fluorochromic images from bone biopsy. Comp. Biol. Med. 13, 27–47.

Huang, H.K., Taira, R.K., Lou, S.L., Wong, A.W.K., et al. (1993b). Implementation of a large-scale picture archiving and communication system. Comp. Med. Imag. & Graph. 17, 1–11.

Huang, H.K., Wong, W.K., Lou, S.L., & Stewart, B.K. (1992). Architecture of a comprehensive radiologic imaging network. IEEE Trans. SA Commun. 10, 1188–1196.

Kangarloo, H. Boechat, M.I., Barboric, Z.,Taira, R.K., Cho, P.S., Mankovich, N.J., Ho, B.K.T., Eldredge, S.L., & Huang, H.K. (1988). Two-year clinical experience with a computed radiography system. Am. J. Radiol. 151, 605–608.

Onoe, M., Preston, K., & Roxenfeld, A., (eds.) (1980). In: Real-Time Medical Image Processing, Plenum Press, New York.

Pressman, N.J. & Wied, G.I. (1979). The automation of cancer cytology and cell image analysis. Ed., Proc. Second Intl. Conf., Chicago, IL.

Rochow, T.G. & Rochow, E.G. (1978). In: An Introduction to Microscopy by Means of Light, Electrons, X-rays, or Ultrasound. Plenum Press, New York.

Udupa, J.K., Goncalves, R.J., Iyer, K., Narendula, S., et al. (1993). Imaging transforms for 3D biomedical imaging: An open, transportable system (3DVIEWNIX) approach. In: Computer Assisted Radiology CAR '93 (Lemke, H.U., Inamura, K., Jaffe, C.C., & Felix, R., Eds.), pp. 370–383, Springer-Verlag, Berlin.

Trambert, M.A. (1986). Cellular logic implementation on a generalized image processor applied to biomedical image processing. Anal. Quant. Cytol. Histol. 8, 131–137.

Valentino, D.J., Mazziota, J.C., & Huang, H.K. (1991). Volume rendering of multimodal images: Applications to MRI and PET imaging of the human brain. IEEE Trans. Med. Imaging 10, 554–562.

0033-8389/96 $0.00 + .20

WORKSTATION DESIGN

Image Manipulation, Image Set Handling, and Display Issues

S.L. Lou, PhD, H.K. Huang, DSc, and Ronald L. Arenson, MD

In the health care community, the trend is to computerize the mechanism of processing medical images and records. The research and development of picture archiving and communication systems (PACS) has been one of the major driving forces in this area. As a result, image management functions of PACS (e.g., image delivery, archival, and retrieval) have been developed and well received by the medical community. Radiologists' acceptance of PACS computer-based (digital) image-display workstations (the point of contact between PACS and user), however, is mixed. This is because the workstation performance strongly depends on three issues: (1) quality of the image, (2) functionality of the image display system, and (3) time required to review images using the system. The major factors that affect the image quality are image creation (although this is not in the scope of our context) and characteristics and specifications of the display media. The main criteria influencing the functionality of the image display system include: (1) ease of operation, (2) fast image access, and (3) simultaneous multiple-image display. The film-alternator system presently in use is a mature system for radiographic reading in clinical radiology. This system has evolved over many years and almost all requirements stated previously have been met. In contrast, the image display quality and efficient display system design remain a challenge to radiologists and engineers of digital-display workstations. This is the main reason today why digital-display workstations have not been widely accepted by radiologists.

This article focuses on the design of effective digital workstations and solutions to these challenging issues. A review of radiology practice is given as a base line for the design of practical digital workstations. The hardware technology of a state-of-the-art workstation is presented. Types of digital workstations used today are outlined. A comprehensive discussion on designing digital workstations for radiologists' use is detailed. Finally, necessary improvements to promote future digital workstations are suggested.

REVIEW OF RADIOLOGY PRACTICE

Today's film-based operation is not perfect. There are significant problems with lost films, delays in accessing films, and high cost of film handling. Yet there is no doubt it is a mature system and generally well accepted by radiologists. Thus, it is important to incorporate key components of the current system

From the Department of Radiology, University of California, San Francisco, California

in the design of a digital image-display workstation. In this section we briefly examine the facilities associated with radiographic reading, such as x-ray films, patient film jackets, and film-alternators. Then, we review the work flow in case preparation including (1) film recording, (2) newly examined and historical film delivery, and (3) film hanging. We use tables and figures to summarize major factors in the conventional film-alternator system that should be incorporated in the digital workstation design.

Radiographic Reading Facility

X-ray Film

In clinical radiology, silver-halide x-ray film is the medium used to acquire, store, and display radiologic examinations. X-ray film is used because of its sensitivity to exposure to x-rays and light, relatively inexpensive and convenient storage, and its contrast characteristic and high spatial resolution for display. The contrast feature easily can be understood from the sigmoid shape of the H and D curve (named after F. Hurter and V.C. Driffield), which shows the relationship between x-ray exposure and photographic density.[3] The photographic density is the measurement of film blackness, and usually is continuous in the range of optical density from 0.2 to 4. The film size commonly used includes, in inches, 8x10, 10x14, 14x14, and 14x17.

Patient Film Jacket

In a film-based system, a patient jacket usually contains various envelopes associated with different imaging modality films, such as CT scan, MR imaging, ultrasound (US), computed radiography (CR), and conventional radiography. Sometimes these film envelopes are organized by organ system or department section. Furthermore, each modality envelope may have several subenvelopes. Each envelope contains examinations that include a series of films containing one or more images. These usually are arranged by date and time of each examination. For example, in a CT scan folder, the envelope may hold films from studies on different dates. An MR imaging examination envelope may contain several sequential scans based on scan orientation, pulse techniques, and applied parameters. Each sequential scan in MR imaging is called a sequence. One MR imaging sequence (or one CT scan study) contains many cross-sectional images and may require more than one film to accommodate. Likewise, a single US examination envelope may contain images from many different scan directions, as well as selected static images from dynamic studies. A CR or x-ray examination envelope may contain films from different views, such as posteroanterior (PA), anteroposterior (AP), and lateral.

Film Alternator

Film alternators, motorized devices containing multiple panels of viewboxes, commonly are used today for reading radiologic films. There are many different configurations in a film alternator. A typical configuration has approximately 40 panels; each panel can hold four 14x17-inch films. Two active panels, one on top of another, may be illuminated at a time. The luminance of an alternator panel usually is more than 400 foot-lamberts (candela/m^2), and when covered by an x-ray film it ranges from 3 to 200 foot-lamberts.

Preparation of Films for Reading

Film Recording

Following an examination, the acquired images are recorded on film. For example, at a CT scan or MR imaging console, the technologist first uses preset keys, which predefine several window and level look-up tables based on body regions and types of examination to obtain an acceptable contrast and brightness setting of the image. Each image then is manipulated manually until the best appearance is obtained according to the technologist's professional judgment. The CR and nuclear medicine (NM) image recorders also allow technologists to select a predefined window and level setting. Instead of adjusting the contrast and brightness setting, manually the CR and NM recording systems automatically process images and provide films with preset contrast and brightness. Unlike CT scan, MR imaging, and CR, US images do not require window and level adjustment because they are preadjusted in the US internal circuitry. But US and NM do require color, which is discussed later in this article. After the window and level setting, images are laser printed onto a film with a predefined format. An optimal choice balances between the size of the film and the number of the images on a film. For example, the 4 x 5 format is used to record 512 x 512 pixel CT scan images on a 14 x 17-inch film. MR images also are recorded on a 14 x 17-inch film with the 4 x 5 format. Because MR images contain 256 x 256 pixels, however, each image is enlarged to 512 x 512 pixels before filming. If there had been no enlargement, MR images would have been recorded on an 8 x 10 format. In that case, anatomic details would be difficult to visualize. CR images usually are much larger in size, such as over 2000 x 2000 pixels. Thus, one CR film usually records one or two views of images (i.e., one-on-one or two-on-one format).

After the films are developed, they are inserted in a modality-specified film envelope. The envelope is marked with the patient name, identification number, and date of examination for identification.

New and Historical Film Delivery

Depending on the individual radiology department, the procedure of delivering newly acquired and historical films for radiologists to review depends on the practice of each individual section or department. Generally speaking, there are two ways to prepare these films. First, the newly examined envelope is inserted into the patient jacket in a staging area, and then the whole patient jacket is delivered from the staging area to each specialty reading room. The second method is to deliver the patient's newly acquired films directly to the reading room. Because most departments today use radiology information systems (RIS), the film library clerks typically receive pull notices for previous studies from the RIS as soon as the new study is scheduled. In this manner, the film library clerks may retrieve the comparison studies and deliver them to the appropriate destination, such as the reading room, even before the new examination is performed. The corresponding patient jacket containing the previous studies and corresponding reports is retrieved from the film library to the reading room before the arrival of the newly examined envelope.

Film Hanging

Radiologists develop image reading habits through their professional training and experience. Arranging films on an alternator is one of these habits. A properly arranged film set facilitates reading. Radiologists either hang films by themselves or train residents or film librarians to do so. Although the preference of film arrangement varies among radiologists, within the same specialty section they more or less follow some common rules. For example, images should be arranged for easy comparison readings between the most current and previous examinations. For a patient who does not have previous examinations, the films may be arranged based on the examination protocol. For example, an MR brain imaging protocol contains four scans: (1) T1 sagittal, (2) T2 axial, (3) multiplanar gradient reconstruction (MPGR) coronal, and (4) T1 axial. This MR imaging examination may be arranged on the film alternator in such a way that the T1 sagittal, which is the first sequence in the scanning protocol, is hung in a manner to be read first. The T1 axial, which is the last sequence in the protocol, is positioned last on the panels, and so forth.

Summary of Film Reading

Table 1 summarizes some characteristics of x-ray films used for image recording. Table 2 gives specifications of alternators for hanging x-ray films. Figure 1 summarizes contents of a patient folder. The regular procedures for preparation of radiologic film reading are summarized in Table 3. These factors, specifications, and required preparations provide a baseline for reference that must be taken into account in the design of a digital image-display workstation.

Table 1. MAIN FACTORS AFFECTING RADIOGRAPHIC READING IN X-RAY FILM

Characteristics	Optical Density	Size (inches)
Image contrast enhancement feature (The characteristic response curve of density vs. exposure is sigma shape. Films with different speed and latitude can be made to suit various body region examinations.)	Range from 0.02 to 4 continuously	8 × 10 10 × 14 14 × 14 14 × 17 and so forth

Table 2. MAJOR FACTORS AFFECTING RADIOGRAPHIC READING IN THE ALTERNATOR SYSTEM

Panels		Lighting		Motor Paddle
Number of Panels	Layout of Panels	Luminance Density	Flicker	Speed of Rotating
e.g., 40	Two active panels (one on top another) (e.g., about the size of four 14 × 17-inch films per panel	>400 foot-lamberts	No	2~3 seconds per panel

WORKSTATION TECHNOLOGY

Generally speaking, display monitors and the computer-imaging system in a workstation are analogous to x-ray films and the alternator in the film-based system. This section examines those factors described previously in the film-based system that are associated with display monitors and the computer-imaging system. It is our intention to provide a better understanding of state-of-the-art technologies in digital workstations.

Image-Display Monitor

Physical Size

The physical size of the display area on the monitor should match the x-ray film size. Although there are various sizes of films used for recording images, a rectangular film with 14x17 inches (approximately 21.5 inches in diagonal) is the most common size used. The physical image display area of the monitors ranges from 20 to 30 inches diagonally and are commercially available. Other challenges including video data rate, frame refresh rate, and intensity brightness of the monitor must be met before they can be completely accepted by radiologists. These are described in the following sections.

Video Data Rate

The video data rate of a display monitor roughly is equal to the multiplication of three parameters: (1) number of pixels per line, (2) number of lines per frame, and (3) number of frames per second plus the various electron beam retrace times. The first two parameters determine the spatial resolution of the display monitor. The third parameter defines the frame refresh rate of the monitor. For example, a currently available high-resolution monitor made by MegaScan display system (E-Systems, Littleton, MA) provides spatial resolution of 2048 x 2560 with noninterlaced vertical refresh rate over 70 Hz. The video data rate of the monitor requires 500 MHz in order to support the specifications.

For an image displayed repeatedly on a monitor, the human visual system is able to integrate the image that is being refreshed. If the frame refresh rate of the monitor is not high enough, it detects flicker. Usually, the flicker diminishes when the refresh rate goes up to 60 Hz. A refresh rate of over 70 Hz is required to ensure an image display monitor is flicker free.

Luminance Intensity

Another important image display monitor characteristic is the luminance intensity. The common measurements of the monitor's luminance intensity are foot-lambert or cd/m^2. Most monitors can provide between 50 to 150 foot-lamberts. (Although there are a few products over 200 foot-lamberts, the scan lines of the monitors become visible, which is not desirable for radiographic reading.) This is low luminance compared with conventional film alternators that have light boxes providing more than 400 foot-lamberts. For a

Table 3. PREPARATION PROCEDURES FOR RADIOGRAPHIC READING

Image Adjustment	Image Recorded Onto Film	Film Retrieval	Film Hanging
Image window & level adjustment Examined body region contrast enhancement	Image format (e.g., 1×1, 2×1, 3×4, 4×4, 4×5, etc.) Image enlargement if necessary	Historical films retrieving for comparison studies	Patient image films are arranged with individual radiologist's preference

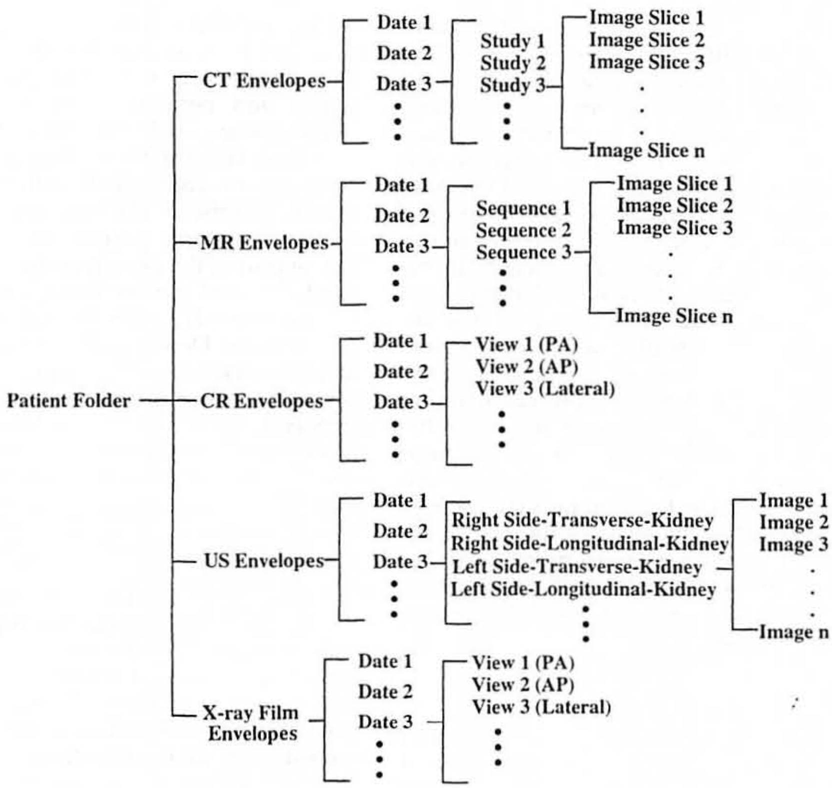

Figure 1. A hierarchy demonstrating the possible content of a patient image folder.

given phosphor surface on a cathode ray tube (CRT), the higher the luminance intensity, the higher the electrical current required. This is because the brightness produced by the phosphor is proportional to the power of electron beam bombarding the phosphor. Thus, one can predict that increasing the spatial resolution (i.e., number of pixels per line and number of lines per frame) results in a lower brightness if the monitor's electrical current is fixed.

Pixel Gray Levels

Photometric resolution refers to the precision of luminance intensity (brightness or photo density) value at each image pixel position.[2] Of particular interest is the number of discrete gray levels that the monitor can generate. These gray levels are related to the number of bits used to control the brightness of each pixel. Currently available gray-level monitors are capable of handling eight-bit data. This means that, theoretically, the monitor can generate 256 distinct levels of gray from dark to bright. Taking noise into account, practically speaking, the effective number of gray levels is never more than the number of gray levels in the digital data. For example, a monitor's root-mean-square noise level accounts for 1% of the entire display range from dark to bright. Even though the monitor is controlled by an eight-bit display system, the monitor is able to display about 100 effective gray levels only.

Gray Scale Linearity

The luminance intensity produced by the monitor is a function of the gray level input, which is called the characteristic curve of the display monitor. In general, a monitor's luminance intensity is controlled by two adjustable knobs: (1) contrast and (2) brightness.

For each contrast and brightness setting there is a corresponding characteristic curve. Ideally, the characteristic curves should remain linearly independent from contrast and brightness settings. Unfortunately, most available gray-scale monitors today do not have linear characteristic curves. Moreover, these nonlinear characteristic curves are not provided to the user. Because the human eye is not sensitive to a slight nonlinearity in the characteristic curve, there is no demand from users to request this information. In the design of an image-display workstation, however, the availability of the characteristic curves is important because one can manipulate them to get a better visual quality of the image. For example, the results of an image manipulated by a processing function are unpredictable because the monitor's curves may enhance or offset the effect of the processing function. For this reason, in order to design effective image processing functions, the characteristic curves of monitors must be known beforehand.

Number of Monitors

As stated previously, the configuration of two active panels that can accommodate a total of eight x-ray films is a common design of an alternator. With today's workstation technology, it is possible to configure eight image-display monitors with one workstation. Issues to consider are the cost of display monitors and the necessity of eight monitors. Few studies have shown that a digital workstation requires more than one display monitor mainly because it allows radiologists to scan rapidly through different image sets.[8, 17] Although the optimal number of monitors of a workstation remains to be determined, and it is task specific, the configuration of two to four monitors gradually becomes a consensus.

Computer System

In addition to image-display monitors, the major hardware components of a display workstation consists of a host computer, user-interface devices, image-storage devices, or display-memory buffers.

Host Computer

The host computer and its peripheral devices perform various tasks, such as user interface, acquiring data from acquisition devices, fetching images for display, and so forth. Performing these tasks requires computing and peripherals input and output (I/O) power. High-end computers usually have high computation power and fast computer buses configured with high-performance peripheral devices. These high-end computer systems perform the tasks faster, but, of course, the price is costly. On the other hand, low-end personal computers (PC) are less expensive; however, the trade off is slower performance. Depending on the applications, display workstations configured with various computer platforms from low-end PC to high-end workstations, such as IBM-PC, Macintosh, Sun SPARC, Hewlett Packard, and Silicon Graphics, are available in today's market.

User Interface

User interface is another important component in the workstation. User-interface devices commonly used in the workstation may include a mouse; a trackball; a keyboard (or keypad); or a dialbox. Depending on the needs of the workstation, more than one of these devices can be configured with the workstation. The mouse is handy because it provides a convenient hand-to-cursor interface. The mouse also is quite comfortable for most users owing to their familiarity using the mouse with their PCs. In addition, clicking the buttons on the mouse provides a means to send a selected signal to the host computer. How many buttons are available on the mouse is dependent on the computer system used. The trackball is a box-like device containing a few buttons and a trackball. The function of the trackball is similar to the mouse except that the operation of the trackball does not require hand maneuvering. Key strokes on the keypad are useful in typing or activating certain settings. The dialbox contains several rotational dials and is useful for fine adjustment of image-processing functions, like window and level, zoom, and scroll. The dialbox, although quite functional, is not intuitive and tends to confuse the occasional user.

Image Storage

Requirements placed on the storage device in image display are stringent. The sheer volume of data calls for a large capacity in excess of gigabyte range, and increasing demands for image processing and graphics at interactive speed require a very high throughput capability. Magnetic disks are the common storage media for images that allow an average I/O transfer rate of one to two megabytes per second from the disk to the video display. In order to archive higher I/O rate, two types of high-speed image storage can be used. One is the random access memory (RAM), which is connected directly to the image processor or the host computer bus. This type of image storage has a very fast I/O rate, but is volatile and expensive. The second type is the magnetic disk array, which is slightly slower than the RAM but is permanent and less expensive.

RAM is used as a buffer in an imaging workstation. Because RAM is expensive, however, the nominal size of the RAM memory in a workstation is between 32 to 128 megabytes. This allows the storage from 8 to 32 2K x 2K x 8 bit images. The RAM memory is used as a buffer in the sense that a set of images is first loaded from the disk storage to the RAM. From there, one image at a time is transferred to a video buffer or video RAM (VRAM). VRAM has a much higher I/O rate than the RAM and is even more costly. The VRAM is connected to the video monitor through a fast digital/analog (D/A) converter. A D/A conversion is then performed displaying the image on the video monitor. This architecture allows an image to be displayed rapidly on the video monitor.

A parallel transfer disk (PTD) or disk array can achieve data transfer rates between the disks and the display memory in the neighborhood of 10 megabytes per second. The PTD allows multiple read and write heads simultaneously to transfer data. The disk array, on the other hand, configures multiple conventional magnetic disks in parallel. Two common approaches for the disk array are (1) software striping and (2) hardware paralleling. In software striping, the disks are connected to the system bus through traditional controllers. Blocks of data are segmented and moved to and from the disk drives in parallel. Data segmentation and recombination are handled by the software. In the hardware approach, a parallel drive array controller simultaneously manages multiple disk drives. For example, eight enhanced small device interface disk drives, each capable of 2.5 megabytes per second data-transfer rate and having 1.2 gigabytes, can be configured in parallel to deliver 20 megabytes per second transfer rate with a total storage capacity of 9.6 gigabytes.

Image Processing and Memory Hardware

The engine of a workstation is a special-purpose image buffer and processing hardware (or image processor). The image processors may be board-level units that plug directly into the host computer's general purpose bus (such as VME, S-bus) or they may be chassis-level products that communicate with the host computer via a host-bus adapter. A typical image processor consists of an image memory (or frame buffer); a pixel processor; and a video-output processor. These components share a common image-transfer bus to realize high-speed transfer of data.

Image memory is needed in addition to the main central processing unit (CPU) memory in the host computer because CPU memory normally lacks the capacity and speed to store and process image data. The pixel processor performs arithmetic operations on the data copied from the image memory. These operations include point functions, such as image addition, subtraction, and merging; geometric functions, such as magnification; statistical functions, such as histograms; and transformation functions, such as lookup table operations. Often, optional hardware components are available to speed up the image-processing computation. These components may include a floating-point accelerator, fast Fourier transform coprocessor, and so forth. The video-output processor normally contains three channels of image output to provide either one 24-bit full-color image or three eight-bit gray scale images. In addition to providing the image channels, a well-designed system also supplies an alpha channel for graphics overlay.

TYPES OF IMAGE WORKSTATIONS

Image workstations can be loosely categorized into six types based on their applications: (1) diagnosis, (2) review, (3) analysis, (4) digitizing and printing, (5) interactive teaching, and (6) editorial and research workstations. These applications overlap on most workstations, however, and the best choice often is dictated by the most predominate use.

Diagnostic Workstation

A diagnostic workstation is used by radiologists for making primary diagnoses. The components in this type of workstation should be of the best quality possible. If the workstation is used for displaying a large volume of projectional radiographs, then multiple 2K monitors are needed. On the other hand, if the workstation is used for CT scan and MR images, multiple 1K monitors are sufficient. A diagnostic workstation requires a digital dictating phone to report the findings. The workstation provides software to append the report with the images. In addition to having the functions that are described previously, the diagnostic workstation requires a rapid (about 1 to 2 second) image retrieval time from disks to display memories. Figure 2 shows a two-monitor 2K display workstation at the University of California, San Francisco (UCSF) showing a CT scan study. This 2K workstation is based on the Sun SPARCserver 470 computer and two 21-inch diagonal 2K portrait mode monitors (UHR-4820P MegaScan display system, E-Systems, Dallas, TX). Each 2K station has a parallel transfer disk with 5.2-gigabyte formatted storage that can display a 2048 x 2048 x 2-byte image in 1.5 seconds (Storage Concepts, Irvine, CA).[11] It should be pointed out that the medium resolution monitors (1K x 1K) are better than 2K monitors for diagnostic workstations primarily used for reading studies from the digital modalities, such as MR imaging, CT scan, NM, US, and so forth. These monitors are more stable, provide higher intensity brightness that lasts much longer, are much cheaper, and, perhaps most important, better match the inherent spatial resolution of the images with the proper image size on the monitors for easy viewing. Large volume CR workstations need the 2K monitors, but an occasional CR case can be managed effectively on 1K monitors by zooming in to full resolution and panning around the image.

Review Workstation

A review workstation is used by radiologists and referring physicians to review cases in the hospital wards or high-volume physician offices. The dictation or the transcribed report must be available with the corresponding images. A review workstation may not require 2K monitors because radiologists sometimes read images from the diagnostic workstation and the referring physicians are not looking for every minute detail. Diagnostic and review workstations can be combined as one single workstation sharing both the

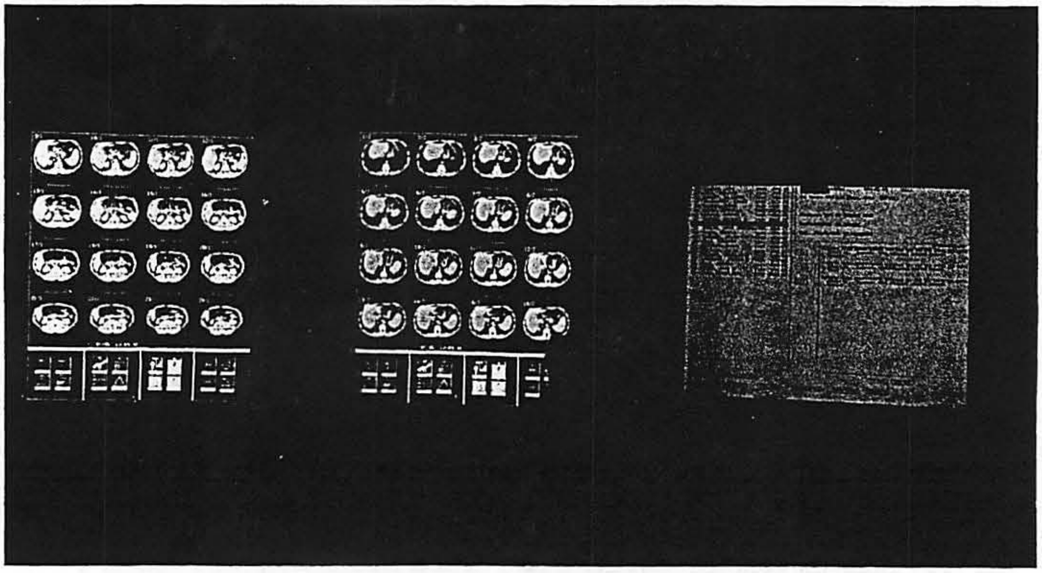

Figure 2. A diagnostic workstation with two 21-inch diagonal 2048 $\times$ 2560 portrait mode MegaScan monitors showing 16 CT scan images on each monitor. This workstation currently is used at the UCSF neuroradiology section.

diagnostic and review function like an alternator. Figure 3 shows a two-monitor 1K (1600 line) display workstation used at the intensive care units at UCSF. This workstation is developed by a partnership between ISG (ISG Technologies, Inc., Ontario, Canada) and UCSF. The system consists of a Sun SPARC-20 workstation with two gigabyte magnetic disks, two GXTurbo video display boards, and two diagonal 24-inch 1600 x 1024 display monitors.

Analysis Workstation

An analysis workstation differs from the diagnostic and review workstations in the sense that it is used to extract useful parameters from images. Some parameters are easy to extract from a simple region of interest (ROI) operation; others, like blood flow measurements from digital subtraction angiography (DSA) and three-dimensional reconstruction from sequential CT scan and MR images are computational intensive. The latter requires an analysis workstation with a more powerful image processor and high performance software.

Digitizing and Printing Workstation

The digitizing and printing workstation is for radiology department technologists or film librarians to digitize historical films and films from outside of the department. The workstation is also used for converting soft copy images to hard copy. In addition to the standard workstation components described previously, this workstation also requires a laser-film scanner, a laser-film imager, and a paper printer. The paper printer is used for pictorial report generation from the diagnostic, review, and editorial and research workstations. A 1K display monitor for quality control purpose is sufficient for this type of workstation.

Interactive Teaching Workstation

A teaching workstation is used for interactive teaching in the department. It emulates the role of a teaching library but with more interactive features. Figure 4 shows a digital mammography teaching workstation from VICOM (Fremont, CA) that is configured

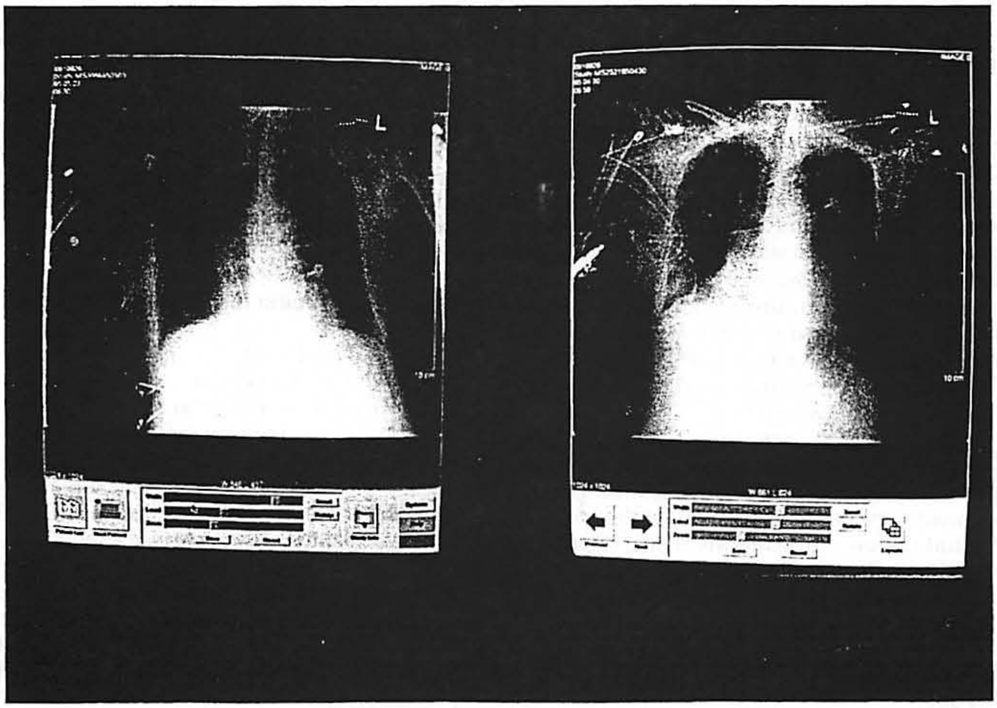

Figure 3. A review workstation with two diagonal 24-inch 1600 × 1024 display monitors showing one CR image on each monitor. The workstation currently is used at the UCSF intensive care units.

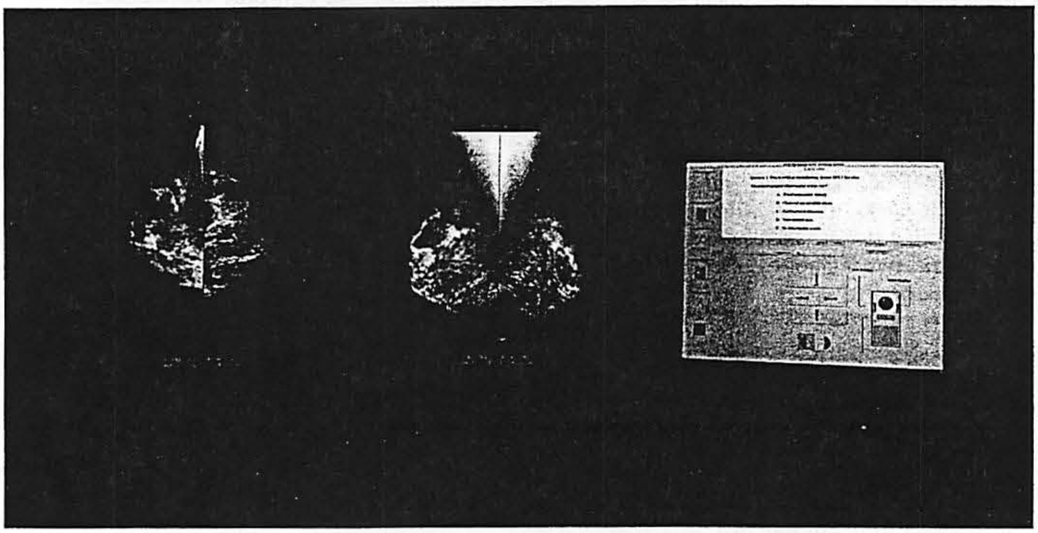

Figure 4. A digital teaching workstation with two 21-inch diagonal 2560 × 2048 MegaScan monitors showing one pair of mammograms on each monitor. The text information and user interface window in the console monitor instructs users to go through questionnaires.

with a Sun SPARCserver-470 computer, PIXAR image processor, and two 21-inch diagonal 2560 x 2048 MegaScan monitors.[14]

Editorial and Research Workstation

An editorial and research workstation is for physicians to generate lecture slides, teaching and research materials, and reports with images. This workstation includes functions in the PC or the Macintosh PC. This workstation uses the paper printer described in the digitizing and printing workstation to generate pictorial report. Figure 5 shows a Macintosh-based editorial and research workstation. The application software is developed within UCSF and has been used widely in the UCSF radiology department.[16]

Although each type of image workstation has specific functions to facilitate physicians' practice, the impact on physicians' practice depends on the development of the diagnostic and review workstations. Thus, the following discussions on workstation design focus on the diagnostic and review workstations.

IMAGE-DISPLAY WORKSTATION DESIGN

Detailed discussions on how to design an effective computer-based workstation for radiologic reading are given in this section. Challenging issues are presented including: (1) handling large image sets prior to review, (2) displaying large image sets with a limited number of display monitors, and (3) implementing simple workstation user interface. The concepts of the Folder Manager including prefetching, auto-sequencing, auto-presets for window and level, preprocessing for background or orientation, and triggers from the RIS that cause events to occur in the PACS are explained.[1,4]

Image Preprocessing

In the film-based system, several manual previewing tasks performed by staff, such as adjustment of window and level, new and historical films delivery, and film hanging on the alternator have made radiologists' viewing practice simpler and easier. Similar tasks must be implemented in computer-based display workstations for them to be competitive with the alternator viewing.

The aim of image preprocessing is to optimize the image appearance on display monitors so that users do not have to adjust the contrast, brightness, and orientation of displayed images manually. Most of today's digital-imaging modalities do not supply information on how to optimize the contrast and brightness associated with the generated im-

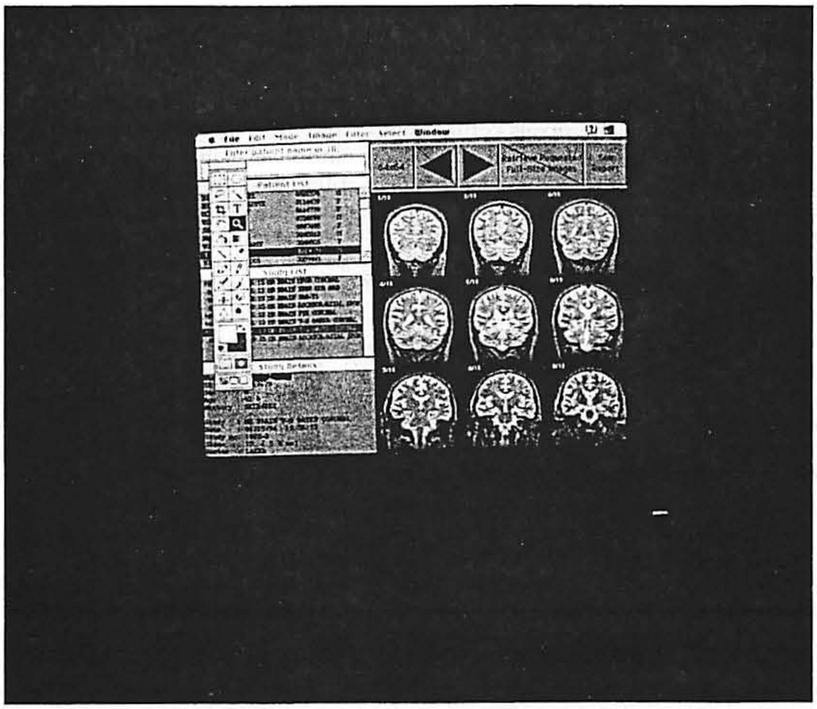

Figure 5. A Macintosh-based editorial and research workstation showing an MR imaging study.

ages because these two parameters are sometimes very subjective. For example, image headers (a set of defined data elements) on MR imaging, CT scan, and CR images contain no information about window and level parameters. Manual adjustments often are necessary to set these parameters for optimal display. Also, CR images often appear on the monitors in improper orientation owing to random placement of the imaging plate by the technologist during the examination. Unlike orientation correction in the film-based system, which easily can be done manually, image rotation and flipping is a time consuming operation in a digital display workstation. Another problem in CR is the unexposed white background in the image that can lower the perceived image contrast. To minimize these problems, image preprocessing is essential before they are displayed on monitors.

Determination of Image Window and Level Parameters

The use of window and level setting is to optimize the presentation of image contrast and brightness. Generally speaking, the level parameter indicates the gray value location of the information of interest and the window parameter shows the gray value range that the major information may be covering. A narrow gray value range usually produces a higher contrast image. If the range is too narrow, however, the information of interest may be excluded during the display.

Optimal window and level selection depends on imaging modality. In the following sections we use MR imaging, CT scan, and CR as examples to describe methods of choosing window and level settings automatically. These methods can be applied to other types of images with minor modification.

MR Imaging Images. Most MR imaging scanners generate either 12-bit or 16-bit data per pixel. Some studies, however, report that useful gray level in an MR image is about six to seven bits. The lower bits contain white or reconstruction noise and bear no useful information.[10, 18] If this is the case, one can simply display MR images by using the most significant 8-bits with the window and level values set for 128 and 127, respectively. Another method is to scale the range between the maximum and minimum gray values between 255 and 0. This method further can be optimized by excluding the pixels containing noise. As a result, the range between the maximum and minimum is reduced, which translates to a higher contrast image.

Two other approaches can be used further to reduce the range between the maximum and minimum values. The first approach is to search the maximum and minimum gray values within a certain area at the central part of the image. The shape and the size of the area can be varied depending on the body part imaged. For example, a commonly used area shape in an axial head MR image can be a central rectangle one fourth the size of the entire image. The rationale of using this area is that the examined body parts usually are placed in the central area of the scanner during the examination for gathering better signal-to-noise ratio data. Obviously, the advantage of this approach is that it is easy and quick in searching the maximum and minimum values within the rectangle. The tradeoff is that the accuracy of the maximum and minimum values is compromised to a smaller area in the image. The second approach is more complicated. It requires an algorithm to outline automatically the examined object (e.g., the head) from the image background. In this way, the maximum and minimum values can be found accurately from the contoured object.

CT Scan Images. The principle of CT scan reconstruction is to calculate the relative linear attenuation coefficients (μ_p) of tissues confined in an imaging area.[3] Usually, the CT scan image is represented by CT scan gray values instead of the relative attenuation coefficients. The following equations show the conversion from the relative linear attenuation coefficient to a CT scan number, and to a CT scan gray value. In general, the term CT scan gray value is used more commonly in a computer-oriented environment.

$$\text{CT scan number} = K(\mu_p - \mu_W)/\mu_W$$
$$\text{CT scan gray value} = \text{CT scan number} + K_o$$

where K is a scaling factor (equal to 1000 for most CT scanners); μ_W is the linear attenuation coefficient for water (0.191 cm^{-1}); and K_o is an offset constant to ensure a nonnegative CT scan gray value.

Because CT scan gray values are tissue dependent, the window and level values can be preset once the examination protocol or the body region is known. For example, brain, pituitary, orbits, cervical spine, temporal bones, chest, abdomen, pelvis, lumbar spine, and so forth each can have a preset window and level value for automatic optimal visual presentation. The easiest way automatically to select the best window and level and associated sequences is to use a protocol table in which the radiologists and technologists establish the proper settings. These protocols can be linked to the examination type in the RIS examination dictionary.[4]

CR Images. CR images require preprocessing by the CR image processor before they are displayed. The preprocessing functions, such as edge enhancement and filtering, are specifically designed for each individual examination protocol (type), such as head, neck, chest, abdomen, pelvis, upper, and lower extremities, as well as the patient size.[7,13] The latter contributes to the brightness and contrast appearance of the image. If the patient is thicker, the image is brighter, and vice versa. In addition, many CR images, such as those of pediatric patients, contain very bright background. For these reasons, extraction of the gray level range for CR image display is not an easy task. If the window and level settings are calculated without considering these factors, the outcome of the soft copy display is unpredictable. Thus, the range determination must rely on the analysis of the gray level distribution within the body regions of interest, which is provided by CR examination protocols.

Removing Unexposed Background

In conventional radiography, especially CR and digital fluorography, sometimes it is necessary to remove the image background owing to x-ray collimation before the images are displayed. Examples appear in pediatric and extremity images where collimation can result in significant white background included in the image. Its removal can reduce the amount of unwanted white background in the image during soft copy display and allow a more accurate display look-up table.

An algorithm that removes image background first searches for the raw edges (left, right, top, and bottom) of the radiation field. The raw edge points are those with standard deviation in the desired direction exceeding an empirically determined threshold. The raw edge points are searched to find the outer corners of the rectangular radiation field. These boundaries are tested to see if any portion of the radiation field had been excluded (i.e., inside the boundaries). This test is based on standard deviations of gray values of the background and the body region (or the radiation field). The background is characterized by lower standard deviations, whereas the body region is characterized by higher deviations. The correct contour is constructed as a collection of left, right, top, and bottom edges of the radiation field. Areas outside of the radiation field are set to the darkest gray level eliminating the unwanted bright background.

Sometimes when the CR imaging plate is not placed properly under the patient (e.g., in a slant angle with respect to the patient's body axis), then the radiation field may not be a rectangle. In this case, the algorithm should have the ability to detect this situation and correct it to search the edges.

After the background removal, the image of interest no longer may be in the central portion of the display field. In order to center and occupy the full monitor screen, it sometimes is advantageous automatically to zoom and pan the background removed image for optimal display.

Orientation

A properly oriented image displayed on a monitor should resemble the conventional hard copy a radiologist reads from the light box. Two examples are provided in CT scan and CR. In CT scan, the orientation of scanned slices appears on the display monitors in certain specific examination protocols different from radiologists' reading preference. For example, in a coronal sinus study with patient's head-first position and prone orientation, images generated by some spiral CT scanners may require a y-axis flip to meet the traditional reading preference. The necessary information to make CT scan image orientation correction automatically can be obtained from the CT scan image header. On the other hand, the automatic rotation correction on CR images requires special a image-processing algorithm.[15]

Local Patient Folder at the Workstation

Historical Image-Set Retrieval

As discussed previously, availability of a patient's current and historical films is important in the radiologic reading. Well designed workstation software should automatically retrieve necessary historical image sets from long-term storage devices (similar to the film library in the film-based system), supplement them with the newly acquired image set, and transfer the complete data file to the image-display workstation. If the historical image set is not prefetched automatically, the second choice is to retrieve it by a query from the workstation. In this case, any historical image sets related to the current image set may be requested to be transferred to the workstation from long-term storage devices. As described previously, the most efficient method of handling the transfer of previous images from the archive to the appropriate workstation is the Folder Manager, with prefetching of the prior studies triggered by the new examination being scheduled in the RIS. Based on the similar examination fields in the RIS examination dictionary, the most useful prior examinations are transferred to the desired workstation the evening before the scheduled new procedure if scheduled in advance. Otherwise, the prior studies could be moved immediately. In this manner, the need to request images manually from the archive is small, avoiding lengthy delays in that process and minimizing archive traffic during midday.[4]

Organization of Patient Folders

Potentially, image sets (including current and historical examinations) of a patient can be a large data file. Thus, when they are in the workstation, they must be organized for easy and efficient access. Commonly, this is done with either a relational database or an object-oriented database. A database contains one or more table files depending on the need of the application. Each table file is a collection of data records, and the fundamental units of a record are fields (or attributes). The contents of the fields is the information associated with an object. For example, a patient record contains fields, such as patient's name, hospital identification number, sex, date of birth, and so forth. In order to access the record, keys (or indices) have to be defined.[6] Usually, a field that is unique throughout a database table is selected as a primary key and fields likely to be accessed frequently can be defined as secondary keys.

There are many ways to implement the hierarchy of the patient folders in a display workstation. The following description is based on a tree-structure of data directory to represent the framework of a display workstation database. The terms of a folder (or a directory) and a file used in the following description are equivalent to a data record and a field of a database table, respectively. The hierarchy starts with a root directory that contains patient folders. Each individual patient is represented by a patient folder and each patient folder is comprised of imaging modality folders. Here, a modality folder is a file underneath its parent directory and also is a directory containing subdirectories and files. Inside a modality folder, it consists of examination folders with different dates. Within an examination folder, image study folders and associated diagnostic reports and various laboratory report files may be enclosed. An image study folder contains image files. For example, in a CR examination, an image file contains one view of an image, such as AP or lateral. On the other hand, in a cross sectional CT scan examination, an image file is a collection of sequential images. This is because a sequence of images provides more complete clinical information, whereas each single image by itself is of less significance. In the database, an image file is a set of indexing information describing the images, such as the image data location, number of images, and so forth. Usually, the physical image data is separated from the database tables and is stored contiguously in high-speed disks for fast image retrieval and display. It is important to emphasize the significance of the unique examination identifier supplied from the RIS. The accession number, which is the unique identifier that relates directly to the consultation report, the order in the patient's medical record, and the bill, is critical to the proper organization of the PACS database. Under the accession number belong the sequences or individual images and there is a date and time associated with each examination and accession number.

Automatic Image-Display Sequencing

In order to mimic the film hanging practice by film clerks using the panel rotation mechanism of the film alternator, the display workstation must possess the function of automatic image-display sequencing. This requires a patient display sequence table (PDST) and an image-set display sequence table (IDST). The PDST contains an ordered list of patients. For each patient in the display workstation, there is an associated IDST. Essentially, the IDST contains records composed of many columns including: (1) image file name, (2) monitor number, (3) panel number, (4) display format, (5) image modality type, (6) window setting, and (7) level setting. These parameters provide information for what, where, and how to display the image data. The image display sequence of a given patient follows the record number of the IDST in order. Based on the IDST, the patient's image sets can be displayed with two selection buttons: (1) "next image file" and (2) "previous image file."

Methods of Generating the PDST

The availability of the PDST enables radiologists to advance patient cases simply by pressing the "next patient" and "previous patient" buttons. This feature imitates the action of stepping on the motor paddle of the film alternator to rotate the light-box panels. The order of the PDST is determined by the combination of the following factors: (1) date and time of the current examination; (2) review status (i.e., patient images read or not); (3) patient status (i.e., in patient or out patient); (4) alphabetical order of patient's last name; and (5) imaging modality. For example, attributes in the PDST are based on the review status and the date and time of the current examination. Thus, only those patients whose current examinations have not been read by radiologists are listed chronologically in the PDST. This ensures that all cases will be read by radiologists. In addition to this example, various PDSTs can be generated by combining different criteria. Useful PDSTs can be implemented into a menu for selection by user interaction. Once again it is important to emphasize the power of the Folder Manager, which triggers the prefetching and linkage of the prior studies to the new studies for each patient to be included in the list.

Methods of Generating the IDST

How to design effective IDSTs is a challenging task. The numerous possible combinations of images and image sequences with or without prior examinations for comparison makes the autosequencing quite difficult. An approach to handle this challenge is presented.

Common Rules and Look-up Tables. The implementation of an automatic image-display sequence in a display workstation includes two steps. The first step is to follow common rules of the film hanging in a selected radiology specialty section. This information can be obtained by studying the film alternator hanging habits in the specialty section. The second step is to handle the preferences of individual radiologists in the section. The common format of arranging films may be implemented by using the rules described previously or by observing the viewing practice of radiologists in the section. To implement the automatic image-display sequence to accommodate individual radiologists' preferences, a user interface needs to be built that allows the radiologists to specify their own image display sequences. Basically, the resultant file is a look-up table that corresponds an input patient case to an output IDST. The input patient case includes a set of image files, such as a series of CT scans or MR images or a single view of CR images. Each image file is uniquely identified by a set of information elements called image file features. The following are examples of information elements of MR images, CT scans, and CR, respectively:

MR images

1. Modality (MR imaging)
2. Name of examination protocol (brain/trauma, stroke, nasopharynx, orbits, and so forth)
3. Name of sequence (T1, T2, fast spin echo, time of fly, and so forth)
4. Scan plane name (axial, sagittal, coronal, and oblique)
5. Contrast agent injection (with or without)
6. Examination date and time

CT Scans

1. Modality (CT scan)
2. Name of examination protocol (brain/trauma, nasopharynx, sinus, parathyroid, and so forth)
3. Name of study (e.g., neck study and mediastinum study in parathyroid examination)
4. Scan plan name (axial and coronal)
5. Contrast agent injection (with or without)
6. Name of preset window and level (soft tissue, bone, and so forth)
7. Examination date and time

CR

1. Modality (CR)
2. Name of examination protocol (orbit, cervical spine, chest, and so forth)
3. Imaging views (PA, AP, and lateral)
4. Type of patient (adult, pediatric, neonatal, and so forth)
5. Examination date and time

The identity of the appropriate protocol is determined by the RIS examination type using a protocol-driven table that the departmental section or individual radiologist generates. These tables use the data fields listed previously to determine the most appropriate sequence and presentation for the examination to be reviewed.

Neural Network on Image-Display Sequence. Another method of generating the appropriate fields for the tables described previously is an intelligent algorithm to derive an output IDST from an input patient case. A supervised neural network (NN) technology may serve this purpose.[5, 9, 12] Theoretically, the supervised NN uses a set of data as the training set, in this case the existing look-up table, to predict some outcome that is the image-display sequence. The NN preserves the one-to-one correspondence capability of the look-up table. In addition, it provides the best predicted output based on what it has learned from the look-up table. Applying NN technology for determination of IDST is a new research area that requires further investigation. This approach might be used for window and level presets and for individual radiologist's preferences.

Image Presentation

Two main issues must be addressed in image presentation. The first has to do with image contrast and brightness optimization on the display monitors. The second is how to display a large amount of image data with limited number of monitors. Both topics are discussed here.

Display Monitor Characteristics

It was mentioned that the nonlinear characteristic curves of gray scale monitors is a factor that may affect the image display quality on CRT monitors. Also, it was discussed that the window and level setting and contrast enhancement function improve image quality. In the final stage of presenting images, all these factors must be taken into account. This implies that conducting a conversion from the monitor characteristic curve to a desired enhancement function (either a linear function or a nonlinear contrast enhancement function) is necessary.

Each individual examination, such as in the head, neck, chest, abdomen, pelvis, and upper and lower extremities requires specific contrast enhancement function related to the monitor. For this reason, these functions should be predefined so that whenever a particular image examination type is displayed on a certain monitor, the corresponding monitor characteristic function is ready to be applied. The examination type can be extracted from the image file header or the organized local patient folder as described previously.

Image-Display Mode

In order to use a limited number of monitors to display a large number of images, various techniques, such as off-screen display, volume display, and montage display are used in the workstation design. The off-screen technique is based on the technology of image memory buffers and high-speed data throughput storage devices, as described previously. Image data are stored in these off-screen buffers and devices whereas other images are already loaded in the on-screen display buffer. As soon as users need the off-screen images, they can be transferred to the display buffer instantaneously. If the update speed matches that of the user's from one film to the other, the display workstation is equivalent to being equipped with virtual-display monitors. The volume-display technique specifically is used to present a cross-sectional image set in a volume object. The montage-display technique is based on the fact that within an image set only a few images are critical for making diagnosis. Thus, only those critical images are displayed. Four methods are described in the following sections: (1) tile format, (2) cine format, (3) three-dimensional format, and (4) montage format.

Tile Display Format. The tile image-display format is used to mimic the way a film-alternator presents images. In this format, each monitor represents one x-ray film. The monitor is logically divided into tiles. The location of each tile is where an image is displayed. The size of the tile varies from the entire screen to a small portion of the screen, depending on the number of tiles that divide the screen. In the case of one tile occupying the whole screen, it simulates the one-on-one film format of projection radiography (see Fig. 3). On the other hand, if there are 16 tiles on one screen, each tile is allocated one-sixteenth of the screen size. This arrangement imitates the 16-on-1 format of CT scan and MR image film recording (see Fig. 2).

There usually are not enough monitors to display images with the tile format. To overcome this limitation, image browsing commonly is implemented using a scrolling method, such as scrolling by page or by row. Here, image browsing is based on the off-screen image buffer and fast storage devices. Let us consider a case of displaying a CT scan image file with 32 images (512 x 512 pixels per image) on a workstation with one monitor (2048 x 2048 spatial resolution). The first half of the images is displayed with the 4 x 4 format while the rest are not displayed. In the page-scrolling mode, these first 16 images are scrolled off the screen and replaced by the next 16 image slices. The scrolling direction, of course, can be reversed. In the row-scrolling mode, the images are scrolled on and off the screen by row (i.e., four images at a time). Although we have used a CT scan examination on a 2K x 2K display in the previous example, keep in mind that the ideal monitors for MR imaging and CT scan are the 1K x 1K for the reasons stated previously.

Cine-Display Format. Cine display shows individual images typically magnified and sequentially presented in rapid succession under user control in a fashion analogous to a slow-motion movie. The third dimension can be either space (CT scan or MR image) or time (US). Cine display not only facilitates the radiologist thought process to translate a set of two-dimensional data into three dimensions but also provides a useful means for visualization of flow in contrast study. Cine display also can be used to view multiple image series simultaneously (multiple-cine mode) as opposed to viewing just one series alone (single-cine mode). The multiple cine format is particularly useful for comparing studies between prior and current, and between precontrast and postcontrast studies. These related sequences should be linked together with similar anatomic levels displayed at the same time. With a well-designed workstation, moving through these sets simultaneously should only require the movement of a mouse.

Technically, all cine modes are implemented as follows. The first image of the data set is displayed on a tile (either the original or magnified version) on initiation of the cine display. The rest of the images are stored in a data buffer, such as the CPU memory, frame memory, or high-speed data I/O disks. As the cine operation proceeds, the stored images are shown successively on the tile either forward or backward at any desired rate.

Three-Dimensional Display Format. There are two methods for implementing three-dimensional display in a workstation. One method, similar to the multiple cine-display mode, divides a display monitor logically into four quadrant windows. One of these four windows is used to present a three-dimensional volume object reconstructed from a two-dimensional cross-sectional image set. The other three windows are used to display three orthogonal images, such as the transaxial, sagittal, and coronal of the same volume object, respectively. Three graphic planes (i.e., the xy plane, yz plane, and zx plane) in the three-dimensional object windows represent the positions where images are sliced in the transaxial, sagittal, and coronal planes. Users may move one of the planes to view different cuts of images. For example, when the xy plane is moved along the z direction, the transaxial images are displayed similar to the cine-display format. This implementation can be expanded from one monitor to multiple monitors so that comparison studies are possible. This display method imitates cross-sectional scanning without a physical scanner system.

The second method is also based on a reconstructed volume object. The three-dimensional object can be partitioned into eight portions with the xy, yz, and zx planes. By removing one of the portions, the internal anatomic structures of the three-dimensional object can be seen. The scope of the removed portion can be controlled by maneuvering the xy, yz, and zx planes along z, x, and y directions, respectively, to reveal the internal structures of the three-dimensional object. Depending on the monitor and image spatial resolution, one or more three-dimensional objects can be displayed simultaneously on one monitor. Users maneuvering the three planes simulate the surgical technique to view internal structures of a volume object.

The three-dimensional display methods described require intensive user interface on the display workstation and demand a high computation power system (most likely a specially designed computer system). The three-dimensional presentation, however, provides a means to cope with the combined problem of limited display monitors and a large amount of image data.

Montage-Display Format. A montage represents a selected subset of individual images from a CT scan, MR image, US, or any other multiimage series. This is useful because only a few images from most series show the particular pathology or interesting features that the user wants to focus on. For an average case, such as MR imaging, comprising six sequences averaging 30 images per series, there are typically 180 images for a given study. A typical montage contains about 20 images. These represent the number of significant images from the radiologist's point of view that are necessary to show the case. Obviously, it is important for the radiologist to view all images for the initial interpretation. This montage is then used for recalling the study later on for comparison with a new study or to show to referring physicians. It is up to the user to select images of significance. The montage feature allows the user to select the images of interest from all sequences into one montage file for future reference. Subsequent reviews of the prior studies can be done simply by referring to the montage file containing the significant images, rather than displaying all sequences done in the examination. This montage set also can be printed on paper or film for the referring physician, the patient, or teaching conferences.

There is one major issue regarding the montage internal design that needs to be considered. This is whether to store the actual image pixel data in the montage file or simply to store indices of the image data. The tradeoff is between storage space versus immediate access to the images. Storing the image data in the montage has the advantage of being the most efficient way to retrieve and display the images, because the data lies in one contiguous space ready to be loaded into the display workstation. One disadvantage is that the image data is duplicated. The question is how much extra storage is required. Based on the previous discussion, each montage file may require about 10% extra storage per study. If the assumption of two montage files per study is made, a reasonable estimate of extra storage required for the database using this approach is 20%. Another disadvantage is that stored images in a contiguous file makes editing the montage file more difficult. Deleting and inserting chunks of image data requires extensive disk I/O operations.

Storing indices to image data has the advantage of easy editing and requires the least amount of additional storage space. One disadvantage is that the actual image data is contained in various image files. This is because each image file containing images in the montage has to be retrieved from the archive to the local storage of the workstation before the montage images can be displayed. This means a time delay may occur. In the worst case, 20 such retrieval processes may be needed for one montage file, meaning a delay of 10 to 20 minutes before the complete file can be displayed, assuming 30 to 60 seconds required per retrieval process. Of course, the user rarely should see this delay owing to the use of the prefetching from the Folder Manager.

Image Manipulation

The ultimate goal of handling image sets before images are displayed is to minimize the radiologist's interaction with the display workstation. No matter how carefully the workstation is designed to preprocess image sets, however, chances are that the processed images may not satisfy individual preferences of radiologists for all cases. Therefore, radiologists may need to do minimal manipulations or minor adjustments on images providing that the user interface operations are easy to use and the speed of manipulation is fast. The following manual image-manipulation functions are essential: (1) window and level, (2) zoom and pan, (3) rotation, and (4) enhancement. Description of these functions and their need in the automatic mode have been discussed. In the following, our discussion focuses on the user interface in the manual mode. In particular, we focus on (1) a common design for these image manipulation functions, and (2) the implementation of each individual function.

Common Design Issues

An easy method for choosing a target image to be manipulated can simplify the operation of image manipulation. Consider the situation that a multiple-image file is displayed on more than one monitor. If a user is required to maneuver a mouse to activate a monitor where a target image is displayed and then to initiate the target image before an image manipulation can be performed, this maneuvering is considered complicated because it requires three operations. A desirable design is a single operation by pointing the cursor on the targeted image.

Another issue is whether a manipulation applied on a single image affects all images of the image file immediately after the manipulation. Usually, for a multiple-image file it is preferable that the manipulation is on a single image first and then the effect of the manipulation instantaneously propagates to other images within the same file without the user's further interaction. On occasion, the manipulation of a single image is demanded. To cover these two options, an on and off toggle should be implemented.

From time to time, after many image manipulation operations, the result may be worse than the original appearance. In this situation, the user typically wants to restore the initial display parameters and settings. Therefore, a reset function is needed.

Window and Level

The function of the window and level can be implemented in two ways: (1) manually adjusted, and (2) preset. With the current technology, most gray-level monitors can only display 256 shades of gray (i.e., eight-bit). For images containing more than eight bits of information, the function of manually adjusting window and level is required to access the full image gray scale dynamically and to select the best image contrast for viewing. Although manually adjusting window and level provides flexibility, the operation is time consuming. To compensate for this, presetting window and level allows an instant optimal display.

The presets for window and level and sequence are chosen based on the protocols established for each examination type. Examples in CT scan are bone, lung, soft tissues, head, chest, and abdomen; and in MR imaging are T1, T2, axial, sagittal, coronal, and so forth. For the unusual cases in which the automatic selection by protocol does not work properly, the desired settings can be assembled within a menu or they can be listed as a set of icons or buttons.

Zoom and Pan

With this function, the user can magnify (zoom) and pan the image on the screen. The field of view, however, decreases in proportion to the square of the magnification factor. Magnification commonly is performed via pixel replication or interpolation. In the former, one pixel value repeats itself several times in both the horizontal and vertical directions. In the latter, the pixel value is replaced by interpolation of its neighbors. For example, to magnify the image by two by replication is to replicate the image 2 × 2 times. The zoom and pan function is an interactive command manipulated via a trackball, a dialbox, or a mouse. Owing to the decreased field of view after the zoom, the ROI may not be on the screen. By using the pan operation, the user can move the image back to the center of the screen. The default presentation of images on the monitors always should attempt to match the inherent spatial resolution of the images to the resolution of the monitors. For those instances when the full image data is presented on the monitor in a compressed view, the zoom function should allow presentation at full resolution.

Rotation

The image rotation function contains eight orientations, including (1) 0 degrees, (2) 90 degrees, (3) 180 degrees, (4) 270 degrees, (5) x-axis flip, (6) y-axis flip, (7) 90 degrees plus y-axis flip, and (8) 270 degrees plus y-axis flip. Other degree rotations are CPU intensive and take longer to complete one rotation, which is not desirable in an image-display workstation. These eight orientations easily can be implemented by using the method of the pop-up menu or with icons.

Image Enhancement

Another image manipulation function applies different enhancement functions. These enhancement functions are particularly useful for CR images, as described previously. The shape of each enhancement curve explicitly shows the characteristics of the enhancement. For this reason, the implementation of this process should focus on easy manipulation of the shape of enhancement curves.

WORKSTATIONS FOR FUTURE NEEDS

A patient examination can involve several imaging modalities. From the radiologist's point of view, gathering as much information as possible for making an accurate diagnosis is a natural tendency. This means that a multipurpose workstation may be necessary in the future. The workstation is not only required to display large amounts of image sets, but also demanded to present combined image information from different modalities. For example, visualization of registered anatomic and functional images, such as positron emission tomography and MR imaging, is one of the means to facilitate radiologists' viewing practice. These images, in addition to Doppler US and general NM images, require color image-display monitors. In addition, radiologists require high-resolution monitors to detect subtle but important information, such as microcalcification in mammography and hairline fractures in bone radiography. This suggests that a multipurpose workstation with hybrid monitor configuration (both high-resolution and color monitors) or high-resolution color monitors may be needed in the future.

One complaint about digital workstations from radiologists is the cumbersome user interface. The main reason is that users have to rely on their hands to operate the workstation, which might divert their attention from the images. This suggests that voice control of the workstation may be a partial solution for future workstation design. But the technology today can provide a very efficient and useful workstation as long as the Folder Manager concepts are implemented in the software.

SUMMARY

The importance of this article is fourfold. First, the introduction of workstation technology and the types of image workstations provides readers with a better understanding of the state-of-the-art and availability of digital image-display workstations in the marketplace. Second, this article identifies primary processes related to image viewing in radiology daily operations. This is crucial because it illustrates the important concepts of the Folder Manager with image preprocessing, patient folder organization, and automatic image display sequencing. With these features incorporated in the workstation design, the number of steps required for a radiologist to interact with a workstation is minimized. Third, the discussions on how to present and manipulate images on the workstations suggest methods concerning the issue of displaying large volumes of image sets on a limited number of monitor screens. Lastly, examples of automatic image sequencing, high-resolution color monitors, and voice-based user interface illustrate current research topics in the future of digital workstation design.

References

1. Arenson RL, Chakraborty DP, Seshadri SB, Kundel HL: The digital imaging workstation. Radiology 176:303–315, 1990
2. Castleman KR: Digital Image Processing. Englewood Cliffs, NJ, Prentice-Hall, 1979
3. Curry TS III, Dowdey JE, Murry RC Jr: Christensen's Physics of Diagnostic Radiology, ed 4. Philadelphia, Lea & Febiger, 1990
4. Feingold E, Seshadri SB, Arenson RL: Folder management on a multimodality PACS display station. SPIE Proceedings 1446:211–216, 1993
5. Freeman JA, Skapura DM: Neural Networks Algorithms, Applications, and Programming Techniques. New York, Addison-Wesley, 1992
6. Gillenson ML: The duality of database structures and design techniques. Communication of the ACM 30:1056–1065, 1987
7. Gonzales RC, Woods RE: Digital Image Processing. New York, Addison-Wesley, 1993
8. Kasaday LR: Human factor considerations in PACS design. SPIE Proceedings 626:581–592, 1986
9. Lippmann RP: An Introduction to computing with neural nets. IEEE ASSP Magazine April: 4–22, 1987
10. Lo SC, Krasner BH, Mun SK: Noise impact on error-free image compression. IEEE Trans on Medical Imaging 9:202–206, 1990
11. Lou SL, Huang HK, Taira RK, et al: 2K radiological image display station. SPIE Proceedings 1899:95–102, 1993
12. McClelland J, Rumelhart D: Parallel Distributed Processing, vol 1 and 2. Cambridge, MA, MIT Press, 1986
13. Merritt CRB: Computed radiography: A new approach to plain film imaging. Diagnostic Imaging January: 58–65, 1985
14. Moskowitz MJ, Huang HK, Wang J, et al: A high resolution display system for mammograms. SPIE Proceedings 2431:447–454, 1993
15. Pietka E, Huang HK: Orientation correction for chest images. J Digit Imaging 5:185–189, 1992
16. Ramaswamy MR, Wong AW, Lee JK, et al: Accessing picture archiving and communication system text and image information through personal computers. AJR Am J Roentgenol 163:1239–1243, 1994
17. Rogers DC, Johnston RE, Brenton B, et al: Predicting PACS console requirements from radiologists' reading habits. SPIE Proceedings 536:88–96, 1985
18. Stewart BK, Lo SC, Huang HK: Gray level dynamic range in magnetic resonance imaging. SPIE Proceedings 626:189–195, 1986

Address reprint requests to
S.L. Lou, PhD
Laboratory for Radiological Informatics
Department of Radiology, UCSF
Box 0628
505 Parnassus Avenue
San Francisco, CA 94143–0628

Pergamon

Computerized Medical Imaging and Graphics, Vol. 20, No. 2, pp. 59–68, 1996

Printed in Great Britain
0895–6111/96 $15.00 + .00

PII: S0895–6111(96)00032–8

TELERADIOLOGY TECHNOLOGIES AND SOME SERVICE MODELS

H. K. Huang
Laboratory for Radiological Informatics, Department of Radiology, University of California, San Francisco, 530 Parnassus Ave., San Francisco, CA 94143-0628, USA

(*Received* 29 *January* 1996; *accepted* 25 *March* 1996)

Abstract—Teleradiology has become increasingly important in the managed care radiology practice environment. In order to fully appreciate the teleradiology operation, we have to understand the current technology available, some service models, and trade-off factors. This paper is organized in three parts. The first part is a review component of a teleradiology operation as well as state-of-the-art technologies. In the second part, we generalize several service models based on our past experience to illustrate the trend in teleradiology applications. The last part on trade-off factors is derived from field data. Four major factors (image capture, workstation, image compression and communication technology) balance a teleradiology operation in terms of cost, image quality, and turnaround time. The major issues in teleradiology yet to be resolved are patient confidentiality and image authenticity. Copyright © 1996 Elsevier Science Ltd.

Key Words: Teleradiology, Networking, Wide area network

BACKGROUND

During the past several years, our country's health care delivery system has been changing from fee-for-service to managed, capitated care. As a result, we see the trend of primary care physicians joining health maintenance organizations (HMOs). HMOs purchase smaller hospitals and form hospital groups under the umbrella of HMOs. Also, academic institutions form consortia to compete with other local hospitals and HMOs. This phenomenon creates an opportunity in radiology practice as radiology expert centers are formed. In the expert center model, radiological images and related data are transmitted between examination sites and diagnostic centers through telecommunications. This type of radiology practice is loosely called teleradiology.

Figure 1 shows an expert center model in teleradiology. In this model, the three modes of operation are shown: telediagnosis—diagnosis is made within 4–24 h after images are produced; teleconsultation—within half an hour; and telemanagement—in real time. Telediagnosis means that an examination is done at a remote site, images and related information are transmitted to an expert center for radiologic diagnosis. This service does not require immediate diagnosis and can wait between 4 and 24 h. Teleconsultation is different in the sense that the patient may be still waiting in the examination site or the primary care physician's office, a second opinion or an immediate diagnosis is required preferably within half an hour. The third service is for telemanagement. In this case, the patient may be still on the examination table and an immediate diagnosis is required for the primary care physician to manage the patient *in situ*. In this expert model, rural clinics, community hospitals and HMOs rely on radiologists at the center for consultation. It is clear from Fig. 1 that in teleradiology, the turnaround time requirement is different depending on the modes of service which in turn determines the technology required and cost involved.

Why do we need teleradiology?

The managed care trend in health care delivery system expedites the formation of teleradiology expert centers. However, even without the health care reform, teleradiology is still an extremely important component in radiology practice for the following reasons. First, teleradiology secures images for radiologists to read so that no images will be accidentally lost in the form of transportation. Second, teleradiology reduces the reading cycle time from when the image is formed to when the report is completed. Third, since radiology subdivides into many subspecialties, even a general radiologist requires an expert's second opinion on occasion. The availability of teleradiology will facilitate seeking the second opinion. Fourth, teleradiology increases radiologists' income since no images would be accidentally lost and subsequently not read. The health care reform adds two more reasons. (1) It saves the health care costs since an expert center can serve multiple sites which reduces the number of radiologists required. (2) It improves the efficiency

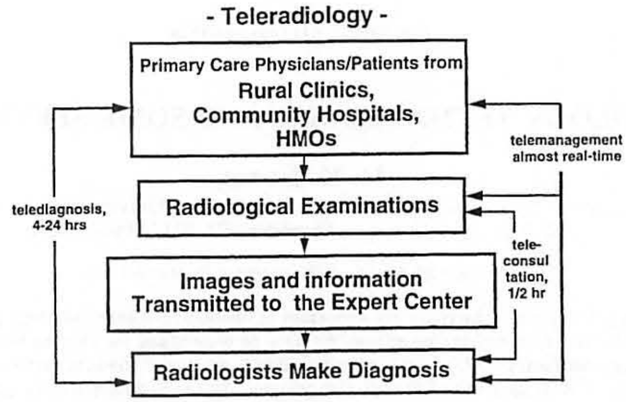

Fig. 1. The expert center model in teleradiology.

and effectiveness of health care because the turn-around time is faster and there is no loss of images.

What is teleradiology?

Generally speaking, teleradiology means that an image is sent from the examination site to a remote site where an expert radiologist will make the diagnosis. The report is sent to the examination site where a primary physician can then prescribe the patient's treatment immediately. Teleradiology can be very simple or extremely complicated. In the simple case, an image is sent from a CT scanner, for example, in the evening to the radiologist's home using low quality teleradiology equipment and slow speed communication technology for a second opinion. During off hours, evenings and weekends, there may not be a radiologist at the examination site to cover the service. A resident normally is in charge and requires consultation occasionally from the radiologist at home during these off hours. This type of teleradiology does not require highly sophisticated equipment. A conventional telephone and simple desktop personal computer with modem connection and display software is sufficient to perform this teleradiology operation. This type of application originated in early 1970 (1).

The second type of teleradiology is more complicated with four different models starting from simple to complicated in ascending order as shown in Table 1. The complications occur when historical images are required for comparison with the current examination, and when information from the radiology information system (RIS) is required to help the expert make a diagnosis. In addition, complications arise when the examination and dictation are required to be archived and appended to the patient image data file. Teleradiology is relatively simple to operate when no archiving is required. However, when archiving and retrieval of previous information of the same patient is required, the operation becomes extremely complicated.

Teleradiology and picture archiving and communication systems (PACS)

When the teleradiology service requires patient's historical images as well as related information, teleradiology and PACS become very similar. For the definition of PACS, refer to (2). Table 2 shows the differences between teleradiology and PACS. The major difference between them is in the methods of image capture. Most current teleradiology still uses a digitizer as the primary method of converting a film image to digital format, although the trend is moving towards DICOM (see next section). In PACS, direct digital image capture using the DICOM (3) is mostly used. In networking, teleradiology uses slower speed

Table 1. Four models in teleradiology

	Historical images/RIS	Archive
Most simplistic	No	No
Simplistic	Yes	No
Complicated	No	Yes
Most complicated	Yes	Yes

Table 2. Differences between teleradiology and PACS

	Telerad	PACS
Image capture	Digitizer	DICOM
Display technology	Same	Same
Networking	WAN	LAN
Storage	Short	Long
Compression	Yes	May be

Table 3. Size of some common medical images

	One image (bits)	No. of images/exam	One examination
Nuclear Medicine (NM)	128 x 128 x 12	30–60	1–2 MB
Magnetic Resonance Imaging (MRI)	256 x 256 x 12	60	8 MB
Ultrasound (US)*	512 x 512 x 8(24)	20–230	5–60 MB
Digital Subt. Angiography (DSA)	512 x 512 x 8	15–40	4–10 MB
Digitized Electronic Microscopy	512 x 512 x 8	1	0.26 MB
Digitized Color Microscopy	512 x 512 x 24	1	0.79 MB
Computed Tomography (CT)	512 x 512 x 12	40	20 MB
Computed Radiograph (CR)	2048 x 2048 x 12	2	16 MB
Digitized X-rays	2048 x 2048 x 12	2	16 MB
Digitized Mammography	4096 x 4096 x 12	4	128 MB

*Doppler US with 24 bit color images.

wide area networks (WAN) comparing with the higher speed local area network (LAN) used in PACS. In teleradiology, the image storage is mostly short-term, whereas in PACS it is long-term. Teleradiology relies heavily on image compression (4) whereas PACS may or may not.

The second column in Table 3 gives sizes of some common medical images. In clinical applications, one single image is not sufficient for making diagnosis. In general, a typical examination generates between 10 and 20 Mbytes. The fourth column in Table 3 shows an average size of one typical examination in each of these image modalities. The highest extreme is in digital mammography which requires 128 Mbytes. To transmit 128 Mbytes of information through WAN requires a very high bandwidth communication technology. One research topic in telemammography is how to transmit this large file size through WAN with acceptable speed and cost.

TELERADIOLOGY COMPONENTS

Table 4 lists the teleradiology components and Fig. 2 shows a generic schematic of their connections. Among these components, reporting and billing are common knowledge and will not be discussed here. Devices which generate images in teleradiology applications include computed tomography (CT), magnetic resonance imaging (MR), computed radiography (CR), ultrasound imaging (US), nuclear medicine (NM), digital subtraction angiography-digital fluorography (DSA, DF), and film digitizer. Images from these acquisition devices are first generated from the examination site and then sent through the communication network to the expert center if they are already in digital format. Or, if these images are stored on films, then they need to be digitized by a film scanner at the examination site.

Table 4. Teleradiology components

- Imaging acquisition device
- Image capture
- Data reformatting
- Transmission
- Storage
- Display
- Reporting
- Billing

Image capture

In image capture, if the original image data are on film, then either a video frame grabber or a laser film digitizer is used to convert them to digital format. A video frame grabber produces lower quality digital images but is faster and cheaper. On the other hand, laser film digitizers produce extremely high quality digital data, but take longer and cost more compared to the video frame grabber (2). During the past several years, computed radiography (CR) has been used extensively in teleradiology. Conventional projection radiography can be obtained with CR which produces a direct digital image as the output (5).

Data reformatting

After images are captured, it is advantageous to convert these images and related data to some

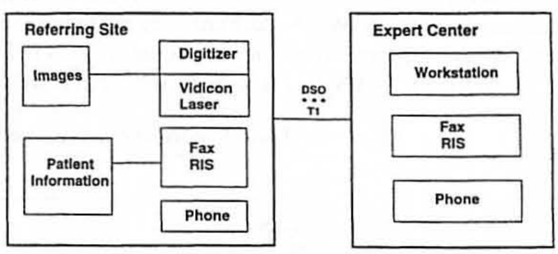

Fig. 2. A generic schematic of teleradiology components and their connections.

industry standards because multi vendors' equipment can be used in the teleradiology chain. The two common standards used in the imaging industry are the Digital Imaging and Communication in Medicine (DICOM) for images and Health Level 7 (HL7) for textual data (6). The DICOM standard includes both the image format as well as the communication protocols, whereas HL7 is only for textual data. The communication for textual information generally uses TCP/IP communication protocols. The description of these two standards is given elsewhere (7).

Storage

At the receiving end of the teleradiology chain, a local storage device is needed for image display. The capacity of this device can range from several hundred Mbytes to 5–10 Gbytes. For teleradiology applications requiring historical images and radiology information retrieval, and current examination and diagnosis archival, a long-term archive, such as an optical disk library, is needed at the expert center. The architecture of the long term storage device is very similar to that used in PACS (8).

Display workstation

For an inexpensive teleradiology system, a low cost 512-line single monitor can be used for displaying images. However, sophisticated multi-monitor display workstations are needed for primary diagnosis. The state-of-the-art technology in image workstations will be described in the next section.

Communication networking

An important component in teleradiology is the communication network used for transmission of images and related data from the acquisition site to the expert center for diagnosis. Since most teleradiology applications are not within the same hospital complex but through inter-health care facilities in metropolitan areas or at longer distances, communication technology involved requires wide area network (WAN). WAN can be wireless or with cables. In wireless WAN, technologies available are microwave transmission and communication satellites. Wireless WAN has not been used extensively due to the cost. Table 5 shows the technology available in WAN using cables. It starts from the low communication rate DS-0 with 56 kbits/s, to a very high communication data rate DS-3 with 45 Mbits/s. All these WAN technologies are available through either a long distance or local telephone carrier. The cost of using WAN is a function of transmission speed. Thus, for a DS-0 line which has low transmission rate, the cost is fairly low compared to DS-3 which is faster but more expensive. Most of the private lines, for example T-1 and T-3, are point-to-point and the cost also depends on the distance between connections. Tables 6 and 7 give an example showing the relative cost between DS-0 and T-1 lines between UCSF and Mt Zion Hospital (MZH), two sites in the San Francisco Bay Area about 2 miles apart.

Comparing Tables 6 and 7 reveals that the initial investment for the DS-0 is $500. The monthly cost is $30 fixed fee plus per local call charge. On the other hand, for the T-1 service the up front investment is $14,500, and the T-1 monthly cost is $554. The user does not have to pay an extra charge per call to use the line. The up front investment for the T-1 is much higher than the DS-0, and for longer distances, its monthly charge is expensive. For example, the charge between San Francisco and Washington, D.C. for a T-1 line could be as high a $10,000 per month. However, the speed of communication using the T-1 is about 30 times faster than the DS-0. Using T-1 line for teleradiology is very popular. Some larger companies lease several T-1 lines from telephone carriers and sub-lease portions of them to smaller companies for teleradiology applications.

User friendliness

One component not listed in Table 4 is the user friendliness in a teleradiology system. User friendliness includes both the connections of the teleradiology equipment at the examination site and the expert center, and the simplicity of using the display workstation at the expert center.

User friendliness means that the complete teleradiology operation should be as automatic as possible requiring only minimal user intervention.

Table 5. Wire technologies available in Wide Area Network (WAN)

Technology	Speed
DS-0 (Digital Service)	56 kbits/s
DS-1 dial up	56 kbits/s to 24 × 56 = 1.344 Mbits/s
DS-1 Private Line (T-1)	1.544 Mbits/s
ISDN Integrated Service Digital Network	56 kbits/s–1.544 Mbits/s
DS-3 Private Line (T-3)	28 DS-1 = 45 Mbits/s

Table 6. WAN cost using DS0 (56 kbits/s) between UCSF-MZH

Modems (2)	$400
Installation (2)	*$100*
Up front investment	$500
DOS Monthly fee	$30+ per call
(30 times slower than the T-1)	

Table 7. WAN cost using T-1 between UCSF-MZH

Modems (2)	$12,000
Ethernet converter (2)	
T-1 Installation	*$2,500*
Up front investment	$14,500
T-1 monthly charge:	$554

For the image workstation to be user friendly requires three criteria to be met: (1) image and related data pre-fetch; (2) automatic image sequencing at the monitors; and (3) automatic look-up table, image rotation and unwanted background removal from the image. Image and related data pre-fetch means that for the same patient examination, all historical images and related data required for comparison by the radiologist should be pre-fetched from the patient folder prior to image transmission and display. When the radiologist at the expert center starts to review the case, these pre-fetched images and related data are available immediately. Automatic image sequencing at the display workstation means that all these images and related data are sequentially arranged so that at the touch of the mouse, properly arranged images and information are shown on the monitors. Pre-arranged data minimizes the times required for the searching and the organizing of them by the radiologist at the expert center. This translates to an effective and efficient teleradiology operation. The third factor, automatic look-up table, rotation and background removal, is necessary because images acquired at the distant site might not have the proper look-up table for optimal visual display, images might not be generated in the proper orientation, and with some unwanted white background in the image due to radiographic collimation. All these parameters will have an effect on the proper diagnosis of the image.

STATE-OF-THE-ART TECHNOLOGY

In the last section we discussed the components in a teleradiology operation. In this section, we present the state-of-the-art technology in teleradiology, especially in communication technology, image compression, and image workstations.

Wide area network-asynchronous transfer mode (ATM) technology

ATM technology is an emerging communication technology both for WAN and LAN. The current commercially available ATM technology is the OC3 with 155 mbits/s. Using ATM for data communication between two nodes requires one adapter board at the computer of each node, an ATM switch connecting both adapters at each node with fiber optic cables (9).

In LAN, ATM is being used by many sites for image communication, whereas in WAN, ATM still has the obstacle to pay for expensive long distance carriers. Table 8 shows the comparison between using T-1 and ATM for communication of images between Mt Zion Hospital and UCSF. Results demonstrate that ATM is almost two orders of magnitude faster than T-1. The cost for using ATM technology is still restricted, not because of the technology, but because of the charges by long distance carriers. One way to make the ATM an affordable WAN communication method is to have the carrier to lower the fiber optic cable utility cost. Figure 3 shows a testbed prototype transmitting CR images from UCSF to a workstation at the San Francisco VA Medical Center. A 10 Mbyte CR image after generated by the CR can be transmitted to the VA Medical Center about 10 miles away in 1.5 s.

Table 8. Time required to send a 10 MB X-ray, 40 MB CT study from MZH to UCSF using T1 and ATM (OC3) (no compression)

	One X-ray exam 2 K × 2.5 K × 2 byte (10 MB)		One CT study (40 MB)	
	One image	Two images	One study	One current + One historical
T1 (1.5 mbits/s) realization 100 KB/s	100 sec (1.6 min)	200 s (3.9 min)	400 s (6.7 min)	800 s (13.4 min)
ATM (155 mbits/s) realization 60 mbits/s	1.3 s	2.7 s	5.3 s	10.7 s

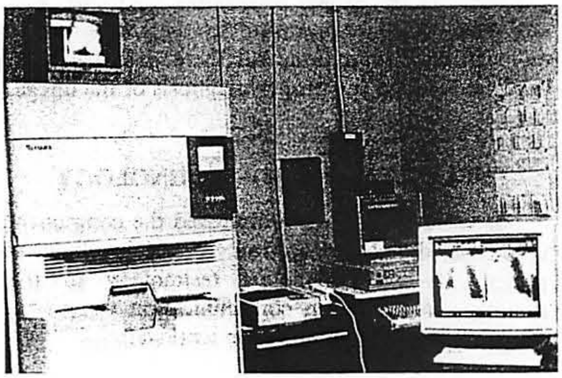

(A)

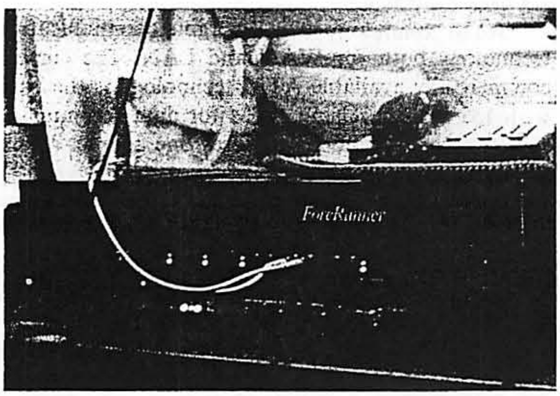

(B)

(C)

Fig. 3. A. FCR 9000; B. ATM Switch; C. ISG image workstation. Radiographs generated by a CR system are transmitted through the ATM at UCSF to the ATM main switch at Pacific Bell in Oakland, then to the ATM switch at the SFVA Medical Center where they are displayed at the 1600 line workstation. The completed process takes less than 2 s after the images are generated (courtesy of Dr Gretchen Gooding).

Display workstations

Table 9 shows the specifications of 2000 line and 1600 line workstations used for teleradiology primary readings. These state-of-the-art technology diagnostic workstation use two monitors with over 2 gigabytes local storage, and 1–2 s for images and reports display. A 2000 line workstation costs between $50,000 and $60,000, whereas a 1600 line costs between $30,000 to $40,000. User friendly software is required for easy and convenient use by the radiologist at the workstation.

Image compression

Teleradiology requires image compression because of the slow speed and high cost of using WAN. For lossless image compression, current technology can achieve between 3:1 to 2:1 compression ratios, whereas in lossy image compression using cosine transform based MPEG and JPEG hardware and software, 20:1 to 10:1 compression ratios can be obtained with acceptable image quality. The latest advance in image compression technology uses the wavelet transform. Wavelet transform has the advantage over cosine transform for higher compression ratio and better image quality after the decompression (10). With the advance in communication technology, image workstation design, and image compression, teleradiology will move closer as an integrated diagnostic tool in daily radiology practice.

TELERADIOLOGY EXAMPLES AND MODELS

Teleradiology services started to proliferate about 2 years ago. One of the earliest health care facilities using teleradiology was the Mayo Clinic. The Mayo Clinic has three sites in Rochester, MN; Jacksonville, FL; and Scottsdale, AZ. In order to provide a service to all three sites, a satellite communication method was used. The Mayo Clinic chose IBM at Rochester as the technical partner for the teleradiology service. Other example is the service to Saudi Arabia provided by the Massachusetts General Hospital (MGH). In these cases, inexpensive regular voice lines, 9.6 kbits/s are used. Table 10 summarizes the MGH operation (11). In the

Table 9. Specifications of 2000 and 1600 line workstations for teleradiology

- Two monitors
- 1–2 week local storage for current + previous exam
- 1–2 second display of images and reports from local storage
- DICOM conformance
- Simple image processing functions

Table 10. MGH operation-two regular grade voice lines (9.6 kbps)

- Customer: Saudi Arabia
- 24–48 hr turnaround time
- 4–6 images/case
- Compression: Radiograph 20:1, CT 10:1
- Transmission: 3–4 mins/image ($7.0)
- Workstation: 2K monitors

following, based on our past experience, we generalize two teleradiology models serving as examples to describe the structure of the teleradiology, how the service is set up, as well as the operational procedure.

Model 1—university consortium. Telequest is a university consortium formed by the departments of radiology at the following universities: Bowman Graduate School of Medicine, Wake Forest University; The Brigham Radiology Foundation in Boston; Emery University Hospital in Atlanta; University of California, San Francisco; and Pennsylvania Medical Center in Philadelphia. A for-profit organization called Telequest was formed in order to provide a nationwide sub-specialty radiology service.

In this model, Telequest provides a turn-key operation for the customer (e.g. an imaging center, a HMO, etc.) and transmits images to the consultation site at one of these five radiology departments. At the customer site, the company provides a turn-key operation, assists the site to interface with the radiology information system, the image acquisition devices, and provides the customer site around-the-clock service coverage. The communication connections is from a third party vendor allowing the customers to select a desired transmission speed. The customer can select consultants from any consultation sites to read the cases. At the consultation site, high resolution workstations described in the previous section are used for the reading, and a rapid turnaround report is guaranteed by the contract. Figures 4 and 5 show, respectively, the teleradiology operation and data flow in a university radiology department consortium model.

Telequest handles all the marketing, service, communication connections, billing and management. As an example, a customer site is an imaging center located at Ohio with two image acquisition systems, a General Electric Signa 5X MR scanner and a Helical CT scanner. The operational hours are from Monday to Friday 7:30am to 10:30pm, Saturday and Sunday is from 8:00am to 2:00pm. The image readings are distributed to the various consultation sites at these five universities. The network used is a fractional T-1 provided by IBM.

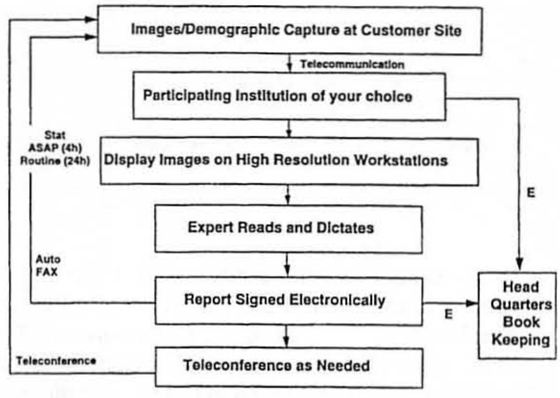

Fig. 4. Teleradiology operation in a university radiology department consortium model.

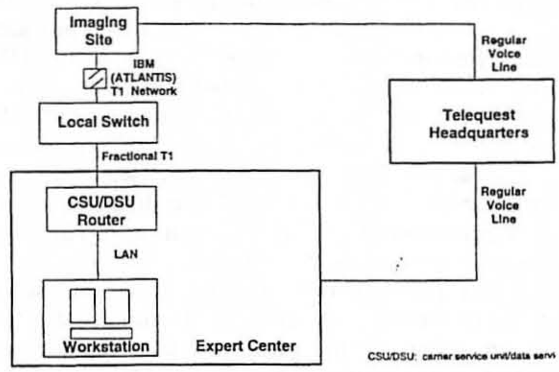

Fig. 5. Data flow in a university radiology department consortium model.

Image compression used is the 2–3:1 lossless compression method. This teleradiology service model uses the strength of these prestigious radiology departments to attract business from imaging centers and HMOs throughout the nation. The result is that images are collected from rural sites, community hospitals, HMOs to the expert centers, and consultations are distributed geographically to these five universities' radiology departments.

Teleradiology service for second opinion. In this model, a health care insurance company in a foreign country initiates an add-on subscription for its policy holder. For an extra amount of money per year on top of the existing health insurance, the subscriber of the add-on policy has the right to request a second opinion on his/her existing medical diagnosis from a premier medical center in the US at the subscriber's own expense. Table 11 shows the operational procedure of this second opinion teleradiology service.

Table 11. Operational procedure of a second opinion teleradiology consultation service

- Subscriber requests a medical second opinion on the radiologic exam to the health insurance company
- The insurance company arranges images to be digitized and transmitted from the foreign country to the US consultation site at the subscriber's own expense
- Images are displayed on high resolution workstation and read by experts at the consultation site
- Second opinion is provided to the subscriber via phone, fax, or teleconference with the subscriber's referring physician at the foreign country
- Subscriber can schedule follow-up exams at the consultation site at his/her expense

An example of this model is an Israel health insurance company, and the premier medical center is The University of California, San Francisco. The current enrolment of this add-on policy is about 800,000 in a country of 5 million people. The physical communication connection between the customer site and the expert site is through international ISDN lines (see Table 5) shown in Fig. 6. The key in this connection is a black box (Ascend) which provides intelligent software to interpret the number of ISDN lines at the sending site, the number of ISDN lines at the receiving site, and the international ISDN standard conversion. Depending on the speed required, multiple ISDN lines can be used to increase the rate of transmission. At the sending site, a film digitizer is used, and at the expert site a 1600 line two monitor workstation is used for interpretations.

The previous two models demonstrate some trend in teleradiology service. In the first model, the expert centers expand their capitations in radiology examinations through a consortium. These radiology departments increase their workload and income which benefits the radiologists as well as the departments. In the second model, second opinion consultation provides the developing country easy access to premier medical centers in the US for consultation. From the customer point of view, a minimal add-on cost on top of an existing health insurance policy is a small amount of pay for peace of mind by allowing them to receive a second opinion consultation if they so desire.

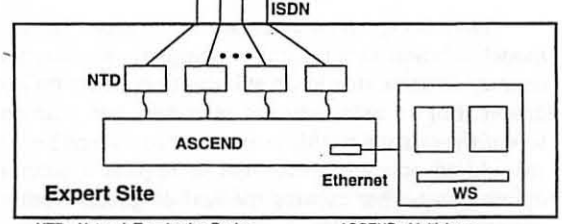

Fig. 6. The physical communication connection between the customer (image capture site) and the expert site of an internatiional second opinion teleradiology service.

SOME IMPORTANT ISSUES IN TELERADIOLOGY

There are two important issues in teleradiology: the trade-off between quality, turnaround time, and cost; and second, data security including patient confidentiality and image authenticity. Table 12 shows the teleradiology trade-off parameters between image quality, turnaround time, and cost. These three parameters are effected by the method of image capture, type of workstations used, the amount of image compressed, as well as communication technology. The cost in teleradiology is determined by all four factors.

In terms of data security, we have to consider patient confidentiality as well as image authenticity. Since teleradiology uses a public communication method to transmit images which has no security, the question arises as to what type of protection one should provide to assure the patient's confidentiality. The second issue is the image authenticity. After the image is created in digital form, can we assure that the image created has not been altered either intentionally or unintentionally? (12) To guarantee image and data authenticity, methods such as data encryption and digital signatures can be used which have been in the domain of defense research for many years. Some of these techniques may be used to

Table 12. Teleradiology trade-off parameters

	Image capture	Workstat	Compress	Comm Tech
Quality	X	X	X	
Turnarnd tm	X		X	X
Cost	X	X	X	X

protect the data authenticity as well as patient confidentiality (13). If high security is imposed on image data, it will increase the cost in decryption and decrease the easy access due to many layers of passwords. The trade-off between cost and performance, confidentiality and reliability will become a major future socio-economic issue in teleradiology. Figure 7 shows a CT image which has been altered digitally by inserting a tumor on the lung (see arrows). Since alterating a digital image is not difficult to do (14), developing methods to protect integrity of image data is essential in teleradiology applications.

DISCUSSION

Teleradiology has been used since the 1970s, however, technology was not ready for massive application until 2 years ago. It has become an important topic involving socio-economic issues because the role telemedicine will play in health care reform. The trend in teleradiology is to balance the cost with the image quality and turnaround time for the service. The four major factors involved are: the method of image capture, the type of workstation used, the amount of image compression, as well as the communication technology. In communication technology, DS lines and ISDN are still the most popular means in low-end teleradiology service. T-1 is expensive when the distance is far apart, but many manufacturers are starting to use it on a shared basis. ATM is an emerging technology which promises to revolutionize the method of image communication. We see this happening in LAN already. In order for teleradiology to fully utilize this new technology, users must exert pressure on carriers to lower the price for using the wide area fiber optic cables. The two models presented demonstrate the trend in teleradiology application as well as type of services using teleradiology. We see the trend that teleradiology will become a necessity in medical practices in the 21st century and it will be an integral part of telemedicine as the method of practicing medicine in the future.

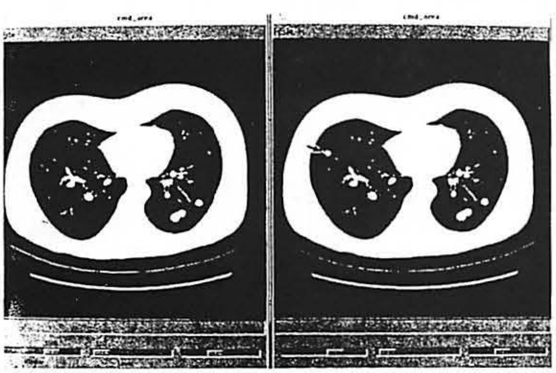

Fig. 7. Left: a CT scan of the chest; right: the same scan with a digitally inserted tumor (see arrow). The insertion process requires minimal image processing (courtesy of Dr X. Zhu).

Regarding the use of internet and World Wide Web (WWW) for teleradiology service; at the moment, both internet and WWW have problems with transmission speed and no control of data confidentiality, security, as well as authenticity. Therefore, the use of internet and WWW for teleradiology application does not look promising at the moment.

SUMMARY

The keys to a successful teleradiology operation require the system to be reliable with minimal user intervention, timely delivery of images with information, rapid display, easy to use, as well as affordable to the users. In this paper we present a loose definition of teleradiology, describe its components, and some state-of-the-art technologies which will effect future teleradiology applications. Two models of teleradiology service are given; one is based on a university consortium which forms the expert center concept and the second is on second opinion teleradiology consultation service. Two important issues of teleradiology are: (i) the trade-off between quality, turnaround time, and the cost of service; and (ii) the patient confidentiality and image authenticity in a teleradiology service.

Acknowledgements—This work was partially supported by NLM Contract No. N01-LM-4-3508.

REFERENCES

1. Steckel, R.J. Daily X-ray rounds in a large teaching hospital using high-resolution closed-circuit television. Radiology 105:319–321; 1972.
2. Huang, H.K. PACS—Picture archiving and communication systems in biomedical imaging. New York: VCH; 1996.
3. ACR/NEMA Digital Imaging and Communication Standard Committee. Digital Imaging and Communications ACR-NEMA. 300-1988. Washington, D.C.: National Electrical Manufacturers Association; 1989.
4. Wong, S.; Zaremba, L.; Gooden, D.; Huang, H.K. Radiologic image compression—a review. Proc. IEEE Trans. 83:194–219; 1995.
5. Sonoda, M.; Takano, M.; Miyahara, J.; Kato, H. Computed radiography utilizing scanning laser stimulated luminescence. Radiology XX:833–838; 1983.
6. Health Level Seven (HL7). An application protocol for electronic data exchange in health care environments version 2.1. Ann Arbor, Michigan: Health Level Seven; 1991.

7. Horii, S.C.; Bridgood Jr, W.D. Network and ACR-NEMA protocols. Syllabus: a special course in computers for clinical practice and education in radiology. Rad Soc. North Amer. XX:97–106; 1992.
8. A.W.K.; Huang, H.K.; Arenson, R.L.; Lee, J.K. Multimedia archive system for radiologic images. Radiograph. 14:1119–1126; 1994.
9. H.K.; Arenson, R.L.; Dillon, W.P.; Lou, A.S.L.; Bazzill, T.; Wong, A.W.K. Asynchronous Transfer Mode (ATM) technology for radiologic communication. Am. J. Roentgen. 164:1533–1536; 1995.
10. Wang, J. 3D Medical image compression by using 3D wavelet transformation. IEEE Trans. Med. Imaging 1996 (in press).
11. Henschke, C.L.; Moreau, J.F. Interactive telecommunication and internet use for radiology education. Radiology 197:42; 1995.
12. Mitchell, W. When is seeing believing?. Sci. American 270:68–73; 1994.
13. Wong, S.T.C.; Abundo, M.; Huang, H.K. Authenticity techniques for PACS images and records. SPIE 2435:68–79; 1995.
14. Mason, R.O. Ethics to information technology issues. Comm. ACM 38:55–57; 1995.

About the Author—H. K. HUANG, D.Sc., FRCR (Hon.) is Professor and Vice Chairman, Director of Radiological Informatics Laboratory, Department of Radiology, UCSF. He has over 25 years' experience in digital image processing research and he established the PACS research program and the medical imaging training program at UCLA. The UCLA PACS has been in clinical operation since 1992. He joined UCSF with a joint appointment in the UCSF/UC Berkeley Bioengineering Graduate Program in October 1992. He is now implementing a second generation PACS as well as doing research in medical multimedia at UCSF. Currently he is the PI of several grants from the CalREN on ATM networking, National Library of Medicine sponsored HPCC Program on WAN Neuro-Imaging. NIH on Image Compression, California State Breast Cancer Research Program in Real-time telemammography.

Reprinted from **JOURNAL OF THE AMERICAN MEDICAL INFORMATICS ASSOCIATION**

Published by Hanley & Belfus, Inc., Philadelphia, PA

Research Paper ■

A Cryptologic Based Trust Center for Medical Images

STEPHEN T. C. WONG, PHD

Abstract **Objective:** To investigate practical solutions that can integrate cryptographic techniques and picture archiving and communication systems (PACS) to improve the security of medical images.

Design: The PACS at the University of California San Francisco Medical Center consolidate images and associated data from various scanners into a centralized data archive and transmit them to remote display stations for review and consultation purposes. The purpose of this study is to investigate the model of a digital trust center that integrates cryptographic algorithms and protocols seamlessly into such a digital radiology environment to improve the security of medical images.

Measurements: The timing performance of encryption, decryption, and transmission of the cryptographic protocols over 81 volumetric PACS datasets has been measured. Lossless data compression is also applied before the encryption. The transmission performance is measured against three types of networks of different bandwidths: narrow-band Integrated Services Digital Network, Ethernet, and OC-3c Asynchronous Transfer Mode.

Results: The proposed digital trust center provides a cryptosystem solution to protect the confidentiality and to determine the authenticity of digital images in hospitals. The results of this study indicate that diagnostic images such as x-rays and magnetic resonance images could be routinely encrypted in PACS. However, applying encryption in teleradiology and PACS is a tradeoff between communications performance and security measures.

Conclusion: Many people are uncertain about how to integrate cryptographic algorithms coherently into existing operations of the clinical enterprise. This paper describes a centralized cryptosystem architecture to ensure image data authenticity in a digital radiology department. The system performance has been evaluated in a hospital-integrated PACS environment.

■ **JAMIA.** 1996;3:410–421.

Medical images form the cornerstone of patient records and often are at the heart of the patient's diagnosis, determination of therapy, and follow-up. They are used not only by radiologists, but also by other clinicians and specialists, such as medical oncologists, radiotherapists, surgeons, neurologists, cardiologists, dermatologists, pathologists, and primary physicians. The trend in medical imaging is increasingly toward a digital and multimedia orientation. The goals are to represent medical images in digital form supporting image transfer and archiving and to manipulate visual information for various clinical services, such as teleradiology and diagnostic workups. Another push is from the picture archiving and communication systems (PACS) community, which envisions an all-digital radiology environment in hospitals for acquisition, storage, communication, and display of large volumes of medical images.[1] The PACS technology provides a systems integration solution for these islands of automation and facilitates the extraction of the rich information contained in multimodality images. Several large-scale PACS have been successfully put into clinical operation and trials.[1] The new thrust of PACS development is to integrate complementary textual information of clinical systems into the central image archive.[2,3]

Affiliation of the author: Department of Radiology, School of Medicine, The University of California, San Francisco, CA.

Correspondence and reprints: Stephen T. C. Wong, PhD, Department of Radiology, UCSF, Box 0628, 505 Parnassus Avenue, San Francisco, CA 94143.
e-mail: stephenwong@radmac1.ucsf.edu

Received for publication: 5/8/96; accepted for publication: 7/1/96.

Along with this digital radiology world comes the problem of establishing trust in medical documents that exist only in the easily altered memory of a computer. Trust can be defined in terms of authenticity—i.e., detect unauthorized modification of image data —and confidentiality—i.e., prevent unauthorized disclosure of image data. One of the advantages of printed film or text is its authenticity—when we see ink on paper or images in print, we feel that these are immutable records, not subject to manipulation or tampering without leaving traces. Few of us, however, have this level of faith in the immutability of medical records committed to electronic media.

People who seek unauthorized access to online medical records do so for several reasons: unauthorized release, industrial espionage, sports hacking, computer theft, and vandalism, to name a few.[4] Examples of unauthorized release include failure to obtain informed consent in writing from the patient or failure to seek an approval from the responsible authority. Industrial espionage occurs, for instance, when a health insurance company seeks a business advantage by obtaining the confidential patient population demographics stored in a competitor's databases. Hacking is another form of unauthorized access by people who view such activities as a sport, and hackers usually leave the data and systems intact. In contrast, computer theft and vandalism are the most dangerous forms of unauthorized access. Individuals penetrating an online medical database seek to steal or alter information about patients and harm the medical system.

Many means have been proposed to improve the security of online medical information: limit physical access to the network, change user passwords frequently, create firewalls to isolate information from other networks, and enforce administrative procedures for data security. Cryptography is one of the strongest and most mathematically sound methods to ensure trust in computerized medical data. There are two major cryptographic techniques: key-based encryption and digital time stamping. These techniques complement one another. Key-based cryptography associates the content of an image with the originator by using one or two distinct keys and prevents unauthorized disclosure of the image.[5] Digital time stamping, on the other hand, generates a characteristic "digital fingerprint" for an image when it is first generated by using a mathematical hash function that permits detection of subsequent modifications. Digital time stamping is not a form of encryption. Research in the past two decades has concentrated on authenticating textual data. The growing use of digital medical images, however, poses new challenges due to their large size and different user requirements. This study investigates the appropriateness of various cryptographic algorithms for improving the security of medical images and derives new methods that incorporate these algorithms seamlessly into digital radiology operations, especially PACS and teleradiology.

Methods

Terminology

This section introduces the basic nomenclature. A message is called plaintext. The process of disguising a message so as to hide its content is called encryption. An encrypted message is called, ciphertext. The process of converting ciphertext back into plaintext is called decryption. Cryptography is the art and science of keeping a message sècure, and cryptoanalysis is the art and science of breaking ciphertext.

A cryptographic algorithm, also known as a cipher, is the mathematical function used for encryption and decryption. To encrypt a plaintext message, apply an encryption algorithm to the plaintext. To decrypt a ciphertext message, apply a decryption algorithm to the ciphertext. If the strength of the security provided by an algorithm is based on keeping the nature of the algorithm secret, it is called restricted (e.g., Zenith's video-scrambling algorithm). By today's data security standards, restricted algorithms provide woefully inadequate security. They are easy to break by experienced cryptanalysts and are not suitable for a large or changing group of users.

Meanwhile, many users and developers have the misconception that data compression can provide protection as certain compression algorithms scramble image data into visually unrecognized forms. The truth is that data compression, similar to restricted cryptographic algorithms, provides little protection once the compression algorithm used is known by the intruder. For high-security applications, all modern encryption algorithms use a key, which can take on one of many values (larger is better). Figure 1 shows the process of encryption and decryption with keys.

A protocol is a series of well-defined steps, involving two or more parties, designed to accomplish a task. A cryptographic protocol is one that uses cryptography. A self-enforcing protocol is the best type of cryptographic protocol because it is independent of the trustworthiness of people or the secrecy of the cryptographic algorithms used. The protocol itself guarantees fairness; if one of the parties tries to cheat, the other party immediately detects the cheating and the protocol stops. Whatever the cheating party hoped would happen doesn't happen. In the teleradiology

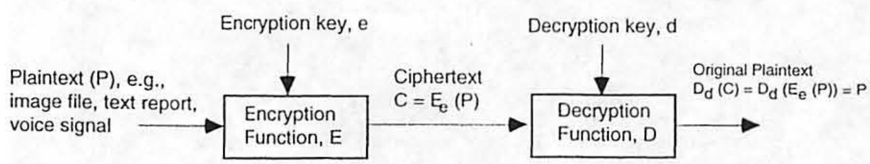

Figure 1 Encryption and decryption with keys.

and PACS environment, the system designer should strive to design and implement cryptographic protocols that are self-enforcing, cost-effective to implement, and can ensure a high level of security.

Cryptographic Algorithms

A cryptographic algorithm is the mathematical function used for encryption and decryption. Table 1 classifies key-based algorithms according to the nature of the encryption and decryption keys.

Secret Key Encryption

In a secret or private-key algorithm, the encryption key can be calculated from the decryption key, and vice versa. In many such cryptosystems, the encryption and the decryption keys are the same. These algorithms require the sender and receiver to agree on a key before they pass messages back and forth. This key must be kept secret; therefore, the level of security provided by such symmetric algorithms rests in the key. The Data Encryption Standard (DES), adopted by the federal government in 1976 and authorized for use on all unclassified government communications, is an example of a secret key algorithm.[6] The key is a 56-bit number and can be changed at any time.

Figure 2 illustrates an example of a secret key cipher on magnetic resonance images (MRIs). The cipher used is based on the International Data Encryption Algorithm (IDEA). The IDEA cipher is a newer and more secure cipher than DES.[7] Its key length is 128 bits—over twice as long as DES. Assuming that a brute-force attack is the most efficient, it would require 2^{128} (10^{38}) encryptions to recover the key. In contrast to the DES cipher, no papers have been published on breaking IDEA messages so far. In addition, there are no obvious patterns in the ciphertext. Figure 3 illustrates this with the even histogram distribution of the encrypted image slice in Figure 2. Pixel values of the 8-bit image slice range from 0 to 255.

The main drawback of secret-key algorithms is that anyone with the key can both encode and decode messages. Thus, any message can be compromised when the key is intercepted. Managing keys involved in a cryptographic protocol creates another problem. Assuming a separate key is used for each pair of users in a network, the total number of keys increases rapidly as the number of users increases. For n users, the total number of keys needed is $(n \times (n - 1))/2$; e.g., 10 users need 45 different keys to talk with one another, while 100 users need 4,950 keys. Such complexity of key management is not feasible for large user groups in a hospital or health maintenance organization (HMO) environment. Further, it is impossible to send someone a secret message unless the sender already can send the receiver a secret message—that is, the sender cannot communicate with the receiver without prior arrangement.

Public-Key Encryption

Public-key algorithms solve the secret-key management problem by having two different keys: one public and one private.[8] Information is encoded by the sender with the recipient's public key but can only be

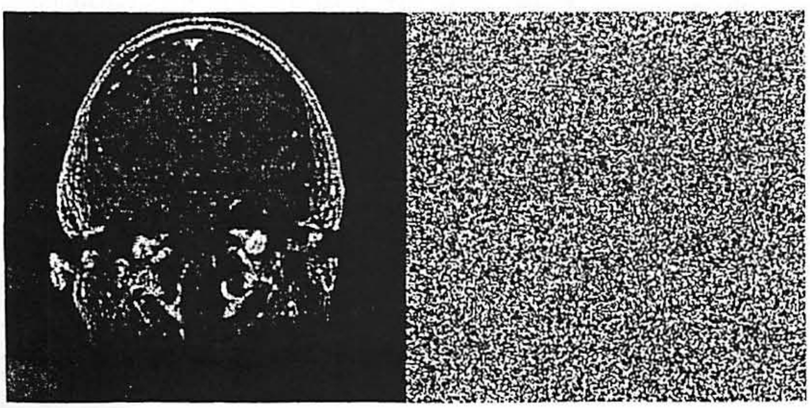

Figure 2 The original MR (left) image slice and the corresponding MR (right) image slice encrypted using the IDEA algorithm.

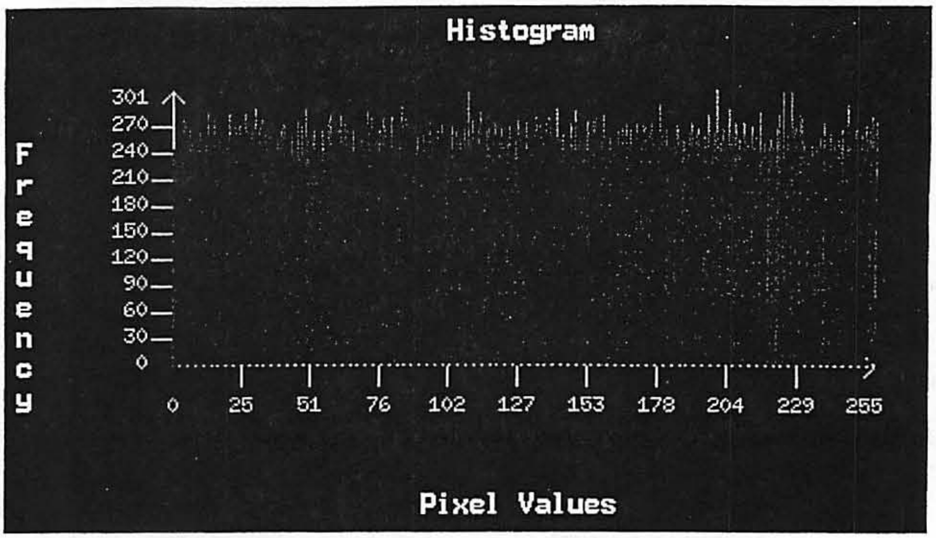

Figure 3 The histogram distribution of the encrypted MR image slice in Figure 2.

Table 1 ■

Three Types of Key-based Cryptography

Type	Nature of keys	Characteristics
Secret-key cryptography	Encryption key (e) = Decryption key (d)	e and d are private
Public-key cryptography	e ≠ d	e public, d private
Digital signature	e ≠ d	e private, d public

decoded by a recipient who possesses the private key. Moreover, the public key contains no hint as to the nature of the private key—it is computationally impossible to deduce the private key from the public key. Anyone with the public key (which, presumably, is made public by the owner) can encrypt a message but can not decrypt it. Only the person with the private key can decrypt the message.

Although public-key algorithms have better and more reliable key management over secret-key algorithms, they are much slower in execution. An example is the Rivest, Shamir, and Adleman (RSA) public-key cryptography, which derives its strength from the difficulty of factoring large numbers.[9] The public and private keys used in RSA are functions of a pair of large (100 to 200 digits or even larger) prime numbers. Recovering the plaintext from one of the keys and the ciphertext is conjectured to be equivalent to factoring the product of the two primes. It is, however, not practical to use pure RSA with large keys to encrypt and decrypt long messages. A 1,024-bit RSA key would decrypt messages about 4,000 times slower than the secret-key cipher. Furthermore, the workload to exhaust all the possible 128-bit keys in the IDEA cipher would roughly equal the factoring workload to crack a 2,304-bit RSA key, which is quite a bit bigger than the 1,024-bit RSA key size that most people use for high-security applications. Given this range of key sizes, and assuming there are no hidden weaknesses in the secret-key cipher, the weak link in this approach of using both private- and public-key cryptography is in the public-key cipher.

Public-key cryptography is attractive not because it is intrinsically stronger than a secret-key cipher—its appeal is that it helps one manage keys more conveniently. Subsequently, the use of public-key encryption for large medical images is better accomplished by using a high-quality, yet faster, single-key encryption algorithm to encipher the message. This original unenciphered message is the plaintext. In a process transparent to the user, a temporary random key, created just for this one session, is used to conventionally encipher the plaintext file. The recipient's public key is then used to encipher this temporary random conventional key. This public-key–enciphered conventional "session" key is sent along with the enciphered text (ciphertext) to the recipient. The recipient uses his or her own secret key to recover this temporary session key and then uses that key to run the fast, conventional single-key algorithm to decipher the lage ciphertext message.

Digital Signature

Digital-signature algorithms are used to prove authorship of, or at least agreement with, the contents of the computerized document. Digital signatures can be accomplished in some public-key algorithms by encrypting messages with the sender's private key and decrypting them with the sender's public key. Encrypting a radiologic image or report using the physician's private key generates a secure digital signature.

When the focus is on the authenticity of medical documents rather than their confidentiality, a digital signature can often be implemented with one-way hash functions.[10] A hash function takes an input data string and converts it to a fixed-size, often smaller, output data string. For a one-way hash function, it is easy to compute a hash value from an input string, but it is difficult to generate a string that hashes to a particular value. Commonly used hash functions in cryptography return values on the order of 128 bits long, so that there are 2^{128} possible hashes. The number of trials required to find a random string with the same hash value as a given string is 2^{128}, and the number of trials required to find two random data strings having the same (random) hash value is 2^{64}. The hash value, known also as the digital fingerprint or message digest (MD), is somewhat analogous to a "checksum" or CRC error checking code in that it compactly represents the message and is used to detect changes in it. Unlike a CRC, however, it is not computationally feasible for an attacker to devise a substitute message that would produce an identical message digest. With the public-key encryption, the message digest is encrypted by the secret key to form a signature. Hash functions are also used extensively in digital time-stamping methods.

Digital Time Stamping

Another proposal for certifying the contents of a document involves using a one-way hash function to create a type of digital time stamp of the document.[11,12] Many secure one-way hash functions are publicly known, however. A forger thus could alter a message, compute a new message digest, and simply attach it to the bogus message. One strategy is to encrypt the hash value with the sender's secret key and attach that value to the original message. The receiver computes a new hash value from the message and compares it with the one recovered from the sender's public key. If they match, then the message was not altered. It is worth noting that computing the hash value of a file is a much faster process than encrypting the entire file.

Another way to strengthen the credibility of a document's time stamp would be to send its hash-value fingerprint to a central time-stamp service. This service would attach the time of arrival and put both in permanent storage. Any question about a document's date and authenticity could be settled by checking the time-stamp service. This observation leads to the concept of digital trust centers for authenticating large volumes of medical images (see Digital Image Trust Centers, below).

Key Length

From the user's point of view, cryptographic keys are similar to the passwords used to operate automatic teller machines and to control access to computer systems. Just as different computer systems allow passwords of different lengths, different encryption algorithms use keys of different lengths. As with passwords, the longer the key, the stronger the security that the algorithm provides. The common way to crack a key used in a robust secret-key algorithm is by brute-force attacks (e.g., by trying every possible key, one after another, until one of the tries succeeds in decrypting the ciphertext).

It is easy to calculate the complexity of a brute-force attack. If the key is eight bits long, there are 2^8, or 256, possible keys. Therefore, it will take 256 attempts to find the correct key, with a 50% chance of finding the key after half of the attempts. If the key is 56 bits long, as in the case of DES, then there are 2^{56} possible keys. Assuming a computer program can try a million keys per second, it will take 2,285 years to find the correct key. If the key is 128 bits long, as in case of IDEA, it will take 10^{25} years. For $1 million, a brute-force cracking machine could be built to crack a 56-bit DES key in an average of 3.5 hours (results guaranteed in 7 hours).[13] This cost is within the budgets of most large companies and many criminal organizations. Fortunately, breaking an 80-bit or higher key is still extremely difficult, if not beyond the realm of possibility, at this stage.

In contrast with secret-key algorithms, breaking public-key algorithms does not involve trying every possible key. Instead, it involves trying to factor the large numbers that are the product of two large primes (see Public Key Encryption, above). Factoring large numbers is difficult. Table 2 lists public-key module lengths whose factoring difficulty roughly equals the

Table 2 ▪

Private-key and Public-key Key Lengths with Similar Resistance to Brute Force Attacks

Private-key Key Length (bits)	Public-key Key Length (bits)
56	384
64	512
80	768
112	1792
128	2304

Table 3 ■

Comparison of Major Cryptographic Algorithms in Image Authentication

Cryptographic Algorithms	Unauthorized Read Detection	Unauthorized Write Detection	Processing Speed	Key Management
Secret Key	+	+	0	−
Public Key	+	+	−	+
Digital Time Stamp	−	+	+	NA

Notations: + means positive (i.e., fast or strong; − means negative (i.e., slow or weak); 0 means average; NA means not applicable.

difficulty of a brute-force attack for private-key lengths.[5] That table states that if one is concerned enough about security to select a private-key algorithm with a 64-bit key, one should choose a module length for the public-key algorithm of about 512 bits.

Algorithm Comparisons

Table 3 summarizes the strengths and weaknesses of the various cryptographic algorithms for improving the security of large image files in digital radiology environments. Because a digital signature can be created by using a public-key method, Table 3 does not evaluate this algorithm.

Digital Image Trust Centers

The purpose of a digital trust center (DTC) is to incorporate systematically a variety of cryptographic algorithms (discussed above) in digital radiology environments. Currently, health care provider organizations lack such a cryptologic model for digital image protection. Figure 4 illustrates the architecture of a digital image trust center within a hospital-integrated PACS environment. In this figure, multimedia data from various image and text sources in a radiology department, such as medical imaging scanners, radiology information systems (RIS), hospital information systems (HIS), individual PAC systems, and film digitizers are linked to a centralized data repository that is managed by the PACS archival server.

In the DTC architecture, the PACS archival server interacts with an authentication server to support the authentication service. The authentication server can attach the hash value and time stamp to an incoming image dataset. The archival server then stores this dataset and its time stamp in the PACS image database and sends a copy of the time stamp back to the imaging source for recording. The image data can be originated by three possible sources. When the imaging source originates from a digital imaging scanner, such as magnetic resonance imaging (MRI) and x-ray computed tomography (CT), the image time stamp should be saved into the database of the acquisition computer of that scanner node. When the imaging source is from a sectional PACS, such as an Ultrasound or Nuclear Medicine PACS, the electronic time stamp should be saved in the local archive of that sectional PACS. When the film digitizer is used to convert external or existing screen films, the time stamp should be saved into the host computer of that film digitizer. Generally, PACS controllers and these acquisition computers can manage time-stamp data through a local database management system (DBMS).

The DTC builds on the infrastructure of the PACS, and so its access control protocols inherited from the PACS. That is, information access is limited to display stations registered in the PACS networks and is granted by patient name or hospital ID only. Also, the PACS does not permit the user to alter the original image and associated data from a display station, although the user can append new findings of an imaging study as separate entries into the central archive. Further work will investigate better access control policies for various kinds of image care services.

Someone who challenges the originality of an image stored in a local imaging site can just query the PACS archival server for verification by providing the image ID. To ease concerns about tampering or backdating at the centralized PACS repository, the scheme can be further refined to blend several sequential time-stamp requests into a chain or a binary tree structure.[12] Such authentication protocols incur little operational overhead with common hash functions; such as Message Digest 4 (MD4) and Message Digest 5 (MD5).[5] Within

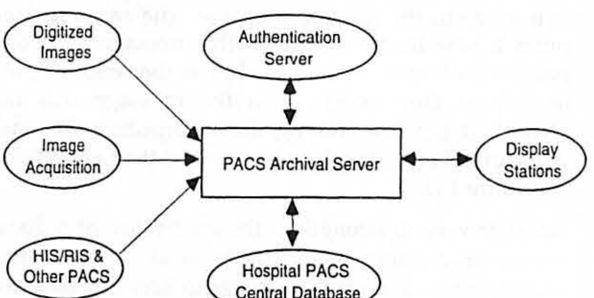

Figure 4 Digital trust center method in PACS for medical image authentication.

the PACS framework, the authentication server can reside in the same computer as the archival center and thus has minimum effect on the overall system architecture. For teleradiology systems without an on-line image database server, an authentication server node should be installed in the expert center site that serves remote small hospitals or rural clinics. The authentication server in this case will calculate and store the electronic time stamps of incoming images.

Moreover, a remote display station can query the PACS server to verify the authenticity of an image received. The display station does so by computing the hash value, or fingerprint, of the image in question and matching this value with the one obtained from the PACS archive. Since massive image transfer is not required, the verification will be done quickly.

The authentication server can also be extended to protect confidentiality. For example, the server creates a random key to encipher an image data file and stores it together with the encrypted image file into the PACS central archive. This assigned key will be sent together with the encrypted image file to the remote display station for confidentiality protection. Such an encryption procedure or protocol, however, can be compromised if the key is intercepted during the transmission. Public-key algorithms are preferable, but they are a thousand times slower than conventional single-key algorithms in encryption. Thus, the

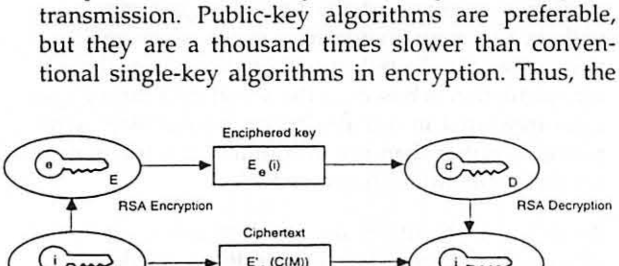

Figure 5 The logical flow of the encryption protocol that incorporates both IDEA secret-key cipher and RSA public-key cipher within a hospital-integrated PACS environment. Medical images are directly retrieved from the PACS central archive. Lossless compression is applied also. Encryption and decryption are performed by two UNIX workstations in the UCSF PACS networks. M'M' = 3D image datasets; C = lossless image compression function; C^{-1} = inverse function of C for lossless decompression; E', E = encryption functions; D, D' = decryption functions; and e, i = encryption keys.

encryption protocols in our authentication server used a mix of private and public key cryptographic techniques. Image encryption imposes added difficulties due to the need to store and transmit massive amounts of image data, instead of their hash values or time stamps for authentication. Thus, we devote the next section to discuss the design and performance of encryption protocols in the digital trust center.

Encryption Protocol

A hybrid encryption protocol has been derived for use in the digital trust center for securing medical image data. This cryptographic protocol takes advantage of the fast encryption of secret-key algorithms and secure key management of public-key methods. This study tested 81 datasets of MRI and positron emission tomography (PET) images retrieved from the UCSF PACS central archive. PET images are converted into 8-bit gray level. The MRI images are divided into 16-bit and 8-bit images. The 8-bit MR images are converted from the heavily T1-weighted scans with no degradation of image quality.

As shown in Figure 5, an image dataset is retrieved from the UCSF PACS archive and subjected to lossless compression. (Since diagnostic and other textual reports are much smaller in size, they are not the focus of this study.) Using data compression together with encryption has three advantages:

- Cryptanalysis relies on exploiting redundancies in the plaintext, and compressing a file before encryption reduces these redundancies.
- Encryption is time-consuming, especially for a large-image file, and compressing a file before encryption speeds up the entire process.
- Transmission time depends on file size, and compressing a file compensates for the expansion due to encryption and reduces the amount of data to be transferred.

It is worth noting that many of the current PAC systems have not yet implemented image compression of any kind. The need for providing image security adds further incentive to incorporate compression into all PAC systems, besides overcoming data storage and transmission limitations. Further, it is important to perform compression before encryption. If the encryption algorithm is any good, the ciphertext will not be compressible; it will look like random data.[5] Thus, most cryptographic packages routinely perform data compression before encryption. The secret-key algorithm known as the International Data Encryption Algorithm (IDEA),[7] is used to encrypt the compressed images, where the secret key is randomly generated for each image encryption. The popular and robust public-key algorithm known as Rivest, Shamir, and Adleman (RSA),[9] is used to encrypt the randomly generated secret key, i, which is a 1,024-bit number. This public-key–encrypted secret key is sent along with the ciphertext (encrypted image dataset) to the receiver. The receiver uses an individual private key to recover this encrypted secret key and then applies that key to run the fast secret-key algorithm to decrypt the large ciphertext.

In this experiment, the sender and the receiver are located in separate SUN SPARC LX workstations (SUN Microsystems, Mountain View, CA) in our PACS networks. The original and the decrypted image datasets were also evaluated to be equivalent; i.e., there was no contamination to the image datasets during this cryptographic process. The software system uses the Pretty Good Privacy (PGP) package[14] and the UCSF PACS data access and transmission programs.[15,16]

Results

Table 4 summarizes the encryption results on 81 volume image datasets of 16-bit MR (18 samples), 8-bit MR (30 samples), and 8-bit PET (33 samples) images. The 8-bit image datasets are postprocessed with a look-up table implemented in a medical workstation.[17] Two types of performance outcome are measured: the encryption time and decryption time with respect to the entire volume dataset and with respect to individual image slices. All these datasets have a uniform image dimension per slice.

As indicated in Table 4, for a few image slices, or even the entire PET volume dataset, it is feasible to incorporate key-based security software into real-time digital radiology applications (i.e., computational overhead is no more than a few seconds) using such common computing platforms as low-end SUN SPARC workstations.

Table 4 shows transmission with encryption and with decryption over low-end SUN SPARC workstations. Note that the reduction in the size of the ciphertext is due to applying lossless compression on image data before encryption. This leads to improvements in transmission time for encrypted files compared with unencrypted files.

This, however, does not apply to the large-volume data of a brain MRI (average about 7.2 MB) or other, even larger image datasets, such as those of mammograms (10 MB per digitized film) and CT (about 30–40 MB for a chest study). Table 4 shows also that the encryption process is slightly slower than the decryption process in our implementation.

One important use of encryption is to ensure the authenticity and confidentiality of radiologic images in telemedicine applications. Tables 5 and 6 give the transmission time performance of unencrypted and encrypted image datasets and slices with respect to three different communications media: narrow band integrated services digital network (56 Kbs N-ISDN), Ethernet (10 Mbs), and OC3-c asynchronous transfer mode (155 Mbs ATM). Figure 6 shows a set of timing performance charts of the three imaging modalities with and without encryption over these communications networks. To reflect real-life situations, the timing calculation is based on the actual data throughput rates measured in our PACS and teleradiology environment, rather than the maximum bit rates allowed for these communications media.[15,16]

As shown in Figure 6, the faster transmission speed of encrypted files is largely due to the lossless compression done before the encryption process. Encryption normally results in similar file size. For low-speed communications media such as N-ISDN, and in the absence of data compression, the hybrid encryption

Table 4 ▪

Time Performance of Encryption and Decryption Based on the Hybrid Scheme in Figure 5

Modality	Image Dimension	Average Volume Size (MB)	s.d.	Average Ciphertext Size (MB)	s.d.	Average Encryp./Decryp. Time per Volume (s)	s.d.	Average Encryp./Decryp. Time per Slice (s)	s.d.
MRI—Brain	256 × 256 × 16-bit	7.21	±0.51	2.51	±0.68	239.17	±26.46	4.24	±0.32
						184.61	±21.47	3.28	±0.27
MRI—Brain	256 × 256 × 8-bit	3.57	±1.20	1.73	±0.72	100.91	±16.90	1.92	±0.23
						88.06	±10.42	1.68	±0.15
PET—Brain	128 × 128 × 8-bit	0.75	±0.00	0.36	±0.15	23.43	±4.88	0.50	±0.10
						20.03	±2.37	0.43	±0.05

Notations: s.d. = standard deviation; MB = megabytes; s = seconds.

Table 5 ■

Effective Transmission Performance of Encrypted and Unencrypted Image Datasets Over N-ISDN (23 Kbs), 10-Base-T Ethernet (1 Mbs), and OC3-c ATM (65 Mbs) Networks

Imaging Modality	Mean Volume Size (MB)	Mean Ciphertext Size (MB)	Communication Medium (averaged data throughput)	Mean Transmission Time per Unencrypted Volume (s)	s.d.	Mean Transmission Time per Encrypted Volume (s)	s.d.
16-bit MRI	7.21	2.51	N-ISDN	2508.06	±176.11	872.55	±237.52
			Ethernet	57.69	±4.05	20.07	±5.46
			ATM	0.89	±0.06	0.31	±0.08
8-bit MRI	3.57	1.73	N-ISDN	1242.56	±417.67	601.16	±251.62
			Ethernet	28.58	±9.61	13.83	±5.79
			ATM	0.44	±0.15	0.21	±0.09
8-bit PET	0.75	0.36	N-ISDN	261.565	±0.00	124.182	±53.884
			Ethernet	6.016	±0.00	2.856	±1.239
			ATM	0.093	±0.00	0.044	±0.019

Kbs = kilobits per second; Mbs = megabits per second.

scheme described in Figure 5 not only ensures data integrity but also provides faster transmission. This is a useful finding, as most teleradiology applications are using low-speed public networks or the Internet for transmission. For high-speed broadband networks of 1 Mbs or more, however, there is a noticeable timing performance degradation when using encryption software, either with or without compression. For instance, Table 5 shows that the mean transmission time per unencrypted (original) 16-bit MRI volumetric dataset is 57.69 seconds (s), with a standard deviation of 4 s. In comparison, the mean transmission time and mean encryption time per encrypted 16-bit MRI dataset is: 20.07 s + 239.17 s = 259.24 s (from Tables 4 and 5), with a standard deviation of 5.46 s + 26.46 s = 31.92 s. The PACS networks are usually built on broadband technology for fast image transmission, so software implementation of image encryption thus incurs noticeable timing overhead. Therefore, the decision whether to apply encryption in a digital radiology environment becomes a tradeoff between time and security.

Discussion

Ready access to medical documents in the coming era of digital radiology carries with it the responsibility for ensuring that information is both authentic and confidential. The growing use of digital medical images in clinical practice poses new security issues due to the large image size and different user requirements. Research in computer cryptography has reached such a level of maturity that many robust algorithms are now available. Recently, papers discussing the use of specific cryptographic techniques in authenticating medical images have also been published. What is still missing, however, is the understanding

Table 6 ■

Effective Transmission Performance of a Single Encrypted and Unencrypted Image Slice Over N-ISDN (23 Kbs), 10-Base-T Ethernet (1 Mbs), and OC3-c ATM (65 Mbs) Networks

Imaging Modality	Mean Volume Size (MB)	s.d.	Mean Ciphertext Size (MB)	s.d.	Communication Medium (estimated throughput)	Transmission Time per Unencrypted Slice (s)	Mean Transmission Time per Encrypted Slice (s)	s.d.
16-bit MRI	7.21	±0.51	2.51	±0.68	N-ISDN	45.59	15.49	±4.22
					Ethernet	1.05	0.36	±0.10
					ATM	0.02	0.01	±0.001
8-bit MRI	3.57	±1.20	1.73	±0.72	N-ISDN	22.80	11.47	±4.80
					Ethernet	0.52	0.26	±0.11
					ATM	0.008	0.004	±0.002
8-bit PET	0.75	±0.00	0.36	0.15	N-ISDN	5.699	2.642	±1.15
					Ethernet	0.131	0.061	±0.03
					ATM	0.002	0.001	±0.0004

Note: Kbs = kilobits per second; Mbs = megabits per second.

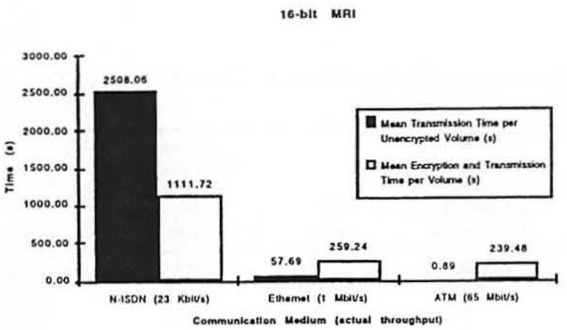

Figure 6.a

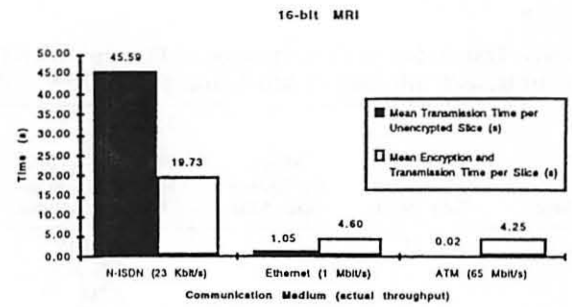

Figure 6.b

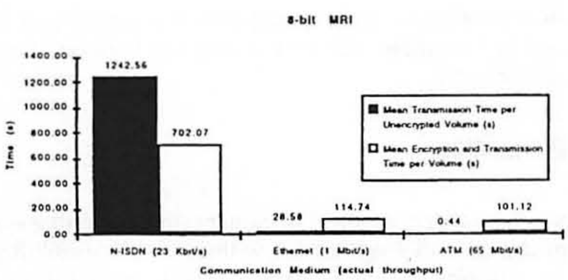

Figure 6.c

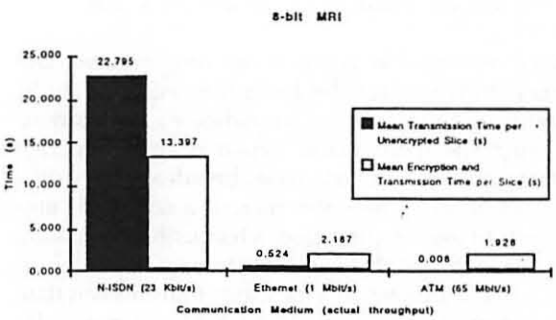

Figure 6.d

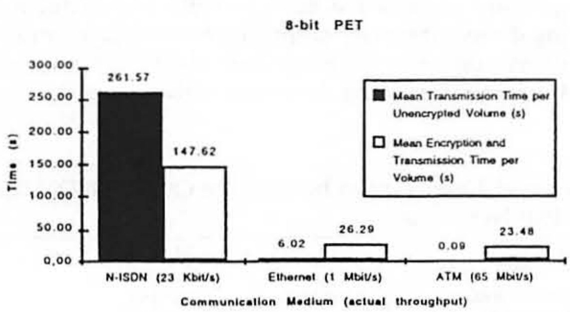

Figure 6.e

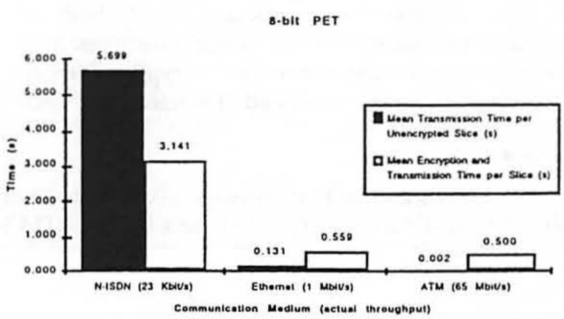

Figure 6.f

Figure 6(A–F) Transmission time performance charts of three types of image files and slices with and without encryption.

of how to integrate these cryptographic algorithms coherently into the existing operations of the enterprise.

This study takes a software system view of creating trust in digital radiology images and investigates the holistic approach of integrating a spectrum of cryptographic algorithms to meet the various security requirements of patient records. The key idea is to introduce a digital trust center as a digital notary to certify and protect the confidentiality of large volumes of medical images in hospitals. We evaluated the performance of our cryptosystem in encrypting several imaging modalities: 16-bit MRI, 8-bit postprocessed MRI, and PET, using cryptographic protocols operated within the hospital's integrated PACS environment. We presented the experimental results based on the sample size of 81 volumetric MR and PET images archived in our PACS repository. Future work will experiment with other encryption techniques to show performance comparisons.

Our result indicates that image authentication can be readily incorporated into the existing PACS architecture without affecting existing operations. Real-time software encryption to protect confidentiality is possible for one or a few selected image slices but not for the entire volumetric dataset (except the low-volume datasets, such as PET images). The encryption of 16-bit MRI and other higher imaging modalities, such as CT and mammography, would require dedicated hardware. Besides the considerable costs, the lack of interface standards also makes the current generation of cryptographic hardware not readily portable across different digital radiology systems.

Over low-speed phone lines, ISDN, and the Internet, the hybridization of lossless compression, public-key cryptography, and secret-key cryptography can reduce the transmission time greatly while providing added security and quality assurance. Certainly, lossy compression can be interchanged with the lossless scheme to further speed up the transmission, but this is done at the expense of image quality.

Many protocols for non-medical applications have been developed recently for securing and authenticating digital information. For example, the Internet Engineering Society developed the Privacy Enhanced Mail (PEM) standard software, which utilizes DES to encrypt e-mail text and RSA to authenticate and sign it. ViaCrypt (Lemcom, Phoenix, AZ) and PGP use IDEA instead of DES for encryption. Digital Notary (Surety Technologies, Morristown, NJ) uses tree-based digital time stamping for data authentication.[11] These protocols can be easily incorporated into the digital trust center model and optimized for digital radiology applications. In addition, most encryption software packages come with automatic key management software that contains files of public- or secret-key material, the owner's user ID, and a time stamp showing when a certain key pair was generated. Often, the secret key files are encrypted with their own passwords or pass phases for protection.

Although cryptography is a powerful system for protecting medical data, it is not a panacea. For instance, cryptography can not protect against stolen encryption keys. The whole point of using encryption is to make it possible for people who have your encryption keys to decrypt your files. Thus, any attacker who can steal your keys can decrypt your files. Also, cryptography cannot protect against destructive attacks. Sometimes, an attacker does not want to read your files but just wants to keep you from reading them. Even an attacker who cannot get access to your encryption keys can still cause you a lot of pain and suffering by breaking into the image archive and erasing relevant medical documents. To solve such problems, the health care provider organizations must enforce proper protocols or procedures for access control.[18] A rudimentary form of access control, inheriting the current data access protocol of PACS, is provided in the digital trust center model. Future work will investigate this important security issue for more specialized image care services in more detail.

In the past, the whole issue of cryptography was clouded by disputes over export and government access for law-enforcement purposes. The discovery and publication of public-key algorithms and digital time stamping open up many vistas for using robust cryptography in non-federal sectors. These two kinds of cryptographic algorithms are the core techniques to establish the trust in multimedia medical records among hospitals using digital images. Research should now focus on the coherent integration of these algorithms into existing hospital information systems.

Nevertheless, there can never be a purely technologic soluton to privacy, and social issues must be considered in their own right. The digital trust center provides a systematic approach for integrating various cryptographic techniques and constructing computer systems that are privacy enabled, giving power to the individual or local hospital. But only the medical community's proper appreciation for these techniques and an understanding of their interrelations can cause the right cryptosystem to be used.

The author thanks Mr. Macro Abundo of the San Francisco VA Medical Center for his assistance in software implementation and data analysis. He also thanks Dr. H. K. Huang and Dr. Ronald Arenson of the Department of Radiology, UCSF, for informing him of the security issues in digital radiology departments. Their practical concerns motivated this investigation and development.

References ■

1. Huang HK, Ratib O, Bakker AR, Witte G. NATO ASI Series F, PACS in Medicine, vol. 74. New York: Springer-Verlag, 1991.
2. Osteaux M (ed). A Second Generation PACS Concept. Berlin: Springer-Verlag, 1992.
3. Huang HK, Arenson RL, et al. Second generation PACS at UCSF. Radiology. 189:1993;290.
4. Smith JP. Authenticating digital medical images with digital signature technology. Radiology. 194:1995;771-4.
5. Schneier B. Applied Cryptography: Protocols, Algorithms, and Source Code in C. New York: John Wiley & Sons, 1993; Chapter 7.
6. Branstad DK, Gait J, Katzke S. Report on the workshop on cryptography in support of computer security. NBSIR 77-1291, National Bureau of Standards, Sept. 21-22, 1976.
7. Lai XJ. On the design and security of block ciphers. In: Massey JL (ed). ETH Series on Information Processing, vol. 1. Konstanz, Switzerland: Hartung-Gorre Verlag, 1992.
8. Diffie W, Hellman ME. New directions in cryptography. IEEE Trans Information Theory. 22:1976;644-54.
9. Rivest R, Shamir A, Adleman L. A method for obtaining digital signatures and public-key crytosystems. Communications of the ACM. 21:1978;120-6.
10. Davies DW, Price WL. Digital signature—An update. Proceedings of the International Conference on Computer Communications, Sydney, Oct. 1984. North Holland: Elsevier, 1985;843-7.
11. Cipra B. Electronic time-stamping: The notary public goes digital. Science. 261:1993;162-3.
12. Haber S, Stornetta WS. How to time-stamp a digital document. Journal of Cryptography. 3:1991;99-112.
13. Wiener MJ. Efficient DES key search. TR-244, School of Computer Science, Carleton University, May 1994.
14. Garfinkel S. PGP—Pretty Good Privacy. O'Reilly & Associates, CA, 1995.
15. Wong STC, Huang HK. A hospital integrated framework for multimodal image base management. IEEE Trans. Systems, Man, and Cybernetics. 26:1996;455-69.
16. Wong STC, Huang HK. Limitations of transmission control protocol on high-speed radiologic asynchronous transfer mode networks. Radiology. 197(P):1995;258.
17. Wong STC, Knowlton RC, Hawkins RA, Laxer KD. Multimodal image fusion for noninvasive epilepsy surgery planning. IEEE Computer Graphics & Applications. 16:1996;30-8.
18. Varadharajan V, Calvelli C. An access control model and its use in representing mental health application access policy. IEEE Trans. Knowledge & Data Engineering. 8:1996,81-95.

PACS
Picture Archiving and Communication Systems in Biomedical Imaging

H.K. Huang, D.Sc., FRCR (Hon.)

VCH / John Wiley & Sons

H.K. Huang
Professor and Vice Chairman
Director, Laboratory for Radiological Informatics
Department of Radiology
University of California, San Francisco
530 Parnassus Avenue, Rm CL-158
San Francisco, CA 94143-0628
and
Faculty, Bioengineering Graduate Program
UCSF/UC Berkeley

This book is printed on acid-free paper. ♾

Library of Congress Cataloging-in-Publication Data
Huang, H.K., 1939–
PACS : Picture Archiving and Communication Systems in biomedical imaging / H.K. Huang.
p. cm.
Includes bibliographical references and index.
ISBN 1-56081-685-6 (alk. paper)
1. Picture archiving and communication systems in medicine. 2. Diagnostic imaging. I. Title.
R857.P52H83 1996
616.07'54—dc20 95-38928
CIP

Printed in the United States of America

ISBN 1-56081-685-6 VCH Publishers, Inc.

Printing History:
10 9 8 7 6 5 4 3 2 1

Published jointly by

VCH Publishers, Inc.
333 7th Avenue
New York, New York 10001

VCH Verlagsgesellschaft mbH
P.O. Box 10 11 61
69451 Weinheim, Germany

VCH Publishers (UK) Ltd.
8 Wellington Court
Cambridge CB1 1HZ
United Kingdom

Preface

Picture archiving and communication systems (PACS) is a concept perceived in the early 1980s by the radiology community as a future method of practicing radiology. PACS consists of image acquisition devices, storage archiving units, display stations, computer processors, and database management systems. These components are integrated by a communications network system. During the past 10 years, technologies related to these components became mature, and their applications have gone beyond radiology to the entire health care delivery system. As a result, PACS for special clinical applications as well as large-scale, hospital-wide PACS are being installed throughout the United States and the world.

A literature search related to PACS reveals that there are about two thousand publications, several edited books, several special issues in journals, and three chapters in my earlier book, *Elements in Digital Radiology*. Although these publications provide, chronologically, documentation on research and development advancement of PACS during the past decade or so, they lack coherence in the subject matter. This book is an attempt to introduce this topic systematically, based on the most recent research and development results. Although originating in the radiology community, the PACS concept can be applied to any scientific field that requires the handling of voluminous pictures and textual data. We anticipate that this field will continue to grow in the next 5 years. This book will serve as a foundation for the future training of people entering this area of work.

I owe a debt of gratitude to Dr. Edmund Anthony Franken, Jr., past chairman of the Department of Radiology, University of Iowa, for getting me interested in this field in 1981. Later, Dr. Gabriel Wilson, then the chairman of the Department of Radiological Sciences at UCLA, offered me an opportunity to launch a PACS project in the department. He provided the initial financial support to establish the Image Processing Laboratory, which later became the Medical Imaging Division. In the ensuing years, Drs. Zoran Barbaric, Robert Leslie Bernett, acting chairmen, and Dr. Hooshang Kangarloo, past chairman of the department, all provided generous support to the project. We also received from the National Institutes of Health (NIH) three large long-term grants in PACS, and we established collaboration from private industry including (in chronological order) Technicare Corporation; Gould/DeAnza Graphic System Division; Light Signatures, Inc.; Konica; IBM Corporation; ADAC Laboratories; Philips Medical Systems, Inc.; Mitsubishi Electronic Corporation; 3M; and Kodak. As a result of these efforts, a large-scale PACS was released for clinical use in early 1992. This UCLA PACS was developed with the Department of Radiology in mind and lacks the expanded, open architecture design that is necessary for a hospital-integrated PACS.

In October 1992, Dr. Ronald Arenson, chairman of the Department of Radiology, UCSF, offered me an opportunity to build a second PACS. Kathy Andriole (computed radiography), Todd Bazzill (network), Andrew Lou (acquisition and display), and Albert Wong (PACS controller), who were part of the core team that built the first PACS, also joined UCSF. In addition, Yuki Ishimitsu and Jun Wang came from UCLA to UCSF to finish their Ph.D. dissertations. At UCSF we recruited several staff members, some postdoctoral fellows, and our assistant, Laura Snarr. Together, we established the Laboratory for Radiological Informatics.

Meanwhile, the NIH has continued supporting our laboratory. We also received new support from IBM Almaden Research Center; the CalREN (California Research and Education Network) Program by Pacific Bell; HPCC (High Performance Computing and Communication) Program sponsored by the NLM (National Library of Medicine); Abe Sekkei, Japan; Lumisys; and Sun Microsystems.

It took us about 18 months to complete the second-generation PACS infrastructure including the interface to the hospital and radiology information systems and to the departmental Macintosh users. We released image workstations one by one for clinical use beginning early in 1994. The next step in our PACS growth is to obtain hospital commitment for deployment of many image workstations to the radiology department as well as in the hospital. In the research area, we are moving toward image content base information retrieval, online PACS three-dimensional rendering, and distributed computing in a PACS environment.

From our experience during the past 12 years, we can identify some major contributions in advancing PACS development. Technically, the first laser film digitizers, developed for clinical use by Konica and Lumisys, the development of computed radiography (CR) by Fuji and its introduction from Japan to the United States by Dr. William Angus of Philips Medical Systems, and the large-capacity optical disk storage by Kodak all are critical. Also highly significant are parallel transfer disk technology, 2000-line and 72 Hz display monitors, the system integration methods developed by Siemens Gammasonics and Loral for large-scale PACS, the DICOM committee's effort in standardization, and the asynchronous transfer mode (ATM) technology for merging local area network and wide area network communications.

In terms of events, the annual SPIE PACS and Medical Imaging meeting and EuroPACS are the continuous driving force for PACS. In addition, every two years the Computer-Assisted Radiology (CAR) meeting, organized by Prof. Heinz Lemke, and the Image Management and Communication (IMAC) Conference organized by Dr. Seong K. Mun, provide a forum for international PACS discussion. The InfoRAD Section at the Radiological Society of North America (RSNA) organized in 1933 by Dr. Laurens V. Ackerman with the live demonstration of DICOM interface, sets the tone for industrial PACS open architecture. The annual RSNA refresher courses in PACS organized first by Dr. C. Douglas Maynard and then by Dr. Edward V. Staab, provide continuing education in PACS to the radiology community.

In 1992 *Second Generation PACS*, Michel Osteaux's edited book, gave me confidence that PACS is moving toward a hospital-integrated approach. When Dr. Roger A. Bauman became editor-in-chief of the then new *Journal of Digital Imaging* in 1988, the consolidation of PACS research and development publications became possible. Colonel Fred Goeringer instrumented the Army's project in medical diagnostic imaging support (MDIS) systems, resulting in several large-scale PACS installations that provide major stimulus and funding for the PACS industry.

All these contributions have profoundly influenced my thoughts on the direction of PACS research and development as well as the contents of this book. This book summarizes our experiences in developing the concept of digital radiology and PACS during the past 10 years. Selected portions of the book have been used as lecture materials in graduate courses on medical imaging and advanced instrumentation at The University of California at Los Angeles, San Francisco, and Berkeley. We hope that this book will inspire more researchers to become interested in this field. Together we can move one step closer to the reality of a digital-based health care environment.

H.K. (Bernie) Huang
San Francisco and Agoura Hills, CA

Contents

PACS: PICTURE ARCHIVING AND COMMUNICATION SYSTEMS IN BIOMEDICAL IMAGING

Table of Contents

ORDER FORM

RSNA 1996

progress through partnership

UCSF LABORATORY FOR RADIOLOGICAL INFORMATICS

Chicago, Il
December 1 - December 6, 1996

REFRESHER COURSES

Sunday 1:30–3:00 PM • 1½ hours

Course No. 153
How to Use a PACS Workstation ("Hands-on" Workshop)

Ronald L. Arenson, MD, Moderator, *San Francisco, CA*
David E. Avrin, MD, PhD, *San Francisco, CA*
Ronald L. Arenson, MD, *San Francisco, CA*
Steven C. Horii, MD, *Philadelphia, PA*

PACS continue to hold promise for reducing dependence on film for acquisition, storage, and display of medical images. This will provide radiologists and other health care professionals with hands-on instruction while using state-of-the-art workstations for PACS.

Purpose: Attendees will become familiar with important concepts, including basic image manipulation (window/level, scroll/zoom, and patient selection), image compression, 3D reconstruction, image processing (edge enhancement), and folder manager processes (pre-fetch, auto-sequence, auto-routing, and auto-window/level). Where appropriate, comparison normal images will be shown along with the modified images to demonstrate differences. No more than three participants will share each workstation, allowing sufficient individual time to master the techniques presented.

Repeats on Monday morning, Course 253; Monday afternoon, Course 353; Tuesday morning, Course 453; Wednesday morning, Course 553; Thursday morning, Course 653; Thursday afternoon, Course 753; and Friday morning, Course 853

Wednesday 8:30–10:00 AM • 1½ hours

Course No. 523
Categorical Course in Physics: Technology Update and Quality Improvement of Diagnostic X-ray Imaging Equipment—Computed Radiography

Robert G. Gould, ScD, Co-director, *San Francisco, CA*
John M. Boone, PhD, Co-director, *Sacramento, CA*

A. Computed Radiography Technology Overview

Katherine P. Andriole, PhD, *San Francisco, CA*

Recent technologic advances in computed radiography (CR) have begun to make this modality more prevalent clinically. Hardware and software improvements in the photostimulable phosphor plate, in image reading-scanning devices, in image processing algorithms, and in image output formats have contributed to the increased acceptance of CR as the counterpart to conventional screen-film projection radiography. An overview of the current state of the art in CR systems will be provided. Advantages and disadvantages inherent in CR will be discussed. Recent modifications in high-resolution CR plate technology, image acquisition mechanisms (including high-resolution 4 × 5-K image capture), image processing, and image display presentation will be detailed. New image processing algorithms to be discussed will include dynamic range control and dual-energy subtraction. Examples will be presented of several types of artifacts potentially encountered with CR, some of which are minimized with the latest technology.

Learning objectives: (1) To review the basic principles of CR. (2) To understand recent advances in CR technology.

B. Computed Radiography Quality Improvement

Charles E. Willis, PhD, *Houston, TX*

Although quality-assurance (QA) processes are essential to the operation of a modern radiology department, the clinical experience base with computed radiography (CR) is limited. CR offers unparalleled variation of the appearance of the radiographic projection. Some of this variation is automatic, and some is under operator control. Clinical experience with CR is needed to establish QA indicators and appropriate action levels. Key elements of a comprehensive QA program for CR include thorough acceptance testing, specialized calibrations, diligent maintenance activities, periodic quality-control measurements, contemporaneous exposure assessments, and a concurrent training program. Constituent tests and measurements are adaptations of those practiced in conventional screen-film radiography. Practical QA tests must be straightforward, rapid, and sensitive. Meaningful comparisons of performance rely on standardized measurements and calibrations. This session will discuss each element of a QA program for CR, suggest appropriate indicators, and describe adjustments to conventional screen-film radiography practice to accomodate CR.

Learning objectives: (1) To compare QA for CR versus conventional screen-film radiography. (2) To understand the limitations of the clinical experience base with CR. (3) To emphasize practical QA activities that can yield substantial improvements.

Continues on Thursday morning, Course 623

Monday Afternoon • Room E270 (Lawless)

506 • 2:57 PM

Background Recognition and Removal of Computed Radiographs

J. Zhang, PhD, San Francisco, CA • H.K. Huang, DSc

PURPOSE: The background of computed radiographic (CR) images caused by x-ray collimation shows white and is difficult to remove efficiently because the removal algorithm has to recognize different body contours as well as various shapes of the collimator. This presentation gives a novel method to recognize and remove the CR background with higher successful ratio and better reliability.
MATERIALS AND METHODS: Our department operates two CR systems (Fuji 9000 and AC-2) generating about 1.2 gigabits of image data daily. The method of background recognition and removal (BRR) for CR images presented here is based on several innovative concepts, including (1) a statistical model of background signals in CR images, (2) signal processing, (3) adaptive parameter adjustment, and (4) consistent reliability estimation rules.
RESULTS: With this method implemented in a clinical PACS, we achieved 99% correct recognition and 91% full removal of CR background without cutting off any valid image information.
CONCLUSION: After BRR of CR images, the contrast sensitivity of the eye in reading these images is increased, and the image visual quality improved greatly. The BBR of CR images also offers an immediate lossless data compression and facilitates application of computer-aided diagnosis. [See also scientific exhibit 816PH.]

Monday Afternoon • Room E265 (Room 8)

515 • 2:30 PM

Utilization of DICOM in PACS Operation

A.W. Wong, BS, San Francisco, CA • H.K. Huang, DSc

PURPOSE: We have integrated our PACS into a DICOM-compliant system that facilitates the communication of radiologic images between individual PACS components.
MATERIALS AND METHODS: The image communication software implemented in our PACS was based on the Millinckrodt central test node software with several enhanced features. These features include (1) data encoding to DICOM in image acquisition nodes in support of non-DICOM imaging devices; (2) multilevel TCP/IP-based network interface support; (3) a job control mechanism, which allows images to be transmitted according to different priority levels or re-transmitted in the event of connection failure; and (4) computer host verification for data security and patient confidentiality. This paper describes the functionality of the communication software and its utilization in our PACS operation.
RESULTS: The enhanced DICOM-based communication software has demonstrated a reliable yet efficient transfer for images in a PACS environment. Our PACS infrastructure currently provides DICOM connectivity for multivendor equipment.
CONCLUSION: Adaptation of DICOM to PACS provides interoperability between PACS components. However, the use of DICOM communication protocols requires overhead that tends to slow down the transmission. Therefore, much effort in software integration is necessary in order to increase operation efficiency of a PACS.

516 • 2:39 PM

PACS Module for Intensive Care Units

A.W. Wong, BS, San Francisco, CA • J. Zhang, PhD • K.P. Andriole, PhD • H.K. Huang, DSc

PURPOSE: We have implemented a PACS module for the intensive care units (ICUs) within our hospital-integrated PACS global system. Portable x-ray examinations are reviewed by physicians on the ICUs' local display stations.
MATERIALS AND METHODS: The PACS infrastructure is composed of an archiving system, a database system, and an asynchronous transfer mode communication network. The integrated ICU module features 2 computed radiographic (CR) systems and 3 dual-monitor (1,600 × 1,280-resolution) display stations (located within the pediatric, surgical, and coronary ICUs). Implemented mechanisms include (1) automatic acquisition and routing of the CR images; (2) an image manager, which groups multiple studies from a single patient on a per-hospital-stay basis; (3) image preprocessing, which presets display parameters to minimize image manipulation during review sessions; and (4) image retrieving, which allows physicians to retrieve historical images from any modality for study comparison.
RESULTS: The ICU PACS provides physicians with rapid access to patient studies, hence improving physicians' efficiency in a time-critical clinical environment.
CONCLUSION: With its scalable infrastructure, our PACS has extended its service outside the radiology department. We conclude that a well-designed PACS can be beneficial to clinicians hospital wide.

SCIENTIFIC SESSIONS

Monday Afternoon • Room E265 (Room 8)

519 • 3:06 PM

On-line DICOM Communication Performance

S. Lou, PhD, San Francisco, CA • D.R. Hoogstrate, BS • H.K. Huang, DSc

PURPOSE: To analyze the performance of DICOM communication-supporting auto-transfer, auto-queue, and manual transfer modes.
MATERIALS AND METHODS: Twelve MR studies, including 57 series with 1,538 sections, were randomly transmitted with 3 modes from an imager using Central Test Node DICOM-based software to a PACS computer, through an Ethernet during clinical hours. The auto-transfer mode transmits an MR section whenever it is available. The auto-queue mode transfers all images only when an entire study is completed. The manual transfer mode simulates a series transfer mode, which measures a time of transferring a series.
RESULTS: On average, the transmission rates of the auto-transfer, auto-queue, and manual mode are 9.25 ($\sigma = \pm 2.66$), 81.75 ($\sigma = \pm 11.90$), and 88.64 ($\sigma = \pm 5.84$) Kbyte/sec, respectively.
CONCLUSION: In the auto-transfer mode the time measured includes imaging, reconstruction, and transfer. The actual transmission time is only 13.8%. In the auto-queue mode, there is a long delay before any image is available at the workstation, since the application has to wait for all images to be ready first. In order to minimize the interference of the data transmission with imager operations, we recommend a 4th mode allowing transfer of an entire series automatically once it is ready.

Thursday Morning • Room E270 (Lawless)

1404 • 11:33 AM

Interactive Visualization and Measurement of Epiphyseal Fusion

E. Pietka, PhD, San Francisco, CA • M.I. Jahangiri, MD, MPH • H.K. Huang, DSc

PURPOSE: We have successfully assessed bone age with digitized hand images. To improve accuracy, we quantified the measure of epiphyseal fusion.
MATERIALS AND METHODS: A specifically designed user interface is employed to display the hand image and select 4 points restricting the region of interest near the phalangeal and radial epiphyses. This region is then subjected to a wavelet transform decomposition procedure. The vertically high-frequency component enhances the fusion. In a nonfused area, a solid line is visible. The development of fusion breaks and thickens the line. Automatic measurement of its thickness and length reflects the stage of fusion.
RESULTS: The analysis has been performed on 40 hand radiographs. Line measures have been plotted versus the bone age as assessed by a radiologist. Digitized and computer radiographic hand images of patients between 13 and 18 years of age have been analyzed. Based on these radiographs, a fuzzy membership function has been calculated. It defines the range of measures for each year of bone age. These 40 images as well as another set of 40 hand radiographs have been used to evaluate the algorithm.
CONCLUSION: Adding epiphyseal fusion to assess bone age increases the objectivity and improves accuracy.

SCIENTIFIC EXHIBITS

■ Physics and Other Basic Sciences

SPACE 785PH

PACS Pitfalls and Bottlenecks

H.K. Huang, DSc, San Francisco, CA • S.L. Lou, PhD

PACS pitfalls are created mostly from human intervention, whereas bottlenecks are due to imperfect design in either the PACS or image acquisition machines. These culprits can be realized only through clinical experience. This exhibit categorizes some of these problems, illustrates their effect on PACS operations, and suggests methods circumventing them. Pitfalls due to human errors often occur at imaging acquisition and at workstations. They can be minimized through a good quality assurance program. Some bottlenecks that affect a PACS operation include network contention; computed radiography, CT, and MR images stacked up at acquisition machines; slow response from workstations; and a long wait for image retrieval from a long-term archive. Bottlenecks can be alleviated by improving system architecture and operation through a gradual understanding of the clinical environment.

SPACE 816PH

Automatic Background Recognition and Removal of Computed Radiographic Images

J. Zhang, PhD, San Francisco, CA • H.K. Huang, DSc

The background of computed radiographic (CR) images caused by x-ray collimation shows white and is difficult to remove efficiently because the removal algorithm has to recognize different body contours as well as various shapes of the collimator. This presentation gives a method based on several innovative concepts, including (1) a statistical model of background signals on CR images, (2) signal processing, (3) adaptive parameter adjustment, and (4) consistent reliability estimation rules, to recognize and remove the background with a higher successful ratio and better reliability. After background recognition and removal of CR images, the contrast sensitivity of the eye in reading these images is increased and the image visual quality improved. This exhibit will present various types of CR background from clinical cases and their recognition and removal pictorially. **[See also scientific paper 506.]**

UCSF LRI

Computer-aided Instruction

SPACE 9728CAI

Interactive Breast Imaging Teaching File

F. Cao, PhD, San Francisco, CA • H.K. Huang, DSc • E.A. Sickles, MD • M.J. Moskowitz, MD

The current UCSF breast imaging interactive teaching file is presented. The teaching file is built on a sophisticated computer-aided instruction model with carefully structured questions. Each user can be prompted to respond by making his/her own observations, assessments, and work-up decisions as well as by marking imaging abnormalities. This effectively replaces a traditional "show-and-tell" teaching experience with an interactive, response-driven type of instruction. In this exhibit, our pilot teaching file with a friendly graphic user interface will be demonstrated on a Sun SPARC workstation and available to participants for their test and evaluation.

Learning objectives:
- Become familiar with digital mammograms.
- Obtain hand-on experience with the UCSF interactive mammography teaching file system—its high-resolution image display, graphic user interface, and response-driven type of instruction.
- Understand the computer-aided instruction models used in the interactive teaching file.
- Use a simple script to create one's own teaching file session.

SPACE 114NR

Magnetic Source Imaging: State of the Art in Epilepsy Imaging

H.A. Rowley, MD, San Francisco, CA • R.C. Knowlton, MD • T.P. Roberts, PhD • S.T. Wong, PhD • R.A. Hawkins, MD, PhD • K.D. Laxer, MD

This exhibit will review the imaging principles and clinical utility of magnetic source imaging (MSI) in epilepsy. Surgical treatment can dramatically improve seizure control in patients with medically refractory epilepsy, provided that the irritative zone can be localized and safely removed. MSI is emerging as an important new tool that helps in the preoperative integration of functional and structural data. During the MSI procedure, spontaneous seizures or interictal "spikes" are recorded with large-array biomagnetometer and coregistered to MRI. MSI localizations correlate with MR imaging, PET/SPECT, and surgical pathologic findings. MSI adds novel information in some patients with neocortical epilepsy, where it may soon offer an alternative to depth electrodes. (This work was supported in part by Biomagnetic Technologies, Inc.)

SPACE 9730CAI

Visual Information Retrieval of Medical Images

S.T.C. Wong, PhD, San Francisco, CA • A. Gupta, PhD • K. Soo Hoo, BSc • R.C. Knowlton, MD • E.P. Grant, MD

Current medical image management systems can only index data by artificial keys and lack the ability to search vast amounts of information by content. This greatly hinders the functional scope of image information systems in clinical services, research, and education. We are actively developing experimental testbeds to support visual information management for the next generation of image information systems. Accordingly, the purpose of this exhibition is to demonstrate new techniques and tools for visual information management in radiology.

Learning objectives:
- Understanding of visual information retrieval.
- Learn how to query image database with hands-on laboratory.
- Learn how to use visual information management for clinical practice and education.